PACIFIC GAS AND ELECTRIC COMPANY
GEOSCIENCES DEPARTMENT
TECHNICAL REPORT

Report Number: GEO. DCPP.TR.14.02
Report Revision: Rev. 0
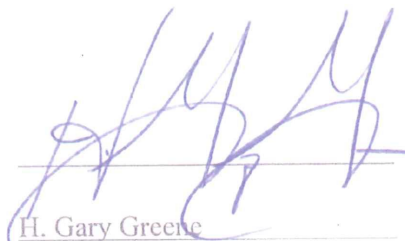Report Date: 7/24/2014
Quality Related: Y
Page 1 of 178

REPORT TITLE: Offshore Low-Energy Seismic-Reflection Studies in Estero Bay, San Luis Obispo Bay, and Point Sal Areas
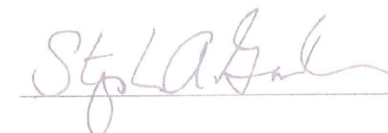
SIGNATORIES

PREPARED BY: _____ DATE: 27 July 2014

H. Gary Greene

Printed Name   Organization

VERIFIED BY: _____ DATE __27 July 2014_____

Stephan A. Graham   Consulting Geologist

Printed Name   Organization

APPROVED BY: _Richard Klimczak_____ DATE: Sept. 10, 2014

Richard Klimczak   Geosciences

Printed Name   Organization

RECORD OF REVISIONS

Rev. No.	Reason for Revision	Revision Date
0	Initial Report. This worked is tracked under SAPNs 505100993 (Greene) and Graham (50533445)	7/27/2014

TABLE OF CONTENTS

Page

LISTS OF TABLES, FIGURES, PLATES, APPENDICES, AND ATTACHMENTS

Tables

Figures

Plates

Appendices

Attachments

ABBREVIATIONS, ACRONYMS, AND SYMBOLS

$\delta^{18}O$	oxygen 18 stable isotope measure
2D	two-dimensional
3D	three-dimensional
CDP	common depth point
CEG	Certified Engineering Geologist (California)
DCPP	Diablo Canyon Power Plant
DEM	digital elevation model
DGPS	differential global positioning system
ELP	early–late Pliocene
FCL	Fugro Consultants, Inc.
GIA	glacial isostatic adjustment
GPS	global positioning system
GSI	Geophysical Service, Inc.
HESS	high-energy seismic survey
HFZ	Hosgri fault zone
Hz	hertz
IHO	International Hydrographic Office
IPRP	Independent Peer Review Panel
IT	independent technical
ITR	Independent Technical Reviewer
ka	thousand years ago *or* thousand years old
kJ	kilojoules
km	kilometer(s)
kyr	thousand years
LCI	Lettis Consultants International
LGM	last glacial maximum
LESS	3D low-energy seismic survey
LTSP	Long Term Seismic Program
m	meter(s)
M	magnitude
Ma	million years ago *or* million years old

MBES	multibeam echosounder
MIS	marine isotopic stage
M_L	local magnitude
MLML	Moss Landing Marine Laboratories
mm/yr	millimeters per year
MPT	mid-Pleistocene transition
ms	millisecond(s)
m/s	meters per second
M_w	moment magnitude
Myr	million years
NQA	Nuclear Quality Assurance
NRC	U.S. Nuclear Regulatory Commission
NTN	near top of Neogene
PG&E	Pacific Gas and Electric Company
QA	quality assurance
QC	quality control
RSA	Rock Solid Attributes
s	second(s)
SSC	seismic source characterization
SSHAC	Senior Seismic Hazard Advisory Committee
TI	technical integration
TWTT	two-way travel time
USGS	U.S. Geological Survey
UTM	Universal Transverse Mercator
WGS 84	World Geodetic System of 1984

1.0 INTRODUCTION

An extensive three-dimensional (3D) low-energy seismic survey (LESS) was undertaken in 2011 and 2012 for Pacific Gas and Electric Company (PG&E) to better define the Shoreline fault zone and to image buried channels that could be used to determine offsets along both the Shoreline and the Hosgri fault zones. This investigation builds upon previous seismic-reflection investigations of the Shoreline fault zone in areas defined by seismicity in the vicinity of PG&E's Diablo Canyon Power Plant (DCPP). These previous investigations were conducted for PG&E in 2009 and 2010 and focused on a microseismicity lineament subparallel to and 1 kilometer (km) west of the coastline that indicated the presence of a previously unidentified fault (Shoreline fault) located approximately 1 km offshore of the DCPP (PG&E, 2012; Hardebeck, 2010). This seismicity lineament was found to comprise two faults in the shallow subsurface; these have been named the Shoreline and Point Buchon fault zones (PG&E, 2011a, 2011b, 2012).

This work is being done by PG&E to comply with the California Energy Commission (CEC) recommendation, as reported in the CEC's November 2008 report titled *An Assessment of California's Nuclear Power Plants: AB 1632 Report*, that PG&E use 3D seismic-reflection mapping and other advanced geophysical techniques to explore fault zones near the DCPP.

For this investigation, detailed three- and two-dimensional (3D/2D) seismic-reflection profile surveys were conducted to determine whether fault offsets of "piercing points" could be imaged and defined for possible slip-rate calculations. These low-energy (~1.5 kilojoules [kJ]) 3D seismic survey areas were located along the southern extensions of the Shoreline fault zone in San Luis Obispo Bay and along segments of the Hosgri fault zone (HFZ) in Estero Bay and the Point Sal offshore areas (Figure 1-1; Plate 1). Evaluation and verification of this report by Professor Stephan Graham can be found in Attachment 1.

1.1 Purpose

The purpose of the 3D LESS was to collect and interpret seismic-reflection data that could be used to determine shallow subsurface relationships between the Shoreline seismicity lineament and crustal faults to refine fault geometry along the various segments of the Shoreline fault zone, and, if possible, to estimate slip rates along the Shoreline and HFZ in the vicinity of the DCPP. The intent was to present these data and interpretations of the structural geometry and morphology in the shallow subsurface for use by the Independent Technical (IT) Team in assessing seismic hazards in the context of a Senior Seismic Hazards Analysis Committee (SSHAC) Level 3 assessment. To accomplish the objectives of this investigation, three different activities took place, as follows:

- Data Collection—High-quality 3D low-energy seismic-reflection profile data were collected for the purpose of imaging seismic stratigraphy that could be interpreted at high resolution and high definition. These data were collected using

state-of-the-art high-precision navigation and high-resolution acoustic sound source, receivers, and recorders.

- Interpretations—The 3D and 2D geophysical data used for this investigation were processed using state-of-the-art signal processing software and interpreted to define and spatially represent the geologic structure and morphology in the shallow subsurface to determine fault geometry and to estimate piercing point offsets and ages that could be used to determine slip rates.

- Technical Report—This Technical Report presents initial geologic and geophysical interpretations of the LESS high-resolution 3D seismic-reflection data (referred to here as the 3D data sets) collected in late 2011 and fall 2012. The intent is for the results of this study to eventually be integrated with more extensive and deeper-penetration 3D seismic-reflection investigations on land, and with the previously reported 3D and 2D investigations offshore of Point Buchon (PG&E, 2012).

1.2 Geologic Background

This section presents a summary of the geologic and tectonic setting of the investigation region to provide a contextual framework for the observations and interpretations made from the newly acquired 3D data sets. The investigation region consists of three 3D survey blocks (Survey Areas 1, 2, and 3) and is located offshore along the coastal margin of the Irish Hills, a west-northwest-trending ridge within the south-central part of the California Coast Ranges, near the city of San Luis Obispo (Figure 1-1; Plate 1).

1.2.1 Tectonic Setting

The central coast of California is characterized by transpressional deformation between the San Andreas fault zone to the east and the San Gregorio–San Simeon–Hosgri fault system of near-coastal faults to the west (Figure 1-2). Transpressional deformation in the region is likely driven by four distinct, but interacting, processes (Lettis et al., 2004):

- A northward left transfer of slip from the San Andreas fault zone to the Rinconada and West Huasna faults to the Hosgri–San Simeon fault zone.

- A past clockwise rotation of the western Transverse Ranges domain (transrotational deformation of Luyendyk, 1991, and Dickinson, 2004a, 2004b) that was mostly completed by the late Miocene or late Pliocene time (Onderdonk, 2005).

- An undetermined amount of plate-normal convergence across the region as described by Zoback et al. (1987), Wentworth and Zoback (1989), Ben-Avraham and Zoback (1992), and Townend and Zoback (2001).

- Complex right-lateral slip faulting associated with the HFZ in the vicinity of the DCPP (Hanson et al., 2004; Lettis et al., 2004; Johnson and Watt, 2012; PG&E, 2012, 2013; Willingham et al., 2013).

The regional transform regime initiated approximately 30 million years ago (Ma) when the transform process between the Pacific and North American Plates introduced a component of strike-slip tectonics (Atwater, 1970). An important aspect of strike-slip tectonic settings is the development of "restraining" and "releasing" bends of a strike-slip fault system, as described by Mann (2007). The resulting "wrench" deformation is reflected in modern topography and bathymetry of en echelon linear to lens-shaped ridges and rhomboid basins (Howell et al., 1980).

Transpressional deformation has produced several distinct but interacting crustal domains and tectonic structures (Figure 1-2; PG&E, 1988). The study areas lie within the western margin of the Los Osos domain, a triangular-shaped structural terrane consisting of northwest-striking reverse, oblique, and strike-slip faults that border uplifted blocks and subsiding basins within the domain. Locally, these include the Santa Maria Valley, San Luis/Pismo, and Los Osos structural blocks, from south to north, respectively (Figure 1-2). The Irish Hills form the structural core of the San Luis/Pismo block (Figure 1-2). A sequence of uplifted marine terraces preserved along the western and southern margin of the San Luis Range record late Quaternary uplift of the San Luis/Pismo block at a rate of approximately 0.2 millimeter per year (mm/yr) in the northwest and approximately 0.1 mm/yr in the southeast (Hanson et al., 1994).

Using earthquake focal mechanisms and borehole breakouts as stress indicators, Zoback et al. (1987) show that fault-normal compression and extension occur along faults of the San Andreas transform fault system in Central California. The change in plate convergence that occurred 4 Ma (3.6 Ma, according to Harbert and Cox, 1986) is documented by northwest-trending folds in the Santa Barbara–San Luis Obispo onshore area and similarly oriented Pliocene and younger structures offshore that indicate that the direction of maximum principal stress is N33°E (McCulloch, 1987; McLaren and Savage, 2001).

1.2.2   Faults and Slip Rates

The faults that contribute most to seismic hazard at the DCPP include the Hosgri, Los Osos, Shoreline, Point Buchon, and San Luis Bay fault zones (PG&E, 2011a, 2011b, 2012). This report provides information that may be used to better characterize the HFZ and the Shoreline fault zone, and thereby reduce uncertainties in the source parameters (i.e., fault length and location with respect to DCPP), and to determine slip rates along these faults based on estimated horizontal fault offsets of defined piercing points (features that are offset by a fault or moved apart).

1.2.2.1   The Hosgri Fault Zone

The HFZ is an active transpressional, convergent right-slip fault zone that within the upper 100 m of section is vertical to steeply dipping and associated with earthquakes (McLaren and Savage, 2001; Hanson et al., 2004; Figure 1-3). The fault zone is 1 to 2.5 km wide and made up of fault traces that cut through various stratigraphic horizons, with some that extend to the seafloor and others that are buried beneath surficial sediment.

Regionally, the HFZ is part of the San Andreas system of faults, which consists of numerous fault strands and is the best seismically imaged fault zone in the offshore region (Figure 1-3; Plate 1). The HFZ trends northwest-southeast for 110 km from north of Point Estero, just north of Estero Bay, to a location approximately 5 km northwest of Point Arguello (Willingham et al., 2013; Figure 1-3; Plate 1A). It is considered the southernmost part of the larger 410 km long San Gregorio–San Simeon–Hosgri fault system (Hanson et al., 2004; Dickinson et al., 2005). The Hosgri and San Simeon fault zones are reported to accommodate 1 to 3 mm/yr of right slip along steeply dipping to vertical transpressional faults (Hanson et al., 2004). Within the longer connected fault zone, the reported slip rate increases to the north, accommodating 6 to 8 mm/yr of slip on the San Gregorio fault zone in the Monterey Bay area and northward (Hanson et al., 2004), although more recently, McFarland et al. (2009) reported a creep rate of 0.8 mm/yr for the San Gregorio fault zone along the San Gregorio–Seal Cove segment. In the vicinity of the DCPP, the HFZ is up to 2.5 km wide and is composed of multiple fault traces PG&E, 2012.

The Hosgri–San Simeon fault zone has a reported slip rate of 0.5 to 6 mm/yr, with a preferred rate of 1 to 3 mm/yr (Hall et al., 1994; Hanson and Lettis, 1994; Hanson et al., 2002). Onshore, the San Simeon fault is well expressed geomorphically and clearly displaces late Pleistocene and Holocene deposits at many locations (Johnson and Watt, 2012; PG&E, 2013). Offshore, the HFZ locally produces scarps on the seafloor and along the fault directly west of the Irish Hills, and abruptly truncates the westward extent of the offshore bedrock platform. In addition, individual traces of faults within the HFZ produce linear escarpments in bedrock, which appear to be pressure ridges that rise above the seafloor sediment. In the area where an eastern strand of the HFZ trends toward the San Simeon fault zone, a submerged, buried sand spit shoreface was evaluated for offset by the fault strand, and an estimated slip rate of 1 to 3 mm/yr was calculated (Johnson et al., 2014).

Locally, the HFZ is the most continuous and complex fault zone in the investigation region. Strands of the fault zone exhibit seafloor expression, either as erosional fault-line scarps or as tectonic scarps. Several strands of this fault zone are identified in a recently obtained 3D/2D data set that show "bright spots" (high-amplitude reflectors resulting from a strong seismic velocity contrast) of presumed associated gas pockets (PG&E, 2012), and also appear in USGS 2D seismic-reflection profiles (Sliter et al., 2009). The 3D/2D data set shows that at depths less than 400 m, this fault zone is more complex than previously mapped in that it consists of multiple en echelon strands (PG&E, 1988, 2011b, 2012). This increased complexity is recognized primarily because of the high resolution of the data and narrow processed line spacing of the 3D/2D data (3.125 m for the 3D surveys and 100 m for the 2D surveys).

The local style of faulting changes along strike of the HFZ in the area where the Point Buchon fault zone extends toward the HFZ (Johnson and Watt, 2012; PG&E, 2012). A graben bounded by right-stepping strands of the HFZ in the central part of the investigation region (PG&E, 2012) indicates extensional strike-slip faulting (transtension). A single fault strand characterizes the fault zone offshore of the Point Buchon coastline (Plate 1). Numerous relatively short strands fan out to the southeast

(Plate 1A) and are associated with folds in the south, indicating compressional strike-slip faulting (transpression). Similar morphology and structure is observed along many strike-slip fault systems, and various researchers have proposed different terminology and models of formation of such features (e.g., see discussion in Mann, 2007). Reading (1980) reported that along strike-slip fault systems in general, small-scale alternate zones of extension and compression are typically present and that these zones can occur along the following structures:

- Curved parts of strike-slip faults.
- Braided faults within a strike-slip fault system.
- Side-stepping, en echelon faults.

This pattern has been described for the San Andreas fault system within the investigation region (Kingma, 1958; Quennell, 1958; Crowell, 1974; Dickinson, 2004b).

1.2.2.2   The Shoreline Fault Zone

As characterized in the Shoreline Fault Zone Report (PG&E, 2011b), the Shoreline fault zone is a vertical right-slip fault that has been divided into several segments (Plate 1) based on changes in the geologic and geophysical expression of faulting at the surface and in the shallow subsurface (PG&E, 2011b). The southernmost segment extends into San Luis Obispo Bay, where it bifurcates. Mapping this bifurcation and extension, along with imaging potential buried channel piercing points that cross the faults, was the primary objective of this investigation (Figure 1.3; Plate 1B).

The Shoreline fault zone lies entirely offshore (Figure 1-3; Plate 1), making it difficult to develop direct quantitative estimates for slip rates. Multibeam echosounder (MBES) bathymetric data from previous PG&E investigations (PG&E, 2012, 2013) were thus examined extensively to identify piercing points (i.e., potentially datable geomorphic features such as paleostrandlines or channel thalwegs on both sides of the fault zone that could be used to constrain cumulative slip and slip rate). However, based on vertical offsets of stratigraphic horizons, the authors of the two PG&E reports estimated a slip rate of 0.05–0.6 mm/yr for the Shoreline fault zone (PG&E, 2011b, 2013).

1.2.2.3   The Point Buchon Fault Zone

The Point Buchon fault zone, northwest of the central segment of the Shoreline fault zone, is a northwest-trending fault that disrupts Tertiary strata east of the HFZ and northwest of the central segment of the Shoreline fault zone (Figure 1-3; Plate 1A). Segments of the fault zone, including the south end and the East Branch, were originally mapped as the N40°W fault zone and described in PG&E (2011b). Both the main and East Branch of the Point Buchon fault zone exhibits probable fault-line scarps, which are clearly evident in MBES bathymetric images. To the south, the Point Buchon fault zone may connect to the central segment of the Shoreline fault zone, although no direct connection has been identified in the shallow-penetration 3D/2D data (PG&E, 2012).

A graben is associated with the north end of the Point Buchon fault zone and may be filled with Pleistocene and younger sediment (PG&E, 2012). A north-trending fault (fault

coded 11008 in PG&E, 2012) that may be part of the HFZ truncates this graben at its northwestern boundary and suggests that transtension may occur near the area where the Point Buchon fault zone approaches the HFZ (PG&E, 2012).

1.2.2.4   The Oceano Fault Zone

The Oceano fault zone is one of several reverse faults, including the San Luis Bay, Wilmar Avenue, and Los Berros faults, that are responsible for uplift of the San Luis Range. The Oceano fault zone has previously been mapped beneath the Nipomo Mesa and Santa Maria River Valley on the basis of seismic data, oil well data, and water well data (PG&E, 1988; DWR, 2002), and its location is well constrained onshore.

1.2.3   Folding

The geometry of folding in Tertiary strata near the DCPP indicates a northeast-southwest horizontal direction of maximum shortening (Plate 1). Deformation within the Hosgri and Point Buchon fault zones is predominantly northwest/southeast-oriented and representative of a strike-slip fault system as described for other strike-slip fault systems (see Reading, 1980; Mann, 2007). Minor discontinuous faults generally occur as north- and east-trending sets and are localized within the Tertiary folded section, indicating they are related to the folding stress field and may be influenced by the fault-normal maximum stress compression occurring along the Pacific–North American plate boundary within the San Andreas fault system today (Zoback et al., 1987; Wentworth and Zoback, 1989; Ben-Avraham and Zoback, 1992; Townend and Zoback, 2001). However, locally within the HFZ, the stress field has been shown to be variable and not dominated by fault-normal maximum stress (McLaren and Savage, 2001).

1.2.4   Seismicity and Slip Rates

Seismicity of the region extending from Estero Bay to Point Sal is scattered, with recent earthquakes ranging in magnitude from 0.1 to 4.1, and focal depths restricted to the seismogenic zone ranging to approximately 14 km (Figure 1-3). Scattering of the earthquakes is most prominent within the Irish Hills onshore and within Estero Bay offshore, although at least three northwest-southeast lineaments of epicenters are recognized. A microseismicity lineament of relocated earthquakes (J.L. Hardebeck, pers. comm. to PG&E, 2013) is aligned along the Shoreline fault zone, with one of the larger-magnitude (M ~ 3.5) earthquakes located near the fault zone's previously mapped south end (Plate 1).

Earthquake epicenters are also aligned along the trend of the HFZ in the central and northern part of the region (Figure 1-3). Few earthquakes have been recorded along the southern extent of the HFZ, in the San Luis Obispo Bay area, and along the HFZ–San Simeon trend north of Cambria.

Observing seismicity patterns constructed from data collected between October 1987 and January 1997, McLaren and Savage (2001) state that the HFZ is an important boundary that separates two regions of contrasting styles and orientations of crustal shortening. Most of the microseismicity in the region is concentrated along the HFZ, the Shoreline

fault, and two additional weak northwest-trending seismicity lineaments within Estero Bay (Hardebeck, 2010). North and offshore of Point Sal, a cluster of seismicity near the HFZ-Casmalia fault intersection occurs near the location of the 1980 local magnitude (M_L) 5.1 and 1984 M_L 3.8 Point Sal earthquakes (McLaren and Savage, 2001). Focal mechanisms from these earthquakes show reverse motion along northwest- and west-northwest-trending fault planes, in close agreement with the mapped strike of the Casmalia fault (McLaren and Savage, 2001).

1.2.5   Regional Physiography

Between Piedras Blancas Point in the north and Point Sal in the south, the continental shelf is gently inclined westward and is 5–20 km wide (Figure 1-1; Plate 1). The shelf break is well defined in the northern part of the region and more diffuse in the south; the shelf break is approximately 120–140 m deep (Plate 1). The Estero Bay study area straddles the shelf break; most of the study area includes the outer continental shelf, but the western part of the study area includes the uppermost part of the continental slope (Plate 1A). The San Luis Obispo Bay and Point Sal study areas are located entirely on the continental shelf (Plate 1B). The region occupied by the study sites includes two broad bays: Estero Bay to the northwest of the DCPP and San Luis Obispo Bay to the southeast of the DCPP. The largest streams and rivers onshore of the study areas drain into San Luis Obispo Bay, including the Santa Maria River, Arroyo Grande Creek, and San Luis Obispo Creek (Figure 1-4). Smaller streams drain into the remainder of the investigation region to the north.

1.2.6   Regional Stratigraphy

Basement rocks exposed in the Central California coastal region generally consist of Jurassic to Cretaceous Franciscan Complex rocks (primarily mélange, metavolcanics, ophiolite, and serpentine) faulted against Cretaceous marine arkosic to lithic sandstone. Along the coastline and in the Point Buchon offshore area, Neogene sedimentary sequences unconformably overlie the basement rocks (PG&E, 2012; Figure 1-5).

Geologic mapping reported in PG&E (2011b) shows that the seafloor is underlain by Quaternary marine sediment in a large part of the investigation region. Where this sediment is absent, most of the seafloor is composed of Tertiary strata exposed in stratigraphic sequences from south to north, including Obispo Formation, Monterey Formation, and the Miguelito Member of the Pismo Formation. Basement rock of the Franciscan Complex and Cretaceous sandstone locally underlie northern San Luis Obispo Bay. Offshore of Point Sal, Neogene units include unnamed Pliocene deposits, Sisquoc, Monterey, Point Sal, Obispo, and Lospe Formations, and the Jurassic-age Point Sal ophiolite.

1.2.7   Seismic Stratigraphy

Two major regional seismic stratigraphic horizons and units have been identified in the study areas (PG&E, 2012, 2013):

- Reflections associated with bedrock and basement rocks.

- Reflections associated with unconsolidated Quaternary sediment.

These units are separated by distinct seismic-reflection boundaries that consist of (1) an unconformity on top of bedrock and (2) the seafloor, which are discussed in stratigraphic order below. Stratigraphic columns representing the stratigraphy for the region of investigation were compiled from previous work (PG&E, 2011b; Willingham et al., 2013; Figure 1-5).

1.2.7.1   Basement and Bedrock

Basement rocks of the Franciscan Complex and Tertiary volcanic intrusions within the investigation region produce acoustically transparent, opaque or chaotic seismic reflections, which form an acoustic basement. Overlying the basement rocks are rocks that comprise the Tertiary stratified bedrock that are acoustically highly variable, reflecting the wide range of lithologies present in the investigation region. In contrast to the acoustics of the basement rocks, the Tertiary sedimentary rocks imaged in the seismic-reflection profiles collected in the region exhibit relatively coherent, continuous reflections that are locally deformed by folding and faulting.

Top of Bedrock

Regionally high-amplitude reflections mark the top of the bedrock (PG&E, 2012, 2013). Locally, this unconformity is coincident with the seafloor, which is exhibited in MBES images as areas of rough, irregular seafloor with differentially eroded layers. Overlying reflections locally lap onto or downlap against the bedrock surface (PG&E, 2012, 2013).

Unconsolidated Quaternary Sediment

Offshore, the late Quaternary stratigraphy varies considerably with depth below modern sea level, and the stratigraphic facies have migrated in geographic position along the continental shelf and upper continental slope. Within the investigation region, this variability is reported to be largely due to geographic differences in sediment supply and exposure to wave energy, rise and fall of sea level, and tectonic deformation (PG&E, 2013).

A sequence-stratigraphic model developed from the interpretation of regional USGS 2D seismic-reflection profile data collected in 2008 and 2009 on the continental shelf from Point Sal to Point San Simeon was constructed for PG&E in 2012 (see PG&E, 2013, for a detailed description). This model is based on the recognition that unconformity-bounded sequences within the Quaternary stratigraphy in the investigation region result from Quaternary sea-level fluctuations that repeatedly exposed and submerged the continental shelf. Ages of these key unconformities are estimated based on correlation to well-documented records of Quaternary global eustatic sea-level cycles. A discussion of Quaternary sea-level cycles, the estimated ages of key unconformities, the ages of channel formation, and the associated uncertainties is presented in Section 1.2.8.

1.2.7.2   Modern Seafloor

The modern seafloor consists mostly of Quaternary sediment (PG&E, 2011, 2013; Watt et al., in preparation). The most prominent unconsolidated sediment packages that make up the seafloor are Upper Pleistocene and Holocene sedimentary units and extensive mobile sand sheets that cover much of the central and outer continental shelf. These sand sheets are separated by seafloor rippled scour depressions that are floored by gravels or smooth bedrock surfaces (PG&E, 2012).

Drop cores taken during the PG&E Long Term Seismic Program (LTSP) indicate that offshore of the DCPP, these sediments consist of sand and silty sand with minor amounts of gravel. These sediments become progressively finer-grained offshore (PG&E, 1988). Bedrock locally crops out on the seafloor, with the highest concentrations of bedrock exposures located offshore of Piedras Blancas Point, Cambria, the stretch of coastline from Point Buchon to Point San Luis, and Point Sal.

1.2.8   Global Eustatic Sea-Level Curves

During the Quaternary, the dominant mechanism responsible for sea-level change was the progressive buildup and decay of continental-scale ice sheets in response to Milankovitch cycles (e.g., see Hays et al., 1976). In addition to these global eustatic changes in sea level related to changing ice volumes, local factors related to tectonics and glacial isostatic adjustment (GIA) in response to ice-sheet melting and hydraulic loading of the continental shelves influence the relative sea-level curve and resulting geologic record of geomorphic features at a specific site (e.g., Peltier, 2004). Furthermore, the timing of relative sea-level maxima varies geographically within individual interglacials due to the patterns and rate of isostatic adjustments (Tamisiea and Mitrovica, 2011; Raymo and Mitrovica, 2012). Because of these local factors, geologic markers of relative sea level are required to calibrate global eustatic sea-level highstands and lowstands to specific sites.

Figure 1-6 presents two sea-level curves that document the timing and amplitude (height) of global eustatic sea-level fluctuations for the past 500 thousand years (kyr). One of these curves represents a composite sea-level reconstruction expressed in meters relative to modern sea level (Waelbroeck et al., 2002; Figure 1-6). This reconstruction is based on a continuous record of oxygen isotope ratios from benthic foraminifera ($\delta^{18}O$), a well-documented proxy for sea-level fluctuations, calibrated to sea temperature data and tied to relative sea-level data, such as in situ fossil coral samples, through statistical transfer functions.

The second curve (Figure 1-6), from Lisiecki and Raymo (2005), represents the timing and amplitude of $\delta^{18}O$ fluctuations sampled from 57 globally distributed records of benthic foraminifera and compiled into a single stacked curve. No attempt has been made to separate the contribution of sea temperature or salinity to $\delta^{18}O$ ratios from that of global ice volume in this curve. Instead, this curve has been scaled vertically to match the last glacial maximum (LGM) sea level in order to produce the equivalent change in sea level (Carlson, 2008). This scaling corresponds to a calibration of 0.011 parts per thousand per meter of sea-level change, with 20 percent removed from the total

amplitude of glacial-interglacial isotopic variation to account for temperature effects (Naish and Wilson, 2009). As shown on Figure 1-6, this scaling provides a reasonable approximation of the timing and magnitude of global eustatic sea-level highstands and lowstands over the past 450 kyr, as represented by the Waelbroeck et al. (2002) curve.

The Lisiecki and Raymo (2005) curve provides an opportunity to evaluate earlier sea-level fluctuations, albeit with more uncertainty, because it extends to 5.3 Ma, much longer than the Waelbroeck et al. (2002) record (Figure 1-7). Within this earlier time frame, the temperature and ice volume components of the $\delta^{18}O$ curve have not been calibrated with data from in situ fossil corals. In the absence of independent sea-level records, direct calibration of this stacked record to actual eustatic sea-level changes requires the assumption that the relative contributions of global ice volume and seawater temperature to the isotopic signature were constant throughout the past 5.3 Ma.

1.2.9   Sea-Level Influence on Local Stratigraphy

Several relative sea-level markers exist locally within the three study areas that allow for correlations to global eustatic sea-level curves and that help minimize uncertainties related to the GIA. Relative sea-level highstands are recorded by flights of emergent marine terraces eroded into the flanks of the uplifting mountain range in the investigation region, which were mapped and dated by Hanson et al. (1994). Elevations of marine-terrace shoreline angles corrected for local tectonic uplift rates suggest that relative sea level in the study area during the highstands from marine isotopic stage (MIS) 5 to MIS 9 ranged between approximately –5 m (during MIS 5a) and +6 m (during MIS 5e), relative to modern sea level (Hanson et al., 1994).

1.2.9.1   Late Quaternary Unconformities

The Quaternary stratigraphy of the continental shelf within the investigation region contains relative sea-level records from past sea-level changes (PG&E, 2013). Sea-level lowstand deposits were recognized in Estero Bay as a distinctive wedge-shaped set of clinoforms localized directly beneath the modern shelf break. Similar distinctive clinoform sets buried beneath the outer shelf were interpreted as deposits from older sea-level lowstands (PG&E, 2013). These lowstand deposits underlie and are truncated by pronounced unconformities that were recognized and correlated widely beneath the outer continental shelf. With one exception (H20 of PG&E, 2013), these unconformities were interpreted to represent surfaces of erosion caused by past sea-level transgressions (PG&E, 2013). The ages of these key unconformities were estimated based on correlation to Quaternary global eustatic sea-level cycles. The preferred ages for the unconformities in the study areas are as follows (after PG&E, 2013):

- Unconformity H10 was interpreted as the post-LGM transgressive surface. Its age was estimated to range from approximately 19 thousand years old (19 ka) to 7 ka, generally decreasing in age with decreasing depth below modern sea level.

- Unconformity H20 was interpreted as the base of the most recent lowstand systems tract that formed a prograding wedge at the base of the shelf margin and whose upper limit was restricted to depths at or near the LGM elevation,

distributed west of and up to the shelf break. Its age was estimated to range from approximately 27 to 19 ka.

- Unconformity H30 was interpreted as the transgressive surface developed between the MIS 6 lowstand and the MIS 5e highstand. Its age was estimated to range from approximately 135 to 125 ka. It is distributed well above the shelf break in San Luis Obispo and Estero Bays.

- Unconformity H40 was interpreted as the transgressive surface developed between the MIS 8 lowstand and the MIS 7 highstand, approximately 250–240 ka.

Uncertainties in the ages of the unconformities stem from the possibility that large hiatuses occur in which entire sequences may have been removed by erosion during sea-level fluctuations, or one or more sequences may have been misinterpreted to represent separate sea-level cycles, when they were actually developed during a single sea-level event. Alternative age models were developed to reflect these uncertainties (PG&E, 2013). The preferred age model for unconformities H10, H30, and H40 is supported by the observation that faults in the investigation region typically vertically offset unconformity H30 several times more than they offset unconformity H10, and faults appear to typically offset unconformity H40 several times more than they offset unconformity H30 (PG&E, 2013). In other words, these are growth faults that continued to move during Quaternary sedimentation. A more complete discussion of the rationale for the preferred and alternative age models is presented in the PG&E seismic stratigraphy project report (PG&E, 2013). An illustration of the preferred and alternative sequence-stratigraphic age models for unconformities in the study areas is presented on Figure 1-6.

1.2.9.2　Older Unconformities

A number of deeper, older unconformities mapped in the offshore Santa Maria Basin and along the HFZ by Willingham et al. (2013) have been used to place the stratigraphy of the study areas in context and provide constraints on the ages of piercing points used to assess fault slip rates. These unconformities include the near top of Neogene unconformity (~2.6–1.8 Ma), the early–late Pliocene unconformity (ELP; ~3.5–2.7 Ma), and the top of Miocene unconformity (~5.5–5.1 Ma; Willingham et al., 2013). In the Estero Bay study area, comparison of stratigraphy to the ELP is accomplished by examining stratigraphy and depth in milliseconds of reflections on 2D seismic-reflection profiles that intersect profiles published by Willingham et al. (2013; Section 6.1). In the Point Sal 3D study area, correlation of stratigraphy with these three unconformities is accomplished through well ties using PG&E's deep-penetration legacy archive seismic-reflection data (Section 6.3) and Willingham et al.'s (2013) data.

1.3　Potential Piercing Points

Since a major objective of this investigation is to determine, where possible, the offsets along the fault zones in close proximity to the DCPP that can be used to determine fault offsets, potential piercing points need to be identified. Any structure or feature that is cut by a fault may be a potential piercing point. Such features as channels or shorelines are

considered good piercing points if they are well imaged and exhibit sharp geomorphology. Both buried fluvial and submarine channels and buried shorelines exist in the investigation region and are well imaged in the LESS data sets collected for this investigation. The thalwegs and margins of the channels, and the shoreline angles of the shorelines, can be used as piercing points for the assessment of fault slip rates.

1.3.1 Fluvial Channel Formation (Continental Shelf)

Fluvial or terrestrial formed channels identified in this investigation are primarily located on the continental shelf, generally in bedrock. The thalwegs and margins of these channels are used as piercing points for the assessment of fault slip rates.

Although many piercing points identified in the LESS data sets are fairly well constrained, and offsets along faults can generally be determined within the resolution of the data (~3 m horizontal and ~2 m vertical), dating of the offsets is less constrained, and is dependent on correlations with the global sea-level curves, and, to a lesser extent, on the estimated ages of erosional horizons (unconformities) indentified in the PG&E (2013 sequence-stratigraphy study (Figure 1-6). Estimated ages of channel cutting and filling events for the investigation of the shelf fluvial channels are primarily based on the four lowest sea-level stillstands in the late Quaternary (Waelbroeck et al., 2002): MIS 10, 8b, and 6b, and the LGM at MIS 2; MIS 12 and 16 are lower yet, but based on isotopic data).

In our analysis of the four latest lowstands shown in the Waelbroeck et al. (2002) curve, we attempt to pick candidate ages on the dropping and rising sea-level curves when channel incision could have been initiated and when channel filling could have begun, bracketing a time increment when continuous channel erosion probably took place. We illustrate this technique on Figure 1-8, where points on the three lowest lowstand curves have been selected to indicate when channel cutting and filling began. Locally, timing of channel incision and filling events is dependent on the geographical location and elevation of the channel on the continental shelf or upper slope of the Central California offshore area. The erosional and filling events are time transgressive and regressive, so that our selection of the time points on the curves is general and based on a possible mid-shelf proximity.

1.3.1.1 MIS 10 Lowstand

The earliest and second lowest lowstand that was analyzed occurred approximately 342 ka (MIS 10), at an elevation of approximately –138 m, with a distinct, and fairly rapid, fall and rise of sea level. During this stage, channel incisions could have occurred at or shortly after approximately 350 ka (Figure 1-8a), and continued eroding until approximately 358 ka (Figure 1-8b). Channel filling could have started approximately 335 ka or before (Figure 1-8c). The probable maximum duration of channel erosion events is approximately 12 kyr, with the peak of thalweg erosion and deepening being approximately 342 ka (see Figure 1-8a).

1.3.1.2   MIS 8b Lowstand

The next earliest lowstand (MIS 8b) that was analyzed occurred approximately 250 ka, at an elevation of approximately –120 m. This lowstand was considerably higher in elevation than the other late Quaternary lowstands discussed here, and channel incisions would not have been as deep as those produced during the other lowstand stages. Consequently, channels formed during this stage may not have survived later erosion, unless, however, they were reoccupied and deepened during the later lowstands.

Channel incisions during MIS 8b could have begun when sea levels dropped below approximately 100 m elevation at or shortly after approximately 255 ka, continuing to erode until approximately 250 ka, when sea level began to rise, but cutting could have continued for a few thousand more years. Channel fill could have begun shortly after sea level started to rise approximately 250 ka (or possibly 245 ka), with significant channel filling occurring from approximately 245 ka and later. The peak thalweg construction would have been approximately 250 ka, with a possible maximum duration for channel erosion of approximately 8–10 kyr.

This stage has provisionally been correlated with the formation of the H40 erosional surface reported in PG&E (2013), although ages as old as MIS 16 (650 ka) are allowed. It was estimated that this horizon ranges in age from approximately 250 to 240 ka, during which time many channels may have been incised into the exposed continental shelf (see Figure 1-7).

1.3.1.3   MIS 6b Lowstand

The second youngest lowstand (MIS 6b) is a double low, with the first lowstand occurring approximately 150 ka, at an elevation of approximately –130 m, and the second occurring approximately 138 ka, at an elevation of approximately –142 m (Figure 1-8d). The second MIS 6b low represents the lowest of the four lowstands discussed here (see Figure 1-6). This lowstand doublet allowed for two generations of channel cutting and filling, or filling and exhumation, or lengthy continuous erosion, depending on the geographical location and elevation of the channels on the continental shelf (Figure 1-8e). Initial channel incisions could have occurred approximately 156 ka, with peak thalweg incision approximately 138 ka (Figure 1-8e). Channel filling would have begun sometime after approximately 135 ka, and perhaps as late as 132 ka (Figure 1-8f).

MIS 6B lowstand and intervening fluctuation in sea level during this stage provided the longest time duration for channel cutting and filling of any of the four late Quaternary lowstands we show on Figure 1-8, with a range in age from approximately 156 to 132 ka, an approximately 24 kyr time period. This is approximately twice as much time available for channel formation as that estimated for the other three lowstands.

This stage has provisionally been correlated with the H30 erosional surface reported in the PG&E (2013) sequence-stratigraphy study, although older ages are allowed. It was estimated that this horizon ranges in age from approximately 135 to 125 ka, or during the lowest lowstand of this stage (MIS 6b on Figure 1-6).

1.3.1.4   LGM Lowstand (MIS 2)

The most recent (youngest) lowstand occurred approximately 19 ka, at an elevation of approximately –123 m (Figure 1-6). Channel incisions could have begun approximately 28 ka and continued to approximately 15 ka (Figure 1-8g). Peak thalweg erosion would have been around 19 ka (Figure 1-8h). Channel filling could have started shortly after approximately 15 ka and continued until approximately 10 ka (Figure 1-8i). The approximate duration of this channel incision event is approximately 13 kyr, and channel infilling likely took place over several thousand years during the major post-glacial rise in sea level. Holocene transgressive nearshore and coastal floodplain marine deposits locally overlie MIS 2 channel fill deposits in many areas on the Central California continental shelf.

Both the H20 and H10 erosional surfaces described in the PG&E sequence-stratigraphy report (2013) appear to be associated with this lowstand stage. The estimated age range of H20 is 27–19 ka and that of H10 is 19–7 ka, which places the erosion of these surfaces at the peak of lowstand and beginning of sea-level rise (Figure 1-6).

1.3.2   Submarine Channel Formation (Continental Slope)

Submarine channels are common on the upper continental slope. These may range from slope gullies or rills that measure less than a few hundred meters across (e.g., Pratson et al., 1994; Greene et al., 2002;Surpless et al., 2009) to deep, wide canyons that measure several kilometers across. Slope gullies are common features on the upper continental slopes, occurring on sediment-laden inclined surfaces, such as delta fronts (e.g., Chiocci and Normark, 1992), as well as on slopes not associated with fluvial processes (e.g., Gardner et al., 2003; Dartnell and Gardner, 2008). Pratson et al. (1994) defined rills on intercanyon divides of the upper continental slope (250–500 m deep) off New Jersey as narrow (20–300 m wide) shallow (20–40 m deep) downward-trending features that merge with troughs and result from downslope sediment flow. These features fit the range of scales summarized by Surpless et al. (2009) for "submarine gullies," ranging from approximately 75 to 600 m wide and from 1 to 30 m relief and forming in water depths from approximately140 to 560 m. Although no consensus term has been adopted in the literature to describe these features, the choice of "submarine gully" to describe features too small to be called channels or canyons in this report follows the usage of Surpless et al. (2009).

In the Santa Barbara Channel, a modern-day analog of slope gullies is well imaged in the MBES data (Greene et al., 2002) and is used in this study to define buried slope channels. These channels are located along the northern flank of the Santa Barbara Basin and originated by several different processes, including subsurface fluid flow (submarine rilling), retrogressive slumping, cross-shelf sediment transport, and shelf-edge delta failures. The channels are ephemeral and vary from being filled to being exhumed. These processes make it difficult to correlate channels from the shelf to the slope.

1.3.2.1   Nested Channels

Within the Central California offshore region, various channels and channel complexes, or nested channels, are present. In this investigation, nested channels refer to channel complexes that consist of smaller channels incised into the fill of a larger incised channel (Figure 1-9). Such a channel complex represents multiple generations of channel cutting and fill that has taken place in one geographic location, such as along the upper continental shelf or inner continental shelf near a fairly continuous sediment source. On Figure 1-9, four, and possibly five, smaller channels are incised into a larger channel and may represent channel erosion that occurred during one stage of sea-level stillstand or during multiple stages of stillstands. While nested channels are common submarine features, similar types of nested channels can form in the terrestrial environment within large, wide river valleys; however, the nested channels observed offshore in the investigation region appear to be submarine features, based on their depth, geographic location, and internal stratigraphy, such as the existence of inner-bend benches as described by Maier et al. (2012).

1.3.3   Paleoshorelines

Previous studies in the investigation region have identified paleoshorelines on the seafloor and in bedrock buried beneath a cover of sediment (PG&E, 2011a, 2012, 2013). Many of these features cross faults and qualify as good potential piercing points if well preserved and imaged. The significance of using paleoshorelines as piercing points is that they can be readily correlated with sea-level lowstands, and ages of formation can be obtained from the sea-level curves discussed above.

1.4   Previously Collected Data

In addition to the reports and information discussed above, specific data sets were accessed to aid in the interpretation of the newly acquired 3D LESS data. These data sets consist of previously collected MBES bathymetry, USGS single-channel shallow-penetration sub-bottom seismic-reflection profiles, PG&E legacy archive deep-penetration high-energy sub-bottom seismic-reflection profiles, magnetic anomaly data, and well-hole data. These data sets are described briefly below, but more details can be found in Fugro Consultants, Inc. (2012a-f, 2013a-e), PG&E (2011, 2012, 2013), and Willingham et al. (2013).

1.4.1   Multibeam Echosounder Data (Seafloor Images)

The seafloor is a distinctly recognizable feature in all three 3D data sets and easily correlated to the MBES data collected previously by PG&E (2011, 2012) and collected recently for PG&E by the USGS. The seafloor horizon was mapped as the first high-amplitude reflector encountered directly beneath the water bottom (PG&E, 2012; this report). Vertical bathymetric relief of the seafloor horizon (as mapped) is commonly associated with two geomorphic features: the rugged bedrock at the seafloor and the margins of mobile sand sheets (well imaged in MBES data; Plate 1).

1.4.2   USGS Seismic-Reflection Profile Data (Shallow Sub-bottom)

Single-channel seismic-reflection-profile data were acquired in 2008 and 2009 by the USGS between Piedras Blancas and Pismo Beach from the R/V *Parke Snavely* using a SIG 2Mille mini-sparker and an EdgeTech SB-0512i™ chirp system. Data were collected along shore-perpendicular transects spaced 800 m apart extending beyond the 3-mile limit of California State territorial waters. Figure 1-10 and Plate 1 show the USGS lines available for this investigation and used in other PG&E reports (2011, 2012, 2013). Additional information regarding data collection of the USGS seismic-reflection profiles, processing, and reprocessing can be obtained from PG&E reports (PG&E, 2011, 2013).

1.4.3   PG&E Legacy Archive Data (Deep Sub-bottom)

Many deep-penetration sub-bottom seismic-reflection profiles located in PG&E's legacy data archives that had been collected in the study areas were used to supplement interpretation of the 3D LESS data and extend the geometry of faults to depths not reachable by the shallow-penetration LESS data. In 1983, PG&E began the LTSP and commissioned a multichannel seismic-reflection survey in California State waters from north of the Piedras Blancas antiform to south of the DCPP. This 1986 survey was one of the last high-energy surveys permitted in California State waters and these data are archived for use in projects such as this LESS investigation. For the LTSP, PG&E also purchased additional exploration survey seismic-reflection profiles collected in this same general area between Point San Simeon and the DCPP. These lines were primarily from the Western Geophysical surveys undertaken in 1974, 1975, and 1982. The interpretation of these new data sets was integrated with the previous PG&E data from the 1970s and presented in the LTSP documentation (PG&E, 1988, 1990). Many of these legacy archive data were included in the study by Willingham et al. (2013).

1.4.4   Magnetic Anomaly Data

The magnetic field within the study area was measured in several surveys to help identify rock units and structures with distinct magnetic signatures (Figure 1-11). Magnetic anomaly data recently acquired by the USGS include an overland fixed-wing aerial magnetic survey and a marine magnetic survey with ship-line spacing at 400 m (see PG&E, 2011b, for details). These surveys were supplemented by a high-resolution helicopter magnetic survey across the Irish Hills coastline at 150 feet above the ground's surface to better define magnetic anomalies associated with the Shoreline fault zone and to gain detailed data in a data gap area between the onshore and offshore measurements (see Appendices B and F of PG&E, 2011b).

1.4.5   Borehole Data

An increase in the level of petroleum exploration in the offshore Santa Maria Basin between 1977 and 1984 resulted in the acquisition of high-quality common-depth-point (CDP) seismic-reflection data and the drilling of more than 50 wells between Point Conception and a point 15 km north of Point Sal (Figure 1-10). Seven of these exploratory wells were used in this study to date seismic-reflection horizons that extend

into the Estero Bay and Point Sal survey areas. Well-log descriptions relate primarily to the late Quaternary and Tertiary strata, and thus do not provide ages for the Upper Pleistocene and Holocene sedimentary units. Further description of these borehole data can be found in the studies reported by Willingham et al. (2013) and Sorlien et al. (1995).

1.5 Study Areas

Three study areas are located offshore of the DCPP, as shown on Figure 1-1 and Plates 1A and 1B and reported in Fugro Consultants, Inc. (2012d, 2013a-e):

- To the north in Estero Bay (Survey Area 1).
- To the south in San Luis Obispo Bay (Survey Area 2).
- Farther to the south off Point Sal (Survey Area 3).

Reconnaissance 2D survey transects of all three survey areas were made before initiating 3D survey operations. The purposes of the 2D reconnaissance lines were to identify high-priority target areas for 3D surveys and refine the limits of the 3D survey areas.

The Estero Bay 3D survey is located within a larger area where 2D reconnaissance lines also were collected (Figure 1-1; Plate 1). In this area, 174.1 km of sail-line (the survey vessel's trackline, along which data are acquired) of survey data were collected. The 3D survey block consists of 1.8 square kilometers (km^2) of 3D binned data resulting in a grid pattern with lines oriented northwest-southeast (333.7°/153.7°; Figure 1-10; Plate 1).

The 2012 San Luis Obispo Bay survey was an extension of the high-resolution low-energy 3D survey conducted in 2011 (Fugro Consultants, 2012a). For both the 2011 and 2012 3D surveys, the bin spacing was 3.125 by 3.125 m. A total of 315.5 sail-line km of survey data were acquired during the 2012 survey operations, with the lines oriented northeast-southwest (034.8°/214.8°). The full-fold survey area was 12.474 km^2. Once the 2011 and 2012 surveys were merged, the total 3D survey area was increased to 27.617 km^2 (Figures 1-1 and 1-10; Plate 1; Fugro Consultants, 2013a).

The Point Sal 3D survey block covers a rectangular area of 13.7 km^2 (Figure 1-10; Plate 1). Several 2D tie lines that connect the Estero Bay and Point Sal survey areas were used to correlate the stratigraphy of the areas with one another.

The 3D survey blocks cover the southern part of the HFZ and Los Osos fault zone intersection in Estero Bay, the southern extension of the Shoreline fault zone in San Luis Obispo Bay, and the southern part of the HFZ off Point Sal. In Estero Bay, the survey block is located in an area where bedrock ridges were previously mapped trending into the eastern margin of the HFZ (PG&E, 1988). The survey coverage of San Luis Obispo Bay is located south of the microseismicity lineament mapped by Hardebeck (2010) and where the southern segment of the Shoreline fault zone was recently imaged (PG&E, 2012), in a region of channel incisions in shallowly buried bedrock. Off Point Sal, the survey area straddles the two major HFZ segments in a region of flat sediment-covered bedrock that is deeply incised by channels (PG&E, 1988; Johnson and Watt, 2012).

1.6   Intended Use of Results

The interpretations of the 3D/2D data will be used by PG&E in its ongoing efforts to characterize seismic hazards at the DCPP. The results of this technical data report will be further evaluated and integrated with interpretations of other data sets, including seismicity surveys, seismic-reflection surveys (both onshore and offshore), potential field (gravity and magnetic) surveys, and geologic and geomorphic mapping onshore. The data inputs and the final report will be provided to the DCPP SSHAC Seismic Source Characterization Technical Integration (SSC TI) team for seismic hazard analysis, and to the California Public Utility Commission's Independent Peer Review Panel (IPRP) for evaluation and comment. Inputs include interpretation and mapping results, estimated offset of piercing points and probable slip rates, and fault geometries for determining overall fault length and connectivity.

2.0   NEW DATA

The primary data interpreted for this report consist of 3D seismic-reflection profile data collected by Fugro Consultants in late 2011 and 2012 and the resultant 3D volumes and cross sections. The data collection procedures and processing are described in the following reports:

- Fugro Consultants (2012a through f)
- Fugro Consultants (2013a through e)

The Fugro reports and data, including the 3D and 2D data SEG-Y files, reside in the PG&E Geosciences offices in San Francisco, California.

A limited number of seismic-reflection profiles were also used from other previous surveys available in PG&E's legacy data archive and from the USGS (Figure 1-10). These data (Table 2-1) were interpreted to reveal the shallow geology in parts of the Estero Bay, San Luis Obispo Bay, and offshore Point Sal areas and are described in Sections 6.0 and 7.0 below. The data acquisition and processing parameters for the most recent (2011–2012) Fugro 3D/2D surveys are summarized in Section 2.2 of this report and are described in more detail in other reports (Fugro Consultants, 2012d,e; 2013a,b,c,d,e).

Table 2-1. Summary of Marine Seismic Surveys Used in This Investigation

Survey	Year	Near-Seafloor Resolution	Source	Data Type	Estimated Vertical Resolution
Aquatronics	1974	Medium	Sparker	2D	~5 m
GSI	1980	Low	Airgun	2D	~15 m
Nekton	1983-1984	Low	Airgun	2D	~15 m
CoMAP	1986	Low	Airgun	2D	~15 m
Digicon	1986	Low	Airgun	2D	~15 m
PG&E/FLEC	1986	Very Low	Airgun	2D	~50 m
Fugro	2010	High	Boomer	2D	~2-3 m
Fugro	2011	High	Boomer	2D/3D	~2 m
Fugro	2012	High	Boomer	2D/3D	~2 m
USGS S-6-08-SC	2008	High	Mini-sparker	2D	~1 m
USGS S-6-09-SC	2009	High	Mini-sparker	2D	~1 m

Electronic copies of previous Fugro data acquisition reports and seismic data, including the 2D and 3D seismic-reflection profile SEG-Y files, currently reside in the PG&E Geosciences offices in San Francisco, California, at Lettis Consultants International, Inc., in Walnut Creek, California, and at the Fugro Consultants, Inc., offices in Ventura, California.

2.1   Data Acquisition

The data used in this study were acquired over a period of two years using standard industry procedures with a low-powered sound source. Low-energy (1.5 kJ), high-resolution (100–700 hertz [Hz] frequency range with a 200–225 Hz fundamental frequency) seismic-reflection profiling systems were used to collect the data (PG&E, 2012). In the San Luis Obispo Bay study area (Survey Area 2), the data were collected between 6 December and 23 December 2011 and August 22 through October 5, 2012, and in the Estero Bay and Point Sal study areas, the data were collected between 22 August and 5 October 2012, with all surveys using a triple-plate boomer as the acoustical source and P-Cable hydrophone streamers as the acoustical signal receiver (Figure 2-1).

The major components of the 3D multichannel data acquisition system were the digital recording system (CNT-2 Controller), 12 or 14 P-Cable-configured streamers of hydrophones, CSP-D power supplies, and a triple-plate boomer seismic energy source (Table 2-2). The GeoEel™ solid digital streamer components, P-Cable, and CNT-2 Controller were supplied by Geometrics of San Jose, California, and the triple-plate boomer seismic source was supplied by Subsea Systems, Inc., of Ventura, California. The streamers were connected to a single P-Cable that was pulled taut from each end by port and starboard paravanes (Figure 2-2). Data were transmitted back to the ship via a signal cable that connected to the P-Cable near the starboard paravane (see Nishenko et al., 2013).

Table 2-2. Fugro 2011-2012 3D Seismic Acquisition Parameters

Number of streamers	12 or 14
Streamer length	50 m
Channels per streamer	8
Group interval	6.25 m
Streamer type	Geometrics GeoEel Solid Digital
3D swath width	37.5 or 43.75 m
Bin size	3.125 m x 3.125 m
Nominal subsurface fold	8
Sample rate	0.250 ms
Record length	0.75 s
Recording format	SEG-D
Source type	AP3000 Boomer
Number of plates	3 (2 active)
Power per boomer plate	625–875 joules
Frequency spectrum	100–800 Hz
Shot interval	3.125 m

The 3D navigation binning system was provided by NCS SubSea, Inc., of Stafford, Texas. Streamer separation on the P-Cable was 6.25 m, and each streamer consisted of eight active channels with a group interval of 6.25 m (Table 2-2). This allowed for tight control of bin spacing by using individual channels or summation of adjacent channels to increase the signal-to-noise ratio. With this configuration, a total of 96 channels (12 streamers) or 112 channels (14 streamers) of data were acquired at a sampling rate of 250 microseconds and a record length of 750 milliseconds (ms). The streamer configuration used in this investigation provided a Nyquist frequency of 2 kilohertz, which was more than sufficient to capture the frequency bandwidth associated with the triple-plate boomer seismic source. All survey navigation data are reported in the Universal Transverse Mercator (UTM) coordinate system, Zone 10N, measured in meters on a World Geodetic System of 1984 (WGS 84) ellipsoid. Survey sail-lines for 3D data collection in all three surveyed areas used a trackline spacing of 37.5 m. Measured water depths in the San Luis Obispo Bay and Point Sal survey areas ranged from 25.7 to 49.9 m and from 52.4 to 120.3 m, respectively, and in Estero Bay the water depth ranged from 86.31 to 104.26 m.

The 3D swath width of this spread was 37.5 m or 43.75 m, depending on the number of streamers deployed. The source to receiver offset varied, but maintained a minimum offset of 20 m. The vessel trackline spacing for the survey was 37.5 m. Shot spacing was at 3.125 m, with a CDP interval of 3.125 m, a 0.25 ms sample rate, and a 0.75-second (s) record length (Figure 2-1; Table 2-2). Due to the similarity of the sound source and digital recording systems used in the 2011 and 2012 seismic surveys, the vertical resolution for all the seismic data is estimated to be 2 m.

A measured dominant frequency of 200 Hz (Figure 2-2) and assumed velocity of 1,600 m/s results in an estimated vertical resolution of 2 m. The assumed velocity is based on seismic velocity determinations of Willingham et al. (2013) and was used in processing of these data, as well as in previous PG&E reports (see PG&E, 2012, 2013; and Section 4.0 below). Vertical resolution can be approximated by the following equation:

$$VR = TT = 0.25\lambda \text{ (of dominant frequency)}$$

where VR = vertical resolution, TT = tuning thickness, and λ = wavelength.

For the 2011 and 2012 surveys, the boomer plates were towed in a sled with the source located 0.3 m beneath the sea surface (Fugro Consultants, 2012a, 2013a). For the 2010–2011 surveys the seismic source was fired on distance (every 3.25 m), and with a group interval of 6.5 m and eight channels per streamer, thus provides for eight-fold acquisition geometry by shooting full-fold (800% CDP coverage) using a shot spacing half of the group spacing (Fugro Consultants, 2012a, 2012b). Calculations for fold are as follows (Sheriff and Geldart, 1995):

Fold = (geophone spacing * number of active channels) / (2 * shot spacing)

Fold = (6.5 * 8) / (2 * 3.25)

Fold = (52) / (6.5)

Fold = 8

2.1.1   2011 Survey

In 2011, 3D high-resolution seismic-reflection profile data were collected using an ultra-high-resolution multichannel seismic-reflection P-Cable system deployed from the M/V *Bluefin*. The P-Cable system configured for this survey consisted of 14 eight-channel hydrophone streamers (Figure 2-1). Survey operations in the winter of 2011 covered an area totaling approximately 19 km^2 in the San Luis Obispo Bay (Survey Area 2) area (Figures 1-1 and 1-10). Data were collected along a predefined survey grid with lines oriented northeast-southwest (034.8°/214.8°) and spaced 37.5 m apart (Table 2-2). Over the course of the seismic survey, a total of 589.9 sail-line km of data were collected. In addition, 18.7 sail-line km of data were collected for data quality assurance and validation purposes in addition to previously acquired 2D data seismic-reflection lines. Water depths in the survey area ranged from 20 to 60 m.

2.1.2   2012 Survey

In 2012, the P-Cable system was deployed from the M/V *Pacific Star*. The configuration of the P-Cable system for this survey consisted of 14 eight-channel streamers (Figure 2-1). A total of 1,130 sail-line km (15,820 surface-line km) of seismic-reflection data were collected. Data collection in Estero Bay encompassed 174.1 sail-line km of data. A total of 1.8 km^2 of 3D binned data resulted from a grid pattern designed with lines oriented northwest-southeast (333.7°/153.7°; Figure 1-10). Data collected in south San Luis Obispo Bay consisted of 315.5 sail-line km of data, with 11.2 km^2 of 3D data coverage following a grid pattern with lines oriented northeast-southwest (034.8°/214.8°; Figure 1-10). The survey area offshore of Point Sal included 141 sail-line km of 2D data and 13.7 km^2 of 3D data following a grid pattern designed with lines oriented northwest-southeast (338°/158°; Figure 1-10; Plate 1).

2.2   Data Processing and Quality Control

The 2D data for Estero Bay, San Luis Obispo Bay, and Point Sal were processed by Fugro Consultants, Inc., in Ventura, California (Fugro Consultants, 2013a). The 3D data for these areas were processed by FSI/CGG in Houston, Texas (Fugro Consultants, 2012e; 2013b,c,d). Fugro Seismic Imaging processed the 3D P-Cable data collected in San Luis Obispo Bay in 2011 (Fugro Consultants, 2012e). New 3D data collected for San Luis Obispo Bay in 2012 were processed by FSI/CGG and merged with the 2011 data (Fugro Consultants, 2013b).

2.2.1   Processing of 2D Reconnaisance Data

The 2D data processing sequence was designed by Fugro Consultants to maximize the usable amount of data in the shallow subsurface between the seafloor and the first seafloor multiple. This was accomplished by using a series of frequency filters, a static correction to compensate for sea state variations during data acquisition, and predictive deconvolution to shape the wavelet of the boomer pulse. A processing flow chart showing the complete 2D high-resolution seismic data processing sequence is shown on Figure 2-3 (Fugro Consultants, 2013a).

2.2.2 Processing of 3D Data

The UNISEIS software was used in processing the 3D data. This software was validated (Fugro Consultants, 2012b) for use in the processing of seismic-reflection profile data for the Central Coastal California Seismic Imaging Project prior to processing the 2012 3D P-Cable survey data.

The 3D data processing was performed in accordance with Fugro Seismic Imaging's Seismic Data Processing Procedure (Project Instruction PI-09; Fugro Consultants, 2011) and Work Instructions issued by Fugro Consultants and developed in conjunction with PG&E requirements. These documents detail the quality control steps that Fugro Seismic Imaging followed during data processing operations (Figure 2-4). At each processing stage, the output data and log files were compared to ensure that the processing algorithms were properly applied to the seismic-reflection data. Quality control checks were recorded in the Fugro Seismic Imaging project file.

Velocity analysis was also performed with Fugro Seismic Imaging's proprietary analysis software package in UNISEIS (Fugro Seismic Imaging, 2012b); for this report, depth is reported in two-way travel time (TWTT) in seconds on seismic-reflection profiles and milliseconds in 3D volume time slices, with sea surface being zero; however, tides ranged from +2.1 to –0.5 m during the surveys, which was determined by the tidal cycles recorded by the National Oceanic and Atmospheric Administration (NOAA) at Port San Luis. Tidal corrections were made to the 3D data during data processing to account for these tidal fluctuations.

The seismic stratigraphy immediately beneath the seafloor is masked by the "bubble pulse," the train of seismic energy produced by the sound source and exhibited in seismic-reflection profiles as a series of closely spaced artifact reflectors. Even though deconvolution processing was applied to the data, this masking by the bubble pulse prevented complete resolution of weak legitimate reflections parallel to the seafloor for approximately 5 ms (~4 m TWTT), using a velocity of 1,600 m/s beneath the seafloor reflection.

2.2.3 Quality Control

The acquisition and processing of the 2011–2012 3D/2D data analyzed in this investigation, as well as the validation of the 3D and 2D processing and interpretation software, were performed under the Fugro Consultants Nuclear Quality Assurance (NQA), which meets the requirements of 10 CFR 50, Appendix A, "Quality Assurance Criteria for Nuclear Power Plants and Fuel Reprocessing Plants," NQA-1, and 10 CFR 21, "Reporting of Defects and Non-compliance." This Technical Report, which interprets the data results, has been written, reviewed, and approved under the PG&E Geosciences NQA program following Geosciences procedure CF3.GE2, "Quality Related Technical Reports." An independent technical review of the report, including inputs and assumptions, was performed by Professor Stephan Graham (under PG&E's CF3.GE2 and NQA-1-2008, Part 3, Sub-paragraph 3.3, Appendix 3.1, "Guidance for Qualification of Existing Data"). Professor Graham's review is documented in the Verification Summary with review comments, and corresponding resolutions in Attachment 1 of this report.

Because Dr. Graham is an independent consultant, a Quality Verification Plan to document his responsibilities is tracked in PG&E's tracking system in Notification 50427212.

Section 10.0 of this report addresses the limitations on the use of the reported results and conclusions presented herein.

2.2.4   Seismic Attributes

Seismic attribute (i.e., derivative) volumes were derived from the time-amplitude 3D data sets using the IHS Kingdom Suite Rock Solid Attributes (RSA) software package. Seismic attributes provide information relating to the amplitude, shape, and/or position of the seismic waveform, which is then compared to similar adjacent waveforms of adjoining traces. Seismic attributes may reveal features or patterns that otherwise might not be apparent in the seismic amplitude volume. For example, the similarity time slice, or derivative, maps show subtle structural features that may not be observable on the amplitude time-slice maps. Derivative maps used in this investigation consist of amplitude and similarity time-slice maps.

2.2.4.1   Tested Attributes

In an effort to derive as much geologic information as possible from the LESS 3D data sets, PG&E and Fugro Consultants held a workshop on 22 March 2013 in Ventura, California, to investigate those attributes that would complement the processed seismic amplitude data. Five geometric attributes were tested:

- Similarity
- Smoothed similarity
- Similarity variance
- Dip of maximum similarity
- Smoothed dip of maximum similarity

Two instantaneous attributes were also generated:

- Trace envelope
- Envelope second derivative

The attribute volumes were evaluated based on the review comments of two IPRP members regarding applicability to paleochannel and fault interpretation. Smoothed similarity and smoothed dip of maximum similarity were identified in the workshop as being the most useful geometric attributes for fault characterization, while 2D trace envelope was found to complement the 2D seismic amplitude profiles for paleochannel margin interpretation.

2.2.4.2   Selected Attributes

The parameters used for the selected attributes are shown in Table 2-3. The smoothed similarity attribute measures the filtered trace-to-trace agreement of the recorded seismic waveform over a user-specified correlation window, initially set to 10 ms (5 ms above

and below each recorded event). Within a 3D volume, areas of flat or laterally continuous reflections (bedding) manifest as zones of strong similarity, while localized discontinuities such as faults and paleochannel margins manifest as zones lacking any trace-to-trace similarity.

Table 2-3. 3D Seismic Data Attribute Parameters

Bandpass		Dip Scan	
Low cut frequency	200 Hz	Number of traces	3
Low cut slope	12 dB/octave	Max dip	0.016 s/ trace
High cut frequency	500 Hz	Dip scan increment	0.002 s/ trace
High cut slope	24 dB/octave		
Similarity		Variance	
Time window	0.01–0.005 s	Time window	0.005 s

In December 2013, the smoothed similarity attribute was tested further to optimize imaging of paleochannel fill deposits and was found to provide much clearer evidence of possible fault offset. This optimized smoothed similarity attribute was derived using a 5 ms comparison window (2.5 ms above and below each recorded event), which allowed for the attribute to be extracted within the 2 to 3 m vertical resolution of the 3D data set, and correlates with IHS Kingdom's suggested window of 20 points, which is 5 ms for these 0.25 ms sample rate data). The parameters used for the smoothed similarity and smoothed dip of maximum similarity attributes are shown in Table 2-3.

Smoothed similarity was primarily plotted on a horizontal time slice or in 3D VuPAK space, because a 2D similarity profile was not often sufficient to capture the significance of the calculated similarity values. The similarity attribute was extracted through the entire recorded section for each of the three data volumes. Comparison of an amplitude and similarity time slice is shown on Figure 2-5.

The smoothed dip of maximum similarity attribute is a measure of the instantaneous trace-to-trace dip angle of maximum agreement of the recorded seismic waveform over a user-specified correlation window. Within a 3D volume, areas of flat or laterally continuous bedding manifest as zones of very low dips, while localized discontinuities, such as faults and paleochannel margins, manifest as zones of very high dip angles. Dip of maximum similarity was primarily plotted on a horizontal time slice or in 3D VuPAK space, as a 2D profile was not often sufficient to capture the significance of the calculated dip similarity values. Comparison of an amplitude and dip of maximum similarity time slice is shown on Figure 2-6.

Attributes for the 3D post-stack time migrated volumes were run using IHS Kingdom, Version 8.6 Hotfix 4 with the RSA add-on module. The parameters used for attribute generation are listed in Table 2-3.

3.0 METHODOLOGY

This section describes the methodology used to interpret the 3D/2D seismic-reflection profile data. The extent of data collection is shown on Figure 1-1 and Plate 1 and described in Section 2.1 above. The post-processed 3D/2D data extend vertically to approximately 500 ms or 0.50 s (~400 m), with better imaging (interpretability) generally in the upper 350 ms or 0.035 s (~280 m) to 100 ms or 0.10 s (~80 m) of the imaged section.

3.1 Interpretation Teams

The interpretation of the 3D/2D data was conducted using a team-based approach. The term "interpretation," as used in the analysis and presented in this Technical Report, means that the visual observations and recognition of features or acoustic signals (reflections) in the 3D/2D data set, assisted by PG&E QA/QC vetted software to interpret 3D/2D seismic-reflection profile data, were used to map stratigraphic layers, geologic structures, and piercing points. Two different teams were established, one with Lettis Consultants International (LCI) and the other with Fugro Consultants (FCL). The LCI team focused on the Estero Bay study area (Survey Area 1), while the FCL team focused on the San Luis Obispo Bay and the Point Sal study areas (Survey Areas 2 and 3). The teams operated in independent locations but achieved continuous project synergy through periodic meetings during the interpretation process. The teams contributed to report production by writing their respective chapters of the results and discussions in the text and providing corresponding figures and plates.

The individuals heading the interpretation teams are listed below with their principal roles:

- Technical Coordinator—Dr. Stuart Nishenko (PG&E)
- Interpretation (Lead Coordinator) and Technical Report preparer—Dr. H. Gary Greene (Moss Landing Marine Laboratories)
- Interpretation—Dr. Phil Hogan (FCL)
- Interpretation—Hans AbramsonWard, CEG (LCI)
- Technical Advisor—Justin Pearce, CEG (FCL)
- Independent Technical Reviewer—Professor Stephan Graham (Stanford University)

The full team structure is shown in Table 3-1.

3.1.1 Data Interpretation

The methodology that the interpretation teams used to interpret data was consistent with the geological and geophysical interpretation of seismic-reflection data outlined by Sheriff (1982), Yilmaz (2001), and Brown (2004). The methodology used to map features to provide fault offsets and determine slip rates (critical elements for a seismic hazard analysis) is as follows:

- Define and map selected stratigraphic layers (horizons), which are either locally relevant or laterally extensive within the 3D/2D data sets, including stratigraphic unconformities where present.

- Define and map structural features, including faults, folds, and/or acoustical anomalies.

- Correlate faults between 2D inlines and crosslines, and selectively use arbitrary slices through the 3D volume to confirm fault orientation and trends.

- Define and map channel margins and thalweg axes and distinguish channel fill sediment type and erosional/transport processes (e.g., braided, meandering, deeply incised), and use time slices to confirm orientation.

- Define and map shorelines that cross faults.

Table 3-1. PG&E 3D LESS Interpretation Team Structure

Study Area	Role	Team Member
Estero Bay	Lead (Project Head)	H. Gary Greene (CapRock, MLML)
	Head Interpreter	Hans AbramsonWard (LCI)
	Associate Interpreter	Brian Gray (LCI)
	GIS Manager	Serkan Bozkurt (LCI)
Point Sal	Lead (Project Head)	H. Gary Greene (CapRock, MLML)
	Head Interpreter	Phil Hogan (FCL)
	Associate Interpreter	Robbie Dame
	Associate Interpreter	Bryan Bergkamp (FCL)
	GIS Manager	Cornelia Dean (FCL)
San Luis Obispo Bay	Lead (Project Head)	H. Gary Greene (CapRock, MLML)
	Head Interpreter	Phil Hogan (FCL)
	Associate Interpreter	Robbie Dame
	Associate Interpreter	Bryan Bergkamp (FCL)
	GIS Manager	Cornelia Dean (FCL)
All Areas	Project Technical Coordinator	Stuart Nishenko (PG&E)

3.1.2   Interpretation Tools

The interpretation teams used IHS Kingdom, Version 8.6 to interpret seismic-reflection data in the Estero Bay, San Luis Obispo Bay, and offshore Point Sal survey areas. The Kingdom software allows the user to view and map horizons on vertical profiles (3D and 2D data sets, cross sections, and user-selected cross sections), as well as on horizontal time slices (3D data set, plan view, user-selected profiles). The vertical cross-sectional profiles and horizontal time slices were primarily displayed as seismic-reflection

amplitudes. Horizontal time slices through seismic attribute volumes generated in the Kingdom RSA software modules were displayed on the seismic base map and in 3D space using VuPAK.

The RSA is a separate program or module that provides additional analysis and visualization capabilities to data in IHS Kingdom. Similarity time slices from RSA were compared to amplitude time slices from IHS Kingdom. The data used for interpretation in the validated version of IHS Kingdom and the data from RSA used in the construction of figures, software validations for SPW, UNISEIS, and IHS Kingdom, and qualification of the data processed using SPW and UNISEIS are all documented (Fugro Consultants, Inc., 2012b,c,f).

Data interpretation was performed on each 3D volume acquired in 2011 and 2012, along with selected 2D legacy archive lines (Figure 1-10) within the vicinity of the Estero and San Luis Obispo Bays and Point Sal areas of investigation. Within the 3D data sets, mapping was conducted initially on 3D inline numbers evenly divisible by 20 to develop an overall understanding of the data set. In areas of interest, or areas having complicated fault geometry, every inline and crossline was interpreted to maximize the accuracy of the mapped seismic horizon or geologic feature. In some cases, interpretations were performed on every other line to better define continuity of a structure or feature. User-selected arbitrary 2D profiles were used to provide different apparent (oblique to structural trends) and true view angles (perpendicular to structural trends) across features to evaluate and aid data interpretation. Crosslines were interpreted as necessary to develop accurate mapping and interpretation of shallow structures. Furthermore, numerous time slices, which include data from every inline and crossline profile, were interpreted.

3.2   Interpretation Criteria

The criteria used by the interpretation team to develop technically consistent mapping within the 3D/2D data sets are specific to the geological features mapped, such as horizons (stratigraphic marker beds and unconformities) and structures (faults and folds), channels, and paleoshorelines, as observed in cross section (acoustic profiles) and/or plan view (attribute time slices). The criteria were developed for piercing points, faults, channels, paleoshorelines (strandlines), and unconformities. Channels (thalwegs and sharp upper walls) and paleoshorelines (strandlines) were selected as the most significant piercing points to be used in this investigation.

3.2.1   Selected Piercing Points

Identifying piercing points that cross and are offset by fault movement is a critical component of this investigation. The criteria for selecting a piercing point as used in this investigation consists of a spatially and temporally restricted (both vertically and horizontally) feature that crosses a fault and has the potential of being offset by the fault (e.g., channel thalweg or the channel line that represents the deepest part of the channel).

A piercing point is defined here as a geologic feature, preferably linear, that is cut by a fault and may be displaced by fault movement (Keller and Pinter, 2002). Geometrically

nonparallel lines intersecting a plane form a point. The sole purpose of selecting piercing points is to reconstruct fault movement. Reconstruction of a piercing point, or moving it back to its original position, is a primary way to determine slip or displacement along a fault. This can be done at various scales, including large scales (m to km), such as those undertaken in this investigation (Lease et al., 2009). Stratigraphic units can also be used as piercing points, and Hill and Dibblee (1953) used the Pelona and Orocopia schists in the first attempt to determine offsets along the San Andreas fault zone. Along the San Gregorio fault zone, Greene (1977) and Clark et al. (1984) used submarine canyons and the relationship and contact between the Cretaceous Monterey mass of Ross and Brabb (1972) that comprise the Monterey Peninsula and the overlying Eocene conglomerate (Carmelo Formation) as piercing points. Reconstructions are best done, however, when a well-defined feature is used to determine offset, such as a channel axis (thalweg), a vertical bedrock fault trace intersecting an eroded bedrock surface, or a shoreline.

In this investigation, piercing points are identified and mapped based on one or more of the following criteria:

- A single similar distinct linear or continuous sinuous geologic feature (channel thalweg, channel margin, shoreline angle) observed on either side of a fault or fault zone in cross section and plan view.
- Two or more structural or geomorphological features observed on opposite sides of a fault or fault zone in plan view.
- Acoustic or stratigraphic relationships that can be correlated across a fault or fault zone in plan view.

The potential piercing points selected in this investigation for determining offsets along faults are listed (in order of confidence level) below:

- Paleoshorelines
- Well-defined thalwegs
- Sharp channel wall breaks

3.2.2   Paleoshorelines (Buried Strandlines)

Buried paleoshorelines that cross faults in the investigation region (San Luis Obispo Bay) were identified using the following criteria:

- Arc-like erosional features identified in coherency time slices (plan view).
- Irregular truncation of acoustic reflectors in cross section.

Paleostrandline depths were estimated using MBES bathymetry and 3D seismic-reflection data. The difference between the gridded seafloor horizon and gridded paleostrandline horizon in time was calculated and converted to depth below seafloor using an assumed estimated velocity of 1,600 m/s with a possible uncertainty of ±15 m/s. Depth below sea level was estimated by adding MBES bathymetry seafloor depth to the depth converted to the paleostrandline grid.

3.2.3   Paleochannels (Buried Channels)

Channels are identified and mapped based on one or more of the following criteria:

- Truncated reflectors separated by a concave upward depression (erosional in nature) in cross section.
- Acoustic contrast between country rock or strata and fill within a concave upward depression in cross section.
- Notched high-amplitude reflector in cross section.
- Buttress unconformities along the lateral margins of interpreted paleochannels in cross section.
- Flattening upward of strata in a cup-shaped or concave downward depression.
- U- or V-shaped depression in acoustic country rock or strata (erosional in nature) in cross section.
- Nested cross-stratified-like cup-shaped reflectors in cross section.
- Sinuous or meandering low-amplitude reflectors in high-amplitude acoustic background in plan view.
- Braided or lobe-shaped reflectors confined to a relatively narrow sinuous or linear area in plan view.
- Sharp linear or sinuous contrast in acoustics in plan view.

Paleochannel depths were estimated in the same fashion as described above for the paleostrandlines.

3.3   Nomenclature

To be consistent in naming and correlating structures and features mapped from the interpretation of the 3D data sets, a nomenclature scheme was constructed and adapted for use in this report. This section discusses the nomenclature and explains the labels assigned to channels, shorelines, faults, and other structures considered in determining offsets of potential piercing points.

3.3.1   Faults and Structural Blocks

This section presents the nomenclature of faults and fault blocks specific to the study areas and as used in labeling channels as piercing points.

3.3.1.1   Estero Bay Study Area

The nomenclature for faults and fault blocks for the Estero Bay study area is as follows:

- The fault trace identified in the central part of the 3D survey is called the eastern trace of the HFZ (fault 11006 in PG&E, 2012).
- The fault trace indentified in the western part of 2D survey is called the western trace of the HFZ (HF 2001 and 2002 in PG&E, 2012).
- The numbered faults were identified in the 2011 2D/3D survey (PG&E, 2012).
- The lettered numbered faults were identified in the 2012 2D/3D survey (PG&E, 2013).

- East of the eastern strand of the HFZ is the Eastern block.
- West of the eastern strand of the HFZ is the Western block.

3.3.1.2   Point Sal Study Area

The nomenclature for channels, faults, and structural blocks for the Point Sal study area is as follows:

- The fault trace identified in the easternmost part of the survey area is called the eastern strand of the HFZ.
- The fault trace indentified in the western part of the survey area is called the western strand of the HFZ.
- The fault indentified in the central area of the survey between the eastern and western branches of the HFZ is called the central strand of the HFZ. Other short, minor unnamed conjugate fault strands that exist in the central area are not named.
- The fault impinging from the east is called the Lions Head fault.
- East of the eastern branch of the HFZ is the Eastern block.
- Between the eastern and western branches of the HFZ is the Central block.
- West of the western branch of the HFZ is the Western block.

3.3.1.3   San Luis Obispo Bay Study Area

The nomenclature for faults and local structural blocks for the San Luis Obispo Bay study area is as follows:

- The fault traces identified in the easternmost part of survey are tentatively called the Shoreline, Southwestern Boundary, Oceano, Pecho, Los Berros, and Central unnamed faults.
- The curved eastern trace of the Shoreline fault is called the Oceano fault.
- The straight trace of the Shoreline fault is called the primary trace of the Shoreline fault.
- The fault trace identified in western part of survey is called the Pecho fault.
- East of the Oceano and Shoreline fault zones is the Eastern block.
- Between the Oceano and Shoreline faults is the Central block.
- West of the Shoreline fault is the Western block.

3.3.2   Channels

The channels identified in the 2D and 3D data sets were labeled according to the guidelines below:

- Starting with the northernmost channel, channels were designated with uppercase letters, starting with "A," progressing in alphabetical order southward.
- Those channels found to be present east of the HFZ or Shoreline/Oceano fault zones were labeled with a lowercase "e." Similarly, those found west of the fault

zones were labeled with a lowercase "w," and those found within the central part of the fault zones were labeled with a lowercase "c."

- In nested channel complexes (channels eroded into channels), the stratigraphically lowest (oldest) channels were designated with a number, starting with "1" and increasing in numerical order upward. Sometimes the code is preceded with a "D" or "S" (for deep or shallow), as indicated in the Estero Bay survey area.

Examples

Examples in using this channel designation scheme are as follows:

- For a nested channel complex with three backfilled incisions within the fill of the large channel incision, each found progressively higher in the stratigraphic complex, all found east of the fault zone, and geographically located in the extreme north of the study area, the designations for all three channels are "Ae1," "Ae2," and "Ae3," respectively.

- For a channel located in the most northerly part of the survey area on the east side of the fault zone, and that crosscuts the next southerly located channel, the crossing channel is designated as "Ae_{x-B}."

- For a channel located in the most northerly part of the survey area on the west side of the fault zone that merges with the next southerly located channel, the combined channel is designated as "Aw_{m-B}."

Piercing Points (Channels)

In labeling those channels used as a piercing point, the thalweg or wall of the channel is designated and the points are labeled according to their channel designation as follows:

- For a thalweg piercing point located in Channel Ae, the point is labeled as "PAe-t."
- For a channel wall piercing point located in Channel Aw, the point is labeled as "PAw-w."
- Channels are lettered from north to south, and are coded to indicate the structural block in which they are located such as Channel Ae, the most northerly channel located on the Eastern block.

3.4   General Working Hypotheses

In the development of the working hypotheses for this investigation, all structures and morphologic features that appeared to cross and be offset by a fault were considered and subjected to a robust geologic analysis to determine with a high level of confidence whether they were potential piercing points. Although only a few features, such as shorelines and channels, made the cut as good potential piercing points, all features were considered. All piercing point candidates considered in our working hypotheses are listed below.

- Buried paleoshorelines (strandlines):

- o Offset reflects true fault displacement.
- o Separation reflects apparent fault displacement.
- o Separation reflects a combination of fault displacement and differential erosion.
- o Separation reflects solely differential erosion.

- Channel thalweg/walls:

  - o Deflections reflect true fault displacement.
  - o Deflections reflect apparent fault displacement.
  - o Deflections reflect a combination of fault displacement and differential erosion.
  - o Deflections reflect solely differential erosion.
  - o Deflections reflects encounter with resistant rock or older structure.

3.5 Interpretation Confidence Levels

The piercing points selected for this investigation are of various confidence levels, and uncertainties exist for each one. Our highest confidence level lies in the selection of strandlines and some channel thalwegs, while less confidence lies in features that are irregular, such as channel walls. Linear and predictable features provide the highest confidence for reconstructing original piercing point locations, while circular or irregular features are less dependable as piercing points. We have taken great care to use features that have a high probability of exhibiting apparent offsets along faults, such as channel walls or broad channel axes that may be controlled by faulting and are erosional in nature rather than truly offset by faulting.

4.0   ASSUMPTIONS

Specific assumptions were made in regard to PG&E's QA/QC oversight validation of all data and software used to produce this report:

1. The previous studies by PG&E (2011a, 2011b) were approved by the NRC and are acceptable for use in this report.

2. Navigation was of the accuracy specified in NCS SubSea's *Navigation Final Reports,* DCPP 3D Geophysical Survey Job Documents (Fugro Consultants, Inc., 2012a,d, and 2013e). The assumption that the specifications are accurate is supported where georeferenced data sets overlap, showing the same structures within the geographical limits of each survey data set (PG&E, 2012).

3. All seismic stratigraphy imaged in the low-energy data set is assumed to have an average bedrock velocity range of 1,600 m/s, which is used in converting time to depth and estimating depths and inclinations (dips). This velocity estimate is based on a seismic source frequency spectrum (PG&E, 2012) and the processing parameters (normal moveout correction using a brute velocity function of 1,600 m/s applied to the seismic data in the CDP domain) used by Fugro Consultants (2013a, 2013b, 2013c, 2013d) in the processing of the seismic-reflection data. This assumed velocity provides reasonable estimated depth calculations down to approximately 400 m, the approximate depth of penetration of the high-resolution energy.

4. Although not validated, it is assumed that MBES bathymetric data collected and processed (2 m grids, with ±1 m resolution) by the Seafloor Mapping Lab of California State University, Monterey Bay, were maintained at IHO S-44 Special Order specifications. Across the entire MBES swath, an average of 95.8 percent of crossline soundings fall within IHO Special Order tolerances, with 99.7 percent within the IHO Order 1 (P. Iampietro, pers. comm. with S. Nishenko, 2010; also see PG&E Multibeam Bathymetry Survey 2009 Quality Control Report, Appendix F of PG&E, 2011b). This assumption is validated through the comparison of various geophysical data sets, including the 3D/2D seismic-reflection data that precisely overlie each other as a georeferenced product (Figure 11 of PG&E, 2012).

5. The seismic-reflection data used in the LTSP Report (PG&E, 1988) were collected to industry standards at the time and are acceptable for use in this report. The data are considered qualified for use under NQA because the LTSP Report (PG&E, 1988), associated data, and responses to the NRC's requests for additional information have been accepted and approved by the NRC.

6. The USGS 2D seismic-reflection profiles are acceptable for use in this report because they were collected in accordance with industry and scientific standards, subjected to peer review, and published (Sliter et al., 2009).

5.0   SOFTWARE

The primary software programs used for this analysis and interpretation of the 3D and 2D seismic-reflection data sets are SPW, UNISEIS, IHS Kingdom RSA (Version 8.6), and ArcGIS. The SPW was used by Fugro Consultants to process the 2D seismic-reflection data, while Fugro Seismic Imaging used UNISEIS to process the 3D seismic-reflection data. IHS Kingdom, a PC-based program for analysis and interpretation of seismic-reflection data, was used in the construction and interpretation of structure maps, cross sections, and time slices. Software validation was undertaken by Fugro Consultants for UNISEIS, SPW, and IHS Kingdom (Fugro Consultants, 2012b, 2012c, 2012f).

ArcGIS Version 10, developed by ESRI, is a software package acceptable to industry, government, and academia that is commonly used to collate and map spatial data in an accurate georeferenced manner. This software was used to construct maps presented in the Shoreline Fault Zone Report (PG&E, 2011b), some of which are reproduced in this report, as well as maps (plates and figures) used for presentation purposes only. Previously interpreted geologic and structural maps in ArcGIS from PG&E (2011b) are used here as base maps for comparison purposes. No calculations were performed on the data using ArcGIS. Therefore, ArcGIS was not validated under NQA.

6.0   THE HOSGRI FAULT ZONE

The interpretation and analyses of the low-energy, high-resolution 3D seismic-reflection data were compared with the previously mapped geology described in earlier reports (PG&E, 2011b, 2013) for both the HFZ and Shoreline fault zone (see Section 7.0 below). Key observations and interpretations of the data are presented here in regard to the HFZ, followed by analysis of the implications of the observations for characterizing faults, piercing points, fault offsets, and slip rates in the Estero Bay and Point Sal study areas.

6.1   The Estero Bay Study Area

The Estero Bay study area (Survey Area 1) is located in a transition zone between the upper continental slope and the outer continental shelf. Bedded sedimentary rock is exposed at the seafloor along the east side of the study area, forming distinct ridges and troughs that are readily evident in a bathymetric image (Plate 1). These strata have been interpreted in previous work as siliceous mudstone of the upper Miocene Miguelito member of the Pismo Formation based on correlation to strata exposed onshore (PG&E, 2011b). In the central and western parts of the study area, the seafloor is underlain by Quaternary sediment. The western edge of bedrock outcrop at the seafloor is broadly parallel to the HFZ. However, in detail, the boundary between rocky seafloor and smooth, sediment-covered seafloor includes several bedrock paleo-embayments of various sizes. The locations and sizes of these embayments appear to be controlled by bedrock structure.

6.1.1   Results

Observations and interpretations of the 3D and 2D data collected within the Estero Bay study area resulted in the identification and mapping of several paleochannels that were considered potential piercing points that could be used to estimate offsets across strands of the HFZ. The relationship of the identified and mapped buried channels to the seismic stratigraphy and key horizons reported in PG&E (2013) provided age constraints for the timing of fault displacements of the piercing points and for the calculation of slip rates.

6.1.1.1   Stratigraphy

The stratigraphy of the Estero Bay study area documents a transition from a continental slope to a shelf-edge environment. The nature of this transition is described below.

Continental Shelf

In the western part of the study area, a thick stratigraphic section beneath the outer continental shelf consists of alternating sequences of onlapping and downlapping reflections that are bounded by a series of unconformities and paraconformities (Figure 6-1). These shallow reflections document episodes of deposition separated by periods of nondeposition or erosion and are interpreted in a sequence-stratigraphic framework as stacked highstand and lowstand-to-transgressive systems tracts that were deposited during late Quaternary sea-level fluctuations (PG&E, 2013) and are well

displayed in the USGS seismic-reflection profiles. To aid in the interpretation of the USGS data, we flattened the seafloor as represented on Figure 6-1a.

Highstand systems tracts (labeled HST on Figure 6-1b) are marked by a series of progradational reflections landward of the shelf break that downlap onto a prominent underlying flatter reflection or surface (Posamentier and Allen, 1999). This pattern of deposition is interpreted to result from increased availability of sediment to the shelf at times of sea-level highstands through times of falling sea level. Lowstand systems tracts (labeled LST on Figure 6-1b) are represented by reflections that lap onto the deeper parts of the highstand systems tracts seaward of the shelf break (Posamentier and Allen, 1999), and are restricted to the outer shelf and slope areas because they were deposited during sea-level lowstands. The top of a lowstand systems tract is defined by the transgressive surface, which marks the onset of sea-level rise in a basin, and is commonly erosional (Posamentier and Allen, 1999). Transgressive systems tracts (labeled TST on Figure 6-1b) are characterized by thin intervals of reflections onlapping onto the erosional transgressive surface. Landward of the lowstand and transgressive systems tracts, the transgressive surfaces exhibit evidence for significant erosion and truncation of underlying reflections (Figure 6-1), which are possibly the result of one or more of the following:

- Wave erosion during a prior sea-level regression.
- Sub-aerial erosion that occurred during a Quaternary sea-level lowstand while the central and inner shelves were exposed.
- Wave erosion during the subsequent sea-level transgression.

Shallow unconformities that separate these systems tracts include parts of the regional unconformities H10, H20, H30, and H40, which were originally described in PG&E (2013). As described in Section 1.2.9, unconformities H10, H30, and H40 are interpreted as transgressive surfaces that were developed following the three most recent sea-level lowstands, MIS 2, MIS 6, and MIS 8, respectively (Figure 1-6). Unconformity H20 is interpreted to mark the base of the most recent lowstand, MIS 2. Two deeper transgressive unconformities, H45 and H48, are recognized locally in Estero Bay. Although the ages of these two are much less well understood, it is possible that they were developed during regressions following the two prior lowstands, MIS 10 and MIS 12 (Figure 1-6).

Continental Slope

Unconformity T05 is the deepest surface marked by significant downlap on Figure 6-1. Beneath unconformity T05, generally uniform, paraconformable reflections are recognized in the deeper parts of the study area, and onlapping, downlapping, or erosional unconformities are notably absent. Reflections below unconformity T05 indicate a different depositional style from the shallower reflections in this figure. These deeper paraconformable reflections suggest relatively uniform sedimentation with very little change in the location or style of deposition. This pattern of sedimentation is consistent with deposition on the continental slope, deeper than the range of Quaternary sea-level fluctuations and associated erosion encountered on the continental shelf. Coast-

parallel seismic-reflection profiles show that channels of various dimensions and depths have cut the reflections that mark this continental slope stratigraphy (Plate 2).

The early–late Pliocene (ELP) unconformity, originally mapped by Willingham et al. (2013), is interpreted to lie within the stack of paraconformable reflections observed at the base of USGS sparker Profile PBS-T2 (Plate 2). Correlation of this unconformity is based on the intersection of Profile PBS-T2 with Line PG&E-1 (collected by Digicon Geophysical, 1986; see profile C-C′ of Willingham et al., 2013).

Middle Pleistocene Transition

Oxygen isotope records compiled by Lisiecki and Raymo (2005) document a change in the amplitude of Quaternary sea-level fluctuations in the middle Pleistocene, beginning with MIS 16, which occurred between approximately 700 ka and 600 ka (Figure 6-2). According to Lisiecki and Raymo's (2005) 5.3 Myr δ^{18}O stack, MIS 16 is associated with a significantly lower oxygen isotope ratio than any previous isotope stage, which implies that global eustatic sea level was significantly lower during MIS 16 than any previous lowstand. This transition is likely related to a climatic transition from relatively frequent low-amplitude 41 kyr sea-level cycles to relatively infrequent high-amplitude 100 kyr sea-level cycles (Bintanja and van de Wal, 2008). This transition, known as the mid-Pleistocene transition (MPT) was gradual, occurring between approximately 1.4 Ma and 600 ka (Bintanja and van de Wal, 2008). Numerous studies have explored potential causes of this change. Most explanations involve details of ice-sheet dynamics (e.g., Clark and Pollard, 1998; Berger et al., 1999; Tziperman and Gildor, 2003; Raymo et al., 2006; Bintanja and van de Wal, 2008), although other explanations have been proposed (e.g., Muller and MacDonald, 1995).

Given that sea-level lowstands prior to MIS 16 appear to have been significantly shallower than they were post–MIS 16, it is possible that the reason for the relatively abrupt transition from a slope to a shelf environment in the western (deeper) part of the Estero Bay study area is that earlier sea-level lowstands were not of sufficient depth to affect stratigraphy in that area. This interpretation implies that the age of unconformity T05 is on the order of 700–630 ka (Figure 6-2). However, sea-level fluctuations indicated by δ^{18}O prior to MIS 11 have not been correlated to precise ice-volume-equivalent paleo–sea levels using geologic indicators of relative sea level, and δ^{18}O ratios provide only approximate estimates of paleo–sea levels. Because of this uncertainty, the precise marine isotope stage of unconformity T05 is not known. Therefore, uncertainty in the age of unconformity T05 is large, and is considered to extend beyond the duration of the MPT, and may range from approximately 1.4 Ma to 540 ka, the age of MIS 14, which is one lowstand older than the probable age of H48 (Figure 6-2).

Migration of Shelf Edge

The edge of the continental shelf was a dynamic feature from middle to late Pleistocene time. This shift in position of the shelf break through time results from a complex interplay of sea-level fluctuations, tectonic uplift and subsidence, and sedimentation. The modern shelf break traverses the Estero Bay study area from south to north, merges with, and extends parallel to the HFZ in the northern part of the area (Plate 1). The

approximate position of the shelf break during late Pleistocene sea-level lowstands may be estimated by mapping the shelf break from buried regional transgressive surfaces (reflections or unconformities in seismic-reflection profiles), as indicated by the line created from points on profiles that demark an increase in steepness of these surfaces. This line represents a transition from regions of distinct erosion (on the continental shelf) to nondeposition or surface-parallel erosion (paraconformities on the upper continental slope), with landward pinch-outs of the lowstand systems tract directly beneath the shelf break. Figure 6-3 is a sketch map showing the approximate position of the shelf edge in the Estero Bay study area following the late Pleistocene sea-level lowstands MIS 2, MIS 6, and MIS 8, as marked by the shelf break in unconformities H10, H30, and H40, respectively, described in PG&E (2013).

The modern shelf break is located seaward of the break in slope in unconformity H10 (Figure 6-3; Plate 1). This relationship with the modern and older breaks reflects deposition at the shelf edge and progradation of the shelf break since the last glacial lowstand and the onset of the most recent transgression, which took place approximately 19 ka (Figure 1-6). A line marking the steepening in slope of unconformity H30 marks the approximate position of the shelf break following the penultimate sea-level lowstand at MIS 6, approximately 135 ka. This break in slope occurs almost directly beneath the paleo–shelf break marked by unconformity H10. In contrast, the break in slope in the deeper unconformity H40 occurs nearly 0.5 to 1.0 km landward of the H10 and H30 shelf breaks. The shallower and more landward break in slope marks the position of the shelf break after the MIS 8 lowstand, which was notably less deep than the subsequent MIS 6 and MIS 2 lowstands (Figure 1-6).

Top of Bedrock

East of the HFZ, the erosional surface of the bedrock is exhibited in the seismic-reflection profiles and, where exposed at the seafloor, in the MBES data used for the study of Estero Bay (Plate 1). A structure contour map of the top of bedrock is presented on Figure 6-4, merged with the regional top-of-bedrock surface mapped for the PG&E seismic stratigraphy project (PG&E, 2013).

Seismic-reflection profiles that image parts of the bedrock surface are shown on Figures 6-5, 6-6, and 6-7 and exhibit variable seismic amplitudes with a fairly low-amplitude reflection marking the top of bedrock. The bedrock unconformity is specifically mapped as the interface between well-imaged coherent reflections (inferred to be Quaternary sediments) and chaotic or semitransparent acoustical units (inferred to represent the underlying bedrock).

The bedrock surface is a broad, gentle, westward-sloping plane that steepens sharply down to the west, where it is truncated by the HFZ (Figure 6-4). Although the shelf extends west of the HFZ in the southern part of the study area (Plate 1), bedrock is not observed west of the primary traces of the HFZ.

Shallow Stratigraphy East of the HFZ

In most of the Estero Bay study area east of the HFZ, the smooth seafloor imaged in the MBES data appears to be underlain by a thin veneer of Pleistocene to Holocene sediment.

The bubble pulse generally obscures seismic reflections from these strata. In locations where the sediment is relatively thicker, thin intervals of transparent to low-amplitude gently dipping reflections occur (PG&E, 2013). Thicker intervals of gently bowed reflections fill the fowllowing three features along the HFZ:

- A broad embayment east of the HFZ and north of the 3D survey.
- A fault-parallel elongate basin localized east of the HFZ in the center of the study area.
- A narrow erosional trough incised into this broad surface in the southern part of the study area (Figure 6-4).

Figure 6-5 shows reflections interpreted as Quaternary strata filling the broad bedrock embayment east of the HFZ and north of the 3D survey. These reflections (strata) are marked by local unconformities, which are correlated with regional unconformities west of the HFZ by tracing them directly on intersecting seismic-reflection profiles (indicated by the intersection with Line PBS-03 shown on Figure 6-5). This correlation suggests that the embayment fill imaged on Figure 6-5 includes strata that range from more than 600 ka to less than 130 ka. A high-resolution sparker profile collected from the same embayment approximately 600 m east of the profile shown on Figure 6-5 exhibits numerous channels carved into the embayment fill (Figure 6-6). Thickening of stratigraphic sequences toward the center of this embayment and progressive steepening of older unconformities suggest that this embayment may occupy a syncline that underwent progressive folding during deposition of these strata. Most of the younger unconformities imaged on Figures 6-5 and Figure 6-6 are truncated at the seafloor on the southeast side of the image, suggesting either active folding and uplift of the anticline to the southeast (imaged on the southeast side Figure 6-5) or onlap and offlap and nondeposition of Quaternary strata in this region.

The southern part of Figure 6-5 overlaps with the eastern half of the Estero Bay 3D seismic-reflection volume, which enables stratigraphy imaged in the volume east of the HFZ to be tied to the stratigraphic markers west of the HFZ. The prominent reflections or stratigraphic markers imaged in the 3D volume and labeled T10, T30, and T50 (Figure 6-5) project beneath unconformities T05 and H48 and, therefore, may be older than 0.6 Ma. Considering the uncertainty in the age of unconformity T05, unconformities T10, T30, and T50 may be substantially older than T05. With the exception of channel fill, no reflections of younger strata appear to be imaged within the 3D volume.

Near the south end of the Estero Bay study area, an erosional trough is located within a graben defined by strands of the Point Buchon fault zone (Figure 6-4). Bedrock contours show that the southern part of this trough extends approximately parallel to the adjacent fault strands, and the northern part bends westward and deepens toward the HFZ (Figure 6-4). Seismic reflections confined to this trough are interpreted to represent Quaternary strata that may be locally deformed by folding, possibly faulting, and incised by channels (Figure 6-7). These reflections underlie unconformity H10, and lap onto the top of pre-Quaternary bedrock, suggesting that these reflections (strata) pre-date the most recent transgression (~19–8 ka). These local unconformities cannot be further tied to the regional unconformities mapped west of the HFZ.

6.1.1.2   Faults

Faults and folds mapped in the Estero Bay study are based on previous mapping completed for the PG&E (2013) report and on new 2D and 3D data collected for this study. Figure 6-8 compares faults mapped previously (Figure 6-8a; PG&E, 2011b; Willingham et al., 2013) with faults mapped for this study.

The increased density of high-resolution 2D and 3D seismic-reflection profiles and updated bathymetry collected and interpreted for this project show that in the Estero Bay study area, the HFZ consists mainly of two dominant subparallel fault strands, faults labeled 10001 and 10006 on Figure 6-8b, with minor secondary strands to the northeast and southwest. These two dominant fault strands are the northern continuation of faults originally mapped and numbered in the PG&E (2012, 2013) report, the numbering system of which is retained for this study. Where well imaged, the strands of the HFZ are generally steeply dipping to vertical. This attitude is consistent with previous characterizations of the HFZ as a dominantly right-lateral strike-slip fault zone (e.g., Hanson et al., 2004; Johnson and Watt, 2012; Willingham et al., 2013). The sense of vertical separation across the HFZ in the study area is dominantly down to the west, as indicated by the presence of the broad, beveled bedrock surface to the east and a relatively thick sedimentary section to the west (Figure 6-4).

In the central part of the study area, the two primary faults of the HFZ bound a northwest-southeast narrow linear ridge (pressure ridge) of uplifted rock and Pleistocene strata (Figure 6-4). This pressure ridge separates an elongate, fairly shallow, enclosed sedimentary basin to the east from the deep offshore Santa Maria Basin to the west. The upper surface of the pressure ridge is eroded flat. To the south, the sense of vertical separation across the two primary faults reverses, and the region between them is downdropped, as exhibited on USGS Profiles PBS-19 and PBS-34 and the 2D profiles at the north end of the Point Buchon 3D survey area (PG&E, 2012).

Newly mapped faults west of the primary HFZ (HF2001, HF2002) trend north-northwest and define the margins of discrete high-amplitude reflections (indicating a "bright spot")[1] between unconformities H30 and H40. The sharp boundaries and orientation of this bright spot are parallel to the HFZ and suggest the presence of shallow gas trapped between the faults. Neither fault HF2001 nor HF2002 exhibits significant vertical separation of abutting reflections. Both faults appear to extend above unconformity H40 (estimated to be approximately 240 ka), and may be associated with some minor vertical separation (a few meters) of the H40 horizon. Both faults are overlain by uninterrupted reflections that lie beneath unconformity H30, which is estimated to be approximately 130 ka.

---

[1] "Bright spots" of high-amplitude reflections localized along or adjacent to faults commonly indicate the presence of gas that has migrated upward along fault planes and into interstices of porous stratigraphic intervals adjacent to the faults. This "gas charging" tends to produce a modulus of elasticity that leads to high-amplitude reflectors and wipes out deeper reflectors beneath it. Sharp boundaries of the bright spots can result from the contrasting density between gas-charged sediment and non-gas-charged sediment.

Patterns of secondary faulting suggest some component of fault-normal contraction within the center of the Estero Bay study area. Figure 6-9 shows a time slice and intersecting seismic-reflection profiles from the northern part of the 3D volume where a series of short faults are interpreted deep in the volume directly east of and parallel to fault 11006. These faults splay upward from fault 11006 (Figure 6-9e). Reflections in the hanging wall of this system of splay faults are deformed into an anticline that extends parallel to fault 11006.

6.1.1.3   Buried Paleochannels East of the HFZ

Four channels and channel complexes are identified within the Estero Bay 3D data set east of the primary trace of the HFZ (Figure 6-10). From north to south, these channels are labeled Channel Complex Ae (consisting of Channels Ae3, Ae2, Ae1.5, and Ae1), Channel Be, Channel Ce (poorly defined), and Channel Complex De. These channels truncate reflections of strata interpreted as lower Quaternary, and they are buried by a thin veneer of sediment that is obscured by the bubble pulse (Figure 6-10). Therefore, the ages of these channels are poorly constrained from the stratigraphy imaged in the 3D data set. These channels are described below; channel locations and geometry are presented on Plate 3.

Channel Complex Ae

Channel Complex Ae includes a series of up to four inset or nested channels that are located near the north end of the 3D volume. The two deeper channels in this complex, Ae1 and Ae1.5, are only poorly defined and may represent reflections of bedding instead of channel margins. The two shallow channels, Ae2 and Ae3, exhibit clear channel morphology in cross section (Figure 6-10), and thus they are mapped with high confidence. They are mapped to extend westward from the eastern margin of the 3D survey, sloping down to the west. However, the western parts of Channels Ae2 and Ae3 are reversed in slope, sloping down to the east. This reverse-sloping geometry is illustrated in the time slice on Figure 6-10, panels f and g, which show that the channel margins narrow and pinch out both to the east and to the west. Channel Complex A3 as imaged in the 3D volume does not appear to intersect with fault 11006. Channel Complex Ae occurs along the southern flank of an anticline, which is imaged by concentric reflections shown in the time slice of Figure 6-10, panels f and g. Channel dimensions and a longitudinal profile of the youngest and best-preserved channel within this complex (i.e., Channel Ae3) are shown on Plate 3.

Channel Be

Channel Be is located near the center of the 3D volume and is well imaged in profile and time slice (Figure 6-10). It trends east-west and extends from the eastern margin of the 3D survey to fault 11006, where it is truncated. It is asymmetric in profile with the southern margin steeper than the northern. Channel dimensions and longitudinal profile for Channel Be are presented on Plate 3.

Channel Ce

Channel Ce is located near the south end of the 3D volume and is moderately imaged in profile (Figure 6-10) and shallow time slices. It extends from the eastern margin of the 3D survey to fault 11006, where it turns to the south, extends along the fault, and trends drains into Channel Complex De. This channel is not imaged on the time slice on Figure 6-10 because it is not incised deeply enough to intersect the position of the time slice.

Channel Complex De

Channel Complex De is located at the south end of the 3D survey, where the northern margin of the channel and a small part of the thalweg are imaged near the location where the channel is truncated by fault 11006 (Figure 6-10). This channel complex is also imaged on USGS 2D seismic-reflection Profiles PBS-19 and PBS-T1A, where the complex appears significantly wider and more deeply incised than any of the channels described above. The USGS seismic-reflection Profile PBS-T1A, located approximately 100 m east of the 3D volume, crosses the entire channel complex and shows that there are at least two smaller channels nested within the main, larger—or basal—channel (shown in the right-hand panel of Figure 6-11). The northern margin of the basal channel is well imaged in the 3D volume, and both margins are well imaged on Profile PBS-T1A, as exhibited by the curved truncation of well-layered reflections at the base of the channel (Figures 6-10 and 6-11). Dimensions and a longitudinal profile for Channel Complex De are presented on Plate 3.

6.1.1.4   Buried Channel Morphology Between Two HFZ Strands

A single-channel complex, Ee, is identified between the primary fault strands (faults 10001 and 11006 that bound a central structural block, a faulted sliver of bedrock) of the HFZ in the study area. The southern part of the central structural block between the two fault strands is downdropped, which appears to have facilitated accumulation of Quaternary sediment and channel preservation. Conversely, in the north, uplift between the fault strands appears to have elevated bedrock and the overlying downslope sections of Channel Complex Ae and Channel Be, thus subjecting them to erosion, which removed all evidence of their past presence. Channel Complex Ee is located within a zone of monoclinal folding in the upper part of the Central block and the fault strand that separates the uplifted part from the downdropped part of the block.

Channel Complex Ee

Channel Complex Ee is well defined both in cross section (in seismic-reflection profiles) and in plan view (in time slices) and includes a well-preserved basal channel with at least two nested channels incised into the larger channel's fill (Figure 6-12). The base of this complex (the basal channel floor) is marked by pronounced curved truncations of the well-layered, south-dipping reflections within the narrow Central block or fault sliver between faults 10001 and 11006. Folding within the narrow within the Central block has produced a slightly asymmetric channel complex geometry. Flattening of the reflection that caps the channels produces a more realistic, symmetrical cross-sectional geometry to

the channel complex, suggesting that the channels were carved prior to folding (Figure 6-12).

Channel Ee1 is the most likely downslope extension of Channel Complex De west of fault 11006, the eastern primary strand of the HFZ. Correlation of these channels is based on the close spatial association that the two channels have on opposite sides of the fault, a similar channel width, trend, and depth of incision, and channel gradient (Plate 3). This correlation is illustrated on Figure 6-11. Because the resolution of the seismic-reflection profiles used in this study was variable, and because of data gaps, the smaller nested channels within Channel Complex Ee could not be correlated to those in Channel Complex De. Channels Ee1 and De are abruptly truncated and separated by fault 11006 (Plate 3). Channel Ee1 extends westward beyond the edge of the 3D volume. Based on the boundaries of imaging in the 3D volume and the fault location uncertainty, Channel Ee1 is imaged within 100–150 m of fault 10001, the primary western strand of the HFZ.

6.1.1.5   Buried Channel Morphology West of the HFZ

Several deeply buried channels are clearly imaged at depth in the USGS seismic-reflection Profile PBS-T2, located approximately 2–3 km west of the primary strand of the HFZ (Plate 2). Several channel-like features are identified on individual Fugro 2D seismic-reflection profiles west of, and closer to, the primary trace of the HFZ based on the criteria described in Section 3.2.3. None of these features exhibit the clear channel morphology imaged in the 3D volume east of fault 10001, likely due to the lower resolution and greater line spacing of the 2D data, as well as the probable presence of shallow gas. Examples of these channel-like features are shown on Figure 6-13 as Channels SBw, SCw, and Unnamed channels. Most of these channel-like features cannot be correlated from one profile to another or mapped for significant distances downslope, which suggests that they are locally isolated and not useful as piercing points. However, three probable channels were identified west of fault 10001 that correlate across at least six adjacent 2D seismic-reflection profiles, indicating that they extend downslope for several hundred meters (Plate 3). These channels, labeled DAw, DBw, and DCw on Plate 3 and described briefly below, are located very deep in the stratigraphic section, well below unconformity T05, and within a sequence of relatively uniform, gently west-dipping reflections, suggesting they formed within a continental slope environment (Figure 6-13; Plate 2).

Channel DAw

Channel DAw is moderately well imaged on the Fugro 2D profiles, but it is clearly imaged on USGS profile PBS-T2. The channel trends east-west with thalweg depths between approximately 275 m and 315 m (~345 ms and 395 ms TWTT; Plate 3). A gap of approximately 1.5 km exists between where Channel DAw is imaged on the westernmost Fugro 2D profile and where it is recognized at depth on USGS 2D Profile PBS-T2. Because of this gap, the channel mapped on Profile PBS-T2 is not included in the grid on Plate 3; instead, an approximate projection of the thalweg profile is shown.

Deep reflections in Profile PBS-T2 suggest that Channel DAw is the youngest of a channel system that episodically occupied approximately the same geographical position

during the late Pliocene and early Quaternary times (Plate 2). Channel DAw is incised into a reflection that is buried approximately 32 m (~40 ms TWTT) beneath unconformity T05. Two deeper channels are also imaged below Channel DAw. The deepest channel in this system apparently extends below the base of Profile PBS-T2 and cuts into the ELP unconformity, which is estimated to be between 3.5 Ma and 2.7 Ma (Willingham et al., 2013).

Channel DBw

Channel DBw is moderately well imaged on the Fugro 2D seismic-reflection profiles, but it is the best imaged and longest in extent of the three deep channels mapped west of the primary western strand of the HFZ. A fence diagram of seismic-reflection profiles illustrating the variability in the geomorphic expression of Channel DBw is presented on Figure 6-14. The depth of DBw ranges between approximately 270 m and 325 m (~335 ms and 405 ms TWTT; Figure 6-14; Plate 3). The channel appears to widen downslope and the incision deepens from approximately 16 to 28 m (~20–35 ms TWTT at its upslope extent to approximately 40 m (~50 ms TWTT) at its downslope extent (Plate 3). Unlike Channels DAw and DCw, this channel is located much nearer fault 10001. The thalweg location is moderately well constrained from the west to within approximately 300 m of fault 10001. Closer to the fault, the thalweg location is more poorly constrained, and two possible alternative thalweg locations are mapped adjacent to the fault (<100 m of fault 10001). A number of meanders or bends are imaged in Channel DBw, as shown by the zigzag thalweg on the map (Plate 3), and the variable asymmetry of the channel's profile (Figure 6-14).

The thalweg of Channel DBw (Plate 3) does not descend smoothly to the west, but instead includes dips and rises of up to approximately 12 m (15 ms TWTT). These variations may reflect uncertainty in depth related to mapping errors or variations in seismic velocity related to the presence of gas; alternatively, they may be an accurate representation of a discontinuous or irregular channel thalweg. Such a channel pattern has been described by Maier et al. (2013) as typical for submarine channels in their early stage of formation. Lee et al. (2002) suggest that channels undergoing erosion by turbidity flows exhibits either stepped channel profiles, such as observed here, or plunge pools, which may result from hydraulic jumps or the impact of high-momentum flows.

Channel DCw

Channel DCw is the southernmost of the deep channels observed west of the HFZ in the study area (Plate 3). Similar to Channels DAw and DBw, channel geometry and depth are moderately well constrained. Channel DCw is relatively straight and displays no significant depth variations in profile, ranging from approximately 270 to 350 m (~340–440 ms) below modern sea level. It is mapped no closer than 500 m west of the western primary fault strand of the HFZ, and its upslope geometry and position is unknown.

A distance of approximately 1.5 km exists between where Channel DCw is imaged on the westernmost Fugro 2D profile and where this channel is recognized deep in the stratigraphy on USGS 2D Profile PBS-T2. Because of this distance, the channel mapped

on Profile PBS-T2 is not included in the grid on Plate 3; instead, an approximate projection of the thalweg profile is shown. As shown on Plate 3, the thalweg gradient of Channel DCw is somewhat steeper than that of the other two channels west of the HFZ. This may be due to a slightly steeper gradient of the continental slope at this location (the modern slope is steeper here, as shown on Plate 1), or it may be that the shallowest channel is not imaged on Profile PBS-T2 because it is masked by the seafloor multiple, and that the downslope extension of Channel DCw is erroneously correlated to a deeper channel.

6.1.1.6   Other Possible Channels

Several additional possible channels or channel complexes are recognized east of the HFZ in the Estero Bay study area. These consist of Channel Fe and channels north of the 3D volume for the Estero Bay study area.

Channel Fe

Near the south end of the study area, the USGS 2D seismic-reflection Profile PBS-T1A shows a channel incised into the sedimentary section bounded by strands of the Point Buchon fault (described as a graben in PG&E, 2012), which is identified here as Channel Fe (Figure 6-7; Plate 3). This channel is located within an erosional trough carved into the top of bedrock (Figure 6-4). The trough extends north-south, bends downslope to the west, and opens westward toward the HFZ, reaching a depth greater than 200 m below modern sea level. This depth is greater than the lowest limit of Quaternary sea-level lowstands (Figure 1-6). The location on the shelf of the deepest part of the channel is currently experiencing tectonic uplift, indicating that Channel Fe was always submerged and that it was likely carved by submarine flows on the upper continental slope. The geometry of this incised trough is similar to the upper reaches of modern shelf-margin channels that are incised into bedrock, suggesting that the trough itself may be the filled remnant of an abandoned shelf-margin channel. The width and depth of this trough constrain the possible geometry of Channel Fe. Therefore, although Channel Fe is recognized on only one seismic-reflection profile (USGS Profile PBS-T1A), the general trend and location of its thalweg may be inferred to extend for a distance of approximately 1 km east of the primary strands of the HFZ.

Channels North of 3D Volume

A series of channels are recognized in USGS seismic-reflection Profile PBS-T1A that incise reflections from probable Quaternary strata that fill the broad paleo-embayment north of the 3D survey area and east of the HFZ (Figure 6-6). Individual channels cannot be correlated from one seismic-reflection profile to another due to variations in data resolution and line spacing. However, as with Channel Fe, limitations on the channel geometry are inferred from the shape of the bedrock embayment that the channels occupy (Figure 6-4). Structure contours on the top of bedrock show that this embayment deepens and widens westward, toward the HFZ, reaching a maximum depth of greater than 200 m below modern sea level. The inclined sides and sloping base of this bedrock paleo-embayment may represent the filled upstream reaches of a submarine channel that previously incised into the edge of the shelf at this location. Although reflections within

the embayment exhibit evidence for minor synclinal folding, clear truncations of reflections on its margins provide evidence for incision and channelization within. The strata that fill this embayment are estimated to range in age from Holocene to greater than 600 ka (Figure 6-5). These strata suggest that this embayment has persisted through much of the late Quaternary.

6.1.2   Discussion

This section provides interpretation and analysis of the data used in this study, based on the results described above. The discussion in this section includes the rationale for selecting the piercing points used for the estimation of offsets along fault strands of the HFZ in the Estero Bay study area, along with the ages used to determine slip rates.

6.1.2.1   Stratigraphy

All buried channels mapped in the Estero Bay study area likely formed on the upper continental slope, beyond the outer edge of the continental shelf. Each of the channels west of the HFZ incises reflections interpreted as continental slope strata (Figure 6-13; Plate 2). On both sides of the HFZ, the channels' thalwegs occur well below the depths of Quaternary eustatic sea-level lowstands, and thus appear not to have been sub-aerially exposed. As shown on Figure 1-6, the LGM and earlier sea-level lowstands are interpreted to have reached depths of approximately 120–125 m below modern sea level. A time slice from the 3D volume at approximately that depth (~120 m below sea level; ~159 ms TWTT) intersects the margins of key channels imaged in the volume (i.e., Channel Complex Ae, Channel Be, and Channel Complex De) and is clearly higher than their thalwegs, which reach depths of approximately 132–140 m (~165–175 ms TWTT) below modern sea level (Figure 6-10; Plate 3). The absence of reflections of Upper Pleistocene or younger strata in the eastern part of the 3D volume suggests that little to no accommodation has been generated at that location within the past 600 kyr and that the site is currently undergoing tectonic uplift. Previous studies of vertical separation across the HFZ also suggest that the east side of the HFZ is uplifting at this site (Hanson et al., 2004; PG&E, 2013). If this is true, then the channels east of the HFZ originally formed at a greater depth than their current position, well below the depth of the shelf break.

The location and pattern of deposition within the study area appear to have been influenced by local depositional accommodation caused by down-to-the-west vertical separation across the HFZ. This accommodation facilitated the deposition of upper Quaternary highstand and lowstand systems tracts west of the HFZ (Figure 6-1). It is also possible that the accommodation was large enough for channels to be completely abandoned west of the fault and that a series of small submarine fans developed that were spread along the primary trace of the HFZ. Alternatively, accommodation may have led to a transition from channel incision east of the fault to channel aggradation west of the fault, as suggested by the geometry of Channel DBw (Figure 6-14). Channel DBw is U-shaped where imaged on seismic-reflection profiles near the primary fault strand of the HFZ, suggesting aggradation within the channel, and V-shaped farther downslope from the fault, suggesting channel incision (see Profile PBS-T2; Figure 6-14; Plate 3).

The geometry and distribution of channels in Channel Complex Ae illustrate the effects of tectonic deformation from dextral slip along the HFZ. The western parts of all the channels in Channel Complex Ae (Figure 6-4) document uplift associated with an underlying anticline, and the older channels exhibit more deformation than the younger channels (Figure 6-9b). This pattern indicates that fold growth continued while the channel complex was developing.

Fluvial Pathways

Three nearshore channels imaged using the MBES bathymetry within the Estero Bay study area are incised into exposed bedrock (dashed blue lines on Figure 6-15). The northern channel is a narrow sinuous channel that heads offshore of Hazard Canyon and can be traced offshore to about the 30 m isobath, where it is buried by sediment. Two possible offshore extensions of this channel are shown on Figure 6-15. The two other channels are located to the south and are wider, more sinuous, and more deeply incised than the northern channel. The southern channels extend offshore from the mouths of Islay and Coon Creeks. Each of these channels widens seaward and at approximately 40–50 m depth is buried by a broad deposit of post-glacial sediment and mobile sand sheets. None of the channels were observed beneath the sediment in the 3D/2D data set collected offshore of Coon Creek and the Point Buchon area (PG&E, 2012).

The sinuous nature of these bedrock-incised channels and their clear association with creeks onshore indicate that they are fluvial in origin and crossed the continental shelf during Pleistocene sea-level lowstands (PG&E, 2011b). None of these channels can be directly correlated with the slope channels described in Section 6.1.1 and shown along the west side of Figure 6-15. No other nearshore channels exist to the south of the study area that could be correlated with the offshore buried channels described here.

6.1.2.2   Faults, Channel Correlations, and Estimated Offsets

Buried paleochannels identified in the Estero Bay study area that cross the HFZ are potential piercing points that can be used to estimate offsets. Correlation of channels from one side of the HFZ to the other is critical to estimating the amount, sense, and rate of displacement across the fault zone.

Correlation of Channels De and Ee1

Of the six channels or channel complexes observed in the study area east of the HFZ, three were considered good potential piercing points. The geometries of the channels located in the bedrock embayment north of the 3D volume, and of Channel Fe within the graben and erosional trough in the south (Figure 6-15) are not as clearly defined as the other three channels, but were found useful in substantiating offsets of the better-defined channels.

The three well-imaged channels and channel complexes in the Estero Bay 3D volume that lie east of the HFZ are considered better potential piercing points. Two of these, Channel Complex Ae and Channel Be, are truncated by the primary eastern fault strand (fault 11006) of the HFZ and are not observed on the west side of that fault (Plate 3), and thus cannot be used as piercing points. Therefore, of the channels observed in the Estero

Bay 3D volume, only Channel Complex De may be correlated across fault 11006. As shown on Plate 3, Channel Complex De extends downslope to the west and is interpreted to be dextrally offset to the north across fault 11006, where it appears to correlate with Channel Ee1. The flattened image of Channel Ee1 (Figure 6-12) shows it to be similar in width and incised to a similar depth as Channel Complex De (Figure 6-11; Plate 3). Correlation of the thalwegs of Channel Ee1 and Channel Complex De suggests a right-lateral separation of 260 ± 60 m and a vertical separation of 40 ± 8 m (50 ± 10 ms TWTT), down to the west, across fault 11006 (Figure 6-16).

Correlation of Channel De-Ee1 to Channels West of HFZ

Of all the channels and channel complexes observed on USGS profile PBS-T2 west of the HFZ (Plate 2), three channels, DAw, DBw, and DCw, are imaged on the Fugro 2D profiles to extend far enough east to be viable candidates for the downstream continuation of Channel D3-Ee1 (Plate 3). These three channels are similar in width (~250–450 m), depth of incision (~20–50 m), and gradient to the combined Channel De-Ee1 (Plate 3). Channel DCw is rejected as a candidate downslope extension of Channel De-Ee1 because this correlation would require either left-lateral slip on the HFZ or a left jog of over 1 km of the channel axis. Left-lateral slip along the HFZ is not compatible with the regional tectonic models (Lettis et al., 1994, 2004) or previous research on the HFZ that clearly documents evidence for right-lateral movement (Hall et al., 1994; Hanson and Lettis, 1994; Hanson et al., 2004; Johnson and Watt, 2012). A left jog in the channel would require the channel to extend parallel to and along the primary trace of the HFZ for more than 1 km before bending again and extending downslope to the southwest along the course of Channel DCw. The existence of such a fault-parallel channel within the requisite depth is not seen in seismic-reflection Profile PBS-19 or in the southwestern part of the 3D volume. Rejection of Channel DCw as a candidate piercing point through correlation with Channel De-Ee1 allows consideration for one of the following correlations:

- Channel DBw is the offset equivalent downslope extension of Channel De-Ee1.
- Channel DAw is the offset equivalent downslope extension of Channel De-Ee1.
- One of the intervening channels observed deep in the stratigraphy of Plate 2 is the offset equivalent downslope extension of Channel De-Ee1.
- None of the mapped channels are correlatable to Channel De-Ee1.

To evaluate alternative channel correlations, slip was restored on the primary traces of the HFZ (Figure 6-17) to match potential offset equivalent channels across the fault zone and evaluate the regional implications of the correlations. Two alternative correlations were tested. In both correlations, 250 m of slip was restored on the primary eastern strand of the HFZ, fault 11006, to align the thalweg of Channel Complex De with Channel Ee1. Correlation A (Figure 6-17a) illustrates a correlation of Channel De-Ee1 with Channel DBw by restoring 850 m of slip on the primary western trace of the HFZ, fault 10001. Correlation B (Figure 6-17b) illustrates a correlation of Channel De-Ee1 with Channel DAw by restoring 4,850 m of slip on the primary western trace of the HFZ. These two alternative correlations are discussed below, followed by brief discussions of the two other correlation scenarios described above.

Alternative A: Correlation of Channel De-Ee1 with Channel DBw

The correlation of Channel De-Ee1 with Channel DBw is strongly favored because it is the simplest correlation that is supported by geomorphic and tectonic evidence. Each of the five channels observed west of the HFZ is paired with a candidate channel east of the fault. The most compelling arguments in favor of Alternative A are listed below:

- It aligns Channel DBw, the best expressed and most continuous channel west of the HFZ, with Channel De-Ee1, the best expressed and most continuous channel east of the HFZ.
- It approximately aligns Channel DAw with the broad, channelized embayment north of the 3D volume.
- It approximately aligns Channel DCw with the bedrock-incised erosional trough that contains Channel Fe.

Channel DBw trends in a similar direction, is incised to a similar depth, and is slightly wider than Channel De-Ee1. The upstream end of Channel DBw is nearly equivalent in width and depth of incision as the downslope end of Channel Ee1 (Plate 3). These comparisons are consistent with both channels being offset parts of a single paleochannel that widens and deepens to the west (Plate 3). Therefore, these relationships suggest that Channel DBw is a favorable offset equivalent of the downslope extension of Channel De-Ee1.

The approximate geometry of the paleo-embayment north of the 3D volume is illustrated by contours on top of the bedrock shown on Figures 6-4 and 6-15. The localization of stacked unconformities within reflections of probable Quaternary strata that fill the paleo-embayment indicates that this embayment has persisted through much of the late Quaternary, possibly due to ongoing folding (Figures 6-5 and 6-6). The truncation of older reflections by unconformity T05 near the base of the section (Figure 6-6) indicates that localized incision into a depositional basin occurred at this location shortly after the formation of the deep channels west of the HFZ (Channels DAw, DBw, and DCw). If this embayment served to channelize downslope submarine flow prior to development of unconformity T05, the embayment then may represent the upstream extension of Channel DAw.

Although Channel Fe is imaged on only one 2D seismic-reflection profile, the approximate trend of the channel may be inferred from the geometry of the incision into bedrock. Contours on the top of bedrock suggest that a precursor to Channel Fe incised into bedrock and created the erosional trough that the channel currently occupies. This trough descends to more than 200 m (>250 ms TWTT) depth as it approaches the HFZ. The incision into bedrock widens to approximately 0.5 km near its intersection with the HFZ. These dimensions are compatible with those of Channel DCw, which range up to approximately 470 m wide, and its thalweg reaches a depth of approximately 270 m (~340 ms TWTT) below modern sea level at its upslope end. These comparisons suggest that the erosional troughs occupied by Channels Fe and DCw are favorable candidates for offset equivalents of the same channel.

It is possible that the two deep channels imaged on the USGS sparker Profile PBS-T2 between Channels DAw and DBw are the downslope parts of Channel Complex Ae and Channel Be (see Figures 6-14 and 6-17). However, no intervening channels were seen in the Fugro 2D data west of the HFZ to establish this correlation.

Precise constraints on the amount of offset implied by Alternative A may be measured from the offset thalwegs of Channel DBw from Channel Ee1 (Figure 6-16). Two sources of uncertainty in the offset of this channel exist. The first is uncertainty in the projection of the channel thalweg, from where it is mapped on each side of the fault to where it intersects the fault. The second is based on the mapping of Channel DBw itself. Channel DBw is not as well imaged near fault 10001 as it is farther from the fault (Figure 6-14b). On the nearest profile to the fault, two channel-like features are recognized that could represent the upslope extension of Channel DBw. Although the southern channel-like feature appears more likely to be the upslope continuation of Channel DBw, the northern channel-like feature is also considered to be a candidate equivalent channel (Figure 6-16). Therefore, uncertainty in the thalweg offset measurement is large. The best estimate of horizontal offset across the primary trace of the HFZ (fault 10001) is between approximately 700 and 1,000 m. Based on the uncertainties described above, the maximum horizontal offset is 1,650 m and the minimum is 450 m (Figure 6-16). The vertical separation is 100 ± 25 m, down to the west.

Alternative B: Correlation of Channel De-Ee1 with Channel DAw

The correlation of Channel De-Ee1 with Channel DAw is rejected for the following reasons:

- It aligns Channels DBw and DCw with a section of the middle shelf where the smooth top-of-pre-Quaternary-bedrock surface indicates that deep channel incision is absent.
- It aligns Channel Fe with a section of the outer shelf/upper slope where continuous reflections in the seismic stratigraphy show no obvious channels incising strata beneath the outer continental shelf.

The juxtaposition of Channel DBw with a section of the middle shelf that contains a relatively smooth, unbroken top-of-bedrock surface is a particularly compelling argument against Alternative B. The erosional surface at the top of pre-Quaternary bedrock here is between approximately 80 m and 100 m (~100 ms and 125 ms TWTT) below modern sea level. No channel is eroded into the top of rock east of the HFZ at this location, as shown by the structure contours on Figure 6-17. This observation is confirmed by examination of the Point Buchon 3D volume, which clearly images the top of pre-Quaternary bedrock along HFZ in this area (PG&E, 2012). The east end of Channel DBw is imaged at a depth of between approximately 265 m and 305 m (~330 ms and 380 ms TWTT) and is at least 200 m wide, and incised approximately 20 m deep. Given the dimensions of this channel where it is truncated by the primary strand of the HFZ (fault 10001), it is likely that the channel extended farther to the east at the time it formed. This alternative could be feasible if the upslope part of Channel DBw were uplifted and eroded. However, based on the significant depth of Channel DBw, approximately 200 m of vertical separation across the primary strand of the HFZ since Channel DBw formed would be required to

remove any upslope part of the channel. At the post-ELP vertical separation rates of 0.09 to 0.14 mm/yr calculated by Hanson et al. (2004), and the late Quaternary vertical separation rates indicated by offset unconformities across the HFZ of approximately 0.07 to 0.2 mm/yr (PG&E, 2013), it would require between 1 and 3 million years for this vertical separation to occur. As described below in Section 6.1.2.2, available constraints on the age of Channel DBw indicate that it is between 1,530 and 590 ka (within 90% confidence).

Alternative C: Correlation of Channel De-Ee1 with Unnamed Channels on Profile PBS-T2

The two deep channels observed at depth on Profile PBS-T2, located between Channels DAw and DBw, could possibly correlate with Channel De-Ee1, although these channels appear not to extend eastward to the HFZ. However, using the same line of reasoning as for Alternative B, the correlation of Channel De-Ee1 with one or the other of the unnamed channels on Profile PBS-T2 is considered unlikely because such a correlation would juxtapose Channel DCw, and possibly also Channel DBw (depending on which unnamed channel is considered correlative with Channel De-Ee1), with a section of the middle shelf where the smooth top-of-pre-Quaternary-rock surface indicates that deep channel incision is absent.

Alternative D: No Correlation

A fourth possibility exists in which the channels east of the HFZ are completely independent of the channels west of the HFZ. If this is true, then no offset equivalent channels exist in the Estero Bay study area, and a slip rate cannot be calculated. This possibility is considered unlikely because the channels east of the fault are interpreted to have developed in a continental slope environment. Therefore, it is very likely that the parts of the channels imaged east of the HFZ are the uppermost reaches of channels that once extended farther down the slope, like those shown on Plate 2.

6.1.2.3   Age Constraints

Channel DBw is bracketed stratigraphically by two key unconformities (Figure 6-14). This stratigraphic bracketing facilitates the estimation of ages of the channel; thus, using the combined Channels DBw, De, and Ee1 (named here "Channel DBw-Ee1-De") as the preferred piercing point for estimating offset along the HFZ (see Table 6-1), a slip rate along the fault zone can be calculated.

The ages of the bounding unconformities represent absolute limiting minimum and maximum ages for offset of Channel DBw-Ee1-De. The lower unconformity is the ELP unconformity, which was mapped and correlated by Willingham et al. (2013) and is estimated to be between approximately 3.5 and 2.7 Ma, based on microfossil data from wells west of Purisima Point in the southern offshore Santa Maria Basin. Thus, the ELP provides a limiting maximum age of 3.5 Ma for the channel. The upper unconformity is T05, which marks the transition of the western part of the Estero Bay study area from a slope to a shelf environment. We consider the possible age of unconformity T05 to be greater than 540 ka (the age of the MIS 14 lowstand) and less than 1.4 Ma (the onset of

the MPT), as reported by Bintanja and van de Wal (2008; Figure 6-2). Therefore, we use 540 ka as a minimum age for offset of the channel.

It is likely that Channel DBw-Ee1-De is significantly older than 540 ka and much younger than 3.5 Ma. As shown on Figures 6-1 and Plate 2, Channel DBw is buried well below unconformity T05. The depth of burial is at least 40 m (~50 ms TWTT) on Figure 6-1 and at least 32 m (~40 ms TWTT) on Plate 2. A preferred age of approximately 700–630 ka is estimated for unconformity T05, based on the onset of large-scale sea-level fluctuations at the end of the MPT (Figure 6-2). Therefore, the probable age of Channel DBw is somewhat older than 630 ka.

Unconformities H10, H30, H40, H45, and H48 are interpreted as surfaces of erosion caused by sea-level transgressions that followed lowstands during MIS 2, MIS 6, MIS 8, MIS 10, and MIS 12, respectively (Figure 1-6; Section 6.1.1.1). Reflections below unconformity H48 overlie and downlap onto unconformity T05 (or a reflection slightly above it) in a pattern typical of highstand systems tracts (Posamentier and Allen, 1999). This relationship suggests that unconformity T05 predates the MIS 13 highstand and, therefore, must be at least as old as the MIS 14 lowstand. Therefore, a minimum age of 540 ka is used as the limiting minimum age for Channel DBw-Ee1-De (Figure 6-2; Table 6-2).

A preferred age range is estimated based on consideration that additional unconformities recognized deep in the stratigraphy might also represent a record of separate paleo–sea-level cycles. These deeper unconformities are not as pronounced as the shallower unconformities within the upper-shelf-margin stratigraphic sequence (Figure 6-1). However, sea-level fluctuations prior to MIS 16 appear to be less extreme than those represented by the shallower unconformities (Figure 6-2), suggesting that less pronounced unconformities might be expected. Because they are less pronounced, the number of unconformities that exist between T05 and Channel DBw-Ee1-De is not certain. Two unconformities are shown within this interval on Plate 2 and Figure 6-1, suggesting that this interval may contain the reflections of deposits from two full sea-level cycles. Evidence for these is not strong, however, and the strata within this interval may result from fewer or more sea-level cycles. To account for this uncertainty, a preferred age range for Channel DBw-Ee1-De is estimated to be broad and is defined by the range between 630 ka (MIS 16, the most likely age of unconformity T05) and 900 ka (approximately four sea-level cycles earlier; see Figure 6-2; Table 6-2).

A limiting maximum age is estimated to be 1 Ma, based on the consideration that the interval between unconformity T05 and Channel DBw-Ee1-De contains deposits from an additional two sea-level cycles that are not recognized as unconformities in the seismic-reflection profiles (Figures 6-1and 6-2; Table 6-2). This limiting maximum age is selected to reflect the high likelihood that the channel is much younger than the absolute limiting maximum age of 3.5 Ma.

An alternative estimate for the age of Channel DBw-Ee1-De is based on the interpretation that the channel was abandoned and buried as a result of long-term climatic changes affecting the study area. Within this age model, channel abandonment and burial likely resulted from changes in the rate or style of sedimentation associated with the

MPT. Outgrowth of the shelf during the extreme MIS 16 sea-level lowstand at the end of the MPT followed this change in style of sedimentation. Consequently, 630 ka represents a limiting minimum age of the channel (Figure 6-2; Table 6-2).

A preferred age range of 1.4 Ma to 700 ka for abandonment of Channel DBw-Ee1-De is estimated to coincide with the duration of the MPT (Figure 6-2; Table 6-2). A limiting maximum age of 3.5 Ma is taken from the maximum age of the ELP (Figure 6-2; Table 6-2).

6.1.2.4   Slip Rates

The calculation of the slip rate for the HFZ is based on the offset of Channel DBw-Ee1-De, which requires dividing the amount of fault offset by the age of the piercing point. The parameters for both estimated offsets and estimated ages include inherent uncertainty. Uncertainty is represented by preferred ranges, and the limiting minimum and maximum constraints, which are described above and summarized in Tables 6-1 and 6-2.

Table 6-1. Estimated Offset of Channel DBw-Ee1-De and Constraints on Uncertainty

Fault 11006 (East)	Offset (m)	Fault 10001 (West)	Offset (m)
Minimum	200	Minimum	450
Preferred low	**230**	**Preferred low**	**700**
Preferred high	**290**	**Preferred high**	**1,000**
Maximum	320	Maximum	1,650

Table 6-2. Estimated Age of Channel DBw-Ee1-De and Constraints on Uncertainty

Age Model: Stratigraphic Approach (Weight 0.9)	Age	Age Model: Climatic Approach (Weight 0.1)	Age
Minimum	540 ka	Minimum	630 ka
Preferred low	**630 ka**	**Preferred low**	**700 ka**
Preferred high	**900 ka**	**Preferred high**	**1.4 Ma**
Maximum	1.0 Ma	Maximum	3.5 Ma

Offset Estimates

The total offset of Channel DBw-Ee1-De across the two primary strands of the HFZ in the Estero Bay study area is calculated by summing both the eastern and western offset values. Offset estimates used for Channel DBw-Ee1-De across the eastern and western strands are presented in Table 6-1. Based on these distributions, the mean combined offset across both channels is 1,230 +450/–390 m within a 90 percent confidence interval.

Age Estimates

The age of Channel DBw-Ee1-De is characterized by the combination of two age assumptions as described above. These assumptions are not considered equally valid and, therefore, are combined into a joint probability distribution, but are weighted unequally. The stratigraphic assumption is subjectively assigned a high weight of 0.9 because it is considered more likely to accurately represent the true age of the abandonment of Channel DBw-Ee1-De. The climatic assumption is subjectively assigned a low weight of 0.1 because these greater ages are considered unlikely to be correct (but they also cannot be ruled out). This combination of age assumptions yields a mean age of 840 +690/–250 ka within a 90 percent (high) confidence interval.

Slip Rates

Dividing the combined offset distribution by the combined age distribution yields a Quaternary slip rate for the HFZ of 1.6 ± 0.8 mm/yr within a high (90%) confidence level. This range describes the most likely slip rate for the HFZ within the Estero Bay study area over the past approximately 1 Myr, and it accurately represents the uncertainty in slip rate if the channel correlation (Alternative A) is correct and the age model adequately captures the true age uncertainty. However, if this channel correlation is incorrect, and the true correlation involves more slip on the fault (such as the correlations described in Alternatives B and C), then the calculated slip rate will be higher. Whereas alternative correlations are not supported by the available data, the data are not adequately resolved to preclude alternative correlations. Thus, our offset and slip-rate estimates are subject to model uncertainty, and future data collection efforts may focus on testing alternative channel correlations.

6.2   The Point Sal Study Area

The Point Sal 3D study area (Survey Area 3) was selected to identify and evaluate piercing points for use in determining offsets and estimating slip rates along the HFZ. The stratigraphy, structure, buried channel morphology, and piercing points in the Point Sal study area (Figure 1-1; Plate 1B) are presented in this section. Primary interpretations are based on the Point Sal 3D LESS data set (Plate 1B), while regional structural and stratigraphic interpretations outside the study area are based on 2D seismic-reflection profiles found in the PG&E legacy data archives and USGS seismic-reflection data collected in 2009 and 2010 (Figure 6-18).

Previous mapping in the area (Jennings and Bryant, 2010) shows that to the west of Point Sal, and east of the 120 m isobath, the HFZ is made up of a single fault splay (Figure 1-1) where it is located between the outer and middle continental shelf. The edge of the continental shelf (shelf break) is approximately coincident with the 125 m isobath located approximately 3 to 4 km west of the area. To the north, in San Luis Obispo Bay, the shelf broadens and the HFZ traverses the outer continental shelf (Plate 1B).

6.2.1   Results

The 3D volume generated from the seismic-reflection data was used to define geologic structure (e.g., faults) and geomorphic features (e.g., buried paleochannels). This resulted in the identification and mapping of features that can be used as potential piercing points to determine displacement along faults.

6.2.1.1   Stratigraphy

The 3D data and PG&E legacy archive seismic-reflection profiles were used in conjunction with offshore well data to identify seismic reflections and seismic signatures corresponding to lithologic units and unit boundaries (unconformities) in the Point Sal 3D volume. The stratigraphy of the Point Sal study area documents a transition from a middle continental shelf to a shelf break/upper-slope environment. Three stratigraphic units were identified in the data from the study area and are informally named "Mesozoic basement rocks and Neogene strata," "unnamed Pleistocene deposits," and "uppermost Pleistocene-Holocene deposits." Several major unconformities were also identified: the ELP unconformity, the "near top of Neogene" (NTN) unconformity, and the "late Quaternary" unconformities. The late Quaternary unconformities developed during glacially induced lowstands in sea level, as discussed in Sections 1.2.8 and 6.1.

Outcrops of Neogene and older bedrock are present in the offshore Point Sal study area (Plate 1B). These older rock units (Figure 1-5) underlie Quaternary sediments.

Mesozoic Basement Rocks and Neogene Strata

Mesozoic basement rocks include Jurassic-age Point Sal Ophiolite and Jurassic- to Cretaceous-age Franciscan Complex mélange. Neogene marine rocks in the Point Sal 3D study area include the stratified Miocene-age Point Sal and Monterey Formations and the Miocene-Pliocene Sisquoc Formation.

Unnamed Pleistocene Deposits

Inferred Pleistocene sediment and local late Pliocene deposits are based on well-layered, fairly continuous reflections observed overlying the top of bedrock. There are numerous unconformities in the unnamed Pleistocene deposits unit, likely resulting from erosional and depositional events during sea-level fluctuations throughout the Pleistocene. Channelized deposits of inferred middle to late Quaternary age are locally present in this unit (Figures 1-8 and 1-9).

Uppermost Pleistocene–Holocene Deposits

The uppermost Pleistocene–Holocene deposits (<20 ka) of the youngest, uppermost stratigraphic unit in the study area were deposited during and after the approximately 120–130 m sea-level rise following the MIS 2 LGM (Figure 1-6). Sedimentary layers of this unit are characterized on seismic-reflection profiles as low- to moderate-amplitude, low- to high-frequency, parallel, fairly continuous reflections (Johnson and Watt, 2012). However, in some areas, the Holocene deposits appear unstratified and acoustically transparent and homogeneous. The Holocene marine deposits in the 3D survey area are not resolvable in most of the northern part of the area and thicken toward the south.

Analogous post-LGM Holocene shelf facies have been identified and mapped in many other locations along the California Central Coast (e.g., Grossman et al., 2006).

Early–Late Pliocene/Near Top of Neogene Unconformities

The ELP unconformity is a prominent horizon in the late Pliocene section throughout the Santa Maria Basin (Willingham et al., 2013); the middle Pliocene strata are reportedly absent in all wells drilled in the basin (J. Rietman, pers. comm., 2013), likely the result of erosion during the onset of regional compression and uplift during the mid-Pliocene (Sorlien et al., 1999). This unconformity is imaged seismically as a combination of truncated reflections and variations in the seismic signatures representative of the upper Sisquoc Formation and overlying unnamed sedimentary units (Willingham et al., 2013). Figure 6-19 illustrates the ELP unconformity on GSI Line 97 in central San Luis Obispo Bay (Figure 1-10 and Figure 6-18 inset; see also Figures A-1 and A-2 in Appendix A).

In addition to the ELP unconformity, a shallower unconformity imaged by deep-penetration 2D seismic-reflection profiles, the NTN unconformity is present across basement highs in much of the offshore Santa Maria Basin (Figures 6-19 through 6-21). Willingham et al. (2013) refer to this as a possible Wheelerian-Hallian unconformity.

Locally, near the HFZ, the ELP and NTN unconformities merge into a single erosional surface. Where the NTN unconformity cuts across large folds and faults, it truncates the ELP unconformity (Figure 6-19). This erosional surface is recognized throughout the Point Sal 3D study area as a high-amplitude basal reflection that represents the top of the Mesozoic basement rocks and Neogene strata (Figures 1-5, 6-19, and 6-20) and is referred to here as the ELP/NTN unconformity (Figure 6-19). It generally underlies gently folded Quaternary-age reflections (Figure 6-22); however, locally, these reflections are strongly folded and faulted where they are in close proximity to Quaternary-active structures, as apparent in time slices obtained from the 3D volume (Figures 6-23, 6-24, and 6-25) and in 3D seismic-reflection profiles (e.g., Figure 6-26).

In most areas of the 3D data set, the ELP/NTN unconformity is recognized as the interface between well-imaged coherent reflections (inferred to be Quaternary sediments) and chaotic or semitransparent acoustical units (inferred to represent the underlying bedrock). On the 2D deep-penetration high-energy seismic survey (HESS) seismic-reflection profiles west of the HFZ (Figures 6-19 and 6-20), an inverse relationship is observed: reflections representing Quaternary reflections above the NTN unconformity appear to be less stratified and continuous as in the Miocene and early Pliocene units.

The age of the ELP/NTN unconformity is constrained by offshore well data, but it encompasses a variable and broad range of time and varies by location. The age of the ELP unconformity has been estimated by Willingham et al. (2013) to be approximately 3.5–2.7 Ma (Figure 1-5). The age of the NTN unconformity is interpreted to have formed between approximately 2.5 Ma and 2 Ma. In this study, the estimated age range of the combined ELP/NTN surface is 3.5–2.0 Ma. The extents and mapped surface of the NTN/ELP unconformity in the Point Sal 3D study area are shown on Figure 6-21.

The "unnamed" Pleistocene deposits overlie the NTN/ELP unconformity (Willingham et al., 2013), and underlie a transgressive erosion surface (<20 ka) associated with the latest

Pleistocene sea-level rise subsequent to the LGM (Johnson and Watt, 2012). These surfaces are commonly characterized on seismic-reflection profiles as continuous parallel to subparallel, moderate to high-amplitude, high-frequency reflections (Johnson and Watt, 2013).

Correlation of ELP/NTN Unconformity with Well Data

Regional 2D seismic-reflection profiles and exploratory well data were used to characterize and date the key ELP/NTN unconformity mapped in the 3D data set. Seven exploratory wells and several 2D seismic-reflection profiles from PG&E legacy archive (Figure 6-18) were used to map Quaternary and Neogene stratigraphic boundaries (unconformities) identified in previous investigations, which focused on the deformational nature of the HFZ and the regional offshore Santa Maria Basin structures (Sorlien et al., 1995, 1999; Willingham et al., 2013). Most of the exploratory wells used in this study are located within 5 km of the Point Sal 3D study area (Figure 6-18).

The seismic stratigraphic nomenclature, formation and unconformity names and ages, and well data used in this correlation are modified from Willingham et al. (2013). Seismic-reflection horizons interpreted from the PG&E 2D deep-penetration legacy archive lines (Figures 6-19, 6-20, A-1, and A-2) include the following:

- The top of Miocene unconformity (~5.5–5.1 Ma).
- The ELP unconformity (~3.5–2.7 Ma).
- The NTN unconformity (~2.6–1.8 Ma).

To map these stratigraphic boundaries, the interpreted unconformities (reflections) were digitized across seismic reflections that corresponded to the time-converted values of the stratigraphic picks on the well logs, or reflections that correlated to an unconformity near a stratigraphic well pick. Wells used in this study are listed in Table 6-3 below.

Table 6-3. Offshore Wells Used in This Study

Exploratory Well	Surface Easting	Surface Northing	2D Seismic Tie Line
415-1	699465	3862779	H-2028
415-2	700677	3861684	H-2028
397-1	701304	3874861	SM85-201
409-3	701364	3867189	SM85-203
060-1	693748	3877422	SM85-205
416-1	701724	3859832	H-2026
422-1	701841	3857308	H-2024

Late Quaternary Unconformities

Several shallow upper Quaternary unconformities were mapped in the Point Sal 3D data set. Horizons H10, H30, and H40, which were previously identified from interpretations of seismic-reflection profiles in a regional sequence-stratigraphy study (PG&E, 2013) and mapped in the Estero Bay study area, were used to correlate the Point Sal 3D data set

with these horizons. These Quaternary unconformities provide a rough geochronologic framework and inferred age estimates (Figure 1-6) of the upper Quaternary sedimentary units mapped in the investigation region (PG&E, 2013).

The unnamed Pleistocene deposits are bounded above by the H10 horizon (PG&E, 2013), and below by the NTN/ELP unconformity (Figure 1-5). The mapped distributions of reflections H10 and H30 and the NTN/ELP unconformity in the Point Sal study area are shown on Figure 6-21.

Integration of Statigraphic and Structural Data

The ELP/NTN unconformity, fault traces, and paleochannels incised into Quaternary strata are clearly visible on the time slices from the 3D volume (Figure 6-26). A shallow time slice at 150 ms (Figure 6-23 shows channel fill deposits from Channels Ee and Fe) bounded on the south by bedrock, to the north by Quaternary strata, and to the west by the Hosgri fault. A time slice at 180 ms, located in the northern part of the 3D survey area (Figure 6-24), shows isoclinal folds in Quaternary strata to the east of the Hosgri, the ELP/NTN unconformity and underlying Neogene strata, and Quaternary channel fill deposits of Channels Ac and Aw in the axis of a broad syncline (Figure A-3). A deeper time slice at 213 ms in the same area (Figure 6-25) clearly shows the HFZ, Quaternary channel fill deposits Ac and Aw in a structural syncline, older, strongly folded Quaternary strata, the ELP/NTN unconformity, and underlying Neogene strata. Structural results for the Point Sal study area are presented in Section 6.3.2.

6.2.1.2   Faults

The HFZ is the dominant structural feature within the Point Sal study area. A restraining bend of the zone at the southwestern boundary of Casmalia/Point Sal structural block appears to influence the structural pattern of the area (Figure 1-2; Plate 1B). Here the structural block is impinging upon the HFZ, where significant changes in structural style take place, such as changes in fault orientation at the intersections of faults (Hanson et al., 2004; Johnson and Watt, 2012; Sorlien et al., 1999).

Faults within and adjacent to the HFZ were primarily identified and mapped using 3D seismic amplitude data (Figures 6-23, 6-24, and 6-25) and refined using the smoothed similarity time slices (Figure 6-27). The results of the high-resolution fault mapping for this study show that the HFZ is considerably more complex than previously mapped (Figure 6-28). Previous investigators (e.g., Jennings and Bryant, 2010) depicted the HFZ as a single fault trace located west of Point Sal. Willingham et al. (2013) showed several subparallel fault traces, with a single primary fault strand west of Point Sal (Figure 6-28). Relative to the previous mapping efforts (Jennings and Bryant, 2010; Johnson and Watt, 2012; Willingham et al., 2013), the most significant changes in the Point Sal 3D study area are as follows:

- Recognition of three primary HFZ fault strands (eastern, central, and western) and several secondary fault splays in the broad paired bend of the HFZ (Figure 6-27).

- Extension of the Lions Head fault farther to the west to near the eastern strand of the HFZ (Figures 6-28 and 6-29).

- Detailed refinement of fault mapping throughout the 3D study area (Figure 6-27), as well as throughout San Luis Obispo Bay and offshore Point Sal (Figure 6-28; Plate 1B).

The Hosgri Fault Zone

A distinct change in structural style occurs from south to north in the Point Sal study area, with the HFZ splitting from a single splay in the south to multiple splays in a broad paired fault bend, which then converge into a single fault splay in the north (Figure 6-30). The strike of the HFZ in the southern part of the study area is 336 degrees, and in the northern part, 330 degrees. To the north of the 3D survey area, the HFZ extends north-northwest across San Luis Obispo Bay with an average trend of 340 degrees (Johnson and Watt, 2012), approximately 10 degrees more northerly than the strike of the fault in the northern portion of the 3D study area (Plate 1B).

An abrupt change in strike of the eastern strand of the HFZ occurs near the center of the study area, approximately 2 km south of the Lions Head fault (Figure 6-28). Seismic-reflection profile Crossline 8200 (Figure 6-31) illustrates the relatively simple structure of the HFZ in the southern part of the study area. At this location, the eastern and western strands of the HFZ bound a localized graben in a small releasing bend. The structural blocks to the east of the HFZ are uplifted relative to the Western (Santa Maria Basin) block (Figures 6-27 and 6-34). On seismic-reflection profile Crossline 9140, located in the central part of the study area (Figure 6-32), the central structural block is uplifted and folded into a broad (1,200 m wide) anticline. This anticline is cut by many short secondary faults, as well as by the central strand of the HFZ. The western strand of the HFZ bounds the west side of the uplifted central structural block and is interpreted as a paired-bend bypass fault. Farther north, within the restraining bend, seismic-reflection profile Crossline 9360 (Figure 6-33) shows the central structural block to be uplifted and the crest of the anticline truncated. In this area, reflections representative of Holocene sediments (H10 and younger) appear to directly overlie a reflection at the top of strongly folded pre-Neogene strata. In the northern part of the 3D study area, the multiple strands of the HFZ identified and mapped in the paired fault bend converge to form a single fault splay that exhibits little apparent vertical separation of the uppermost Pleistocene–Holocene deposits (Figures 6-27 and 6-34).

The eastern strand of the HFZ locally appears to vertically displace unconformity H10, and possibly upper (younger) horizons, by approximately 4 ± 2 m (~5 ms; Figure 6-21b). Both the eastern and western strands of the HFZ offset reflection H30 (Figures 6-21c and 6-31). All the mapped faults appear to offset and/or fold the ELP/NTN unconformity (Figures 6-21a, 6-32, 6-33, and 6-34).

To the north of the Lions Head fault, the ELP/NTN unconformity and overlying reflections exhibit tight folding, with northwest fold vergence (Figure 6-29). A series of short faults bifurcate the central structural block. These faults vary in length from approximately 150 to 1,500 m. The northern termination of this set of faults is approximately coincident with the eastern strand of the HFZ to the north of a 20-degree bend in the fault zone (Figure 6-27). Several of the short faults cut and dextrally offset the ELP/NTN unconformity along the axis of Anticline Ac (Figure 6-34). Additional

short faults are also imaged west of the central strand of the HFZ in the 3D volume, but they are not as common as to the east (Figures 6-27 and 6-34).

The Lions Head Fault Zone

The integrated mapping of the LESS 3D data, which includes the previously collected deep-penetration PG&E legacy archive data and USGS 2D seismic-reflection profiles, indicates that the northwest-trending Lions Head fault zone converges with the HFZ in the 3D study area (Figure 6-28). There is an approximate 10-degree restraining bend in the eastern strand of the HFZ approximately 1,400 m south of this point of convergence. This bend is approximately 1,200 m north of the 20-degree releasing bend in the eastern strand of the HFZ (Figure 6-27). The primary Lions Head fault strand is vertical to steeply dipping where imaged in the 3D data and expresses approximately 35 m vertical displacement of the ELP/NTN unconformity (Figure 6-29b). Uplift to the north of the intersection of the Lions Head fault with the HFZ is suggested by the absence of the H10 unconformity and Holocene sediments (Figure 6-21).

The Casmalia Fault Zone

The Casmalia fault zone lies outside the Point Sal 3D LESS study area; therefore, only the PG&E 2D legacy archive data and reconnaissance 2D seismic-reflection data collected for this study in 2012 were used to characterize and map the fault zone. The surface trace of the Casmalia fault zone, as modified after Sorlien et al. (1999), Lettis et al. (2004), Jennings and Bryant (2010), Johnson and Watt (2012), PG&E (2013), and Willingham et al. (2013), is shown on Figure 6-28b and Plate 1B. Several subparallel fault traces extend from the coast approximately 2 km north of Mussel Point toward the west-northwest and extend approximately 12 km offshore to near the south end of a trace of the HFZ in south-central San Luis Obispo Bay. The Casmalia fault forms the northern boundary of the Casmalia/Point Sal block (Figure 1-2).

The Blind Thrust Fault NE

A buried thrust fault, referred to here as the "Blind Thrust fault NE," is interpreted to lie beneath the folded ELP/NTN unconformity (Figure 6-29). Seismic reflections representative of Quaternary and Neogene strata above and below the ELP/NTN surface are uplifted and folded in the hanging wall of the inferred blind thrust fault (Figures 6-24 and 6-34b, d). Given the observed structural and stratigraphic relationships, some shortening may have occurred along the ELP/NTN unconformity itself prior to folding (Figure 6-29). Analogous low-angle faulted unconformities have been recognized elsewhere in California, including onshore in the Great Valley (O'Connell et al., 2001) and offshore Southern California (Rivero and Shaw, 2011). Transpressional deformation is also evidenced by isoclinal folds in reflections of possible Quaternary strata above the ELP/NTN unconformity (Figures 6-24 and 6-25), and in northeast-southwest-verging shortening beneath, along, and in reflections above the ELP/NTN surface. Deformation of all the mapped reflections in the section above the ELP/NTN unconformity/Blind Thrust fault NE is recognized on 2D seismic-reflection profiles. Folding is particularly pronounced in strata below the H40 unconformity (Figure 6-29).

6.2.1.3   Folds

There is significant structural relief on the mapped ELP/NTN unconformity (Figure 6-34). The maximum structural relief from the crest of Anticline Ae to the trough of Syncline Ae is approximately 120 m (150 ms). Slope gradients on the ELP/NTN surface are variable; the steepest slopes coincide with fault scarps and the flanks of folds (Figure 6-34). Fold axes on the top of the mapped ELP/NTN unconformity to the east and west of the HFZ (Figure 6-34) are oblique to the overall trend of the HFZ and vary in strike from 280 to 320 degrees.

The ELP/NTN surface is strongly folded throughout the Point Sal study area. The largest and most prominent folds in the 3D study area, designated Anticline A and Syncline A, are labeled on each section. As is apparent on Figures 6-29 and 6-30, structural deformation, including folding and uplift, is significantly greater in the Los Osos domain to the east of the HFZ than in the Santa Maria Basin to the west (Figure 1-2).

An example of deformation within the Quaternary strata above the ELP/NTN unconformity is shown on inline seismic-reflection Profile 1020 (Figure 6-30); this indicates syndepositional deformation and subsidence of Syncline Aw concurrent with uplift of structural highs to the north and south. Similar growth folding is apparent in Syncline Ae on inline seismic-reflection Profile 1370 (Figure 6-29). Quaternary deformation and syntectonic sediment accumulation associated with fold growth is also apparent in the northern part of the study area on the Eastern block, as imaged on Figure 6-29.

6.2.1.4   Buried Paleochannels

Seven channels or channel complexes are identified within the 3D data set in the Point Sal study area (Figures 6-35 and 6-36). From north to south, these include Channel Complex Ac and Aw (Channels Ac1, Ac2, Aw1, and Aw2), Channel Be and Bc, Channel Ce, Channel De, Channel Ee, Channel Complex F (Channels Fe1-3, Fc1-2, and Fw1-3), and Channel Ge (Figure 6-36). The paleochannels were identified based on the criteria outlined in Section 3.4.3. Most of the channels appear to be structurally controlled and are incised into reflections interpreted as folded Quaternary deposits. Other channels (e.g., Channel Bc) are incised into reflections of the Neogene bedrock. The paleochannels are incised into both structural lows (synclines) and highs (anticlines). Some paleochannels (i.e., Channels Ce, De, Ee, and Ge) are recognized only on the eastern structural block. Others have been mapped in the central structural block and in either the western or eastern structural blocks (i.e., Channels Ac/Ae and Be/Bc). The only channel complex present on all three structural blocks of the HFZ is Channel Complex F, consisting of Channels Fe, Fc, and Fw (Figure 6-36).

Channel Complex A

Channel Complex A includes a master channel (lowest and largest channel) and a nested channel (Figure 6-37), which is located in the north-central part of the Point Sal 3D study area (Figure 6-36). Both channels are recognized in the central and western structural blocks (Figures 6-36, 6-37, and 6-38) and terminate abruptly at the western and central

strands of the HFZ (Figure 6-39). Channel Complex A is structurally controlled in that it is located in Syncline Ac/Aw on the northern flank of Anticline Ac/Aw (Figure 6-30). Growth folding is apparent in the syntectonic reflections in Syncline A (Figures 6-37 and 6-38). Seismic reflections of channel fill deposits in Channels Ac2 and Aw2 (the uppermost, youngest channels) are only slightly folded. In the deeper channels (Channels Aw1 and Ac1), the reflections are more strongly folded, exhibiting truncation of underlying reflections on the northern and/or southern flanks of the syncline that are characteristic of broad erosional surfaces. The morphology of the upper channel (Ac2) is better preserved than Channel Ac1, and erosional truncation of underlying reflections is clearly apparent on the southern channel margin (Figure 6-37). The channel is located within the axis of a growth syncline, and erosional truncation is not as apparent on the northern channel margin as on the southern channel margin. The interpreted channel margins for Ac1 and Aw1 are best shown in the time slice of Figure 6-39.

Channel Complex Be/Bc

Channel Complex Be/Bc is located near the center of the Point Sal 3D volume and is well imaged in 3D seismic-reflection profiles (Figures 6-40 and 6-41) and time slices (Figure 6-42). Channel Be is oriented southeast-northwest and extends from near the eastern margin of the 3D survey to the eastern strand of the HFZ, where it terminates abruptly (Figure 6-42). Channel Bc is incised into the uplifted central structural block, and terminates at the western strand of the HFZ. Channel Bc does not extend across the entire uplifted central structural block, and does not abut the eastern strand of the HFZ or the central strand of the HFZ (Figures 6-36 and 6-42). The central structural block uplift likely elevated the segments of Channel Bc that once crossed this block, exposing them to wave erosion and removal during late Quaternary sea-level lowstands. Channel B is not identified in the western structural block and, because of the limited extent and discontinuous nature of the channel, cannot be used as a piercing point for determining offsets across the entire width of the HFZ. However, the Channel B thalweg piercing point along the eastern strand of the HFZ can be used to estimate offset on the eastern strand of the fault zone.

Channels Ce, De, Ee, and Ge

Channels Ce, De, Ee, and Ge are all relatively short channels confined to the eastern structural block in the central and southern part of the 3D study area (Figure 6-35 and left panel on Figure 6-36). All these channels are truncated by the eastern strand of the HFZ and do not extend to the west across the fault. Due to their small size, limited extent (confined to the eastern structural block only), and variable geometry, no attempt was made to constrain fault offsets using these channels.

Channel Complex Fe

Channel Complex Fe consists of three nested channels (Channels Fe1, Fe2, and Fe3) located near the south end of the Point Sal 3D study area and restricted to the eastern structural block, where it terminates abruptly at the eastern strand of the HFZ (Figure 6-43). This nested channel complex is located adjacent to a bedrock high at the southern margin of a broad syncline, where it is bounded on the south by the ELP/NTN

unconformity. To the north, Channel Fe1 is incised into gently folded reflections representative of inferred early to middle Quaternary strata.

The margins of the master (or basal) channel are well imaged in the 3D volume and in USGS Line PBS-324 of Johnson and Watt (2012) as pronounced angular unconformities that separate well-layered reflections (bedded strata) from low-amplitude, chaotic-to-transparent reflections (channel fill material) of the incised channels. The shallower nested Channels Fe2 and Fe3 are mapped based on apparent truncation of gently dipping to fairly flat-lying reflections (apparent erosional angular unconformities) within previously deposited channel fill. The thalweg and margins of the Channels are illustrated on a time slice at 160 ms (Figure 6-44a) and a representative time slice at 170 ms (Figure 6-44b) shows the approximate lateral margins of Channel Fe1. The margins of Channel Fe2 are also visible on the time slices.

Channel Fe1 is approximately 500–800 m wide (Figure 6-44) and approximately 60 m (~75 ms TWTT) deep, with the master channel (Fe1) thalweg located at a depth of approximately 170 m (~200 ms TWTT; Figure 6-43). Given the depth of the channel thalweg, which is below the lowest Quaternary sea-level lowstand, and the bench-like reflections shown on the walls of the nested channels (see Maier et al., 2013), Channel Fe1 likely formed as a submarine channel near the top of the upper slope. It is possible that a terrestrial stream incised the eastern part of Channel Fe3 sometime during a late Quaternary sea-level lowstand, as the thalweg depth is approximately 125–130 m below sea level. The channel deepens toward the west, with a maximum thalweg depth of approximately 180 m below sea level. The character of the seismic reflections within the Channel Fe3 fill deposits are more chaotic and less stratified than Channel Fe2 and Fe1 fill deposits, suggesting a shallow marine or possible fluvial origin (Figure 6-43). Channel Fe1 has a U-shaped geometry, and Fe3 is narrower and exhibits a V-shaped geometry (Figure 6-43).

Channel Complex Fc

Channel Complex Fc has a different structural geometry and channel morphology from the other channels to the east and west of the HFZ in Channel Complex F. The apparent Channel Complex Fc is located in the axis of an east-west-trending syncline within the central structural block (Figures 6-35, 6-36, 6-45, and 6-46). Although distinct channel morphology of cut and fill (Figure 1-8) is not exhibited in the 3D data set for this channel complex, the complex's proximity to distinct channels east and west of it, and the structure's general trend suggest that a depression formed by the syncline could have acted as a conduit for sediment transport. The synclinal depression could have connected the eastern and western channels during the Quaternary when sea level was lower, but it has experienced little erosion and much aggradation of sediment in the axis of the syncline. In contrast, erosional truncation of the flanks of the syncline to the north and south of the channel margins is apparent on Figure 6-45.

Syndepositional subsidence and growth of the syncline are suggested by progressive unconformities on the syncline's flanks (Figure 6-45). This structure is well defined in both 2D profiles and 3D time slices, and it includes the two apparent channels that are now preserved because they are located within a graben bounded by two primary strands

of the HFZ. The eastern strand of the HFZ is a releasing bend along the east side of the transtensional pull-apart graben (Figure 6-46). The western strand of the HFZ is a relatively straight bypass fault. The base of this channel complex is marked by a fairly high-amplitude reflection that truncates dipping, and folded reflections from what appears to be the prominent angular unconformities on the flanks of the syncline.

The reflection at the base of the inferred Channel Fc2 truncates the inferred Channel Fc1 channel fill reflections on both the east and west sides of the syncline, which appears to merge (coeval) with unconformity H30 (Figure 6-45). Truncation of the inferred Channel Fc2 folded reflections of possible channel fill synclinal deposits is observed below the H10 reflection (Figure 6-45). The apparent Channel Complex Fc is approximately 750 m wide and approximately 96 m (120 ms TWTT) deep, and the inferred Channel Fc1 thalweg lies at a depth of approximately 200 m (~245 ms TWTT). Given the depth of this thalweg and its internal stratigraphy, Channel Fe1 appears to have formed as a submarine channel within an actively subsiding synclinal depocenter on the upper continental slope. Alternatively, Channel Fe1 may have formed at a shallower depth on the outer shelf and subsequently subsided.

The deepest part of Channel Complex Fc is adjacent to the eastern strand of the HFZ (Figures 6-36 and 6-46). This is likely due to eastward tectonic tilting and subsidence of a small transtensional structure located at the south end of the central structural block. The syncline where the apparent Channel Complex Fc is located appears to be a small pull-apart basin that formed within the releasing bend of the eastern strand of the HFZ (Figure 6-36 and 6-46). Based on the 2D deep-penetration PG&E legacy archive seismic-reflection profile data, the depth (to NTN/ELP Unconformity) of the transtensional basin/syncline in this releasing bend is estimated to be approximately 320–440 m (~400–550 ms TWTT).

Channel Complex Fw

Channel Complex Fw is less well defined in both seismic-reflection profiles and time slices than Channel Complex Fc. It includes a well-preserved upper channel (Fw3) and two poorly imaged lower channels, Channels Fw1 and Fw2 (Figures 6-22, 6-47, and 6-48). Only the southern channel margin of Channels Fw1 and Fw2 is clearly imaged. These two channels are stratigraphically lower (older) than Channel Fw3, which lies to the south (Figure 6-47). The better-imaged channel, Channel Fw3, has a thalweg depth of approximately 260 m (320 ms TWTT). This depth is greater than the lower limit of reported Quaternary sea-level fluctuations (Figure 1-6), and the channel's internal stratigraphy is consistent with channels and gullies formed on submerged continental slopes elsewhere (Greene et al., 2002; Gardner et al., 2003; Dartnell and Gardner, 2009; Surpless et al., 2009). The channel is approximately 500 m wide at the top (Figure 6-48) and approximately 200 m deep (250 ms TWTT). Channel Fw3 is overlain by a thick (~80 m; 100 ms TWTT) sequence of relatively flat-lying to gently folded inferred upper Quaternary strata (Figure 6-47). Horizons H30 and H10 are mapped near the top of this sequence. The dip of the reflections inferred as late Quaternary strata, as well as the underlying reflections, is toward the east, with an increase in inclination toward the western strand of the HFZ (Figures 6-31 and 6-36).

Channel Complex F Summary

Channels Fe1, Fe3, and Fw3 (Figures 6-43, 6-44, 6-47, and 6-48) are the most extensive and best-defined channels within Channel Complex F. In the western structural block, the geometry of Channel Fw3 is much better defined than Fw1 and Fw2, and its internal stratigraphy and geometry are similar to Fe3's. Channels Fe1 and Fw3 are located south of the axis of a syncline and adjacent to the ELP/NTN unconformity (Figures 6-43 and 6-47). Channel Fe3 is incised into Channel Fe2 deposits and has a narrow, V-shaped channel (Figure 6-43). Channel Fw3 appears to be the most likely candidate channel to be correlated with Channel Fe3, and thus can be used as a piercing point to determine offset across the entire width of the HFZ.

There are three channels in the Channel F complex to the west of the HFZ. Channels Fw1 and Fw2 are stratigraphically lower (older) than Channel Fw3 (Figure 6-47), and may correlate with Channels Fe1 and Fe2 east of the fault (Figure 6-43). The southern channel margins of Channels Fw1 and Fw2 are not clearly resolvable in the data, and the channel thalwegs thus were not mapped. However, Channels Fw3 and Fe3 are well resolved in the data, and offer the preferred channel correlation that is evaluated herein. Alternate channel correlations (Fe1/Fw3) are possible, and as such were also evaluated.

6.2.1.5   Piercing Points

Several geomorphic piercing points are recognized in the Point Sal 3D data set and consist of paleochannel thalwegs offset by strands of the HFZ. The locations of Channel Complex A, B, and F piercing points are shown on Figure 6-36, but Channel Complexes A and B do not cross the entire HFZ and thus cannot be used to estimate vertical and lateral separation across the fault zone as a whole. These channels' thalweg piercing points can be used, however, to estimate separation across individual fault strands within the HFZ. These estimates are summarized in Table 6-4 and illustrated on Figures 6-49, 6-50, and 6-51a and b.

Channel Complex A Thalweg Piercing Point

Although Channel A is well imaged on the 3D seismic-reflection data, and the correlation of the channel across the western strand of the HFZ is clear (Figure 6-39), the confidence level for a thalweg piercing point is low because of the broad channel thalweg (particularly on the Western block) at the piercing point (Figures 6-37 and 6-38) and rounded upper channel margins (see Section 3.5—Interpretation Confidence Levels). The Channel Aw2/Ac2 thalweg dextral offset of approximately 95 ± 20 m across the western strand of the HFZ is illustrated on Figure 6-49.

Channel Complex B Thalweg Piercing Point

Channel Complex B is a well-imaged channel incised into bedrock on the central structural block, but on the eastern structural block (Channel Be) has a relatively broad thalweg. Part of Channel Bc is absent on the central structural block due to uplift and erosional removal. Consequently, the confidence level for the Channel B piercing point is medium. However, the thalweg offset is estimated to be 356 m, with an estimated maximum offset of 510 m and a minimum of 193 m (Figure 6-50).

Table 6-4. Summary of Piercing Point Offset Measurements for Point Sal

Piercing Point	Dextral Offset (m)			Vertical Separation (m)			Confidence Level
	Min.	Max.	Pref.	Min.	Max.	Pref.	
Preferred Entire HFZ–Channel Fe3/Fw3	550	700	**600–650**	80	110	**95, down to the west**	Highest
Eastern Strand HFZ–Channel Be/Bc	193	510	**356**	20	60	**40, down to the east**	Medium
Western Strand HFZ–Channel Fc1/Fw3	376	490	**432**	55	95	**75, down to the west**	Medium
Eastern Strand HFZ–Channel Fe3/Fc1	150	250	**200**	15	45	**30, down to the west**	Medium
Western Strand HFZ–Channel Ac2/Aw2	75	115	**95**	5	15	**10, down to the west**	Low
Alternate Entire HFZ–Channel Fe1/Fw3	450	600	**500–550**	70	100	**85, down to the west**	Low

Note: 3D P-Cable survey data resolution is 3 m horizontal and 2 m vertical.

Channel Complex F Thalweg Piercing Point

The thalwegs of Channel Complex F (Channels Fe1-3, Fc1-2, and Fw1-3) cross the entire HFZ; the estimated lateral and vertical separation across the eastern and western strands of the HFZ for this channel complex is provided in Table 6-4 and illustrated on Figure 6-51a and b. The proximity of Channel Complex F to the mouth of the Santa Maria River suggests that perhaps this complex represents the cutting and filling of submarine channels near the shelf edge by a relatively large stream or river source. This river or stream may have meandered across an emergent coastal plain (the modern continental shelf) during sequential sea-level lowstands, thereby shifting the erosional channels to cut into previous channel-filled areas. San Antonio Creek to the south of Point Sal provides another possible sediment source, but the size of the watershed is not as large as the Santa Maria River watershed (Figure 1-4).

Correlation of Channel Fe3 with Fw3 (Figure 6-51a) is highly preferred. Channels Fe3 and Fw3 appear very similar in their cross-sectional shape and fill. In addition, a small channel incised into the upper fill of both channels suggests that these channels are two segments of the same channel. The channel geometry of these two channels is similar, with narrow, V-shaped cross-sectional geometry. Channel Fe3 is narrower than Fe1 (Figure 6-43) and shares morphologic similarities with Channel Fw3. Channel Fe3 is approximately 30 m deep and 400 m wide. It is inset within, and incised into, Channel Fe1 and Fe2 deposits (Figure 6-43). Channel Fe3 fill deposits are unconformably overlain

by Holocene marine shelf sediments (above reflection H10; see Figure 6-43). The channel complex of nested channels, of which Channel Fe3 and Fw3 are the youngest (upper) channels, appears to have formed in a submarine environment along the distal part of the continental shelf or upper-slope environment where a meandering river source of sediments on the shelf was supplied during a Quaternary sea-level lowstand. The stratigraphically highest (youngest) channels of the Channel Complex F, Channels Fw3 and Fe3, may therefore be correlative in age. Therefore, correlation of the Channel Fe3 thalweg with the Channel Fw3 thalweg across the entire HFZ provides a highly preferred estimated offset of 600–650 m, with a maximum of 700 m and minimum of 550 m (see Table 6-4). The estimated vertical separation of the alternate correlation of Channel Fe3/Fw3 thalweg is 95 m, down to the west. The correlation confidence level for the Channel Fe3/Fw3 piercing point offset is the highest.

The highly preferred correlation and measured offsets of Channel Fe3 with Fw3 can be compared with the combined measured offsets of Channel Fe3/Fc1 and Fc1/Fw3 piercing points across the HFZ. Although Channel Fc1 is well imaged on the seismic-reflection data, and the preferred correlation of the channel across the eastern and western strands of the HFZ is clear, the confidence level for the Channel Fc1 piercing points with Channel Fw3 and Fe1 is medium because Channel Fc1 has rounded upper channel margins and the thalweg follows the axis of a syncline (Figures 6-45 and 6-46). The preferred correlation of the Channel Fe3 thalweg piercing point with the Channel Fc1 thalweg is clear, and the preferred offset across the eastern strand of the HFZ is estimated at 200 m, with a maximum offset of 250 m and a minimum of 150 m (Figure 6-51a). Correlation of the Channel Fc1 thalweg with the Channel Fw3 thalweg across the western strand of the HFZ provides a preferred estimated offset of 432 m, with a maximum of 490 m and minimum of 376 m. The total preferred offset using the combined measured offsets of Channel Fe3/Fc1 and Fc1/Fw3 piercing points across the HFZ is therefore 632 m (see Table 6-4). This value falls within the highly preferred 600–650 m measured offset of Channel Fe3 with Fw3.

An alternative correlation of the Channel Fe1 thalweg with the Channel Fw3 thalweg across the entire HFZ provides an estimated offset of 500–550 m, with a maximum of 600 m and minimum of 450 m (see Table 6-4 and Figure 6-51b). The alternate correlation of Channel Fe1 with Fw3 through Fc1 is based on the reasonable geometric match of the channels in plan view. While the resultant offsets appear reasonable in light of past predicted offsets for the HFZ, the channels also are well imaged on either side of the HFZ with similar channel thalweg dimensions that exhibit the same east-west trend on all three structural blocks. Channel Fe1 is approximately 60 m deep and 700 m wide. Channel Fw3 is approximately 60 m deep and 600 m wide (Figure 6-51a). The channel morphology and width of Channels Fe1 and Fw3 are similar, and both channels are incised into reflections of inferred Quaternary strata adjacent to bedrock, which suggests a possible match. Although the channels appear to be stratigraphically inverted, the lower (oldest) Channel Fe1 connecting with the upper (younger) Channel Fw3, we suspect that this apparent stratigraphic relationship could result from a channel complex being formed at one sea-level lowstand near the mouth of a large fluvial sediment source. Therefore, Channels Fe1, Fc1, and Fw3 can be correlated with a medium degree of confidence

across all the mapped faults in the southern part of the 3D survey area (Figures 6-36 and 6-51b). The estimated vertical separation of the alternate correlation of Channel Fe1/Fw3 thalweg is 85 m, down to the west.

Another alternative correlation of Channel Complex Ee with Channels Fc and Fw was considered but was discarded because it would require sinistral, rather than dextral, motion on the eastern strand of the HFZ (Figure 6-51b), which is incompatible with published literature and knowledge about this fault zone (Hanson et al., 1994; Johnson and Watt; 2012; Willingham et al., 2013). In addition, strong similarities between the geometry, internal stratigraphy, depth, and stratigraphic position of Channels Fe3 and Fw3 provide compelling evidence for the preferred correlation of Channel Complex F across the HFZ (Figures 6-43, 6-47, and 6-51a).

6.2.2   Discussion

The results of mapping faults and buried paleochannel morphologies and thalweg piercing points within the Point Sal study area can be used to estimate offsets along the faults. Slip rates can be calculated using these estimated offsets along with estimated ages of the channels. This section discusses the use of stratigraphy, structure, and channel morphologies to determine potential slip rates across the HFZ.

6.2.2.1   Stratigraphy

The stratigraphy of the Point Sal study area represents both a distal continental shelf and upper-continental-slope depositional environment. In this study, buried paleochannels have been found to provide the best piercing points to use in estimating fault offsets, which are incised into the Quaternary stratigraphy. All the channels west of the HFZ incise reflections interpreted as continental slope strata. The thalwegs of channels west of the HFZ occur below the depths of Quaternary eustatic sea-level lowstands, and thus are likely submarine (upper continental slope) in origin, as the LGM and earlier sea-level lowstands reached a depth of approximately 120–125 m below modern sea level (Figure 1-6). A time slice from the 3D volume at a depth of approximately 118 m (146 ms TWTT) intersects the margins of Channel Complex B, whose thalwegs are found at depths of approximately 120 m (150 ms TWTT) below modern sea level (see Figures 6-40, 6-41, and 6-42). These observed submarine-like channels appear to have formed in an upper-slope depositional environment similar to ones described for channels in other parts of California (Shepard, 1965; Greene et al., 2002; Surpless et al., 2009), as well as in other parts of the world (Adeogba et al., 2005). The bench-like morphology along the margins of Channel Complex F (Figure 6-43) is characteristic of features described by Maier et al. (2013) for submarine channels formed on the upper slope of the Big Sur offshore area.

Active uplift of the central structural block (Figure 6-27) and along the Lions Head fault is suggested by the absence of reflections H10 and H30 in these areas (Figure 6-21). Reflections of inferred Holocene sediments, where present, are considerably thinner to the east of the HFZ than to the west. A similar stratigraphic pattern is present in inferred Upper Pleistocene reflections above the H30 horizon (Figure 6-21). Previous studies of

vertical separation across the HFZ also suggest that the east side of the fault zone is presently experiencing uplift (Hanson et al., 2004; Willingham et al., 2013).

Similar to the stratigraphy observed in the inner Estero Bay, sediment depositional patterns are influenced by local accommodation created by down-to-the-west vertical separation across faults, specifically, in the Point Sal study area by faults of the HFZ. It is likely that this vertical subsidence affected the processes of channel erosion and deposition by controlling the trend and spatial geometry of the channel thalwegs (e.g., Figures 6-39, 6-44, and 6-48).

The southern parts of the master and nested channels that make up Channel Complex A exhibit evidence for uplift associated with the folding of the anticline to the south, which is most pronounced in the central structural block. The lower (older) channels exhibit more deformation than the upper (younger) nested channels, indicating that fold growth continued during development of Channel Complex A. Growth of Anticline Ac and dextral and vertical separation on the eastern and western splays of the HFZ may have influenced channel position and geometry, as nested Channel Ac2 is located farther south than Channel Ac1, closer to the axis of uplift (Figure 6-37). Given the staggered positions of the channels over the northern limb of the anticline, contemporaneous fold growth suggests a progressive southward channel migration through time, resulting in the observed erosional truncation of the southern flank of Channel Ac1 by the thalweg of Channel Ac2 (Figure 6-37). Similar relationships are observed to the west, where the thalweg of Channel Aw2 is offset farther south relative to the thalweg of Channel Aw1. Truncation of reflections in the upper part of Channel Aw1 is apparent on Line 997 (Figure 6-38) and probably represents erosion of the channel fill deposits. The most likely source of sediments supplied to Channel Complex A when active was the Santa Maria River via longshore drift from the northeast (Figure 1-4). The channel thalwegs of the Channel Complex A are located at a depth of 160–200 m, deeper than the lowest Quaternary sea-level lowstand, and are thus considered to have formed in a submarine environment, along the axis of an actively subsiding syncline on the upper continental slope.

6.2.2.2   Faults

The results of mapping faults within the Point Sal study area indicate that the HFZ dominates the structure of the region. However, new insights into the complexity of the fault zone itself and the interaction with other faults in the region has resulted from this study. Presented below is a discussion of the HFZ, the Lions Head and Casmalia faults, and a new fault named here the "Blind Thrust fault NE."

The Hosgri Fault Zone

Three primary fault strands of the HFZ are mapped in the central part of the Point Sal study area, where the central structural block is uplifted and folded into a broad (800–1,000 m wide) anticline (Figure 6-32). This anticline is cut by many secondary faults, as well as by the central strand of the HFZ, creating complex fault relationships and small, slivered, fault-bounded blocks (Figure 6-27). Pull-apart basins and other transtensional structures (e.g., grabens) have formed in the southern part of the central structural block,

where the central and eastern strands of the HFZ exhibit releasing bends (Figures 6-27, 6-31, and 6-34). The central part of the central structural block has been uplifted and folded into a faulted anticline (Figure 6-32). Farther north, the central structural block is strongly uplifted, with the crest of the anticline beveled off within a 10-degree restraining bend (Figures 6-27 and 6-33). In the northern part of the Point Sal 3D study area, the multiple strands of the HFZ mapped in the south converge and form a single fault splay with little apparent vertical separation (Figure 6-34).

The three primary strands are located in the central part of the 3D survey area, with transtension displayed in the south and transpression displayed in the north. This change is reflected in the mapped distribution and thickness of sediments above the H10, H30, and ELP/NTN Unconformities (Figure 6-21). There is an approximate 6-degree change in the strike of the HFZ from approximately 336 degrees in the south to approximately 330 degrees in the northern part of the 3D survey area (Figure 6-27). To the north of the 3D survey area, the HFZ extends north-northwest across San Luis Obispo Bay with an average trend of 340 degrees, approximately 10 degrees more northerly than the strike of the fault in the northern portion of the 3D study area (Plate 1B). This releasing fault bend has been attributed impingement of the Casmalia/Point Sal block toward the northwest into the HFZ (Johnson and Watt, 2012). The 3D survey area is located at the southwest boundary of the Casmalia/Point Sal block, where the Lions Head fault converges with and indents the HFZ (Figures 6-27 and 6-28).

To the south of the intersection of the Lions Head fault with the HFZ, a minor restraining bend in the eastern strand of the HFZ is located 1 km north of an abrupt 20-degree releasing bend in the fault. The abrupt 20-degree bend in the eastern strand of the HFZ is inefficient and is being cut off by transfer of slip onto the straighter central and western strands, which serve as a paired-bend bypass faults (Figure 6-27). Bypass occurs when it becomes more efficient for a fault to cut across an indentor block or paired bend than to bend circuitously around it (Johnson and Watt, 2012). The central strand of the HFZ is the longest and has the greatest amount of lateral offset (Figure 6-34) of the many faults cutting across the central structural block, which is being slivered by transcurrent motion. The relatively straight, linear western strand (Figure 6-27) is the primary bypass fault, and bounds the western side of the Central block. A large-scale analog of this relationship is the San Jacinto fault, which is accommodating increasingly greater amounts of slip along the Pacific–North American plate boundary as it cuts off part of the 'Big Bend' on the San Andreas Fault Zone in Southern California.

The westward deflection of the eastern strand of the HFZ to the south of the intersection with the Lions Head fault zone over the last several million years has occurred concurrently with clockwise rotation of the Point Sal block (Sorlien et al., 1999). The transfer of slip from the eastern strand to the central and western strands of the HFZ is consistent with paired-bend, rigid-basement block indentation (Swanson, 2005), as recently described by Johnson and Watt (2012), at the intersection of the Los Osos and Shoreline fault zones with the HFZ in Estero Bay to the north. Similar fault bends, fault slivers, and bypass faults have been described by Sims (1993) for the San Andreas fault zone near Parkfield. Bending of the eastern strand of the HFZ and slivering of the central structural block (Figure 6-27) is interpreted to be a direct result of shortening and

transpressive uplift due to fault convergence and impingement of the Casmalia/Point Sal block toward the northwest into the HFZ (Figures 1-2 and 6-28).

The piercing points identified in this study that cross the HFZ suggest that much of the late Quaternary dextral offset has been accommodated by the eastern and central strands, but that the western strand is also active, particularly to the south of the bifurcation of the central strand from the western strand. This is consistent with analog models for restraining and releasing bends in strike-slip fault zones (Crowell, 1974; McClay and Bonora, 2001).

The Lions Head Fault Zone

The Lions Head fault zone forms the southern boundary of the Casmalia/Point Sal block (Figure 1-2), and, on the basis of the PG&E deep-penetration legacy archive data and the observed surface fault geometry (Plate 1B), is interpreted as a steeply dipping oblique reverse fault, which may be an inverted Miocene structure (Figures 6-28 and 6-29). Left-lateral oblique reverse slip is indicated by slickenslides and fault striations on the Lions Head fault onshore (Clark, 1990), as well as by the geomorphology of the coastline south of Point Sal (Plate 1B). The fault zone trends nearly east-west and onshore to the east of the survey area, bounds the southern flank of the Casmalia Hills, and then projects into the ocean at Point Sal (Figure 6-28). The Casmalia Hills mountain range is most likely the result of compression and uplift occurring from regional transpression and rotation of the Point Sal block (Sorlien et al., 1999).

The Casmalia Fault Zone

The Casmalia fault zone is interpreted as an oblique right-lateral reverse fault that may be transferring slip from the Los Osos domain onto the HFZ. Focal mechanisms from earthquakes associated with the fault zone show reverse motion along northwest- and west-northwest-trending fault planes (McLaren and Savage, 2001), which is in close agreement with the mapped strike of the Casmalia fault zone. Several north/northwest-verging imbricate reverse-fault splays exhibiting displacement of basement and Quaternary strata are apparent on the 2D legacy archive data (Figure A-4). Approximately 5 km north of Point Sal, the Casmalia fault zone extends onshore and bounds the northern flank of the Casmalia Hills to the east (Figure 6-28).

The strike of the main strand of the HFZ changes from N24°W to N19°W where the westward projection of the Casmalia fault intersects the HFZ. This fault bend has been interpreted as resulting from northwest translation of the Casmalia/Point Sal block and indentation of the HFZ, causing a releasing bend in San Luis Obispo Bay (Johnson and Watt, 2012).

The Blind Thrust Fault NE

A buried thrust fault, "Blind Thrust fault NE," has been interpreted beneath the folded ELP/NTN unconformity in the northeastern part of the Point Sal study area (Figure 6-29). Transpressional deformation is evidenced by folds in the reflections above the ELP/NTN unconformity that probably represent Quaternary strata (Figures 6-24 and 6-25), and northeast-southwest shortening beneath, along, and in the reflections (sediment) above

the ELP/NTN surface (Figures 6-21, 6-29, and 6-34), thus the fault is interpreted as being active in the Quaternary. Deformation of all the mapped reflections in the section above the ELP/NTN unconformity/Blind Thrust fault NE is recognized on the 2D seismic-reflection profiles, and folding is particularly pronounced in strata below the H40 unconformity (Figure 6-29). This fault is interpreted in the 3D data as a southeast-trending, low-angle splay of the Lions Head fault zone and/or HFZ within the Casmalia/Point Sal block. The structural block bounded by this fault and the Lions Head fault (Figure 6-29) likely deformed due to convergence and shortening along the southern boundary of the Casmalia/Point Sal block.

Active uplift of an anticline above the inferred tipline of the fault is suggested by growth folding near the north end of the 3D LESS study area (Figure 6-29). The observed northeast-southwest shortening east of the HFZ and across the Los Osos domain (Figure 1-2) has been documented by other investigators (e.g., Sorlien et al., 1999; Hanson et al., 2001; Lettis et al., 2004; Willingham et al., 2013).

6.2.2.3   Channel Correlations and Estimated Offsets

Of the seven paleochannels or channel complexes identified in the Point Sal 3D data set (Figures 6-35 and 6-36), two (Channels B and F) have significant lateral and vertical displacement (Figure 6-36; Table 6-4). Of the three major fault strands within the mapped HFZ, the estimated amount of lateral and vertical separation of piercing points varies as a result of differential deformation and strain partitioning along the HFZ since its inception in the Pliocene (Compton, 1991; Sorlien et al., 1999; Johnson et al., 2012; Willingham et al., 2013). All the other channels that cross the mapped faults have little or no observed offset (i.e., Channel Complex A), while Channel Complexes A and B are limited in extent to only one or two of the three structural blocks. The thalweg piercing points of Channel Complex F are the best features to use to determine total offset across the entire HFZ, as this complex extends across all structural blocks.

There is a change in fluvial architecture and morphology between Channel Fc, which is structurally confined to the axis of a broad subsiding, syndepositional syncline (Figure 6-45), and Channels Fe and Fw, which are narrower and are incised into reflections of inferred Quaternary strata. The axis of the syncline, which coincides with the thalweg of Channel Fc (Figure 6-46), trends east-west and aligns well with the trends of Channels Fe and Fw (Figure 6-51a and b). The depths of the thalwegs of Channels Fe, Fc, and Fw suggest flow toward the west in an upper-slope depositional environment, although block rotation and near-fault effects, possibly the result of transtensional structural rollovers, affect the eastern parts of Channels Fc and Fw. Modern analogs of mid-upper-slope channels and gullies resulting from downslope gravity-driven sediment transport are commonly linear (Field et al., 1999; Spinelli and Field, 2001; Greene et al., 2002; Mitchell and Huthnance, 2007).

Channels Fe3, Fc1, and Fw3 can be correlated with a high degree of confidence across all the mapped faults in the southern part of the 3D survey area (Figures 6-36 and 6-51a). The channel thalwegs exhibit the same east-west trend on all three structural blocks. Channel Fe3 is approximately 30 m deep and 400 m wide. It is inset within and incised

into Channel Fe1 and Fe2 deposits (Figure 6-43). Channel Fe3 fill deposits are unconformably overlain by Holocene marine shelf sediments (above reflection H10; see Figure 6-43). Channel Fw3 is approximately 60 m deep and 700 m wide (Figure 6-51a). The channel morphologies of Channels Fe3 and Fw3 are very similar. Given that both of these channels are incised into reflections of inferred Quaternary strata, and that their stratigraphic position and similarities are analogous to upper-slope channels observed elsewhere along the California continental margin, they thus provide a channel correlation of the highest confidence level, independent of Channel Fc.

The alternative correlation of Channel Fe1 with Fw3 was considered (Figure 6-51b). Channel Fe1 is wider than Fe3 (Figure 6-43) and is U-shaped, rather than V-shaped. Channel Fe1 is approximately 60 m deep and 700 m wide. Given the geomorphic differences between Channels Fe1 and Fw3, and their stratigraphic position, the alternative correlation is considered much less likely than the preferred correlation (Figure 6-51a). The western and central strands of the HFZ converge immediately north of where Channels Fc1 and Fw3 are juxtaposed across the fault (Figures 6-27, 6-36, and 6-51), so the amount of offset on Channel Complex F by these two fault strands cannot be independently resolved. For discussion purposes, we refer to this as the Channel F–western strand piercing point.

Clear vertical and lateral separation of the Channel F thalwegs is noted on the eastern and western strands of the HFZ (Figure 6-51a; Table 6-4). Across the entire HFZ in the preferred Channel Fe3/Fw3 correlation, the total measured lateral separation of the Channel F thalwegs is approximately 550–700 m of dextral offset, with a preferred value of 600–650 m. The preferred estimated vertical separation across the entire HFZ is approximately 95 ± 15 m, down to the west (Table 6-4). The confidence level of this correlation is the highest.

The alternative correlation of Channel Fe1 with Channel Fw3 (Figure 6-51b) exhibits 450–600 m of dextral offset, with a preferred value of 500–550 m (Table 6-4). Relative to the preferred correlation (Fe3/Fw3), the alternate correlation exhibits a 100 m smaller dextral offset for Channel F, and implies a younger age for Channel Fw3. The confidence of this correlation is low.

Across the western/central strands of the HFZ, measured lateral separation of Channel Fc1 from Channel Fw3 is approximately 376–490 m, with a preferred value of approximately 432 m of dextral offset (Figure 6-51a). The estimated vertical separation across the western/central strands of the HFZ is approximately 75 ± 20 m, down to the west (Table 6-4). The correlation confidence level of Channel Fc with Channels Fe and Fw is medium.

Across the eastern strand of the HFZ, the lateral offset of the Channel Fe1 thalweg from the Channel Fc1 thalweg is estimated in the preferred correlation to be from 150 to approximately 250 m of dextral offset, with a preferred value of approximately 200 m (Figure 6-51a). The estimated vertical separation across the eastern strand of the HFZ is approximately 30 ± 15 m, down to the west (Table 6-4). Given the higher correlation confidence level of Channel Fe3 and Fw3 (exclusive of Channel Fc1), offset measurements of these channel thalwegs are used for estimating the preferred dextral slip

rates across the HFZ. The alternative correlation of Channel Fe1 with Channel Fw3 thalwegs (Figure 6-51b) is used for estimating alternative dextral slip rates across the HFZ.

6.2.2.4   Age Constraints

The ages of the channels in the Point Sal study area are poorly constrained. Consequently, the ages of channel incision and infilling must be estimated through the use of observed stratigraphic relationships, estimated sediment accumulation rates, and previously published climatic (sea-level) models. These models are all subject to significant uncertainty.

The channels mapped in this study are bracketed stratigraphically by two key unconformities, the lower ELP/NTN unconformity and the upper H10 unconformity. The H10 unconformity is interpreted to represent the pre-Holocene transgressive surface formed during the sea-level rise from MIS 2 and MIS 1 between approximately 18 ka and 8 ka, respectively (Waelbroeck et al., 2002; Siddall et al., 2003; Lisiecki and Raymo, 2005).

The preferred age model for Point Sal Channel Complexes A, B, and F is presented on Figure 6-52a. The estimated ages shown on the figure are for Channels Aw2, Ac2, Bc, Be, Fw3, Fc1, and Fe3, which were used to correlate channel thalweg piercing points for estimating preferred slip rates across the HFZ. An alternative age model is presented on Figure 6-52b and is based on the alternative channel correlation for Channel Complex F (Channels Fe1/Fc1/Fw3). The estimated ages of Channels Aw2, Ac2, Bc, and Be remain the same in both the preferred and alternative models.

Channel Complex A

Channel Complex A is structurally controlled, and likely developed in an actively subsiding syncline during late Quaternary sea-level lowstands. Growth folding in Syncline A suggests active syndepositional subsidence of the channel axis; therefore, the Channel A thalwegs formed at a shallower depth than their present-day depth. Channels Ac1, Ac2, Aw1, and Aw2 are all below the maximum depth of Quaternary sea-level lowstands, and are likely of marine origin. In both Channel Complex Ac and Channel Complex Aw, erosional truncation of older channel deposits has occurred along the southern flank of the channels (Figures 6-37 and 6-38). A southward migration of both the channel thalweg and syncline axis in younger, shallower strata is apparent, and is particularly pronounced in Channel Ac (Figure 6-37). This relationship is consistent with syndepositional dextral, southward translation of the central structural block along the eastern strand of the HFZ through time.

The H30 horizon, with an estimated age of approximately 140–130 ka (PG&E, 2013), is present approximately 30 m below the seafloor and approximately 40 m above Channel Aw2 (Figure 6-38). The confidence level of the stratigraphic position and age of H30 to the east of the western strand of the HFZ in the Point Sal 3D survey area is low. The thalweg of Channel Aw2 is approximately 70 m below the seafloor. Based on the estimated age of H30, the sediment accumulation rate in the axis of Syncline Aw over the

past 140 ka is approximately 20 cm/ka. Assuming relatively uniform subsidence and sediment accumulation rates at the site in the late Pleistocene, the preferred age for Channel Aw2 is approximately 270–245 ka (MIS 8b and 8c). The thalweg depths of Channels Aw2 and Aw1 are 75 m and 100 m, respectively, below the seafloor. Assuming relatively uniform subsidence and sedimentation rates in the axis of Syncline Aw, and presuming that the unconformities associated with Channels Aw1 and Aw2 formed during sea-level lowstands since the MPT, the estimated ages of Aw1 and Aw2 are approximately 350–340 ka (MIS 10) and approximately 270–245 ka (MIS 8b and 8c), respectively.

The relative position of Channel Aw2 below reflection H30 (Figure 6-38) fits the age model, and it is likely that the channels were most active and the observed erosional unconformities developed during low sea–level stands, when sediment sources from the coast were more proximal to the shelf break (Pratson et al., 2007; Sommerfield et al., 2007) and sediment delivery to river channels and the coast was generally greater than during interglacial periods (Reneau et al., 1990; Knox, 1995; Orange, 1999). Increased frequency of El Nino–Southern Oscillation (ENSO) in the late Holocene starting approximately 3 ka resulted in increased sediment accumulation rates in many California offshore basins fed by submarine canyons that cross the shelf and extended to the nearshore zone (Romans et al., 2009), but most submarine canyons that do not cross the shelf are stranded and inactive during high sea-level stands (Normark et al., 2009).

The assumption of relatively uniform subsidence and sediment accumulation rates may not be valid, however, and there is considerable uncertainty in the age of Channel Aw. Alternative ages are also possible and were considered. The estimated minimum age for Channels Ac2 and Aw2 is approximately 20 ka (MIS 2), and the estimated maximum age is 1.4 Ma (Figure 6-52a and b).

The similarities in stratigraphic relationships between Channel Complexes Ac1-2 and Aw1-2 (Figures 6-37 and 6-38), as well as the continuity and depth of the thalwegs for Channels Ac2 and Aw2 (Figure 6-49), indicate that the channels mapped in Channel Complex A are similar in age in both the central and western structural blocks (Figure 6-36).

The preferred interpretation is that channel erosion events represent the dominant 100 kyr late Quaternary sea-level cycle, and as observed, both Channels Ac2 and Aw2 are one cycle older than H30 (Figure 6-38). Given that the preferred age for H30 is approximately 155–135 ka (MIS 6b), the estimated preferred age of approximately 270–245 ka (MIS 10) for Channels Ac2 and Aw2 is consistent with this interpretation. Therefore, the preferred age model (Figure 6-52a) for paleochannels within Channel Complex A is that the channels developed during the late Quaternary, since the end of the MPT (~625 ka). Older ages are possible, however, so the maximum age of Channel Complex A is 1.4 Ma.

Channel Complex B

Within Channel Complex B, Channel Bc is incised into the ELP/NTN unconformity in the uplifted Central block (Figure 6-41). Channel Be is incised into reflections inferred to

be Quaternary sediments that lie within the axis of a syncline of the eastern structural block (Figure 6-40). The Channel Be thalweg is located approximately 20 m below the seafloor and approximately 85 m above the ELP/NTN unconformity in the axis of the syncline (Figure 6-40).

The thalwegs of Channels Be and Bc are located at a depth of approximately 120 m. The post-ELP/NTN reflections into which Channel Be is incised are strongly folded inferred Quaternary strata (Figure 6-40). Erosional truncation of these reflections by Channel Be is clearly apparent on the northern flank of the channel (Figure 6-40). Horizon H40, which is mapped along the same truncation surface (angular unconformity) to the north, exhibits structural and stratigraphic relationships similar to the syncline where Channel Be is located (Figure 6-40) and likely coincides with the unconformity at the base of Channel Be. Given a preferred age of 250–240 ka for H40 (PG&E, 2013), it appears that Channel Be was incised during the MIS 8b lowstand (Figures 1-6 and 6-52a).

An alternative model that was evaluated and rejected is that Channel Be was incised during MIS 2, approximately 28–15 ka (Figure 6-52a). However, this would require the unconformity at the base of Channel Be to be reflection H10, which is not supported by the regional mapping studies (Figures 6-21 and 6-29; PG&E, 2013). Reflection H10 is not recognized above Channels Bc and Be, and it appears to be located within the bubble pulse. In addition, if Channel Bc was incised during MIS 2, there should be a continuous channel incised into pre-Neogene rock across the Central block, contrary to the observed relationships (Figure 6-42). Consequently, it appears that Channel Be was incised prior to MIS 2 (Figure 6-52a).

The age model for Channel Be indicates that incision and infill took place during a sea-level lowstand in the late Quaternary between MIS 6b (138 ka) and 1.4 Ma, with a preferred age of approximately 250–240 ka during MIS 8b (Figures 1-6 and 6-52a and b). Given the observed structural and stratigraphic relationships, and the similarities in geometry, depth, and morphology between Channels Be and Bc, it is likely that these paleochannels are coeval in age, and that they were incised either during MIS 8b or during a previous glacially induced sea-level lowstand after the MPT.

Channel Complex F

The thalwegs and margins of Channel Complex F to the east and west of the HFZ are well imaged in the 3D volume as pronounced angular unconformities where the channel is incised into layered reflections of the unnamed Pleistocene deposits, above the ELP/NTN unconformity (Figures 1-5, 6-43, and 6-47). Channel Complex Fc is located in the inferred Quaternary sediments within the axis of a subsiding syncline (Figures 6-36, 6-45, and 6-46), and the base of Channel Fw3 is marked by a pronounced angular unconformity that truncates north-dipping reflections in Quaternary sediments to the west of the western strand of the HFZ (Figure 6-47).

Estimating the age of Channel Complex F incisions and channel infilling is problematic. The depths of the Channel Fe1 and Fc1 thalwegs are approximately 160 m (~200 ms TWTT) and 200 m (~250 ms TWTT), and the depth of the Channel Fw3 thalweg is approximately 260 m (~320 ms TWTT). These depths are significantly greater than the

reported 120–125 m sea-level lowstands of the late Quaternary since the MPT. Either Channel Complex F has subsided significantly since initial fluvial channel incision, or the channels are of marine origin and formed below sea level. The submarine origin is considered more likely.

Channel Complex F is approximately 700 m wide near the top of Channel Fw3 (Figure 6-47), which lies at a depth of approximately 200 m (~250 ms TWTT). Channel Fw3 is overlain by a thick (~80 m; ~100 ms) sequence of fairly flat-lying reflections inferred to be of late Quaternary age, and horizons H30 and H10 have been mapped near the top of this sequence (Figure 6-47). The age of Channel Complex F is constrained by a lower-bound limit of the ELP/NTN and an upper-bound limit of reflections H10 and H30. Approximately 50 m of relatively flat-lying, undeformed reflections separate the top of Channel Fw3 and the H30 horizon (Figure 6-47). Consequently, Channel Fw3 is interpreted to be significantly older than the H30 horizon. A reflection observed approximately 40 m below H30 may represent the H40 unconformity (Figure 6-47), which is not regionally mapped in this area (PG&E, 2013). The confidence level of the age of H30 to the west of the western strand of the HFZ in the Point Sal 3D survey area is medium.

Channel Fe1 is overlain by reflection H30, and Channel Fe3 is overlain by reflection H10 (Figure 6-43). The oldest age for Fe3 allowed by the observed relationships is H30, approximately 150–130 ka (Figure 6-52a). The confidence level of the age of H30 to the east of the eastern strand of the HFZ in the Point Sal 3D survey area is low.

The preferred age model for Channel Complex F (Channels Fw3, Fc1, and Fe3) suggests that incision and infilling took place during a low sea-level lowstand in the late Quaternary, sometime between MIS 6b (~150–130 ka) and 1.4 Ma, with a preferred age of approximately 350–340 ka, at the MIS 10 lowstand (Figure 6-52a).

The alternate age model (Figure 6-52b) for Channel Complex F (Channels Fw3, Fc1, and Fe1) also assumes that incision and infilling took place during MIS 10, approximately 350–340 ka. The only difference between the two age models is that the preferred model (Figure 6-52a) is for Channels Fw3, Fc1, and Fe3 to be correlative in age, whereas the alternate age model (Figure 6-52b) is for Channels Fw3, Fc1, and Fe1 to be correlative in age.

6.2.2.5   Slip-Rate Estimates (Paleochannel Piercing Points)

Calculation of the slip rates of the HFZ in the Point Sal study area is based on the offsets of the channel thalweg piercing points within Channel Complexes A, B, and F, which is done simply by dividing the amount of fault offset by the age of the piercing point. Both of these parameters include inherent uncertainty. The uncertainty in both of these parameters is represented by the limiting minimum and maximum constraints, which are described above and summarized in Tables 6-5, 6-6, 6-7, and 6-8.

Channel Complex A

The Channel Complex A piercing points (thalwegs of Channels Ac2 and Aw2) that cross the western strand of the HFZ exhibit measurable lateral and vertical displacements.

These channels are better imaged than Channels Ac1 and Aw1, and more clearly exhibit erosional truncation of underlying reflections (Figures 6-37 and 6-38). Consequently, only the thalweg piercing points of Channels Ac2 and Aw2 are presented in the age models (Figures 6-52a and b) used for estimating slip rates. Estimations of dextral slip rates on the western strand of the HFZ are presented in Table 6-5 below.

Table 6-5. Western Strand HFZ–Channel Ac2/Aw2 Dextral Slip-Rate Estimates

Age	Min. Offset (75 m)	Max. Offset (115 m)	Pref. Offset (95 m)	Comments
20 ka (MIS 2)	3.75 mm/yr	5.75 mm/yr	4.75 mm/yr	Minimum age (MIS 2) of Channel Ac2/Aw2
250 ka (MIS 8b/8c)[a]	0.3 mm/yr	0.46 mm/yr	**0.38[a] mm/yr**	Preferred age (MIS 8b/8c) of Channel Ac2/Aw2 from interpretation that channel incision events represent 100 kyr sea-level cycles. Channel Ac2/Aw2 is ~one cycle older than H30
1.4 Ma (MIS 45)	0.05 mm/yr	0.08 mm/yr	0.07 mm/yr	Maximum age of Channel Ac2/Aw2 at onset of MPT

[a] Preferred age model and slip rate.

The preferred slip-rate estimate for the western strand of the HFZ, based on the age model for Channel A, is 0.38 mm/yr, within a range of 0.3–0.46 mm/yr. The estimated minimum slip rate is 0.05 mm/yr, and the maximum slip rate is 5.75 mm/yr. As discussed previously, the preferred age of incision of Channel B is 250 ka (MIS 8b).

Channel Complex B

The Channel Complex B piercing points (thalwegs of Channels Be and Bc) that cross the eastern strand of the HFZ suggest dextral offsets of approximately 193–510 m (Figure 6-50) and vertical displacement of approximately 20–60 m. This apparent thalweg displacement, however, may be the result of erosion or other processes that are not representative of fault movement. Nevertheless, these apparent offset estimates are used to determine a potential slip rate for the eastern strand of the HFZ and are presented in Table 6-6 below.

The preferred slip-rate estimate for the eastern strand of the HFZ, based on the age model for Channel B, is 1.42 mm/yr, within a range of 0.77–2.04 mm/yr. The estimated minimum slip rate of the preferred correlation is 0.14 mm/yr, and the maximum slip rate is 3.70 mm/yr. As discussed previously, the preferred age of incision of Channel B is 250 ka (MIS 8b).

Table 6-6. Eastern Strand HFZ–Channel Be/Bc Dextral Slip-Rate Estimates

Age	Min. Offset (193 m)	Max. Offset (510 m)	Pref. Offset (356 m)	Comments
138 ka (MIS 6b)	1.40 mm/yr	3.70 mm/yr	2.58 mm/yr	Minimum age (MIS 6b) of Channel Be/Bc from absence of continuous channel across central block
250 ka (MIS 8b)[a]	0.77 mm/yr	2.04 mm/yr	**1.42[a] mm/yr**	Preferred age (MIS 8b) of Channel Be/Bc from interpretation that Channel B is same age as H40, and the preferred age model for H40 (PG&E, 2013)
1.4 Ma (MIS 45)	0.14 mm/yr	0.36 mm/yr	0.25 mm/yr	Maximum age of Channel Be/Bc

[a] Preferred age model and slip rate.

Channel Complex F

Slip rates for the preferred Channel F correlations were calculated based on offsets illustrated on Figure 6-51a, as summarized in Table 6-4, and the preferred age model (Figure 6-52a). The preferred slip rates for the HFZ are calculated from measured lateral offsets and estimated ages for Channels Fe3 and Fw3. The correlation confidence level for these two channels is high because they are very well defined and geomorphically similar, and they share the same trend and same stratigraphic position. The estimated dextral slip rates for the preferred Channel Fe3/Fw3 correlation are shown in Table 6-7.

Table 6-7. Preferred Channel Fe3/Fw3 Dextral Slip-Rate Estimates for Entire HFZ

Age	Min. Offset (550 m)	Max. Offset (700 m)	Pref. Offset (600 to 650 m)	Comments
138 ka (MIS 6b)	3.98 mm/yr	5.07 mm/yr	4.35-4.71 mm/yr	Minimum age (MIS 6b) for incision of Channel Fe3/Fw3 thalweg
342 ka (MIS 10)[a]	1.61 mm/yr	2.05 mm/yr	**1.75–1.90[a] mm/yr**	Preferred age (MIS 10) of Channel Fe3/Fw3 based on superposition and depth below reflectors H10 and H30 west of HFZ, and preferred ages for these reflectors (PG&E, 2013)
1.4 Ma (MIS 45)	0.39 mm/yr	0.5 mm/yr	0.43-0.46 mm/yr	Maximum age of Channel Fe3/Fw3

[a] Preferred age model and slip rate.

The preferred slip-rate estimate for the entire HFZ based on the Channel Fe3/Fw3 correlation is 1.75–1.90 mm/yr, within a range of 1.61–2.05 mm/yr. The estimated minimum slip rate of the preferred correlation is 0.39 mm/yr, and the maximum slip rate is 4.71 mm/yr. As discussed previously, the preferred age of incision of Channel Fe3/Fw3 is 342 ka (MIS 10). This range describes the most likely slip rate for the HFZ within the Point Sal study area over the past approximately 500 kyr, and accurately represents the uncertainty in slip rate based on the conditions that the channel correlations are correct and the age model adequately captures the true age uncertainties. However, if the correlations are incorrect, and the true correlations involve more slip on the fault, then the calculated slip rate will be higher. Alternative correlations are also possible (see below in next section).

Channel Complex F Slip Rates Estimated from Alternative Correlation and Age Model

Slip rates for the alternative Channel Complex F correlation were also evaluated. The estimated dextral slip rate for the alternative correlation is based on Channel Fe1 and Fw3 being of the same age. The alternate Channel Complex F piercing points' correlation (thalwegs of Channels Fe1 and Fw3) across the HFZ suggest approximately 450–600 m of dextral separation since incision of the channel thalweg. Channels Fe1 and Fw3 are interpreted as marine channels that originally incised into reflections of sediment deposited on the middle and upper slope. The correlation confidence level for these channels is low because they are not well defined and geomorphically similar. However, Channel Fe1 is stratigraphically lower than Fe2 and Fe3, is U-shaped, and is about the same width as Channel Fw3. There is considerable uncertainty in the age of Channels Fe1 and Fw3 because of the lack of age control. The range of possible ages for the horizons that stratigraphically bracket Channels Fe1 and Fw3 and the apparent dextral slip rates for the preferred channel correlation are given in Table 6-8.

Table 6-8. Alternate Channel Fe1/Fw3 Dextral Slip-Rate Estimates for Entire HFZ

Age	Min. Offset (450 m)	Max. Offset (600 m)	Pref. Offset (500–550 m)	Comments
138 ka (MIS 6b)	3.26 mm/yr	4.35 mm/yr	3.62–3.98 mm/yr	Minimum age (MIS 6b) for incision of Channel Fe1/Fw3 thalweg. Not preferred due to stratigraphic position of Fw3 relative to H30 west of HFZ
342 ka (MIS 10)[a]	1.32 mm/yr	1.75 mm/yr	**1.46–1.61[a] mm/yr**	Preferred age (MIS 10) of Channel Fe1/Fw3 based on channel elevation and depth below reflectors H10 and H30, and preferred ages for these reflectors (PG&E, 2013)
1.4 Ma (MIS 45)	0.32 mm/yr	0.43 mm/yr	0.36-0.39 mm/yr	Maximum age of Channel Fe1/Fw3

[a] Preferred alternate age model and slip rate.

The alternate slip rate estimate for the entire HFZ based on the Channel Fe1/Fw3 correlation is 1.46 to 1.61 mm/yr, within a range of 1.32 to 1.75 mm/yr. The estimated minimum slip rate of the preferred correlation is 0.32 mm/yr, and the maximum slip rate is 4.35 mm/yr. As previously discussed, the preferred age of incision of Channel Fe1/Fw3 is 342 ka (MIS 10).

7.0 THE SHORELINE FAULT ZONE

This section focuses on the southern extension of the Shoreline and associated fault zones that are acoustically imaged in the San Luis Obispo Bay area. Here we address the stratigraphy and structure associated with possible fault movement and describe channels and paleoshoreline morphologies that are potential piercing points identified from the interpretations of the San Luis Obispo Bay (Survey Area 2) 3D LESS data set and supplemented with interpretations of the USGS and PG&E legacy archive seismic-reflection profiles.

7.1 The San Luis Obispo Bay Study Area

The San Luis Obispo Bay study area (Survey Area 2) is located on the middle continental shelf in central San Luis Obispo Bay (Figure 1-1; Plate 1). The Santa Maria River and other smaller, locally sourced coastal drainages (Figure 1-4) feed into the bay and provide abundant sediment to the coast and shelf. The Santa Maria River is fed from an extensive watershed and throughout the Holocene has formed a substantial delta, which is classified as a high-energy, wave-dominated delta regime (Galloway, 1975; Boggs, 2005), characterized by a linear coastline, a large coastal dune complex, braided and meandering streams on a wide coastal floodplain, a lagoon, and back-dune lakes.

7.1.1 Results

Identification, mapping, and descriptions of the faults and geomorphic features used in determining the potential slip rates associated with the Shoreline and other fault zones within the San Luis Obispo Bay study area result from the interpretation of the extensive data sets available during the time of this study. The results stem mainly from extensive assessment and visualization of the 3D data volume, as well as from the PG&E 2D legacy archive data.

7.1.1.1 Stratigraphy

Neogene and Mesozoic-age rocks underlie Holocene continental shelf sediments in San Luis Obispo Bay (Figure 7-1). Outcrops of Neogene and older bedrock at the seafloor are common on the inner shelf of the northern and southern parts of the bay, while Holocene marine shelf sediments cover most of the seafloor elsewhere. Four basic stratigraphic units are imaged from the 3D seismic-reflection and bathymetric data, which were correlated with the stratigraphic units described by Johnson and Watt (2012). These units, described below, consist of Mesozoic basement rocks, Neogene marine rocks, Upper Pleistocene deposits, and latest Pleistocene to Holocene strata.

Mesozoic Basement

Basement rocks consist of Jurassic Coast Range ophiolite, Jurassic to Cretaceous Franciscan Complex mélange, metavolcanics, and serpentine, and Cretaceous sandstone. These older rocks are highly deformed and generally acoustically homogeneous, indicative of massive units (Figure 7-1). Deformed bedding is locally visible in 3D time slices within the Cretaceous sandstone unit. Volcanic intrusive and extrusive rocks form

large, rounded tectonic clasts ("knockers"), which are commonly more resistant to erosion than other basement units. The interpreted serpentinite units (Plate 4) appear curvilinear to sinuous in plan view and are locally present along fault zones. On the LESS seismic-reflection profiles, all the basement and Neogene rocks are represented by a high-amplitude reflector and have been mapped as the top-of-bedrock surface.

Neogene Marine Rocks

Neogene marine rocks in the 3D survey area include tuffaceous sandstone and siltstone of the Miocene Obispo Formation (Figure 7-1). Stratified Miocene-age Monterey Formation and Pliocene Pismo Formation are locally present on the inner shelf in San Luis Obispo Bay (PG&E, 2011a), but are not mapped in the 3D survey area. On seismic-reflection profiles, the inferred Miocene Obispo Formation is similar in appearance to the Mesozoic basement rocks (Plate 4); however, on the 3D time slices, the texture of this unit is characterized by chaotic, unstratified intervals with large angular blocks embedded within a finer-grained matrix of zeolitized tuff (Hall, 1973). Volcanic intrusions of Miocene age are also locally present within the Obispo Formation. Across the 3D survey area, the Neogene rocks and Mesozoic basement rocks are collectively mapped as a top-of-bedrock horizon. Faults and channels are mapped on the top-of-bedrock surface and are locally overlain by Quaternary strata (Figures 7-2 and 7-3).

Upper Pleistocene Deposits

Upper Pleistocene deposits unconformably overlie the top-of-bedrock surface and underlie a transgressive erosion surface (<20 ka) associated with the latest Pleistocene sea-level rise (Johnson and Watt, 2012). These strata are present in the southeastern part of the 3D survey area, and thicken dramatically to the south in central San Luis Obispo Bay (Figure 7-4). They are commonly characterized on seismic-reflection profiles and time slices (Figure 7-5) by an upper sequence of channelized Upper Pleistocene deposits that lap onto the bedrock surface in the southern part of the 3D survey area (Figure 7-6). Onshore these deposits have been mapped by the California Department of Water Resources (DWR, 2002) as the Paso Robles Formation. Offshore, these deposits are locally underlain by continuous parallel to subparallel, moderate- to high-amplitude, high-frequency reflections (Johnson and Watt, 2013). This unit occurs above a heavily incised bedrock surface (Figure 7-7) throughout much of San Luis Obispo Bay, and presumably was deposited in shelf, nearshore, and coastal floodplain/deltaic environments during the late Quaternary (Johnson and Watt, 2012). The Upper Pleistocene deposits are bounded above by the H10 horizon (PG&E, 2013) and below by the top-of-bedrock surface (Figures 7-8 through 7-11).

Upper-Most Pleistocene to Holocene Strata

The latest Pleistocene to Holocene (<20 ka) strata make up the youngest, uppermost stratigraphic unit in the survey area, having been deposited during and after the approximately 120–130 m sea-level rise following the LGM (MIS 2; Figure 1-6). These strata are characterized on seismic-reflection profiles (Figures 7-8, 7-10, and 7-12) by low- and moderate-amplitude, low- to high-frequency, parallel, moderately continuous reflections (Johnson and Watt, 2012). The Holocene marine deposits in the 3D survey

area vary in thickness from 0 to 25 m (Figure 7-9), and thicken toward the south (Figures 7-6c and 7-10). Analogous post-LGM Holocene shelf facies strata have been identified and mapped in many other locations along the California Central Coast (Grossman et al., 2006).

The isopach of Quaternary sediments (Figure 7-6a) consists of all sediments between the top-of-bedrock surface and the seafloor, including channel fill deposits, Upper Pleistocene coastal floodplain deposits, and Holocene marine shelf sediments. The Holocene sediment cover thickens toward the south, with a maximum thickness of approximately 25 m. The maximum thickness of Quaternary strata in the 3D survey area is 75 m. Similar to the Holocene sediment, the Quaternary deposits thicken gradually from north to south and dramatically from west to east where the top-of-bedrock surface steeply slopes into the Santa Maria River embayment. The Upper Pleistocene coastal floodplain deposits also thicken toward the south, varying from 0 to 45 m in thickness. The limit of onlap of the Upper Pleistocene deposits onto the top of bedrock is shown as a green line on Figure 7-6, and, because of its geochronological significance in constraining the age of channel formation and fault offset, is referred to repeatedly in the text and shown on maps throughout this report.

Continental Shelf

On the continental shelf, the Holocene sediment cover is generally thin, with local exposures of bedrock in the northern part of the study area. The southern edge of bedrock seafloor exposures is broadly on trend with the Los Berros fault zone. Within the central part of San Luis Obispo Bay, the transition from rocky seafloor in the north to smooth, sediment-covered seafloor is characterized by a submerged bedrock paleo-embayment that extends north toward Avila and Point San Luis. The location and size of the embayment appears to be controlled by the paleo–San Luis Obispo Creek drainage pathway that crosses the continental shelf (Figure 1-4). Other paleo-embayments or breaks in the seafloor outcrop pattern are present to the east, offshore of Pismo and Arroyo Grande Creeks. To the south, a continuous wedge of Holocene and Quaternary sediment covers the seafloor across San Luis Obispo Bay to immediately north of Point Sal. Throughout the study area, the distribution of Holocene sediment tends to reflect the irregular morphology of the top of bedrock and local Quaternary creek and river drainage systems (Figure 1-4; Plate 1).

Seismic-reflection horizons (unconformities) H10, H20, H30, and H40 (Figures 1-6 and 1-8) were mapped to the south, across the HFZ, and into western San Luis Obispo Bay (PG&E, 2013) using regional sequence stratigraphy reported in PG&E (2013) and recognized offshore of Estero Bay. The mapping provides loose geochronologic bracketing and approximate age estimates of late Quaternary sedimentary units that lie beneath the shelf. The preferred age model for these unconformities is illustrated on Figure 1-6 (modified from PG&E, 2013).

Stratigraphic units and mapped horizons in the San Luis Obispo Bay 3D data set include the H10 horizon and the top-of-bedrock surface (Figures 7-3 and 7-4). The H10 horizon was also mapped using 2D seismic-reflection profiles from the PG&E legacy archive. The correlation confidence in the top-of-bedrock horizon is high across most of the 3D

data set (see inset on Plate 4), but is lower to the south below the depth of the seafloor multiple.

Continental Shelf Break

North and south of San Luis Obispo Bay, the edge of the continental shelf is approximately coincident with the 125 m isobath (PG&E, 2013) and with the HFZ in Estero Bay (Plate 1B). To the north of Point San Luis, the HFZ roughly marks the boundary between the continental shelf and the continental slope. However, in San Luis Obispo Bay, the shelf broadens and the HFZ traverses the outer continental shelf (Figure 1-1; Plate 1B), resulting in a poorly defined shelf break. Johnson and Watt (2012) attribute this to progradation of a thick deltaic sedimentary wedge offshore of the Santa Maria River. A minor break in slope occurs at approximately 160 m depth west of San Luis Obispo Bay and may represent the western terminus of a downlapping, distal progradational wedge of the paleo–Santa Maria River delta (Johnson and Watt, 2012).

Paleochannels

Pre-Holocene buried paleochannels incised into the top of bedrock were identified using the seismic amplitudes and post-stack smoothed similarity attribute (Figures 7-2 through 7-11; Plate 4) and were further refined using a structural contour map (Figure 7-7; Plate 5). The buried channels are generally well defined and filled with material that produces a distinct acoustical signature of transparent to chaotic character or weakly layered (Figure 7-12). Other pre-Holocene channels not incised in bedrock are locally apparent in the unnamed Upper Pleistocene deposits (Figure 7-5). An age model for paleochannels incised into bedrock in the 3D data survey area is presented in Section 7.2.1.5 of this report. The channels in the Upper Pleistocene deposits were not mapped because they are small, discontinuous, meandering channels and do not cross Quaternary-active faults. The channels are discussed in Sections 7.1.1.3 and 7.2.1.4 below.

7.1.1.2   Faults

In San Luis Obispo Bay, several faults were recognized and mapped within the 3D LESS area and to the southeast. Fault identification was based on the criteria presented in Section 3.2. After detailed mapping of the reflection identified as the top-of-bedrock horizon in the 3D volume, a smoothed similarity attribute was extracted over the horizon (Figure 7-2) to image lineaments associated with the shallow subsurface traces of many faults, which formed the basis for mapping faults. Definition of fault dip below the bedrock surface was challenging in the 3D data set because of limited penetration below the reflection of the bedrock surface (Figures 7-8, 7-10, and 7-12). However, given the resolution and clarity of fault traces visible on the top-of-bedrock surface, fault traces were interpreted and mapped with a high level of confidence throughout the survey area (Figure 7-2; Plate 4).

Considerable detail of the fault geometry is provided in the 3D volume, and the pattern of faulting in plan view is complex (Figure 7-13). In the northwestern and central parts of the 3D survey area, several faults converge and split near Souza Rock (Figures 7-13, 7-14, and 7-15; Plate 4). The Shoreline fault zone has been mapped as the throughgoing

structure in this area; it extends southeastward through the entire survey area and to the southeast across San Luis Obispo Bay (Plate 1B). The Oceano fault bifurcates from the Shoreline fault near Channel A west of Souza Rock and continues to the southeast as a narrow linear fault strand across the 3D survey area (Figures 7-3 through 7-7; Plates 4 and 5). Outside the 3D survey area, this fault continues and connects with the Oceano fault zone, which then aligns with the previously mapped Santa Maria River and Oceano fault zones onshore near the mouth of Arroyo Grande Creek (Figure 7-15). The total length of the Oceano fault from Souza Rock to the shoreline is 10.7 km (Figure 7-15).

Just north of Souza Rock, the western terminus of the Los Berros fault appears to be truncated by, or merge with, the Shoreline fault zone (Figure 7-2; Plates 1B and 4). A general east-west-trending inferred fault, here called the North Pecho fault, appears to merge with the southeastern strand of the Shoreline fault zone in the central part of the survey area, and a more westerly inferred strand, called the Pecho fault, appears to bifurcate from the North Pecho fault strand near the northwestern corner of the survey area and extend a short distance to the southeast (Figure 7-15). A well-defined east-west trending unnamed fault terminates at the Shoreline fault zone in the central part of the survey area, just south of where the North Pecho fault appears to merge with the Shoreline fault zone.

Faults were also mapped throughout northern San Luis Obispo Bay outside the 3D survey area using 2D seismic-reflection profiles from PG&E's legacy archive data set (Figures 7-14 and 7-15). The convergence of many faults can be observed in plan view, with the previously mapped Pecho, Oceano, Shoreline, and Los Berros fault zones and several unnamed faults merging within the 3D survey area (Plates 4 and 5). These faults are mapped on the top-of-bedrock surface and are also identified in the USGS 2D seismic-reflection profiles (e.g., Line PBS-09 on Figure 7-16). On Profile PBS-09, all the faults can be seen to offset the reflection identified as the bedrock surface where the reflection is imaged, and none of the faults appear to extend above the H10 reflection.

The Oceano and Los Berros fault zones and the central unnamed fault are well represented in seismic-reflection profile CoMAP 86-3 (Figure 7-17), where all mapped faults appear to offset reflections of pre-Quaternary rock and cut shallow subsurface reflections interpreted to be of late Quaternary age (Figure 7-17). The USGS seismic-reflection Profile PBS-10 (Figure 7-18) clearly shows offset of the deep, high-amplitude reflection identified as top of bedrock by the Los Berros fault, as well as deformation, folding, and tilting of shallow, thinly layered reflections of probable Quaternary strata overlying the bedrock surface. The USGS seismic-reflection Profile PBS-283 (Figure 7-19) exhibits faults that offset and deform well-layered, continuous reflections beneath the H10 reflection, which suggests late Quaternary activity of the "South Pecho" (named for a fault that extends from the 3D study area to the south), Shoreline, and central unnamed faults. To the south of the 3D survey area, the Shoreline fault zone is interpreted to cut the reflection that represents the H10 unconformity, as shown on USGS Profile PBS-283 (Figure 7-19). Faults associated with the Hosgri, Shoreline, Oceano, Los Berros, and Los Osos fault zones are exhibited on a composite cross section that includes seismic-reflection profiles of Nekton Line 229, CoMAP Line 3, and the 2011 PG&E Price Canyon Line (Figure 7-20).

The Los Berros and Oceano faults are part of the Southwestern Boundary zone, which also includes the Wilmar Avenue fault (Figure 7-20). Willingham et al. (2013) previously mapped these faults offshore of Pismo Beach, and the results of the present study confirm and refine the locations of these faults (Figure 7-15). The onshore extension of the Wilmar Avenue fault is modified from Lettis et al. (2004), and the onshore extension of the Los Berros fault is from AMEC (2011), which aligns well with the trace mapped offshore. The Oceano fault is interpreted to extend onshore to the east beneath Nipomo Mesa, where it splays onto two separate fault strands (Oceano and Santa Maria River faults), both of which appear to offset Quaternary sediments on Vibroseis Line SM-05 (Figure A-5). The locations of these faults are modified from Lettis et al. (2004) and the California Department of Water Resources (DWR, 2002). The Shoreline and South Pecho faults offset bedrock and overlying reflections interpreted to be Quaternary strata in southern San Luis Obispo Bay, near the mouth of the Santa Maria River, and appear to connect with a fault mapped in the Guadalupe Oil Field onshore (Figure 7-21a; CDOGGR, 1992).

The Los Berros fault trace in the 3D data set is curved and in places is not clearly defined in the smoothed similarity map of the top-of-bedrock surface (Plate 4). This fault has a distinctly different strike from the southeast-trending Shoreline fault strand and the east/southeast strike of the Oceano fault (Figure 7-15b). The strike of the Los Berros fault changes along different parts of the fault, but is generally east-west. Seafloor exposures of bedrock are common on the north side of the fault in northern San Luis Obispo Bay (Plate 1B). The geometry and shallow dip of the fault, as interpreted from CoMAP seismic-reflection profile Line 86-3 (Figure 7-17), suggest that the fault dips to the north and is a thrust fault. On the CoMAP profile, we interpret a hanging-wall anticline on the north side of the fault, and a footwall syncline on the south side of the fault. This geometry is also apparent on USGS Line PBS-10 (Figure 7-18), and on the regional line across San Luis Obispo Bay (Figure 7-20). A magnetic lineament correlates with the fault trace (Figure 7-14), suggesting basement offset at depth.

Three separate fault-bounded structural blocks—the eastern, central, and western structural blocks (Figures 7-2b, 7-7b, and 7-22b; Plate 5) were identified in the San Luis Obispo Bay 3D volume. The Eastern block is separated from the Central block by the Oceano fault, and the Central block is bounded by, and separated from, the Western block by the Shoreline fault zone. As mapped on Figure 7-7b and Plate 5, the Los Berros fault is in the eastern structural block, several unnamed faults are in the central structural block, and numerous strands of the Pecho fault zone are in the western structural block.

Fault activity was evaluated based on paleochannel crosscutting relationships and stratigraphic units deformed by faults. Evidence for Quaternary activity was noted on the Shoreline, Oceano, South Pecho, Central unnamed, and Los Berros fault zones. Piercing points were identified on the Shoreline and Oceano fault zones and unnamed faults; these are discussed in Section 7.1.1.3. Analyses of San Luis Obispo Bay faults, piercing points, age models, and slip-rate constraints are discussed in Section 7.2.

7.1.1.3   Piercing Points

Numerous piercing points were identified in the 3D LESS data set (Figure 7-23). Two piercing points were mapped at the intersection of paleostrandlines and the Shoreline fault (Figure 7-24). The other piercing points are buried paleochannels where they cross various mapped Quaternary faults (Figure 7-23). The results of the interpretations that defined piercing points along the Oceano and Shoreline fault zones and other unnamed faults in the central structural block mapped in the San Luis Obispo Bay 3D survey area are presented below.

Paleoshoreline (Strandline) Piercing Points

Four buried shorelines were recognized and mapped in the southern part of the San Luis Obispo Bay study area (Figures 7-23 and 7-24). Time slices of the two paleoshorelines that cross the Shoreline fault zone are presented on Figures 7-25 and 7-26. These paleoshorelines are incised into reflections identified as Upper Pleistocene deposits that overlie the bedrock surface (Figures 7-27 and 7-28). The inner edges (shoreline angles) of the paleostrandlines imaged in 3D time slices (Figures 7-25 and 7-26) define linear to circular geomorphic features (Figure 7-24) that are stratigraphically isolated, and an age of incision can be estimated from these stratigraphic relationships (Section 7.1.2.5).

The paleostrandlines and shoreline angles were mapped using the same methodology as described in PG&E (2011, 2013) reports. The mapped paleostrandlines vary in depth from approximately 79 to 97 m (Figure 7-24). Two paleostrandlines that cross the Shoreline fault zone were identified and mapped at depths of 84 m and 92 m (Figures 7-24 through 7-28). Both of these strandlines exhibit lateral and vertical separation across the Shoreline fault zone. Vertical separation was measured in IHS Kingdom and is estimated to be approximately 0.8 to 1.6 m (~1–2 ms), near the resolution of the data. Dextral offset on both the 84 and 92 m deep strandlines is 9.4 ± 6 m, with a preferred value of 10 m (Figure 7-29).

Dextral and vertical offset estimates for paleostrandline–Shoreline fault zone piercing points are summarized in Table 7-1.

Table 7-1. Shoreline Fault Zone–Paleostrandline Offset Estimates

Paleostrandline Elevation (m)	Dextral Offset (m)			Vertical Offset (m)		
	Min.	Max.	Pref.	Min.	Max.	Pref.
–84	3.4	15.4	**10**	0.8	1.6	**1**
–92	3.4	15.4	**10**	0.8	1.6	**1**

Note: Minimum dextral offset of 3.4 m is based on measured offset of 9.4 m minus combined 6 m of geologic uncertainty and data resolution.

The geomorphic expression of the paleostrandlines (Figures 7-24, 7-25, 7-26, and A-6) consists of several buried bedrock paleo-embayments separated by bedrock paleo-headlands. The geometry (in plan view) and morphology of the buried paleoshorelines and paleo–sea cliffs interpreted from the 3D data set are similar to the geomorphology of

the present-day shoreline along the coast of the San Luis Hills between Avila and Los Osos, although less irregular.

Buried Channel Piercing Points

Twelve buried paleochannels incised into the bedrock surface were recognized and mapped using the 3D LESS data set (Figures 7-7, 7-30, 7-31, and 7-32). These have been designated Channels A through L, from north to south (Figures 7-2, 7-7, and 7-22; Plates 4 and 5), and labeled according to the channel nomenclature described in Section 3.3.2 above. Channels were mapped in the 3D volume using amplitude time slices (Figure 7-31) and attributes, as well as interpretation of 2D lines displayed within the 3D volume (Figures 7-8 and 7-12). Relative ages of channel fill deposits were evaluated based on depth of incision and channel crosscutting relationships (Figure 7-32; insets shown on Plates 5 and 6).

Stream channel axis (thalweg) profiles were created for each mapped channel (Plate 6). Three separate channel complexes were designated based on inferred watershed source (Figures 1-4 and 7-30). Source Channel Complex 1 (Channels A through E) appears to have been sourced from San Luis Obispo Creek. Source Channel Complex 2 (Channels F through I) was probably sourced from Pismo Creek (Figure 7-30) and Source Channel Complex 3 (Channels J, K, and L) appears to be sourced from very small, local watershed areas on the eastern structural block or perhaps from overflow from Pismo Creek. A surface slope map of the top of bedrock illustrates that steeper slopes are associated with channel margins (Plate 7) and fault scarps. The length, width, depth, and average inclination of the mapped channels in the 3D survey area are presented in Table 7-2 below.

Table 7-2. Summary of Paleochannel Dimensions for San Luis Obispo Bay

Channel	Complex	Length (m)	Width (m)	Depth (m) avg./max.	Avg. Inclination (%)
A	1	7,688	74–128	14/23	3.6
B	1	4,039	85–116	13/23	4.5
C	1	6,559	76–180	15/27	3.5
D	1	2,706	63–120	7/14	2.6
E	1	852	25	4/9	3.5
F	2	5,440	50–170	10/14	2.8
G	2	930	32–45	5/7	2.5
H	2	852	40–50	8/12	2.8
I	2	4,083	50–115	7/15	4.3
J	3	584	26	3/5	2.8
K	3	143	20	1/3	4.9
L	3	229	15	1/2	2.7

A complex paleochannel morphology is imaged in the 3D volume (Figures 7-33 through 7-42; Plates 4 and 5), where channels range from small, fairly straight narrow-thread channels with V-shaped channel (Figure 7-41) to broad, flat channel floors representative of a braided fluvial system (Figures 7-39 and 7-42). The margins of the channels are generally sharp in the thread channels, while they are gently rounded in the larger, broader channels. The sharp upper margins of many of the channels are well exhibited in slope maps that were constructed to define the line of greatest slope declivity in high resolution (within 3–6 m), as shown on Plate 7, and the upper margins are used as potential piercing points for determining fault offsets.

The crosscutting relationships and bifurcation of the paleochannels that are apparent on the horizontal and inclined time slices of the 3D volume suggest varying ages of initial channel incision and reoccupation of the channels mapped in San Luis Obispo Bay (Figure 7-32; Plates 4, 5, and 6). The relative ages of the stream channels were interpreted using channel elevations or depths within the stratigraphic sequences, cross-channel profiles, crosscutting relationships, and thalweg gradient maps (Figure 7-22; Plates 6 and 7). Older and younger relative ages of initial channel incision are distinguished (Figure 7-23; Plate 6), but in some cases, the relative ages of channels are unclear. Contradictions in the relative ages of individual channels exist in different parts of the 3D data set, suggesting that some channels were abandoned and subsequently reoccupied at different periods through geologic time. The relative ages of initial channel incision (Figures 7-23; Plates 5 and 6) are inferred based on channel depths, bedrock surface contour map, and the geomorphic relationships at channel crossings. Crosscutting relationships of the upper (youngest) channel fill deposits in each channel and their stratigraphic position and relationship to Holocene marine and Upper Pleistocene deposits were also evaluated and used in developing channel age models (see Section 7.1.2.5 below).

Confidence Levels in Selecting Piercing Points

Geologic and measurement uncertainties contribute to the total uncertainty in piercing point offset estimates. Measurement uncertainty is a function of data resolution, which for the 3D P-Cable system used in this study, is approximately 3 m horizontal and approximately 2 m vertical (see Section 2.2). Geologic uncertainty is variable, but for the San Luis Obispo Bay 3D data set, is generally 3 to 6 m. For those piercing points that cross the Shoreline fault, which is characterized as a vertical right-slip fault zone, and where no horizontal separation is observed, the minimum value of dextral separation is taken as 0, and the maximum value as 6 m. Vertical separation across faults in the 3D data set locally exhibits opposite senses of motion (north vs. south side up) and in some cases varies along strike. For those piercing points where no vertical separation is observed, the range is –2 m to +2 m (see Tables 7-3 through 7-10). Offset estimates and associated measurement uncertainties are summarized in Table 7-11. Geologic uncertainties related to the following factors are considered in determining offsets of the piercing points:

- Fluvial geomorphology.
- River avulsion and deflection.

- Differential erosion.
- Juxtaposition across fault-line scarps of bedrock units with differences in rock hardness.
- Erodability of lithologic units.

Channel Complex A–Shoreline-Oceano Fault Zone Piercing Points

The Channel Complex A piercing points are located in Source Channel Complex 1 of San Luis Obispo Bay (Figure 7-30), west of Souza Rock at the intersection of the Shoreline and Oceano faults (Figures 7-2, 7-33, 7-34, and 7-35). Channel Complex A consists of two well-defined channels, one incised (nested) into the other (Figure 7-35), as well as two offset channel margins (Figure 7-35c). The deeper (older) channel is incised into the reflection identified as bedrock (Figures 7-34 and 7-35a). The lower (older) channel fill deposits are offset by the Shoreline fault zone, as apparent on a smoothed similarity time slice at 0.73 s (Figure 7-33a). The upper (younger) nested channel is incised into the channel fill of the lower (older) bedrock-incised channel (Figure 7-33, panels e and f, and Figure 7-35b). The thalweg of this incised nested channel does not appear to be offset by any fault strands of the Shoreline or Oceano fault zones.

Both channel margin and channel thalweg piercing points were used as strain gauges to estimate separation of piercing points across the primary strand of the Shoreline fault zone. Figure 7-33 shows mapping results, including a 3D smoothed similarity time slice (panel a), a slope gradient map (panel b), a contoured bedrock/paleochannel surface (panel c), and three uninterpreted and interpreted amplitude sections (panels d, e, and f). The Shoreline fault is interpreted to dextrally offset the shallow (~50 m below sea level) Channel Complex A's margins by 20 to 40 ± 10 m (see amplitude time slice on Figure 7-35c). The channel margin on the southeast side is disrupted, and apparent dextral offset on the Shoreline fault zone is greater than that observed on the northwest channel margin. The eastern Channel Complex A margin also appears to be vertically offset by the Oceano fault zone (Figure 7-33b and c; Figures 7-34 and 7-35); vertical separation at this location is estimated to be 3 ± 2 m. The Oceano fault zone structural style is reverse, north side up. Souza Rock is uplifted in the hanging wall of the Oceano fault zone at this location, which is near the point of bifurcation from the Shoreline fault zone (Figure 7-2).

The lower Channel Complex A fill deposits are cut by the Shoreline fault zone, as expressed by a lineament visible on a time slice at 0.73 ms (TWTT; Figure 7-33a). The time window of the smoothed similarity attribute displayed on Figure 7-33a is 5 ms (TWTT), and the time-slice depth is approximately 8 to 10 ms (TWTT) above the top of the bedrock surface. The younger narrow and linear nested channel incised into the upper part of the lower (older) channel fill is not offset by the Shoreline or Oceano fault zones (Figure 7-35b). The younger channel's position in relation to the bedrock-incised channel indicates that it reoccupied Channel Complex A during a recent sea-level lowstand in the late Quaternary, subsequent to the initial incision of Channel A into bedrock, channel filling, and approximately 30 m (±10 m) of offset of its thalweg (Figure 7-35a and c). Of the 10 m uncertainty, approximately 3 m is based on the pixel size of the 3D imaging and approximately 7 m on the geologic uncertainty of the Channel A piercing points. Dextral

and vertical offset estimates for Channel A–Shoreline and Oceano fault zone piercing points are summarized in Table 7-3.

Table 7-3.Shoreline-Oceano Fault Zone–Channel A Offset Estimates

	Dextral Offset (m)			Vertical Offset (m)		
Fault	**Min.**	**Max.**	**Pref.**	**Min.**	**Max.**	**Pref.**
Shoreline	10	50	**30**	1	5	**3**
Oceano	0	6	**0**	1	5	**3**

Note: P-Cable survey data resolution is 3 m horizontal and 2 m vertical.

Channels B/C–Shoreline Fault Zone Piercing Points

Potential fault offsets were investigated farther southeast in Source Channel Complex 1, where the Shoreline fault zone crosses the paleochannel thalweg and channel margin piercing points of Channels B and C (Figure 7-36). The 3D seismic time slice (Figure 7-36a) at 0.083 s (TWTT), a slope gradient map (Figure 7-36b), and a contoured bedrock surface/paleochannel plot (Figure 7-36c) were used to interpret the relationships between the paleochannels' morphology and fault lineaments. In the vicinity of the North Pecho fault, Channels B and C overlap and cut across the lower (older) Channel Complex A, and are incised into bedrock at a depth nearly equal to Channel A (Figure 7-36d). South of the Los Berros fault, Channels B and C are incised into bedrock at a depth lower than Channel A (Plate 6). Locally, Channel C is incised into Channel B, but in other areas, these channels lie adjacent to each other at nearly equal depths (Figure 7-36, panels e and f).

No visible lateral or vertical offsets along the Shoreline fault zone of either Channel B or C thalwegs or margins were observed. Given the dextral sense of motion proposed for the Shoreline fault zone reported in previous studies (PG&E, 2011a), we consider offsets to be only right-lateral along the fault zone. We consider the potential range of offset along the fault zone in this location to be 0–6 m, with approximately 3 m being the pixel size of the 3D imaging, and approximately 3 m representing the geologic uncertainty. Consequently, the range of dextral offset is 0 to 6 m, with a preferred offset of 0 m.

The range of vertical offset is –2 to +2 m, with a preferred offset of 0 m. The dextral and vertical offset estimates for Channel B/C–Shoreline fault zone piercing points are summarized in Table 7-4.

Table 7-4. Shoreline Fault Zone–Channel B/C Offset Estimates

Dextral Offset (m)			Vertical Offset (m)		
Min.	**Max.**	**Pref.**	**Min.**	**Max.**	**Pref.**
0	6	**0**	–2	2	**0**

Note: P-Cable survey data resolution is 3 m horizontal and 2 m vertical.

Channel F–Shoreline Fault Zone Piercing Points

Near the center of the 3D survey area, channel margin and thalweg piercing points associated with buried paleochannels F, G, and H were investigated for potential offsets (Figure 7-37). Interpretation of the 3D volume resulted in the construction of a smoothed similarity time slice (Figure 7-37a) at 0.092 s (TWTT), slope gradient map (Figure 7 37b), and contoured bedrock surface/paleochannel plot (Figure 7-37c) that are used to show the paleochannels' morphologies and the location of Shoreline fault zone. Channel F is a northeast-southwest-oriented, fairly wide (75–85 m) and deep bedrock-incised channel that diagonally cuts across the generally east-west-oriented, relatively shallower bedrock-incised Channels G and H (Figure 7-37, panels c, d, and e), where it truncates both channels, leaving them as small hanging valleys to the wider and deeper Channel F. The thalweg of Channel F has a very low gradient in the vicinity of the Shoreline fault zone, more so than to the northeast and southwest. The line of onlap of Upper Pleistocene sediments crosses the Shoreline fault at the location where Channel F crosses the Shoreline fault zone (Plates 5 and 6).

Channels G and H do not cross the Shoreline fault zone and thus cannot be used as piercing points. Channel F crosses the Shoreline fault zone, just southeast of the Channel Hw hanging valley, and in this vicinity, the thalweg is relatively straight and does not indicate significant dextral offset. However, the sharp upper wall breaks are bowed away from the channel and more irregular than the channel margins, both upslope and downslope of the fault zone (Figure 7-37, panels b and c). This irregularity of the Channel F margin could be erosional or may reflect some displacement associated with the fault zone.

No clear offsets of the channel margins are observed, but the margins do appear to be warped and disrupted. The channel is significantly wider and shallower on the southwest (Western block) side of the fault zone than on the northwest (Figure 7-37, panels e and f). Therefore, although the thalweg of Channel F does not exhibit distinct dextral offset, considering the resolution of the 3D data and geologic uncertainty, the preferred dextral offset is 1 m within a range of 0–6 m. Minor down-to-the-north vertical offset of the thalweg is suggested by the channel profile (Plate 6). The vertical offset is –3 to +1 m, with a preferred vertical offset of –1 m.

Dextral and vertical offset estimates for Channel F–Shoreline fault zone piercing points are summarized in Table 7-5.

Table 7-5. Shoreline Fault Zone–Channel F Offset Estimates

Dextral Offset (m)			Vertical Offset (m)			
Min.	Max.	Pref.	Min.	Max.	Pref.	Comments
0	6	**1**	–3	1	**–1**	3 m horizontal and 2 m vertical data resolution

Channel I–Shoreline Fault Zone Piercing Points

In the southern part of the 3D survey area, Channel I is incised into the bedrock and generally trends northeast–southwest to the northeast of the Shoreline fault zone and trends north-south to the south of the fault zone (Figure 7-38). Using a 3D smoothed similarity time slice (Figure 7-38a) at 0.103 s (TWTT), slope gradient map (Figure 7-38b), and contoured bedrock surface/paleochannel plot (Figure 7-38c), potential channel thalweg and margin piercing points were examined to determine whether any offsets are observed along the fault zone. No clear fault offset of channel thalweg, margins, or fill is apparent on the 3D data at this location. The data suggest that Channel I is incised through a very thin wedge of the Upper Pleistocene deposits, and that it is buried beneath Holocene sediments (Figure 6-38d through f). The thalweg of Channel I has a very low gradient and is bowed upward in the vicinity of the Shoreline fault at this location (Plates 5 and 6), suggesting possible deformation along the fault zone.

Based on the data resolution and geologic uncertainty, the range of dextral offset of Channel I by the Shoreline fault zone is estimated to be 0 to 6 m, with a preferred offset of 1 m. No vertical separation of the Channel I thalweg is observed; therefore, the range of vertical offset is estimated to be –2 to +2 m based on the data resolution.

Dextral and vertical offset estimates for Channel I–Shoreline fault zone piercing points are summarized in Table 7-6.

Table 7-6. Shoreline Fault Zone–Channel I Offset Estimates

Dextral Offset (m)			Vertical Offset (m)			
Min.	Max.	Pref.	Min.	Max.	Pref.	Comments
0	6	**1**	–2	2	**0**	3 m horizontal and 2 m vertical data resolution

Channels B, C, D, and E–Oceano Fault Zone Piercing Points

Within the central part of the San Luis Obispo Bay 3D survey area, Channels B, C, D, and E cross the Oceano fault zone. An amplitude time slice (Figure 7-39a) at 0.073 s (TWTT), a bedrock slope plot (Figure 7-39b), a contoured bedrock surface map (Figure 7-39c), and 2D seismic-reflection profiles (Figure 7-39d, e, and f) that cross the channels were examined to define and map channel thalweg and margin piercing points that could be used for estimating offset along the Oceano fault zone. All channels are incised into the bedrock, with the larger incised channels, Channels A and B, being deeper and wider than Channels D and E. Channel B lies west of Channel C north of the fault zone, and trends north-south, parallel to Channel C. At the fault zone, Channel C crosses over Channel B such that Channel B then lies east of Channel C south of the fault zone, and the two channels resume their parallel trend. Channels D and E are located east of Channels B and C and are parallel in trend, but they curve into the larger channels near the fault zone. Channel E is the most sinuous of all the channels, meandering across Channel D upslope of where Channel E appears to connect with Channel B (Figure

7-39c). Channel D also connects with Channel B, near where the Oceano fault zone crosses the channels.

Examination of the bedrock surface contours, channel profiles, and crosscutting incisions into lower (older) channel fill (nesting) suggests that filling and abandonment of Channels C and E has occurred more recently than it did for Channels B and D, but that Channel E has been reoccupied. Although evidence for minor vertical separation was observed on the Channel B and C thalwegs (Figure 7-39d), the upper channel fill deposits of all four channels do not appear to be cut by the Oceano fault zone.

No visible dextral offsets of Channel B, C, and D thalweg or margin piercing points are observed in the data, as each channel displays little or no variability in trend or width across the Oceano fault zone. Channel E does change trend across the fault zone, but it is a small, meandering channel that exhibits similar bends to the north, away from the fault zone. Although the location of the Channel C crossover of Channel B and the merging of Channels D and E into Channel B is near where the channels cross the Oceano fault zone, any relationship to fault motion or relief is not evident in the 3D data set. Given the lack of observable dextral offset of the piercing points for these channels, a maximum lateral offset of approximately 6 m, which falls within the geologic uncertainty and horizontal resolution of the 3D data set and bin size of the bedrock/paleochannel grid, is estimated for the Oceano fault zone at its intersection with these channels. The range of right-lateral offset of the Oceano fault zone is 0 to approximately 6 m, with a preferred value of 0 m.

Examination of the channel profiles (Plate 5) suggest a vertical bedrock separation along the Oceano fault-line scarp of approximately 3 ± 2 m on the Channel B thalweg, 2 ± 2 m on the Channel D thalweg, and 2 ± 2 m on the Channel E thalweg where they cross the Oceano fault zone. The Channel C thalweg exhibits minor vertical separation across the fault-line scarp; the estimated offset value is 1 ± 2 m (with a range of -1 to $+3$ m). The Channel E thalweg also exhibits minor vertical separation across the fault-line scarp, and the estimated offset range is 2 ± 2 m, with a preferred value of 2 m.

Dextral and vertical offset estimates for Channel B, C, D, and E–Oceano fault zone piercing points are summarized in Table 7-7.

Table 7-7. Oceano Fault Zone–Channel B, C, D, and E Offset Estimates

	Dextral Offset (m)			Vertical Offset (m)		
Channel	**Min.**	**Max.**	**Pref.**	**Min.**	**Max.**	**Pref.**
B	0	6	**0**	1	5	**2**
C	0	6	**0**	−1	3	**1**
D	0	6	**0**	0	4	**2**
E	0	6	**0**	0	4	**2**

Channel F–Oceano Fault Zone Piercing Points

Channel F crosses the Oceano fault zone near the center of the northeastern edge of the San Luis Obispo Bay 3D survey area. Identification of potential channel thalweg and

margin piercing points involved using a smoothed similarity time slice (Figure 7-40a) at 0.0755 s (TWTT), a bedrock slope plot (Figure 7-40b), a contoured bedrock surface map (Figure 7-40c), and 2D seismic-reflection profiles (Figure 7-40, panels d, e, and f) across the paleochannel where it crosses the Oceano fault zone produced from the 3D volume.

Where Channel F crosses the Oceano fault zone, an abrupt change in thalweg orientation from northeast-southwest to northwest-southeast is apparent; the thalweg is oriented parallel to the northwest-southeast-trending unnamed fault that intersects the Oceano fault zone at the western margin of the channel. The channel morphology and style also change from a narrow, bedrock-incised channel northeast of the fault to a much wider and shallower meandering and anastomosing channel system south of the fault (Figure 7-40, panels a, b, and c). Channel F's thalweg is not laterally offset at the fault zone. The change in fluvial style observed across the Oceano fault zone and the unnamed faults (Figure 7-40f) is coincident with a change in thalweg gradient and apparent vertical separation along the Oceano fault-line scarp (Plates 5 and 6).

No dextral fault offset of Channel F is observed in the 3D data at the resolution and geologic uncertainty of approximately 6 m. Therefore, the estimated right-lateral offset range for Channel I at the Oceano fault is 0 to approximately 6 m, with a preferred offset of 0 m.

Vertical separation of the channel thalweg across the Oceano fault zone as observed on the channel profile (Plate 6) is approximately 3 ± 2 m, with a preferred value of 2 m.

Dextral and vertical offset estimates for Channel F–Oceano fault zone piercing points are summarized in Table 7-8.

Table 7-8. Oceano Fault Zone–Channel F Offset Estimates

Dextral Offset (m)			Vertical Offset (m)			
Min.	Max.	Pref.	Min.	Max.	Pref.	Comments
0	6	**0**	1	5	**2**	3 m horizontal and 2 m vertical data resolution

Channels J, K, and L–Oceano Fault Zone Piercing Points

The easternmost set of paleochannels, Channels J, K, and L, mapped across the Oceano fault zone is located near the northeast margin of the San Luis Obispo Bay 3D study area in Source Channel Complex 3. A time slice (Figure 7-41a) at 0.0675 s (TWTT), a bedrock slope plot (Figure 7-41b), a contoured bedrock surface map (Figure 7-41c), and 2D profiles (Figure 7-41, panels d, e, and f) near where the channels cross the Oceano fault zone were all used to identify potential channel thalweg and margin piercing points.

In the eastern structural block, Channels K and L are confined as bedrock gullies (Figures 7-23 and 7-41) that terminate at the bedrock fault scarp associated with the Oceano fault zone (Figure 7-41). Channel K continues southeastward a short distance as a channel incised into Upper Pleistocene deposits (Figure 7-41, panels a and e). Only Channel J was mapped to continue across the Oceano fault as a bedrock-incised channel. Consequently,

Channel J's thalweg and margins are used as potential piercing points to constrain fault offset within this area.

No lateral offset of Channel J's thalweg or margins is observed where Channel J crosses the Oceano fault zone, and no distinct change in thalweg gradient occurs (Figure 7-41c). However, the bedrock surface at the juncture of Channel J and the Oceano fault zone exhibits a vertical separation of approximately 2 m (±2 m), down to the southwest. The bedrock surface outside the channel thalweg along profile A-A′ (Figure 7-41d) also exhibits a vertical separation of approximately 2 m, producing a fault-line scarp. The channel margins are disrupted and vertically offset approximately 2 m (±2 m), down to the southwest. The vertical separation across this fault-line scarp and the steepness of the fault scarp increase to the southeast (Figure 7-41b and c; Plate 7). The Oceano fault-line scarp along the bedrock surface is preserved where it lies beneath the Upper Pleistocene deposits, which onlap onto bedrock immediately west of the Channel J–Oceano fault piercing point (Figure 7-41b and c). The surface of onlap follows the Oceano fault trace for approximately 150 m.

Dextral and vertical offset estimates for Channel J–Oceano fault zone piercing points are summarized in Table 7-9.

Table 7-9. Oceano Fault Zone–Channel J Offset Estimates

Dextral Offset (m)			Vertical Offset (m)			
Min.	Max.	Pref.	Min.	Max.	Pref.	Comments
0	6	**0**	0	4	**2**	3 m horizontal and 2 m vertical data resolution

The −60 m contour at the top of bedrock exhibits an apparent dextral offset of approximately 150 m (Figures 7-7 and 7-41c; Plate 5), which appears to result from vertical (reverse) separation of the Oceano fault zone where it intersects the southeast-dipping bedrock surface at an oblique angle. In addition, the Upper Pleistocene sediment isopach map (Figure 7-6c) displays approximately 150 m of apparent dextral separation.

Channels F, G, and I–Unnamed Fault Piercing Points

Near the center of the San Luis Obispo Bay study area, paleochannels F, G, and I cross the central unnamed fault. These channels' potential thalweg and margin piercing points are confined to the central structural block (Figure 7-23). Examination of a smoothed similarity time slice (Figure 7-42a) at 0.083s (TWTT), a bedrock slope plot (Figure 7-42b), a contoured bedrock surface map (Figure 7-42c), and 2D seismic-reflection profiles near the intersection of the channels and the central unnamed fault (Figure 7-42, panels d, e, and f) reveal the structural relationship of the channels with the fault.

The central unnamed fault exhibits vertical, south-side-up displacement at this location, but the sense of motion varies along strike. Channel G and I thalwegs are not offset. However, Channel F exhibits an abrupt change in trend from northeast-southwest to east-west across the unnamed fault, where the thalweg (Channel Fc) is deflected by approximately 120 m and its southern margin is aligned along (possibly fault controlled)

the fault for over 200 m (Figure 7-42, panels c, e, and f). Channels F and I merge to the north of the unnamed fault, where they diverge from an aggradational system incised by Channel F. To the south of the unnamed fault, the linear, north-south-trending Channel I becomes more deeply entrenched into bedrock as a V-shaped channel. The fill of Channel G is crossed and incised into by Channel I. Channel G is truncated along the eastern margin of Channel F, forming a hanging valley (Figure 7-42, panels b and c). The geomorphologies of the channels and their geometric pattern of erosion and aggregation suggest that Channel F is younger than Channel I (although they could be of the same age).

A change in all channels' fluvial morphology occurs where they cross the unnamed fault as they are much broader and more sinuous to the north of the fault zone and more linear and deeply incised to the south. To the east of Channels Gc and Ic, beneath the Upper Pleistocene deposits, the bedrock surface is vertically offset 1 to 2 m by the unnamed faults, down to the north (Plate 7).

Based on the data resolution and geologic uncertainty, the range of dextral offset of Channels F, G, and I by the unnamed fault zone is estimated to be 0 to approximately 6 m, with a preferred offset of 0. Vertical offset along the unnamed fault-line scarp by Channels F, G, and I was observed in the 3D volume. A vertical offset of 0 ± 2 m, down to the north, is interpreted for Channel I, and vertical offsets of 1 ± 2 m, down to the north, are observed for Channels F and G. To the east of where these channels are mapped, a vertical offset of 1 ± 2 m, down to the north, is observed at the unnamed fault forming a fault-line scarp at the bedrock surface. In this area, the scarp is well preserved beneath the Upper Pleistocene deposits.

Dextral and vertical offset estimates for Channel F, G, and I–unnamed fault zone piercing points are summarized in Table 7-10 below.

Table 7-10. Unnamed Fault Zone–Channel F, G, and I Offset Estimates

	Dextral Offset (m)			Vertical Offset (m)		
Channel	Min.	Max.	Pref.	Min.	Max.	Pref.
F	0	6	0	−1	3	1
G	0	6	0	−1	3	1
I	0	6	0	−2	2	0

7.1.2   Discussion

The interpretations of the shallow faults, paleochannels, shoreline geomorphologies, and stratigraphy for evaluating fault geometry and activity are discussed in this section. The results of the interpretations of the 3D volume and 2D seismic-reflection data in the San Luis Obispo Bay study were used to refine fault locations and to determine potential piercing points and fault offsets along the Shoreline and Oceano fault zones.

We provide the rationale for adopting those piercing points used to determine offsets along faults, along with the preferred age model used to constrain slip rates. Refinements

and changes to mapped fault locations and geometry relative to previous mapping studies are also discussed (Figure 7-15).

7.1.2.1   Stratigraphy

All buried paleochannels imaged in the 3D survey area located on the middle continental shelf appear to have formed during Quaternary low sea-level stands. The thalwegs of the channels are well within the depths of Quaternary eustatic sea-level lowstands, and thus were sub-aerially exposed, as expressed in their fluvial geomorphology. The LGM (MIS 2) and the many older Quaternary sea-level lowstands reached depths of approximately 120–125 m below modern sea level (Figures 1-6 and 7-7; Plate 5). The –120 m contour is located at the southern margin of the survey area.

The presence of seafloor bedrock outcrops and the paucity of Pleistocene or younger sediments in the northern part of the 3D survey area suggest that it is undergoing tectonic uplift, subjected to high-energy seafloor current activity, being starved of sediment, or a combination of all these factors. However, tectonic subsidence is occurring locally, such as in the southeastern part of the 3D survey area, where a wedge of Upper Pleistocene deposits is imaged that increases in thickness toward the south (Figure 7-6b).

The location and pattern of deposition within the study area are influenced by local uplift on the Oceano and Los Berros fault zones in the north, and by accommodation created by down-to-the-south subsidence in the San Luis Obispo embayment. This accommodation has facilitated the deposition of Quaternary sediments in the offshore and onshore Santa Maria Valley block, between the Casmalia/Point Sal block to the south and the San Luis–Pismo block (Figure 1-2) to the north (Lettis et al., 2004).

The geometry and distribution of channels in the San Luis Obispo Bay study area illustrate the effects of tectonic uplift from crustal movement along the Southwestern Boundary zone, which bounds the south margin of the Irish Hills and San Luis block (Figure 7-20) and influences stratigraphy. The channels in the eastern structural block (Figure 7-7) document uplift associated with this deformation and are more deeply incised into the bedrock surface than the channels located on the central and western structural blocks.

Younger channels (i.e., Channel C) appear to be incised progressively deeper than predecessor channels (Plate 6). Given the position of the channels on the southern margin of the Irish Hills/San Luis block, deeper channel incision of younger channels suggests active tectonic uplift of the area and fluctuating sea levels through geologic time.

Fluvial Pathways

To the north and east of the San Luis Obispo Bay 3D survey area, two major source channel complexes are recognized that are carved into bedrock on the continental shelf (Figure 7-30). The geomorphology and internal architecture (threadlike to braided) of these bedrock-incised channels and channel complexes, together with their clear association with creeks onshore, indicate that they are fluvial in origin and that they formed on the exposed continental shelf during Pleistocene sea-level lowstands (PG&E, 2011a).

Source Channel Complex 1 (Figure 7-30) is made up of several narrow, straight to sinuous channels incised into the bedrock on the inner shelf offshore of San Luis Obispo Creek. This channel complex can be traced offshore to a depth of approximately 40 m before becoming buried by Holocene sediment (Figure 7-6). This source channel complex comprises Channels A through D (Figure 7-7; Plate 4). Channels A, B, C, and D can be traced offshore across the shelf to west of the Shoreline fault zone (Figure 7-31; Plate 5). Channel E is sourced on the shelf, but it feeds into Channel B and is included in Source Channel Complex 1 (Figures 7-7, 7-30, and 7-31).

Source Channel Complex 2 (Figure 7-30) is also made up of narrow, straight to sinuous channels incised into the bedrock of the inner shelf offshore of Pismo Creek. Arroyo Grande Creek (Figure 1-4) may have also influenced the formation of this channel complex. In the 3D survey area, at water depths greater than approximately 50 m, this source channel complex is imaged as bedrock Channels F, G, H, and I (Figure 7-7; Plate 5). Channels F and I can be traced offshore across the shelf to the west of the Shoreline fault zone, where they are buried beneath both Holocene and Upper Pleistocene sediments (Figures 7-6, 7-7, 7-12, and 7-31). Channel G appears to be sourced on the shelf, but feeds into or is cut by Channel F. Channel H may represent the westward extension of Channel G or it may have been sourced from Channel F. Both Channel G and H are included in Source Channel Complex 2 (Figures 7-7, 7-30, and 7-31).

Channels J, K, and L appear to be locally sourced. These three channels comprise Source Channel Complex 3 (Figures 7-7 and 7-31). Channel J may also represent overflow from Channel F in Source Channel Complex 2.

7.1.2.2   Faults

Three primary fault zones extend through or nearly through the San Luis Obispo Bay study area: the Shoreline, Oceano, and Los Berros fault zones. These fault zones are well imaged and mapped from the 3D volume and 2D seismic-reflection profiles (Figures 7-2, 7-3, 7-4, 7-10, 7-13, and 7-23). Several shorter faults, such as the two strands of the Pecho fault zone (Pecho and North Pecho faults), and two previously unidentified unnamed faults (the central unnamed fault and the other unnamed fault) are also mapped using the 3D volume. Outside the 3D survey area, 2D seismic-reflection profiles (Figures 7-14 through 7-21) are used to extend the Shoreline fault zone onto land to the south near the Santa Maria River mouth, to map the South Pecho fault, and to connect the Los Berros and Oceano faults with faults previously mapped by others onshore (Figure 7-15; Plate 1B).

The Shoreline Fault Zone

Previous maps of the Shoreline fault zone (PG&E, 2011b, 2012) showed the southern segment terminating immediately south of Souza Rock (Figure 7-15a). Using the interpretations of the 3D data set, we extend the Shoreline fault zone south from where it was previously mapped north of San Luis Obispo Bay (PG&E, 2011a,b, 2012). Mapping results using all available PG&E 3D and legacy archive seismic-reflection data (Plate 1B) indicate that the Shoreline fault zone extends approximately 22 km south of Souza Rock. The fault is clearly imaged for 6.5 km within the limits of the 3D survey area, 5.3 km of

which is south of Souza Rock. The Shoreline fault extends offshore from the the southern extent of the 3D survey for another 13.7 km , where it comes ashore near the mouth of the Santa Maria River (Figure 7-21a,b). Nearshore seismic-reflection data collected for the State Lands Commission (Digicon, 1986; Nekton, 1986) were used to constrain the location of Shoreline and South Pecho fault in southern San Luis Obispo Bay (Figures 7-21a,b, A-7, and A-8). The Shoreline fault projects towards an onshore, 3 km long strike-slip fault that offsets the top of the Sisquoc Formation that was previously mapped at this location (CDOGGR, 1992) based on onshore well and seismic reflection data, with the fault showing dextral offset (Figures A-7 and A-8). The fault could not be mapped south of the Guadalupe Oil Field, but it trends toward and may connect with the Casmalia fault to the south (Figures 7-15b, 7-21a, A-7, and A-8; Plate 1B). Assuming that the Point Buchon fault zone north of the San Luis Obispo Bay study area is part of the Shoreline fault zone, then the fault zone north of Souza Rock is approximately 23 km long (PG&E, 2011b), and the Shoreline fault zone in its entirety is approximately 45 km long.

Considerable detail of the structural fault geometry is provided in the 3D volume, and the pattern of faulting in plan view is complex (Figure 7-2). The convergence of many faults can be observed in plan view, with the previously mapped Pecho, Oceano, Shoreline, and Los Berros fault zones and several unnamed faults merging within the 3D survey area (Plates 1B, 4, and 5). In the northwestern and central parts of the 3D survey area, several faults converge (Figure 7-7). The Shoreline fault zone bifurcates west of Souza Rock, where one strand trends toward the east-southeast as the Oceano fault zone. The Shoreline fault zone is mapped as a linear throughgoing structure, and extends southeastward through the entire 3D survey area. Just north of Souza Rock, the western terminus of the Los Berros fault appears to be truncated by, or to merge with, the Shoreline fault zone (Figures 7-2 and 7-3).

The linear northwest-southeast trend (~N33W strike; Plate 4) of the mapped primary trace of the Shoreline fault zone in the 3D survey area is clearly expressed as a narrow lineament on the smoothed similarity bedrock surface map (Figure 7-2). To the south of the 3D survey area, the Shoreline fault exhibits a similar trend, with a strike ranging from N25W to N30W.The attitude of the fault is near vertical, and the estimated ratio of dextral-to-vertical separation based on the offset paleostrandlines is approximately 10:1 (see Section 7.1.1.3). The style of faulting is thus almost purely right-lateral strike-slip.

Given the estimated ages of Upper Pleistocene deposits and the paleostrandlines that are offset by the Shoreline fault, the fault is thus interpreted to have been active in the late Quaternary. In some areas of San Luis Obispo Bay, Holocene sediments may be deformed by the fault (Figure 7-19), but in most areas the youngest sediments offset by the fault are late Pleistocene in age (Figures 7-16, 7-20, 7-21, and 7-33). Within the 3D survey area, the timing of last movement on the Shoreline fault is loosely constrained to be between MIS 6e and MIS 5e (Figures 7-27 and 7-28), although younger ages are possible. Age models and estimated slip rates are presented in Sections 7.1.2.5 and 7.1.2.6.

The Oceano Fault Zone

The Oceano fault is one of several reverse faults, including the San Luis Obispo Bay, Wilmar Avenue, and Los Berros faults, that previously were mapped onshore and nearshore as the Southwestern Boundary Zone (PG&E, 2011a). The Oceano fault bifurcates from the Shoreline fault in Channel A west of Souza Rock and continues to the southeast as a narrow linear fault strand 5.0 km across the 3D survey area (Figures 7-2, 7-3, 7-4, and 7-7; Plates 4 and 5). Outside the 3D survey area, this fault continues offshore for 10.7 km to near the mouth of the Arroyo Grande Creek, where it connects with the previously mapped Santa Maria River and Oceano fault zones onshore (Figure 7-15; Plate 1B). The length of the fault from Souza Rock to the shore is 15.7 km. Onshore, the Oceano fault zone has previously been mapped 17.5 km to the southeast (DWR, 2002; Lettis et al., 2004).

The Oceano fault is expressed on the offshore bedrock surface as a fault scarp, or a fault-line scarp that abruptly ends where Upper Pleistocene deposits pinch out near Channel J's crossing of the fault (Figures 7-4, 7-5, 7-6, 7-7, and 7-41b; Plate 7). This suggests that little or no surface fault rupture and associated vertical separation has occurred on this segment of the Oceano fault zone since the pre-Holocene MIS 2-1 sea level transgression, although minor offset of unconformity H10 is apparent on some profiles (Figure 7-11).

The strike of the Oceano fault zone is distinctly different from the more southeast-trending primary trace of the Shoreline fault zone; it changes strike from about N40°W at Souza Rock to N65°W 1.5 km to the southeast, in the central part of the 3D survey area. Souza Rock appears to be an uplifted block (pop-up) in a 25-degree restraining bend in the Oceano fault zone. This geometry of the mapped trace of the Oceano fault zone (Figure 7-15), together with buried fault scarps on the bedrock surface (Plate 7), and the observed vertical separation of the Upper Pleistocene deposits (Figures 7-10 and 7-11), suggest that the fault dips to the northeast and is primarily a reverse fault (Figures 7-16, 7-17, and 7-20), similar to a previously mapped onshore segment of the fault (Figures 7-15 and Line SM-5a presented on Figure A-5; Plate 1B).

The Oceano fault zone is shown in this study to offset reflections of late Quaternary age and possibly of early Holocene age (Figure 7-1), and thus is considered an active Quaternary fault zone (Figures 7-4, 7-10, and 7-11). Age models and estimated slip rates for the Oceano fault zone are presented in Sections 7.1.2.5 and 7.1.2.6, respectively.

The Los Berros Fault

The mapped geometry of the faults imaged in the 3D volume shows that the Los Berros, Shoreline, and Oceano fault zones converge northwest of Souza Rock. These fault zones splay in a radial pattern toward the east and southeast into San Luis Obispo Bay (Figure 7-15b; Plate 1B).

Previous maps of the Los Berros fault (Willingham et al., 2013) show that this fault, along with the Wilmar Avenue and Oceano faults, bisect the coastline and extend onshore (Figure 7-15a). As reported by AMEC (2011), an inferred trace of the Los Berros fault was mapped beneath Nipomo Mesa and extends 5 km to the coastline. The results of this study suggest that the Los Berros fault extends from onshore beneath Nipomo Mesa

offshore to 10.5 km west of Shell Beach, where the fault connects with, or is truncated by, the Shoreline fault zone northwest of Souza Rock (Figures 7-2, 7-15b; Plates 1B, 4, and 5).

The Los Berros fault intersects the Shoreline fault near the northern boundary of the 3D survey area (Plates 1B and 4) where the 10 August 2000 M_L 3.5 earthquake is located approximately 1 km northwest of Souza Rock (Figure 7-43; Hardebeck, 2010). A dextral strike-slip focal mechanism with a nodal plane parallel to the Shoreline fault zone (Figure 7-43), in combination with offset paleostrandlines revealed by this study, indicates that the zone is an active right-lateral structure.

Activity of the Los Berros fault, however, is poorly constrained. There is no apparent, clear offset of the top of bedrock, channel margins, or channel thalwegs along the trace of this fault in the LESS 3D data set (Plates 4 and 5). There is a change in the gradients of the thalwegs of Channels A, B, C, and D where these channels cross the fault zone (Plate 6), and the fluvial style of these paleochannels changes to the north. However, the observed change in thalweg gradient may be due to differences in rock strength (erodability) and differential erosion of rock units juxtaposed by the fault.

Horizons H10, H30, and H40 could not be mapped with confidence from the Estero Bay area into northern San Luis Obispo Bay. On CoMAP Line 86-3 (Figure 7-17), the ages of the strata and rock units displaced by the fault zone are poorly constrained. However, on PBS-10 (Figure 7-18), top of bedrock, unnamed Quaternary deposits, and inferred Holocene deposits in the footwall of the fault are all deformed and cut by the Los Berros fault. A hanging-wall anticline on the north side of the fault and a footwall syncline on the south are clearly apparent on both seismic-reflection lines CoMAP 86-3 and PBS-10 (Figures 7-17 and 7-18). The Los Berros fault is thus considered an active, north-dipping reverse fault in northeastern San Luis Obispo Bay. This is consistent with evidence for Quaternary activity on the onshore portions of the Wilmar Avenue fault (Lettis et al., 1994), which connects with the Los Berros fault offshore of Shell Beach (Figure 7-15b; Plate 1B).

The Pecho Fault Zone

Previous mapping of the Pecho fault zone showed the zone as having two arcuate, diverging strands in central San Luis Obispo Bay (Figure 7-15b; Willingham et al., 2013). The results of this study indicate that the Pecho fault zone is more complex than previously mapped, and that it consists of multiple, shorter fault strands that are clearly expressed as narrow lineaments in the 3D volume. To the south, the South Pecho fault consists of a single strand that closely parallels the Shoreline fault to near the mouth of the Santa Maria River in southern San Luis Obispo Bay (Figures 7-15, 7-20, and 7-21; Plate 1B). The South Pecho fault, as mapped by Willingham et al. (2013), coincides with the northern portion of the South Pecho fault mapped in this study (Figure 7-15a and b).

Although the South Pecho fault is located approximately 500 m to the west, it is considered a splay of the Shoreline fault zone (Figures 7-20 and 7-21). Here, the South Pecho fault strand appears to displace sediment of Quaternary age, although bright spots (gas) prevent clear interpretations on some seismic-reflection lines (Figure 7-19).

Unconformity H30 (dated at 150–130 ka) appears not to be vertically separated by the South Pecho fault strand on USGS Profile PBS-19 (Figure 7-19). However, based on the estimated ages of the inferred Upper Pleistocene deposits cut by the fault (Figures 7-1, 7-16, 7-20, and 7-21), as well as its fault style and sense of motion (almost pure 10:1 right-lateral strike-slip), the South Pecho fault is interpreted to be a Quaternary-active splay of the Shoreline fault.

Unnamed Faults

Several unnamed faults (i.e., the central unnamed fault and other unnamed faults) are mapped in the 3D survey area and are located between the Shoreline and Oceano fault zones (Figure 7-15b; Plates 1B, 4 and 5). These faults offset the bedrock surface along the margins of several paleochannels. The central unnamed fault (Figure 7-15b; Plates 4 and 5) is a linear northwest-southeast-trending fault located between the Oceano and Shoreline fault zones in central San Luis Obispo Bay. A magnetic lineament correlates with the fault trace (Figure 7-14), suggesting basement offset or juxtaposition of varying lithologies at depth. The central unnamed fault cuts shallow subsurface reflections of strata inferred to be of Quaternary age (Figures 7-15b, 7-17, and 7-19) and is thus interpreted to be active.

The unnamed faults that intersect the Shoreline-Oceano fault zone typically have curved fault traces. These faults offset the bedrock surface along the margin of several paleochannels and beneath the Upper Pleistocene deposits. Except for fault-line scarps offsetting bedrock along paleochannel margins, which may be fault controlled, no fault scarps were observed on the Holocene sediment-covered bedrock surface northwest of the onlap edge of the Upper Pleistocene deposits (Plate 7). The unnamed faults in the 3D survey area appear to have experienced surface rupture in the Quaternary, but do not exhibit evidence for Holocene activity.

7.1.2.3   Paleostrandline Correlations and Estimated Offsets

Two of the four paleostrandlines (−82 and −92 m depths) imaged in the 3D volume cross the Shoreline fault zone and are considered excellent piercing points that exhibit distinct dextral and vertical separations (see Section 7.1.1.3). Vertical separation is estimated to be approximately 0.8 to 1.6 m (1–2 ms), with a preferred value of 1 m. Lateral offset of both strandlines is approximately 9.4 ± 6 m, with a preferred value of 10 m.

Given the clear geomorphologic expression of the paleostrandlines that erode reflections of Upper Pleistocene sediment and the unambiguous, distinct measurable dextral and vertical separations across the fault zone, offset estimates of the mapped paleostrandline piercing points are considered of the highest confidence level (see Section 3.6; Plates 4 through 7).

Paleostrandline and paleochannel piercing point measurements for the San Luis Obispo Bay 3D study area are summarized in Table 7-11 below.

Table 7-11.Summary of Piercing Point Offset Measurements for San Luis Obispo Bay

Piercing Point	Dextral Offset (m)			Vertical Offset (m)		
	Min.	Max.	Pref.	Min.	Max.	Pref.
Shoreline Fault–84 m paleostrandline	3.4	15.4	**10**	0.8	1.6	**1**
Shoreline Fault–92 m paleostrandline	3.4	15.4	**10**	0.8	1.6	**1**
Shoreline Fault–Channel A	10	50	**30**	1	5	**3**
Shoreline Fault–Channels B and C	0	6	**0**	–2	2	**0**
Shoreline Fault–Channel F	0	6	**1**	–3	1	**-1**
Shoreline Fault–Channel I	0	6	**1**	–2	2	**0**
Oceano Fault–SE Margin Channel A	0	6	**0**	1	5	**3**
Oceano Fault–Channel B	0	6	**0**	1	5	**2**
Oceano Fault–Channel C	0	6	**0**	–1	3	**1**
Oceano Fault–Channel D	0	6	**0**	0	4	**2**
Oceano Fault–Channel E	0	6	**0**	0	4	**2**
Oceano Fault–Channel F	0	6	**0**	1	5	**2**
Oceano Fault–Channel J	0	6	**0**	0	4	**2**
Unnamed Fault–Channel F	0	6	**0**	–1	3	**1**
Unnamed Fault–Channel G	0	6	**0**	–1	3	**1**
Unnamed Fault–Channel I	0	6	**0**	–2	2	**0**

Note: 3D P-Cable survey data resolution is 3 m horizontal and 2 m vertical.

7.1.2.4   Channel Correlations and Estimated Offsets

Twelve channels (Channels A through L) are observed in the San Luis Obispo Bay 3D volume, and most cross the mapped faults in the area but have little or no observed lateral separation (see Section 7.1.1.3). However, the exception is the well-defined bedrock-incised Channel A, which exhibits the largest potential dextral separation across the Shoreline fault zone of all the paleochannels mapped, having a range of offsets of 10–50 m and a preferred value of 30 m (Table 7-11). Given the clear geomorphologic expression of the paleochannels incised into pre-Quaternary bedrock, and that the channels observed in the San Luis Obispo Bay 3D data set exhibit either little or no vertical or lateral separation across the mapped faults, correlation of most of the mapped channels across the faults is clear and unambiguous, providing the highest confidence level for the correlations (Section 3.5; Plates 4 through 7). Specifically, above the intersection of the seafloor multiple with the bedrock surface, all the channels, with the exception of Channels G, H, K, and L, can be correlated with confidence across the mapped faults (Figures 7-23, 7-33 through 7-42; Plates 4 and 5). However, in the southern part of the 3D volume southwest of the Shoreline fault zone, signal convolution of the seafloor multiple with the primary reflections of Channels Fw and Iw prevented clear resolution of these channels, and thus lowered the correlation confidence level to medium (Figures 7-38 and 7-40; Plate 4).

The thalwegs for each channel were mapped in the 3D volume and were used to create 2D channel profiles in ArcGIS (Plate 6). Minor slope inflections and changes in thalweg gradient were noted where Channels A through D cross the Los Berros fault zone in the northern part of the survey area. However, with the exception of Channel A, evidence for clear and unambiguous lateral separation of the channel thalwegs across the mapped fault zones was not found (Plate 6). Vertical separation of thalwegs was noted where the Oceano fault crosses all channels (Channels A through F and J; Plate 6). Vertical offsets of Channel F and G thalwegs were also apparent where these channels cross the unnamed fault (Plates 6 and 7).

Where the Shoreline and Oceano fault zones bifurcate to the west of Souza Rock, at the location of Channel A, they exhibit clear evidence of Quaternary activity (Figures 7-33, 7-34, and 7-35; Plates 1B, 4, and 5). Vertical separation of the bedrock surface is observed on both the Shoreline and Oceano fault zones in areas that lie below the limit of onlap of the Upper Pleistocene deposits onto top of bedrock (Figures 7-4 through 7-7; Figure 7-12; Plates 5 through 7). The Upper Pleistocene deposits are offset by these faults, both within and outside mapped paleochannels (Figures 7-1, 7-5, 7-6, 7-11, and 7-13). Several minor unnamed faults between these two major fault strands also offset the top of bedrock below the limit of onlap of Upper Pleistocene deposits (Figure 7-10; Plates 5 and 7).

West of Souza Rock Channel A is laterally offset by the Shoreline fault zone (Figures 7-33, 7-34, and 7-35). Lateral separation is interpreted to be approximately 10–50 m, with a preferred (dextral) offset of approximately 30 m (Table 7-11). Channel A is the only channel within the resolution of the San Luis Obispo 3D volume that is interpreted to exhibit significant, measurable dextral offsets of its channel margins and thalwegs along the Shoreline fault zone. Lower channel fill deposits are offset by the fault (Figure 7–33a), while a younger, nested channel is unfaulted (Figure 7-35b).

The 3D seismic data reveal an abrupt inflection in the orientation of Channel A's thalweg from roughly north-south to east-west, as well as a substantial increase in channel width from approximately 100 m to more than 200 m and a shift in thalweg orientation back to north-south just west of the intersection of the Shoreline and Oceano fault zones near Souza Rock (Figures 7-33 and 7-34). The apparent right-step of approximately 140 m of the observed stream morphology may have resulted from deflection of the channel around the resistant uplifted Souza Rock.

Estimated vertical offsets of paleochannels across the Oceano fault zone range from 1 to 3 m within a range of −1 to +5 m. Channels B, D, F, and J exhibit measurable, preferred vertical offsets of approximately 2 m. Channel C is vertically offset by approximately 1 m (±2 m) by the Oceano fault zone (Table 7-11). The base Holocene reflection (H10) also appears to be locally disrupted by the fault (Figures 7-10 and 7-11). The Channel E thalweg and margins are sinuous (meandering) where the channel crosses the Oceano fault zone, and they are deflected approximately 80 ± 20 m, although no measurable lateral offsets of the piercing points (thalweg and margins) are observed. However, the Channel E thalweg exhibits approximately 1–2 m of vertical separation across the Oceano fault-line scarp, within a range of 0–4 m. The apparent vertical separation across

the Oceano fault-line scarp could be the result of differences in rock strength and erodability, however, rather than fault offset. Channels K and L are restricted to the eastern structural block, and thus do not provide piercing points.

7.1.2.5   Age Constraints

Age estimates of when paleochannels formed (eroded) are primarily based on the periods when sea-level lowstands occurred, as reflected in the sea-level curves (Figures 1-6 and 1-7). By bracketing a time on a curve when channels began to erode into bedrock or fill, and when erosion ceased and sedimentary deposition and channel filling probably occurred, an age window is produced that can be used to date the features (see Figure 1-8). In addition, a feature's stratigraphic position relative to mapped horizons is used to estimate its age of formation; ages have been established for the mapped horizons by using sequence stratigraphy (e.g., located between bedrock and H10; see Figure 7-27). Fault activity is similarly estimated, for example, by observing the uppermost reflections that are noticeably displaced or deformed by a fault and correlating the reflection with a mapped horizon or unit that is bracketed by two horizons. Sedimentation rates can also be used to estimate relative ages when depositional rates are fairly well known, but these were not used in the San Luis Obispo Bay study area because of a lack of good data on sedimentation rates and because of variable sediment accumulation across the shelf as a result of variations in bedrock topography, subsidence rates, and proximity to the Santa Maria River.

Paleostrandline Age Constraints

The buried paleostrandlines mapped in this study are incised into Upper Pleistocene deposits above the mapped bedrock surface and that lie above the geomorphic expression of the paleoshorelines (Figures 7-24, 7-25, and 7-26). The preferred geologic model for the formation of the strandlines is that they developed during a late Quaternary intermediate sea-level stand (e.g., MIS 4, 6e, or 8c) and were subsequently preserved by slowly aggrading estuarine and/or deltaic sedimentation on a coastal floodplain landward of a coastal dune complex during a glacial maximum (i.e., MIS 2, 6b, 8b, 10).

An age model for the paleostrandlines, presented on Figure 7-44, is based on the preferred ages for seismic reflections mapped as horizons H30 and H40 (PG&E, 2013) and the observed stratigraphic relationships between these horizons and the depths of the mapped paleostrandlines (Figures 7-27 and 7-28). Reflected in the age model is an assumption that little tectonic uplift has occurred in central San Luis Obispo Bay since the paleostrandlines formed during the late Quaternary. The best evidence for estimating the age of the shorelines is exhibited on Figure 7-27, where unconformity H40 (~250–240 ka) appears to be statigraphically lower than the paleostrandline. The H40 horizon onlaps the bedrock surface southwest of the paleostrandlines at a depth of approximately 120 m, whereas unconformity H30 (~135–125 ka) lies stratigraphically higher than the paleostrandlines and is thus considered younger than the strandlines. Therefore, the paleostrandlines are interpreted to have incised into Upper Pleistocene deposits (Figure 7-1) sometime between 185 ka and 155 ka (MIS 6c through 6e), when sea levels

stabilized for several tens of thousands of years at depths between 75 m and 92 m below modern sea level (Figures 7-28 and 7-44).

In consideration of the other potential ages for the formation of the paleoshorelines, a maximum age would be MIS 14 (~550 ka), and a minimum age of would be MIS 3 and 4 (~28–70 ka). The maximum and minimum ages are not consistent, however, with the observed stratigraphic relationships and estimated ages for H30 and H40 (PG&E, 2011a).

Paleochannel Age Constraints

Given the lack of available radiometric ages, magnetic stratigraphy, or biostratigraphy, the ages of the channels in the San Luis Obispo Bay study area are poorly constrained. Consequently, channel ages were estimated through the use of sea-level curves and stratigraphic models.

Crosscutting relationships allow relative ages of channel incision, reoccupation (exhumation), and abandonment to be determined (Figure 7-32; Plate 5). The channels that appear to have been abandoned most recently are Channels C through F and Channels K and L. The incision of Channel B and Channels G through J is interpreted to have occurred more recently than the formation of Channel A. Channels K and L appear to be locally sourced, and are interpreted to have been incised into the exposed shelf during MIS 3 or 4, prior to deposition of the youngest Upper Pleistocene deposits that cover the channels (Plate 5). During this period (MIS 3 and 4), sea levels varied between –50 m and –80 m, and the shoreline was near or adjacent to the Oceano fault zone scarp at the location of Channels K and L. This hypothesis explains why Channels K and L, as fluvial channels, are only incised into the eastern structural block to the north of the Oceano fault zone, and why they are not present in bedrock on the central structural block. Channel K was likely reoccupied during MIS 2, as evidenced by a channel incised into the Upper Pleistocene deposits to the southwest of the Oceano fault.

Age models for the paleochannels identified in the San Luis Obispo Bay study area are presented on Figure 7-45. The channels are bracketed stratigraphically by two key unconformities that extend across most of the survey area that have been correlated with well-established sea-level curves for the late Quaternary (Figures 1-6 and 1-7; Waelbroeck et al., 2002; Siddall et al., 2003; Lisiecki and Raymo, 2005). The lower unconformity is the bedrock surface (Figure 7-7; Plate 5), and the upper unconformity is H10. The H10 horizon is located at the base of the Holocene (Figure 7-6b), which is interpreted to represent the pre-Holocene transgressive surface formed during the sea-level rise from MIS 2 to MIS 1 (~15–8 ka; Figure 1-8).

The age of initial incision of Channel A is poorly constrained. However, given the observed bedrock channel morphology, piercing point (thalweg and channel margins) offsets, fault cut channel fill deposits, and a nested younger channel west of Souza Rock (Figures 7-33 and 7-35), Channel A is likely significantly older than MIS 2, and likely older than MIS 6. Sea-level-curve metrics and stratigraphic control provided by the observed relationship between the Channel A fill and Upper Pleistocene deposits provide additional constraints on the channel age.

Channels A, F, and I extend south of the onlap edge of the Upper Pleistocene deposits, and thus appear to have been initially incised prior to deposition of these sediments in the late Pleistocene, when the southernmost, deeper parts of these channels were buried (Plate 5). There is clear evidence that some channels have been repeatedly reoccupied (see Section 7.1.1.3). Channel I is incised into the Upper Pleistocene deposits at the Shoreline fault piercing point, and the channel fill deposits are overlain by Holocene sediments, demonstrating that the channel was reoccupied during MIS 2 (Figure 7-38, panels d, e, and f). The timing of initial incision of Channel F into the bedrock surface is unclear based on the 3D data set, but given the depth of this channel and its inferred stratigraphic position where unconformity H40 laps onto the bedrock surface to the southwest of the study area at approximately 120 m (Figure 7-46), it may be coeval with H40 (MIS 8b).

A shallow channel that is incised into bedrock approximately 35 m below horizon H40 (~155 m), observed on USGS Profile PBS-319 to the southwest of the 3D survey area (Figure 7-46), may represent Channel I. This location is 5 km south of the 3D survey area, and the uncertainty in this age is large. The preferred age model for Channel I is that it was initially incised during MIS 10 (~345 ka), when sea level was at approximately 125 m below modern sea level (Figures 1-8 and 7-45). Given the elevation of inferred Channels F and I on USGS Profile PBS-319, this would imply that this part of San Luis Obispo Bay has undergone net subsidence in the last several hundred thousand years.

Initial incision of Channels C, D, E, and J is interpreted to have occurred more recently than for Channels A, B, F, and I. Channels K and L appear to be locally sourced (no known river or creek input) and are interpreted to have been initially incised into the exposed shelf during MIS 3 or 4, prior to deposition of the uppermost Pleistocene sediments (Plate 5). During this period (MIS 3 and 4), sea levels varied between –50 m and –80 m, and the shoreline was near or adjacent to the Oceano fault zone scarp at the location of Channels K and L. Differential uplift across the Oceano fault led to greater channel incision into the hanging wall (eastern structural block) relative to the footwall (Central block), creating a fault-line scarp that may have coincided with the shoreline during MIS 3 (Figures 7-41 and 7-45). This explains why Channels K and L, as fluvial channels, are only incised into the eastern structural block bedrock to the north of the Oceano fault zone, and why they are not present on the bedrock of the central structural block.

The highest preferred age model for Channel A, based on estimated ages for H10, the eustatic sea-level curve metrics, and other criteria, is MIS 12, the sea-level lowstand that stabilized approximately 450–430 ka. During this lowstand, sea level fell below –80 m elevation for approximately 45,000 years (470–425 ka, as shown on Figure 1-6), which is the longest duration of any lowstand since the end of the MPT (Figure 6-2). Sea levels were below –80 m elevation for only approximately 20 kyr during MIS 10, and for 30 kyr during MIS 8. The elevation of sea level during MIS 12 was also lower than during MIS 10 and 8b (Figures 6-2 and 7-45).

The lowest preferred age model for Channel A (Figure 7-45), based on the eustatic sea-level curves and on the estimated age of unconformities outside the 3D survey area, such

as horizons H30 and H40 (PG&E, 2013), is MIS 8b and 8c, the sea-level lowstand that stabilized between approximately 275 and 245 ka. This alternate age model is weakly supported from interpretations of USGS seismic-reflection profiles PBS-09 and PBS-319 (Figure 7-46), which show a possible channel incised into bedrock to a depth of approximately 110–120 m, where it lies below the H30 horizon and at about the same depth as the H40 horizon. On PBS-319, the channel is shallow (~3 m) and is approximately 100–150 m wide, likely due to being close to base level on a relatively flat coastal floodplain. Based on the location of this channel in relation to the 3D survey area, however, it is more likely to be the seaward extension of Channel F. Channel A is not interpreted to be present on USGS profile PBS-319 (Figure 7-46), and it may have been removed by erosive coastal processes during MIS 10, 8b/c, and/or 6b/c. Thus, within the extents of 3D survey area (Figure 7-7), the highest preferred age model for the initial incision of Channel A into the bedrock surface is during the extended MIS 12 sea-level lowstand, an extended period when sea levels were within a depth range between approximately 80 and 130 m below modern sea level (Figure 7-46). Reflected in both of the preferred age models for Channel A is an assumption that little tectonic uplift and likely some subsidence have occurred in this part of San Luis Obispo Bay during the late Quaternary, which is consistent with the observed elevation of onlap of horizon H40 onto the bedrock surface (Figure 7-46).

On USGS profile PBS-319, the observed bulge in reflection H40 near its onlap onto the bedrock surface may represent a sand bar near the ancestral San Luis Obispo Creek mouth, indicating proximity to the shoreline in this area. An analogous modern progradational sand bar is observed in the inner shelf offshore of Avila, where the creek enters San Luis Obispo Bay. It is possible that Channels F and/or A formed from ancestral stream flow sourced from the San Luis Obispo Creek Watershed (Figures 1-5 and 7-30), which incised into sub-aerially exposed Jurassic metamorphic basement rocks, Cretaceous sandstones, and Neogene tuffs, basalts, and sedimentary rocks.

Dextral offset of channel thalwegs, margins, and fill by the Shoreline fault occurred after initial incision of Channel A and subsequent infilling either during the MIS 8b–MIS 7e or the MIS 12-MIS 11 transgressions (Figure 7-45). The presence of unfaulted nested channel fill (Figure 7-35c) indicate that Channel A was subsequently reoccupied, possibly during MIS 2.

The preferred age model for the incision of Channel C is the MIS 2 LGM, between approximately 28 ka and 15 ka, with infilling between approximately 18 ka and 10 ka (Figures 1-8 and 7-45). Given Channel C's crosscutting and incision into Channel B's upper fill deposits, Channel C is interpreted to be younger than Channel B. The preferred age model for Channel B is MIS 6b, between approximately 155 ka and 130 ka for initial incision, with possible reoccupation during MIS 2 prior to incision of Channel C.

The ages of the paleochannels in San Luis Obispo Bay (Figures 7-7 and 7-45; Plate 5) are estimated as follows:

- Channels C, D, and E were incised during MIS 2 (~20–10 ka).
- Channels K and L were incised during MIS 3 and 4 (~70–40 ka).
- Channels B and J originated during stage 6b and 6c (~160–140 ka).

- Channel F originally formed during MIS 8b and 8c (~275–245 ka).
- Channel A may have originated during sea-level lowstands recorded during MIS 8b/8c, 10, or 12.
- Channel I may have been incised during MIS 10 (~350–340 ka).

As previously noted, Channels A, B, F, and I appear to have been reoccupied during subsequent sea-level lowstands. While it is considered unlikely that any of the channels are older than MIS 16, the upper-bound maximum age of the initial incision of all the channels is conservatively placed at approximately 1.4 Ma, at the beginning of the MPT transition (Figure 6-2).

7.1.2.6   Slip-Rate Estimates

In the simple calculation of the slip rates for the Shoreline and Oceano fault zones, the estimated amount of fault offset is divided by the estimated age of the piercing point. Both of these parameters include inherent uncertainties, which are described above in Section 7.2.1.5. Uncertainty in both of these parameters is represented by the limiting minimum and maximum constraints.

Paleostrandline Slip-Rate Estimates

Slip-rate estimates for the paleostrandlines across the Shoreline fault zone in the San Luis Obispo Bay study area are based on the age model shown on Figure 7-44 and presented in Table 7-12. The lateral offset of the two strandlines' piercing points (the −84 and −92 m strandlines) that cross the Shoreline fault zone is approximately 9.4 ± 6 m, with a preferred value of 10 m (Figure 7-29). Vertical separation is estimated to be approximately 0.8–1.6 m (1–2 ms).

Based on the age model and measured separation of the paleostrandlines' piercing points reported above, the maximum estimated dextral slip rate is 0.51 mm/yr, and the minimum slip rate is 0.01 mm/yr. The preferred estimated dextral slip rate for the Shoreline fault at the paleostrandline piercing points identified in this study is 0.06 mm/year. Since the estimated vertical separation is 0.8 to 1.6 m (1–2 ms), the ratio of horizontal to vertical slip is approximately 10 to 1, and the preferred vertical slip-rate value is less than 0.01 mm/yr.

Paleochannel Slip-Rate Estimates

The ages of the buried pre-Holocene paleochannels in San Luis Obispo Bay are poorly constrained. Consequently, estimates of fault slip rates based on offset paleochannel thalwegs and margins are conjectural. However, even with this significant uncertainty, the estimated ages for paleochannels presented in the age model (Figure 7-44) can be used effectively to develop slip-rate estimates for the Shoreline and Oceano fault zones, providing valuable constraints on maximum allowed slip rates for the faults in these fault zones.

Table 7-12. San Luis Obispo Bay Paleostrandline Dextral Slip-Rate Estimates

Age	Min. Offset (3.4 m)	Max. Offset (15.4 m)	Pref. Offset (10 m)	Comments
70–28 ka [30 ka]	0.11 mm/yr	0.51 mm/yr	0.33 mm/yr	Minimum age of paleostrandlines allowed by PG&E (2013) minimum age model for H30 and H40
185–155 ka (MIS 6e) [160 ka][a]	0.02 mm/yr	0.10 mm/yr	**0.06 mm/yr[a]**	Preferred interpretation based on relationship to and preferred ages for H30 and H40 (PG&E, 2013). Assumes paleostrandlines were incised during transgressive intermediate MIS 6c/6e lowstands when sea-level elevations were at ~–84 to –92 m
275–250 ka (MIS 8c) [255 ka]	0.01 mm/yr	0.06 mm/yr	0.04 mm/yr	Alternative age (MIS 8c) from interpretation that paleostrandlines were incised during transgressive lowstands at ~–84 to –92 m
550 ka (MIS14)	0.01 mm/yr	0.03 mm/yr	0.01 mm/yr	Maximum age of paleostrandlines during MIS 14

Note: Ages in square brackets were used to calculate the preferred slip rate.

[a] Preferred age model and slip rate.

Shoreline Fault Zone–Channel A Slip-Rate Estimates

Channel Ae/Ac piercing points, where bedrock channel thalwegs and channel margins cross the Shoreline fault zone west of Souza Rock, suggest that approximately 10–50 m of dextral separation may have occurred since initial channel incision and initial infilling (Figure 7-33). Based on measured channel thalweg and margins offsets, the preferred estimate of dextral separation is 30 m, which is within the 10–50 m range of measured channel margin offsets and the 20–40 m range of measured offset of the channel thalweg (Figure 7-35). Given the uncertainties with regard to thalweg locations, offset measurements, and the range of possible ages of the sequence-stratigraphic horizons that stratigraphically bracket Channel Ae/Ac, several potential slip-rate estimates were calculated for the Shoreline fault zone, as shown in Table 7-13 below.

Using the highest preferred age of approximately 430 ka (MIS 12) and the preferred Channel A thalweg piercing point offset of approximately 30 m, an estimated slip rate of approximately 0.07 mm/yr (within a range of 0.02–0.12 mm/yr) is calculated for the Shoreline fault zone using Channel A. Using the lower preferred age of approximately 250 ka (MIS 8b/8c) and the preferred Channel A thalweg piercing point offset of approximately 30 m, the estimated slip rate is approximately 0.12 mm/yr (within a range of 0.04–0.20 mm/yr). Considering the other potential ages (135 ka of MIS 6b, and 1.4 Ma of MIS 45) for Channel A incision, a minimum estimated slip rate of 0.01 mm/yr (1.4 Ma at 10 m minimum offset) and a maximum estimated slip rate of 0.37 mm/yr (135 ka at

50 m maximum offset) is calculated for the fault zone. Based on the observed unfaulted nested channel at the top of the Channel A complex, the Shoreline fault zone does not appear to have ruptured since channel abandonment and filling (Figure 1-8) during the MIS 2-1 transgression (~10-15 kyr).

Table 7-13. Channel Ae/Ac Shoreline Fault Dextral Slip Rate Estimations

Age	Min. Offset (10 m)	Max. Offset (50 m)	Pref. Offset (30 m)	Comments
135 ka (MIS 6b)	0.07 mm/yr	0.37 mm/yr	0.22 mm/yr	Minimum age (MIS 6b/6c) of bedrock Channel A inferred from the channel age model
250 ka (MIS 8b/8c)[b]	0.04 mm/yr	0.2 mm/yr	**0.12 mm/yr**[b]	Lowest preferred age (MIS 8b/8c) of initial Channel A bedrock incision and infilling, based on possible relationship to H30 and H40 to the southwest of the 3D survey area
430 ka (MIS 12)[a]	0.02 mm/yr	0.12 mm/yr	**0.07 mm/yr**[a]	Highest preferred age (MIS 12) of initial Channel A bedrock incision, based on sea-level metrics and the apparent absence of Channel A to the west of the 3D survey area
1.4 Ma (MIS 45)	0.007 mm/yr	0.04 mm/yr	0.02 mm/yr	Maximum age of Channel A allowed by the channel age model

[a] Highest preferred age model and slip rate.

[b] Lowest preferred age model and slip rate.

Oceano Fault Zone–Channel A Slip-Rate Estimates

The preferred dextral offset of Channel A's thalweg and margin piercing points at the Oceano fault zone is 0 m (Table 7-11). Only the eastern margin of Channel A intersects the Oceano fault where the fault zone bifurcates from the Shoreline fault zone near the middle of Channel A, west of Souza Rock (Figure 7-7b). This intersection exhibits approximately 3 m of vertical separation across the Oceano fault, with a range of 1–5 m. A fault scarp associated with the Oceano fault zone does not appear to be present on the bedrock surface outside the channel, suggesting that the surface was beveled by erosion during the MIS 2 lowstand and has remained undeformed since that time. Given the uncertainties with regard to offset measurements and the range of possible ages of the sequence-stratigraphic horizons that stratigraphically bracket Channel Ae/Ac, several potential slip-rate estimates were calculated for the Oceano fault zone, as shown in Table 7-14 below.

Table 7-14. Oceano Fault Zone–Channel A Vertical Slip-Rate Estimates

Age	Min. Offset (1 m)	Max. Offset (5 m)	Pref. Offset (3 m)	Comments
135 ka (MIS 6b)	0.01 mm/yr	0.04 mm/yr	0.02 mm/yr	Minimum age (MIS 6b/6c) of Channel A inferred from the channel age model
250 ka (MIS 8b/8c)[b]	0.004 mm/yr	0.2 mm/yr	**0.012 mm/yr**[b]	Lowest preferred age (MIS 8b/8c) of initial Channel A bedrock incision and infilling, based on possible relationship to H30 and H40 to the southwest of the 3D survey area
430 ka (MIS 12)[a]	0.002 mm/yr	0.01 mm/yr	**0.007 mm/yr**[a]	Highest preferred age (MIS 12) of initial Channel A bedrock incision and infilling, based on sea-level metrics and the apparent absence of Channel A to the west of the 3D survey area
1.4 Ma (MIS 45)	0.001 mm/yr	0.004 mm/yr	0.002 mm/yr	Maximum age of Channel A allowed by the channel age model

[a] Highest preferred age model and slip rate.

[b] Lowest preferred age model and slip rate.

Oceano Fault Zone–Channels B and F Slip-Rate Estimates

Channel B and F thalweg piercing points (Plate 6) cross the Oceano fault zone (Figures 7-23, 7-39. and 7-40) and exhibit approximately 2 m (~1–5 m range) of vertical separation and 0 to 6 m dextral offset. Several other channels (C, D, E, and J) also exhibit 1 to 2 m of offset across this fault zone. It is possible that these measured offsets represent differential erosion due to variable rock strength and erodability, with older, more resistant rocks on the upthrown, north side of the fault-line scarp. However, the fault scarp is well preserved both beneath the Upper Pleistocene deposits and, locally, within the buried channels thalwegs, and it is not present outside channels to the west of the limit of onlap of the Upper Pleistocene deposits onto the top of bedrock (Plates 5 and 6).

Given the uncertainties with regard to offset measurements and the range of possible ages of horizons that stratigraphically bracket Channels B and F, three potential slip rates were calculated for the Oceano fault zone in the vicinity of Channels B and F, as shown in Table 7-15 below.

Table 7-15. Oceano Fault Zone–Channel B and F Vertical Slip-Rate Estimates

Age (ka)	Min. Offset (1 m)	Max. Offset (5 m)	Pref. Offset (2 m)	Comments
20 ka (MIS 2)	0.05 mm/yr	0.25 mm/yr	**0.1 mm/yr[b]**	Higher preferred (Model 1) age (MIS 6b/6c) of reoccupied Channels B and F inferred from the channel age model
135 ka (MIS 6b)[a]	0.01 mm/yr	0.04 mm/yr	0.015 mm/yr[a]	Alternative, lower preferred (Model 2) age of reoccupied Channels B and F at the Oceano fault
1.4 Ma (MIS 45)	0.001 mm/yr	0.004 mm/yr	0.001 mm/yr	Maximum age of Channel F allowed by the channel age model

[a] Model 2 slip rate.

[b] Preferred (Model 1) age model and slip rate.

The highest preferred vertical slip-rate estimates (Model 1) for the Oceano fault zone are 0.1 mm/yr at the Channel B and F piercing points. The sense of fault motion is reverse, north side up. The highest preferred slip-rate estimates for Channels B and F are based on crosscutting relationships visible on time slices in the 3D volume (Figure 7-22), which suggest reoccupation of Channel F and Channel B during MIS 2. An alternative lower preferred model (Model 2) suggests that these two channels were not reoccupied during MIS 2 at the Oceano fault zone piercing points, and developed during MIS 6b (Figure 7-45). If the alternative model is valid, then the slip rate on the Oceano fault zone at the Channel B and F piercing points is 0.015 mm/yr over the past 135 kyr, an order of magnitude lower than the Model 1 scenario. The data resolution and geologic uncertainties allow for both models to be possible.

Oceano Fault Zone–Channel C Slip-Rate Estimates

Channel C exhibits −1 to 3 m of vertical separation across the Oceano fault zone. The Channel C thalweg piercing point (Plate 5) where the channel crosses the Oceano fault zone (Figures 7-23 and 7-39) suggests approximately 1 m of vertical separation, and 0 to 6 m of lateral offset (Table 7-11). Given the uncertainties with regard to offset measurements and the range of possible ages of surfaces that stratigraphically bracket Channel C, three potential slip rates were calculated for the Oceano fault zone, as presented in Table 7-16.

The estimated slip rate for the Oceano fault zone at the Channel C piercing point is 0.05 mm/yr, based on a preferred offset of 1 m and an age of 20 ka at MIS 2.

Table 7-16. Oceano Fault Zone–Channel C Vertical Slip-Rate Estimates

Age	Min. Offset (–1 m)	Max. Offset (3 m)	Pref. Offset (1 m)	Comments
20 ka (MIS 2)[a]	–0.05 mm/yr	0.15 mm/yr	**0.05 mm/yr[a]**	Preferred age of initial incision of Channel C at the Oceano fault piecing point
135 ka (MIS 6b)	0.007 mm/yr	0.02 mm/yr	0.007 mm/yr	Alternative age (MIS 6b/6c) of Channel C inferred from the channel age model
1.4 Ma (MIS 45)	<0.001 mm/yr	0.002 mm/yr	<0.001 mm/yr	Maximum age of Channel C allowed by the channel age model

[a] Preferred age model and slip rate.

Oceano Fault Zone–Paleochannels D and E Slip-Rate Estimates

Channel D and E thalweg piercing points (Plate 5) cross the Oceano fault zone (Figures 7-24 and 7-40) and exhibit 2 m (0–4 m range) of vertical separation and 0 to 6 m dextral offset. Channel E thalweg and margins are deflected by approximately 80 m (±20 m) in a meander bend in the vicinity of the fault zone (Figure 7-39). It is possible that the measured offsets represent differential erosion due to variable rock strength, with older, more resistant rocks on the upthrown, north side of a scarp produced by the fault zone, as well as erosional downcutting and lowered based level to the west of the fault zone by Channels B and C.

Given the uncertainties with regard to offset measurements and the range of possible ages of surfaces that stratigraphically bracket the channels, three potential slip rates were calculated for the Oceano fault zone and these piercing points, as shown in Table 7-17.

Table 7-17. Oceano Fault Zone–Channel D and E Vertical Slip-Rate Estimates

Age	Min. Offset (0 m)	Max. Offset (4 m)	Pref. Offset (2 m)	Comments
20 ka (MIS 2)[a]	0 mm/yr	0.2 mm/yr	**0.1 mm/yr[a]**	Preferred age (MIS 2) of Channels D and E at the Oceano fault, as it is stratigraphically above H10 and the limit of onlap of unnamed Quaternary deposits
135 ka (MIS 6b)	0 mm/yr	0.03 mm/yr	0.015 mm/yr	Alternative age (MIS 6b/6c) of Channels D and E inferred from the channel age model
1.4 Ma (MIS 45)	0 mm/yr	0.003 mm/yr	0.001 mm/yr	Maximum age of Channels D and E allowed by the channel age model

[a] Preferred age model and slip rate.

The preferred slip-rate estimate for the Oceano fault zone is 0.1 mm/yr at the Channel D and E piercing points, with a reverse sense of motion, north side up.

Oceano Fault Zone–Paleochannel J Slip-Rate Estimates

Channel J thalweg and margin piercing points exhibit approximately 2 m (0–4 m range) of vertical separation across the Oceano fault zone. Channel J is incised into bedrock beneath the Upper Pleistocene deposits. Channel J also incises into the Upper Pleistocene sediments (Figure 7-41), however, which suggests reoccupation during MIS 2.

Given the uncertainties with regard to offset measurements and the range of possible ages of horizons that stratigraphically bracket Channel J, three combined lateral/vertical slip rates were calculated for the Oceano fault zone, as shown in Table 7-18.

The highest preferred model suggests that Channel J was incised during MIS 2, and that the channel is incised into the Upper Pleistocene coastal floodplain deposits that buried Channel Jc to the southwest of the Oceano fault zone (Figures 1-8i, 7-5, and 7-41). If this model is valid, then the slip rate on the Oceano fault zone in the vicinity of Channel J during the last approximately 20 kyr is 0.1 mm/yr. The lower preferred slip-rate estimate for the Oceano fault zone is 0.015 mm/yr, based on an age of 135 ka at MIS 6b.

Table 7-18. Oceano Fault Zone–Channel J Vertical Slip-Rate Estimates

Age	Min. Offset (0 m)	Max. Offset (4 m)	Pref. Offset (2 m)	Comments
20 ka[a] (MIS 2)	0 mm/yr	0.2 mm/yr	**0.1 mm/yr**[b]	Highest preferred age (MIS 2) of Channel Je/Jw incision and/or reoccupation, as it incises into the Upper Pleistocene deposits and bedrock
135 ka (MIS 6b)[b]	0 mm/yr	0.03 mm/yr	0.015 mm/yr[a]	Lower preferred age (MIS 6b/6c) of Channel J inferred from the channel age model
1.4 Ma (MIS 45)	0 mm/yr	0.003 mm/yr	0.001 mm/yr	Maximum age of Channel Je/Jw

[a] Highest preferred (Model 1) age model and slip rate.

[b] Lower preferred Model 2 slip rate.

Shoreline Fault Zone–Channels B and C Slip-Rate Estimates

The Channel B and C thalweg piercing points across the Shoreline fault (Figures 7-23 and 7-36) show no distinct offsets, with 0 m (–2 to +2 m range) of vertical separation and 0 m (0–6 m range) dextral offset (Table 7-11). Given the uncertainties with regard to offset measurements and the range of possible ages of the horizons that stratigraphically bracket the channels, three different slip rates were calculated for the Shoreline fault zone, as shown in Table 7-19.

Table 7-19. Shoreline Fault Zone–Channel B and C Slip-Rate Estimates

Age	Min. Offset (0 m)	Max. Offset (6 m)	Pref. Offset (0 m)	Comments
20 ka (MIS 2)[a]	0 mm/yr	0.15 mm/yr	**0 mm/yr[a]**	Preferred age (MIS 2) of Channels B and C at the Shoreline fault, as these channels are stratigraphically below H10 and above the limit of onlap of unnamed Upper Pleistocene deposits
135 ka (MIS 6b)	0 mm/yr	0.02 mm/yr	0 mm/yr	Alternative age (MIS 6b/6c) of Channels B and C inferred from the channel age model
1.4 Ma (MIS 45)	0 mm/yr	0.002 mm/yr	0 mm/yr	Maximum age of Channels B and C allowed by the channel age model

[a] Preferred age model and slip rate.

The preferred slip-rate estimate for the Shoreline fault zone is 0 mm/yr for the past approximately 20 kyr at the Channel B and C piercing points, within a range of values of 0–0.15 mm/yr. Therefore, the Shoreline fault zone appears not to have ruptured within the past 15–20 kyr at this location.

Shoreline Fault Zone–Channel F Slip-Rate Estimates

The Channel F thalweg and margin piercing points that cross the Shoreline fault zone (Figures 7-23 and 7-37) do suggest minor vertical fault separation, with −1 m (−3 to + 1 m range) of vertical separation and 1 m (0–6 m range) of lateral offset (Table 7-11). Both the northern and southern channel margins are disrupted, and the channel width and depth of incision change upgradient and downgradient from the fault (Figure 7-37). Given the uncertainties with regard to offset measurements and the range of possible ages of the horizons that stratigraphically bracket the channels, and with evidence for reoccupation of Channel F, three potential slip-rate estimates were calculated for the Shoreline fault zone and this location, as shown below in Table 7-20.

The preferred slip-rate estimate for the Shoreline fault zone is 0.05 mm/yr for the past approximately 20 kyr at the Channel F piercing points with the range of values from 0 to 0.30 mm/yr.

Table 7-20. Shoreline Fault Zone–Channel F Slip-Rate Estimates

Age	Min. Offset (0 m)	Max. Offset (6 m)	Pref. Offset (1 m)	Comments
20 ka (MIS 2)[a]	0 mm/yr	0.30 mm/yr	**0.05 mm/yr**[a]	Preferred age (MIS 2) of Channel F reoccupation at the Shoreline fault
250 ka (MIS 8b/8c)	0 mm/yr	0.02 mm/yr	0 mm/yr	Preferred age (MIS 8b/8c) of initial Channel F incision based on the relationship to H30 and H40, to the west of the 3D survey area. Assumes no reoccupation during MIS 2 or 6
1.4 Ma (MIS 45)	0 mm/yr	0.004 mm/yr	0 mm/yr	Maximum age of Channel F allowed by the channel age model

[a] Preferred age model and slip rate.

Shoreline Fault Zone–Channel I Slip-Rate Estimates

The Channel I thalweg and margin piercing points observed at the Shoreline fault zone (Figures 7-23 and 7-38) suggests 0 m (±2 m range) of vertical separation, and possible 1 m (0–6 m range) of lateral offset (Table 7-11). With the understanding that uncertainties are significant with regard to offset measurements and the range of possible ages of the horizons that stratigraphically bracket the channels, and with evidence for reoccupation of Channel I, three potential slip-rate estimates were calculated for the Shoreline fault zone and this location, as presented in Table 7-21.

Table 7-21. Shoreline Fault Zone–Channel I Slip-Rate Estimates

Age	Min. Offset (0 m)	Max. Offset (6 m)	Pref. Offset (1 m)	Comments
20 ka (MIS 2)[a]	0 mm/yr	0.30 mm/yr	**0.05 mm/yr**[a]	Preferred age (MIS 2) of Channel I reoccupation at the Shoreline fault
250 ka (MIS 8b/8c)	0 mm/yr	0.02 mm/yr	0 mm/yr	Alternative age (MIS 8b/8c)of Channel I reoccupation based on the relationship to H30 and H40, to the west of the 3D survey area
1.4 Ma (MIS 45)	0 mm/yr	0.004 mm/yr	0 mm/yr	Maximum age of Channel F allowed by the channel age model

[a] Preferred age model and slip rate.

The preferred slip-rate estimate for the Shoreline fault zone is 0.05 mm/yr for the past approximately 20 ka at the Channel I piercing points, with a range of values of 0–0.30 mm/yr.

8.0   SYNTHESIS

The objectives and goals of the 3D LESS studies were all accomplished. The primary objectives of this investigation were to identify and map the southward extension of the Shoreline fault zone and estimate offsets along both the Shoreline fault zone and the HFZ. The goal was to provide a range of offset distances and estimated ages of piercing points to constrain slip rates along the fault zones. To accomplish this, potential piercing points (primarily buried paleochannels and buried paleoshorelines or strandlines) were identified and mapped in accordance with the criteria outlined in Section 3.2.1, using the 3D volumes and 2D seismic-reflection profiles outside the 3D survey areas. These survey areas (see Figure 1-1; Plates 1A and 1B) consist of three disparate 3D survey blocks, as follows:

- Survey Area 1 is located in Estero Bay.
- Survey Area 2 is in San Luis Obispo Bay.
- Survey Area 3 is offshore of Point Sal.

From each of these areas, a 3D volume was constructed (e.g., Figure 7-31), and several different attributes were tested to determine those that would image the paleochannels and shoreline piercing points best. Of the seven attributes tested (five geometric and two instantaneous attributes), two (smooth similarity and smoothed dip of maximum similarity; Figures 2-5 and 2-6) were compared with a selection of amplitude time slices to define the piercing points.

Two structures, the HFZ and the Shoreline fault zone, are the primary focus of this investigation (Figures 1-1 and 7-20a; Plates 1A and 1B). For the HFZ, buried paleochannels provide the best geometric piercing points for use in estimating offsets across the entire fault zone. The channels imaged in the Estero Bay and Point Sal study areas appear to be primarily submarine channels, with possible fluvial heads, formed on a paleo–continental slope, as they exhibit submarine channel morphologies (Figures 1-9 and 6-6) and are located beneath the modern outer continental shelf (Estero Bay study area) or beneath the modern middle to outer continental shelf (Point Sal study area). For the Shoreline fault zone, by contrast, the buried paleochannels imaged in the San Luis Obispo Bay study area exhibit fluvial channel characteristics (Figures 7-3 and 7-8).

Given the lack of available radiometric ages, magnetic stratigraphy, or biostratigraphy, the ages of the channels in the study areas are poorly constrained. Age models were constructed to estimate ages of piercing points and calculate slip rates associated with the mapped faults. The primary basis for the age models is the Quaternary sea-level curve (Waelbroeck et al., 2002; Lisiecki and Raymo, 2005; Figures 1-6 and 6-2); sequence-stratigraphic horizons (Figure 6-1b), which were dated using the sea-level curves (PG&E, 2012); and recognized unconformities correlated with biostratigraphic well-hole data in the offshore Santa Maria Basin (Willingham et al., 2013; Figures 6-18 through 6-20). For fluvial channels, the sea-level curves (Figures 1-6 and 1-7) were examined to estimate the age range in which channel incision and abandonment, or filling, occurred by selecting points on the sea-level curves where the depth range of a falling or rising sea level correlates with the identified depth of the channel thalweg (Figure 1-8). By bracketing a time interval on the sea-level curve when shorelines and channels began to erode into

bedrock or fill and when erosion ceased and sedimentary deposition and channel filling probably occurred, an age window is produced that can be used to estimate the age of the features (see Figure 1-8).

Ten general unconformities were used to statigraphically constrain the ages of piercing points. Three of the 10 are the regional top of Miocene unconformity (~5.5–5.1 Ma), the ELP (~3.5–2.7 Ma), which is described by Willingham et al. (2013; Figure 1-5), and the NTN (~2.6–1.8 Ma), which is described in Section 6.2. One relatively deep unconformity located above the NTN is T05, which was locally identified in the Estero Bay study area and has been assigned an estimated preferred age of approximately 700–630 ka (Figure 6-1). Unconformity T05 is the deepest surface marked by significant downlap in Estero Bay. Six unconformities are recognized because they bound Quaternary stratigraphic sequences (Figure 6-1b). The 4 youngest unconformities (Figures 1-5 and 6-1b), based on a PG&E sequence-stratigraphy study (PG&E, 2012), were H40, H30, H20, and H10. Ages for all 6 of these unconformities were estimated from Quaternary sea-level curves; their ages are estimated as follows:

- H48 formed between the MIS 12 lowstand and the MIS 11 highstand, approximately 460–425 ka.
- H45 formed between the MIS 10 lowstand and the MIS 9 highstand, approximately 370–330 ka.
- H40 formed between the MIS 8 lowstand and the MIS 7 highstand, approximately 250–240 ka.
- H30 formed between the MIS 6 lowstand and the MIS 5e highstand, approximately 135–125 ka.
- H20 formed near the LGM elevation and below, approximately 27–19 ka.
- H10 formed post-LGM, approximately 19–7 ka.

Fault activity is estimated by correlating the uppermost reflections displaced or deformed by a fault with mapped horizons that bracket the deformed reflections.

8.1 The Hosgri Fault Zone

A series of buried paleo–submarine channels and channel complexes are used as piercing points for estimating offsets along the HFZ. These channels are imaged in the 3D volumes and associated 2D seismic-reflection profiles of the Estero Bay and Point Sal study areas (Figures 6-8 and 6-18); thus, two separate and distinct sites along the HFZ located approximately 45 km apart are used to determine offsets.

8.1.1 Faults of the Estero Bay Study Area

In the Estero Bay study area, the HFZ consists mainly of two dominant subparallel fault strands, faults labeled 10001 and 10006 on Figure 6-8b (PG&E, 2013), with minor secondary strands to the northeast and southwest. Where well imaged, the fault strands of the HFZ are generally steeply dipping to vertical, consistent with previous characterizations of the HFZ as a dominantly right-lateral strike-slip fault zone (e.g., Hanson et al., 2004; Johnson and Watt, 2012; Willingham et al., 2013). The sense of

vertical separation across the HFZ in the study area is dominantly down to the west, as indicated by the presence of the broad, beveled bedrock surface to the east and a relatively thick sedimentary section to the west (Figure 6-4). Faults within the HFZ have produced slivers or a central structural block in Estero Bay and Eastern, Central, and Western blocks in the Point Sal and San Luis Obispo Bay study areas.

8.1.1.1   Piercing Points

Several channel complexes and many channels are identified in the Estero Bay study area (Figure 6-17); however, only seven are well enough constrained by the data to be considered for use as thalweg piercing points, with three of these located east of the eastern primary strand of the HFZ (eastern structural block), one between the eastern and western strands (central structural block), and three east of the western primary strand (western structural block).

In the eastern structural block, Channel Complex Ae (consisting of Channels Ae3, Ae2, Ae1.5, and Ae1); Channel Be; Channel Ce (poorly defined); and Channel Complex De (Figure 6-10b) were considered potentially correlative with channels identified west of the HFZ. Channel Complex Ee is the only potential piercing point located in the central structural block, as it is well defined both in cross section (in seismic-reflection profiles) and in plan view (in time slices) and includes a well-preserved basal channel with at least two nested channels incised into the larger channel's fill (Figure 6-12).

In the western structural block, three channels were considered potentially correlative with channels east of the HFZ (Plate 3): Channel DAw, with a thalweg depth of approximately 275–315 m below modern sea level; Channel DBw, with a thalweg depth of approximately 270–325 m; and Channel DCw, with a thalweg depth of approximately 270–350 m.

8.1.1.2   Offsets of Piercing Points

Of the channel thalweg piercing points observed in the study area east of the HFZ, on the eastern structural block, only Channel Complex De may be correlated across fault 11006. As shown on Plate 3, Channel Complex De extends downslope to the west and exhibits dextral offset to the north across fault 11006, where it appears to correlate with Channel Ee1 on the central structural block. The flattened image of Channel Ee1 (Figure 6-12) shows it to be similar in width and incised to a similar depth as Channel Complex De (Figure 6-11; Plate 3). Correlation of the thalwegs of Channel Ee1 to Channel Complex De suggests a right-lateral separation of 260 ± 60 m and a vertical separation of 40 ± 8 m, down to the west, across fault 11006 (Figure 6-16).

Of the channels imaged west of the HFZ, three extend far enough to the east and are incised deeply enough to suggest that they may correlate to channel remnants east of the HFZ. These three channels are DAw, DBw, and DCw (Figure 6-15). Restoring approximately 850 m of slip on fault 10001 aligns each of these three channels with candidate upgradient extensions east of the fault. This restoration suggests that Channel DBw is the downgradient extension of Channel De-Ee1 (Correlation A on Figure 6-17).

Precise constraints on the amount of offset are measured from the offset thalwegs of Channel DBw from Channel Ee1 (Figure 6-16). Two sources of uncertainty in the offset of this channel exist. The first is uncertainty in the projection of the channel thalweg from where it is mapped on each side of the fault to where it intersects the fault. The second is based on the mapping of Channel DBw itself. Channel DBw is not as well imaged near fault 10001, as it is farther from the fault (Figure 6-14b). On the nearest profile to the fault, two channel-like features are recognized that could represent the upslope extension of Channel DBw. Although the southern channel-like feature appears more likely to be the upslope continuation of Channel DBw, the northern channel-like feature is also considered a candidate equivalent channel (Figure 6-16). Therefore, uncertainty in the thalweg offset measurement is large. The best estimate of horizontal offset across the primary trace of the HFZ (fault 10001) is between approximately 700 and 1,000 m. Based on the uncertainties described above, the maximum horizontal offset is 1,650 m and the minimum is 450 m (Figure 6-16). The vertical separation is 100 ± 25 m, down to the west.

8.1.1.3   Age Constraints and Slip Rates

Slip rate along the HFZ is calculated using the combined Channel DBw-Ee1-De as the preferred piercing point. Channel DBw is bracketed stratigraphically by two key unconformities, the ELP and the T05 horizon, which provide absolute minimum and maximum constraints on the possible age of the channel (Figure 6-14). As shown on Figures 6-1 and Plate 2, Channel DBw is buried well below unconformity T05. The depth of burial is at least 40 m as shown on Figure 6-1, and at least 32 m as shown on Plate 2. However, the timing and rate of sedimentation that led to abandonment and burial of Channel DBw is not well understood. Two alternative approaches, based on stratigraphic and climatic assumptions, are applied to estimating the channel age in order to account for this uncertainty (see Section 6.1.2.2 and Figure 6-2). These assumptions yield a mean age of 840 +690/–250 ka, within a high (90%) confidence interval.

The preferred slip-rate estimate for the entire HFZ in the Estero Bay study area based on the Channel Fe3/Fw3 correlation is 1.75–1.90 mm/yr, within a range of 1.61–2.05 mm/yr. The estimated minimum slip rate of the preferred correlation is 0.39 mm/yr, and the maximum slip rate is 4.71 mm/yr. As discussed previously, the preferred age of incision of Channel Fe3/Fw3 is 342 ka (MIS 10).

8.1.2   *Faults of the Point Sal Study Area*

The Point Sal study area is located along the trend of the HFZ approximately 45 km south of the Estero Bay study area (Figure 1-1; Plates 1A and B). A distinct change in structural style occurs from south to north in the Point Sal study area, with the HFZ splitting from a single splay in the south to multiple splays in a broad paired fault bend, which then converge into a single fault splay in the north. An abrupt change in strike of the eastern strand of the HFZ occurs near the center of the survey area, where multiple shorter faults are mapped and slice the central structural block into many slivers that deform a broad anticline (Figure 6-28). This complex fault pattern is representative of a restraining bend that is actively undergoing transpression, as the eastern strand of the HFZ appears to

vertically displace unconformity H10, and possibly upper (younger) horizons, by approximately 4 ± 2 m (Figures 6-21), and both the eastern and western strands of the HFZ offset an unconformity represented by reflection H30 (Figures 6-21 and 6-31).

Just north of the restraining bend, where the central structural block tapers to the north, the northwest-trending Lions Head fault zone converges with the HFZ (Figure 6-28). Here the primary Lions Head fault strand is vertical to steeply dipping where imaged in the 3D data and it expresses substantial vertical displacement of the ELP/NTN unconformity (Figures 6-21 and 6-29).

The Casmalia fault zone consists of several subparallel fault strands that extend (1) from the coast approximately 2 km north of Mussel Point toward the west-northwest and (2) approximately 12 km offshore to near the south end of the eastern strand of the HFZ in south-central San Luis Obispo Bay, where it forms the northern boundary of the Casmalia/Point Sal block (Figure 1-2). This fault zone represents the northern boundary of an uplifted bedrock block whose southern boundary is represented by the Lions Head fault zone, forming an uplifted fault block onshore known as the Casmalia Hills. The Casmalia/Point Sal block projects into the outer southern part of San Luis Obispo Bay as Point Sal (Figure 6-28; Plate 1B).

The buried thrust fault, "Blind Thrust fault NE," is interpreted to lie beneath the folded ELP/NTN unconformity (Figure 6-29). Seismic reflections representative of Quaternary and Neogene strata above and below the ELP/NTN surface are uplifted and folded in the hanging wall of the inferred blind thrust fault at this location (Figures 6-24 and 6-34).

8.1.2.1   Piercing Points

Seven channels or channel complexes are identified within the 3D data set in the Point Sal study area (Figures 6-35 and 6-36). From north to south, these include Channel Complex Ac and Aw (Channels Ac1, Ac2, Aw1, and Aw2); Channels Be and Bc; Channel Ce; Channel De; Channel Ee; Channel Complex F (Channels Fe1-3, Fc1-2, and Fw1-3); and Channel Ge (Figure 6-36). Most of the channels appear to be structurally controlled, although some are incised into both structural lows (synclines) and highs (anticlines), and some are incised into reflections interpreted as folded Quaternary deposits (Figure 6-37). Other channels (e.g., Channel Bc) are incised into reflections of the Neogene bedrock. Some paleochannels (i.e., Channels Ce, De, Ee, and Ge) are recognized only on the eastern structural block. Others have been mapped in the central structural block and either in the western or eastern structural blocks (i.e., Channels Ac/Ae and Be/Bc). The only channel complex present on all three structural blocks of the HFZ is Channel Complex F, consisting of Channels Fe, Fc, and Fw (Figure 6-36).

8.1.2.2   Offsets of Piercing Points

Of the seven paleochannels or channel complexes identified in the Point Sal 3D data set (Figures 6-35 and 6-36), three (Channel Complexes A, B and F) appear to have significant lateral and vertical displacement of their thalweg piercing points (Table 6-4). For the three major fault strands mapped within the HFZ, the estimated amount of lateral and vertical separation of piercing points varies due to differential deformation and strain

partitioning along the HFZ since its inception in the Miocene (Compton, 1991; Clark et al., 1994; Sorlien et al., 1999; Johnson et al., 2012; Willingham et al., 2013). The thalweg piercing points of Channel Complex F are used to determine a preferred total offset across the entire HFZ, as this channel complex extends across all structural blocks. We used the offsets and slip rate estimates for Channel Complexes A and B across the western and eastern strands of the HFZ to compare with those of Channel Complex F.

The highly preferred correlation is for Channel Fe3 east of the HFZ to be of similar age with Fw3 to the west. Channels Fe3 and Fw3 appear very similar in their cross-sectional shape and seismic character of channel fill, and a small channel incised into the upper fill, suggests that these channels are segments of the same channel. Channel Fe3 is narrower than Fe1 (Figure 6-43), and shares morphologic characteristics with Channel Fw3. The total measured lateral separation of the preferred Channel F thalweg correlation (Channel Fe3/Fw3; Figure 6-51a) is approximately 550–700 m of dextral offset, with a preferred value of approximately $600–650 \pm 50$ m. The preferred estimated vertical separation across the entire HFZ is approximately 95 ± 15 m, down to the west (Table 6-4). The confidence of this correlation is of the highest level.

An alternative correlation of Channel F is also possible. The alternative correlation of Channel Fe1 with Fw3 through Fc1 is based on the reasonable geometric match of the channels in plan view. The channel widths of Channels Fe1 and Fw3 are similar, and both channels are incised into reflections of inferred Quaternary strata adjacent to bedrock. Correlation of the Channel Fe1 thalweg with the Channel Fw3 thalweg across the entire HFZ provides an estimated dextral offset of 500–550 m, with a maximum of 600 m and minimum of 450 m (see Table 6-4). The estimated vertical separation of the channel thalweg is 85 m, down to the west (Figure 6-51b). The correlation confidence level of Channel Fe1 with Channel Fw3 is medium.

Channel Complex B is incised into bedrock on the central structural block (Figure 6-41) and is well imaged. On the eastern structural block, Channel Be has a relatively broad thalweg incised into reflections of interpreted Quaternary strata (Figure 6-40). Part of Channel Bc is absent on the central structural block due to uplift and erosion (Figures 6-42 and 6-50). Consequently, the confidence level for the Channel B piercing point is medium. The thalweg offset is estimated to be 356 m, with an estimated maximum offset of 510 m and a minimum of 193 m.

Channel A is well imaged on the 3D seismic-reflection data, and the correlation of the channel across the western strand of the HFZ is clear (Figure 6-39). However, the confidence level for the Channel A piercing points (thalweg and upper channel wall break) is low because of the broad thalweg and rounded upper channel margins (Figures 6-37 and 6-38). The Channel Aw2/Ac2 thalweg dextral offset of approximately 95 ± 20 m across the western strand of the HFZ is illustrated on Figure 6-49. Thus, given the higher correlation confidence level of Channels Fe3 a nd Fw3 (exclusive of Channel Fc1), offset measurements of these channel thalwegs are used for estimating the preferred dextral slip rates across the HFZ.

8.1.2.3   Age Constraints and Slip Rates

The channels mapped in the Point Sal study area are bracketed stratigraphically by three key unconformities: the ELP/NTN unconformity, the H30 unconformity, and the H10 unconformity. Given the observed structural and stratigraphic relationships between Channels Be and Bc, along with similarities in geometry, depth, and morphology, it is likely that these paleochannels are coeval in age. Channel Bc is incised into the ELP/NTN unconformity in the uplifted Central block (Figure 6-41). Channel Be is incised into reflections inferred to be Quaternary sediments that lie within the axis of a syncline on the eastern structural block (Figure 6-40). The Channel Be thalweg is located approximately 20 m below the seafloor and approximately 85 m above the ELP/NTN unconformity in the axis of the syncline (Figure 6-40).

The thalwegs of Channels Be and Bc are located at a depth of approximately 120 m, which coincides with several of the past sea-level lowstands in the late Quaternary since MIS 16 and the MPT (Figure 1-6). The post-ELP/NTN reflections into which Channel Be is incised appear to represent strongly folded Quaternary strata (Figure 6-40). Erosional truncation of these reflections by Channel Be is clearly apparent on the northern flank of the channel. Horizon H40 is mapped along the same reflection to the north. It exhibits structural and stratigraphic relationships similar to the syncline where Channel Be is located (Figure 6-40), and it likely coincides with the unconformity at the base of Channel Be. Given the preferred age for H40 (PG&E, 2013), it appears that Channel Be was incised during the MIS 8b lowstand (Figures 1-6 and 6-52a).

The thalwegs and margins of Channel Complex F to the east and west of the HFZ are well imaged in the 3D volume as pronounced angular unconformities where the channel is incised into layered reflections of the unnamed Pleistocene deposits, above the ELP/NTN unconformity (Figures 1-5, 6-43, and 6-47). Channel Complex F is located in the inferred Quaternary sediments. The depths of the Channel Fe1 and Fc1 thalwegs are approximately 160 m and 200 m, respectively. The Channel Fw3 thalweg is at a depth of approximately 260 m. These depths are significantly greater than the reported 120–125 m sea-level lowstands of the late Quaternary since the MPT. Consequently, either Channel Complex F has subsided significantly since initial fluvial channel incision, or the channels are of marine origin and formed below sea level. Given the thalweg depths and morphology, which are similar to other slope channels (Lee et al., 2002; Dartnell and Gardner, 2009; Surpless et al., 2009; Maier et al., 2013), a submarine origin is considered more likely.

The width of Channel Complex F is approximately 600 m near the top of Channel Fw3 (Figure 6-48), which lies at a depth of approximately 200 m and which is overlain by a thick (~100 m) sequence of fairly flat-lying reflections inferred to be of upper Quaternary strata, with horizons H30 and H10 mapped near the top of this sequence (Figure 6-47). The age of Channel Complex Fw is constrained by a lower limit of the ELP/NTN unconformity and an upper limit of reflections H30 and H10. Approximately 60 m of relatively flat-lying undeformed reflections separate the top of Channel Fw3 and the H30 horizon (Figure 6-47). Consequently, Channel Fw3 is interpreted to be significantly older than the H30 horizon. A reflection above a minor angular unconformity at the top of the

Channel Fw3 fill deposits is interpreted as possibly being horizon H40 (Figure 6-47). Given the preferred age (MIS 8b) for H40 (Figure 1-6), incision of Channel Fw3 may have occurred during MIS 10, approximately 350–340 ka. The confidence level of the age of H30 to the west of the western strand of the HFZ in the Point Sal 3D survey area is medium (PG&E, 2013). The confidence level of H40 in this area is poor.

The age model for Channel Complex F (Channels Fe3, Fc1, and, Fw3) suggests that channel incision and infilling took place during a low sea-level lowstand in the late Quaternary, prior to the development of horizon H30. The age of the channel complex is constrained to be between 130 ka (H30 unconformity) and 1.8 Ma (NTN unconformity). Prior to development of Channel Complex F, at least 150 m of syntectonic sediment accumulated above the NTN unconformity in Syncline Ae (Figure 6-29). Growth folding is apparent within the axis of this syncline. Significant post-depositional folding of these deposits is also apparent on the 3D data (Figure 6-29), suggesting a relatively prolonged period of geologic time post-NTN unconformity development, possibly in the early to middle Quaternary. Channel Complex F is incised into the interpreted strongly folded Quaternary strata of Syncline A (Figures 6-22, 6-23, 6-29, and 6-47). Given these relationships, we infer a likely late Quaternary age of Channel Fe3/Fw3 incision, with a maximum age of 1.4 Ma, at the beginning of the MPT (Figure 6-2), as the early age of channel formation of the Channel F complex's older channels (i.e., Fw1 and Fe1). We therefore conclude that Channel Fe3/Fw3 developed sometime between approximately 1.4 Ma and 130 ka, with a preferred age of approximately 350–340 ka, at the MIS 10 lowstand maxima (Figures 1-6 and 6-52).

The Channel Be and Bc thalweg piercing points of Channel Complex B that cross the eastern strand of the HFZ suggest dextral offsets of approximately 193 m (minimum) to approximately 510 m (maximum), with a preferred offset of 356 m and approximately 20–60 m of vertical displacement. However, this apparent thalweg displacement may be the result of erosion or other processes that are not representative of fault movement. Nevertheless, these apparent offset estimates are used to determine a potential slip rate for the eastern strand of the HFZ, and, as shown in Table 6-6, are calculated for three different ages: 138 ka (MIS 6b), 250 ka (MIS 6b), and 1.4 Ma. Using these three ages and the minimum estimated offsets, the estimated slip rates are 1.4 mm/yr for 138 ka, 0.77 mm/yr for 250 ka, and 0.14 mm/yr for 1.4 Ma. For the maximum offsets, the slip rates are 3.7 mm/yr for 138 ka, 2.04 mm/yr for 250 ka, and 0.36 for 1.4 Ma. Given the preferred age of channel formation of 250 ka, and a preferred offset of 356 m, the preferred slip rate for the eastern strand of the HFZ at Channel B was calculated as 1.42 mm/yr, with a minimum slip rate of 0.77 mm/yr and a maximum slip rate of 2.04 mm/yr.

The Channel Fe3/Fw3 thalweg piercing point across the HFZ suggests approximately 550–700 m of dextral separation since incision of the channel thalweg, with a preferred offset of 600–650 m. These channels are interpreted as marine channels that originally incised reflections of sediment deposited on the middle and upper slope. The correlation confidence level for these channels is high because they are very well defined and geomorphically similar. However, given that Channel Complex F is most likely of marine origin, there is considerable uncertainty in the ages of channel incision. The range of possible ages for the horizons that stratigraphically bracket Channels Fe3 and Fw3 and

the apparent dextral slip rates are given in Table 6-6. The slip rates calculated for ages of 138 ka (MIS 6b), 342 ka (MIS 10), and 1.4 Ma at a minimum offset of approximately 550 m are 3.98 mm/yr, 1.61 mm/yr, and 0.39 mm/yr, respectively. In contrast, using the same ages, the slip rates for a maximum offset of approximately 700 m are 5.07 mm/yr, 2.05 mm/yr, and 0.5 mm/yr, respectively. Using the preferred offset of 600–650 m and the same ages, the estimated slip rates are 4.35–4.71 mm/yr, 1.75–1.90 mm/yr, and 0.43–0.46 mm/yr, respectively, and the preferred slip rate is 1.8 ± 0.4 mm/yr. The preferred slip rate of 1.8 ± 0.4 mm/yr for the HFZ, based on Channel Complex F offsets and age estimates, is comparable to, and in general agreement with, previous slip rate estimates for the HFZ.

8.1.2.4   Point Sal Slip Rate Summary

The estimated slip rate for the eastern strand of the HFZ, based on the Channel B measured offsets and age model, is approximately 1.4 mm/yr. The estimated slip rate for the western strand of the HFZ, based on the Channel A measured offsets and age model, is approximately 0.4 mm/yr. Consequently, the combined slip rate for the eastern and western strands of the HFZ, based on the Channel A and B measured offsets and age models, is 1.8 mm/yr. This rate is consistant with the preferred slip rate of 1.8 ± 0.4 mm/yr across the entire HFZ independently calculated (based on measured offsets and the age model) for Channel Fe3/Fw3 at a separate location, confirming the validity of the preferred slip rate. Therefore, the confidence of this slip rate estimate is the highest for all piercing points considered.

8.2   The Shoreline Fault Zone—San Luis Obispo Bay

Given the interpretations of the 3D data set, the Shoreline fault zone is extended south from where it was previously mapped north of San Luis Obispo Bay (PG&E, 2011b, 2012). Within the study area, the fault bifurcates and connects with other previously mapped faults and fault zones (Figure 7-15; Plate 1B). Many potential piercing points, consisting of buried paleoshorelines (paleostrandlines), channels, and channel complexes, cross the Shoreline and other fault zones in the San Luis Obispo Bay study area (Figure 7-2).

Considerable detail of the fault geometry is provided in the 3D volume, and the pattern of faulting in plan view is complex (Figure 7-3). In the northwestern and central parts of the 3D survey area, several faults converge near the location of Souza Rock (Figure 7-7). The Shoreline fault zone is mapped as the throughgoing structure and extends southeastward through the entire 3D survey area. The fault zone bifurcates at Souza Rock, where one strand trends toward the east-southeast, connecting with the Oceano fault zone. In the southeastern part of the 3D survey area, the Oceano fault zone is expressed on the bedrock surface as a fault scarp whose relief disappears toward the northwest, abruptly ending where Pleistocene strata pinch out near Channel Je (Figures 7-3, 7-6, 7-7, and 7-41b; Plate 7). Just north of Souza Rock, the western terminus of the Los Berros fault appears to be truncated by, or merges with, the Shoreline fault zone. A general east-west-trending inferred fault, the North Pecho fault, appears to merge with the southeastern strand of the Shoreline fault zone in the central part of the survey area, and a more

westerly inferred strand, the Pecho fault, appears to bifurcate from the North Pecho fault strand near the northwest corner of the survey area and extends a short distance to the southeast (Figure 7-15b). A well-defined east-west-trending unnamed fault merges with the southwest-trending strand of the Shoreline fault zone in the central part of the survey area, just south of where the North Pecho fault appears to merge with the Shoreline fault zone.

Other faults were mapped throughout northern San Luis Obispo Bay outside the 3D survey area using 2D seismic-reflection profiles from PG&E's legacy archive data set (Figures 7-14 and 7-15). The convergence of many faults can be observed in plan view, with the previously mapped Pecho, Oceano, Shoreline, and Los Berros fault zones and several unnamed faults merging within the 3D survey area (Plates 1B, 4 and 5).

The Oceano fault bifurcates from the Shoreline fault in Channel A west of Souza Rock and continues to the southeast as a narrow, linear fault strand across the 3D survey area (Figures 7-3 through 7-7; Plates 4 and 5). Outside the 3D survey area, this fault continues and connects with the Oceano fault zone, which then aligns with the previously mapped Santa Maria River and Oceano fault zones onshore near the mouth of the Santa Maria River (Figure 7-15). The total length of the Oceano fault from Souza Rock to the shoreline is approximately 10 km.

Based on 2D data the Shoreline fault zone proper is extended approximately 13.7 km from the southeast edge of the survey area (Figure 7-21a) southeast to where it connects with a fault mapped in the Guadalupe Oil Field onshore (CDOGGR, 1992). This distance, added to the approximately 6.5 km length of the fault zone clearly imaged in the 3D volume, extends the newly mapped part of the Shoreline fault zone by approximately 22 km south from Sousa rock; Sousa Rock is 1.2 km south of the north end of the 3D survey boundary. Assuming that the Point Buchon fault zone north of the San Luis Obispo Bay study area is part of the Shoreline fault zone, then the fault zone length north of Souza Rock is approximately 23 km, making the Shoreline fault zone in its entirety approximately 45 km long.

8.2.1   Piercing Points

Many potential piercing points are imaged in the 3D volume and consist of buried paleoshorelines (paleostrandlines in 3D), channel thalwegs, and channel margins (Figure 7-23 and 7-24). Four buried strandlines that vary in depth from 79 to 97 m beneath modern sea level are located in the southern part of the San Luis Obispo Bay 3D study area (Figure 7-24). Two of the paleostrandlines, located at depths of 84 and 92 m, cross the Shoreline fault zone (Figures 7-25 and 7-26). These two paleoshorelines are incised into reflections interpreted as Upper Pleistocene deposits that onlap and overlie the bedrock surface (Figures 7-11 and 7-28). The line that marks the boundary between the wave-cut platform and the paleo–sea cliff (strandlines) define a linear to circular geomorphology (Figure 7-29) that is stratigraphically isolated, so that an age of incision and amount of offset can be fairly well estimated.

Twelve buried paleochannels (Channels A through L on Figures 7-2, 7-7, and 7-23) are incised into the bedrock and well imaged in the 3D volume of the San Luis Obispo Bay

study area (Figures 7-22, 7-31, and 7-32; Plates 5 and 6). These channels range from small, V-shaped fairly straight narrow-thread channels (Figure 7-41) to broad, flat channel floors representative of a braided fluvial system (Figures 7-39 and 7-42). The margins of the channels are generally sharp in the thread channels, while they are gently rounded in the larger, broader channels. The sharp upper margins of many of the channels are well exhibited on slope maps that were constructed to define the line of greatest slope declivity in high resolution (within 3–6 m), as shown on Plate 7, and used as potential piercing points for determining fault offsets.

Given the clear geomorphologic expression of many of these paleochannels (their V-shaped thalwegs and sharp upper wall margins that are incised into the pre-Quaternary bedrock), the correlation of these channels' piercing points is of the highest confidence level. Also, in the southern part of the 3D volume, and southwest of the Shoreline fault zone, signal convolution of the seafloor multiple with the primary reflections of Channels Fw and Iw prevents clear resolution of these channels, and thus diminishes the correlation confidence level to medium (Figures 7-38 and 7-39; Plate 4).

Evidence for little or no fault offset occurs at most of the channel piercing points (see Section 3.6; Plates 4 through 7). However, an exception is the well-defined bedrock-incised Channel Complex A, which exhibits dextral offset across the Shoreline fault zone (Figures 7-33 and 7-35).

8.2.2   Offsets of Piercing Points

Geologic and measurement uncertainties contribute to the total uncertainty in piercing point offset estimates. Measurement uncertainty is a function of data resolution, which for the 3D P-Cable system used in this study, is approximately 3 m horizontal and approximately 2 m vertical (see Section 2.2). Geologic uncertainty is variable, but for the San Luis Obispo Bay 3D data set, it is generally 3–6 m. Those piercing points that cross the Shoreline fault zone, which is characterized as a vertical right-slip fault zone, and where no horizontal separation is observed, the minimum and preferred values of dextral separation is taken as 0, and the maximum value as 6 m. Vertical separation across faults in the 3D data set locally exhibit opposite senses of motion (north vs. south side up), and in some cases vary along strike. For those piercing points where no vertical separation is observed, the range is inferred to be ±2 m (see Tables 7-3 through 7-10). Offset estimates and associated measurement uncertainties are summarized in Table 7-11. Geologic uncertainties related to fluvial geomorphology, river avulsion and deflection, and differential erosion are all factors considered in determining offsets of the piercing points (see Section 7.2).

Five channels (Channels A, B, C, F, and I) cross the Shoreline fault zone, and seven channels (Channels A, B, C, D, E, F, and J) cross the Oceano fault zone. These channels, plus two paleoshorelines (the –84 m and –92 m strandlines), provide multiple potential piercing points for use in estimating offsets and slip rates on the two fault zones (Table 7-11).

8.2.2.1 Strandlines

The 84 and 92 m deep strandlines equally exhibit lateral and vertical separation across the Shoreline fault zone. Vertical separation is estimated to be approximately 0.8 to 1.6 m (down to SW) and dextral offset is 9.4 (3 pixels) ± 6 m, with a preferred value rounded to 10 m (Figure 7-29). Given the clear geomorphologic expression of the paleostrandlines that erode reflections of Upper Pleistocene deposits, and the unambiguous, distinct, measurable dextral and vertical separations across the fault zone, offset estimates of the mapped paleostrandline piercing points are considered of the highest confidence level (see Section 3.6; Plates 4 through 7).

8.2.2.2 Channel Thalwegs and Margins

West of Souza Rock, Channel Complex Ae appears to be laterally offset by the Shoreline fault zone (Figures 7-32 through 7-34). Lateral separation is interpreted to be approximately 10–50 m, with a preferred (dextral) offset of approximately 30 m (Table 7-11). Channel Ae/Ac is the only channel within the resolution of the San Luis Obispo 3D volume that is interpreted to exhibit significant measurable dextral offsets of its channel margins and thalwegs along the Shoreline fault zone.

The channel thalweg mapped in the lower part of Channel Complex A is incised into the bedrock surface (Figures 7-33 and 7-35). The Channel A thalweg is dextrally offset by approximately 30 ± 10 m (Figure 7-35a). Vertical separation of the bedrock channel thalweg is estimated to be 3 ± 2 m, down to the south (Plate 6).

The Shoreline fault is interpreted to dextrally offset the shallow (~50 m below sea level) Channel Complex A's margins by 20 to 40 ± 10 m (Figures 7-33a and 7-35c). The channel margin on the southeast side is disrupted, and apparent dextral offset on the Shoreline fault zone is greater than that observed on the northwest channel margin (Figures 7-33b and 7-35c). Lower channel fill deposits are offset by the fault (Figure 7-33a), while a younger, nested channel is not deformed or displaced by the Shoreline or Oceano faults (Figure 7-35b). The eastern Channel Complex A margin also appears to be vertically offset by the Oceano fault zone (Figure 7-33b and c; Figures 7-34 and 7-35); vertical separation at this location is estimated to be 3 ± 2 m. The Oceano fault zone style is reverse, north side up. Souza Rock is uplifted in the hanging wall of the Oceano fault zone at this location.

Two well-defined channels, Channels F and I, cross the Shoreline fault zone in the southern part of the 3D survey area (Figure 7-2; Plate 5). Channel Fw is very straight and its thalweg and margin piercing points appear not to be significantly offset by the fault zone. Slight bending of both channel margins is apparent, however, and channel depth and width vary across the fault zone (Figure 7-37e and f). Channel I is more sinuous than Channel F, and also does not appears to be significantly offset by the Shoreline fault zone. Although little to no offsets of either channel's piercing points are observed in the 3D data, given the data resolution (approximately 3 m), the uncertainty in the original canyon morphology, and the unknown amount of canyon wall erosion that might have occurred since the canyon was abandoned, it is possible that up to 6 m of offset may have

occurred, yet is undetected in the 3D data. The preferred offset for Channels F and I across the Shoreline fault is 1 m, within a range of 0–6 m.

Estimated vertical offsets of paleochannels across the Oceano fault zone range from 0 to +5 m, down to the southwest. Channels B, D, E, F, and J exhibit measurable preferred vertical offsets of approximately 2 ± 2 m (Table 7-11). The top-of-bedrock surface and Upper Pleistocene deposits are vertically offset (down to southwest) approximately 3 ± 2 m, and the base of Holocene reflection (H10) also appears to be locally disrupted by the Oceano fault zone (Figures 7-10 and 7-11). The Channel E thalweg and margins are sinuous (meandering) where the channel crosses the Oceano fault zone, and they are deflected approximately 80 ± 20 m, but no measurable lateral offsets of the piercing points (thalweg and margins) are observed. However, the Channel E thalweg exhibits approximately 2 m of vertical separation across the Oceano fault zone, with a range of 0–4 m. Channels K and L are confined to the eastern structural block and thus do not provide piercing points.

8.2.2.3   Age Constraints and Slip Rates

In the simple calculation of the slip rates for the Shoreline and Oceano fault zones, the estimated amount of fault offset is divided by the estimated age of the piercing point. Both of these parameters include inherent uncertainties, which are described in Section 7.2.1.5. Uncertainty in both of these parameters is represented by the limiting minimum and maximum constraints. The lack of good geochronologic control on age constraints is the greatest source of uncertainty. Where the Shoreline and Oceano fault zones bifurcate to the west of Souza Rock, at the location of Channel Complex A, they exhibit clear evidence of Quaternary activity (Plates 1B, 4, and 5). Vertical separation of the bedrock surface is observed on both the Shoreline and Oceano fault zones in areas that lie below the limit of onlap of the Upper Pleistocene deposits onto the top of bedrock (Figures 7-6 and 7-12; Plates 5 through 7). The Upper Pleistocene deposits are offset by these faults, both inside and outside mapped paleochannels (Figures 7-1, 7-5, 7-6, 7-11, and 7-13). Several minor unnamed faults between these two major fault strands form fault-line scarps and appear to offset the top of bedrock below the limit of onlap of the Upper Pleistocene deposits (Figure 7-10; Plates 5 and 7). The buried paleostrandlines mapped in this study are incised into inferred Upper Pleistocene deposits that overlie the mapped bedrock surface (Figures 7-25 and 7-26). The preferred geologic model for the formation of the strandlines is that they developed during a period of relatively stable, glacially lowered sea levels, and were subsequently preserved by slowly aggrading estuarine and/or deltaic sedimentation on a coastal floodplain landward of a coastal dune complex sometime during a late Quaternary intermediate sea-level stand (e.g., MIS 4, 6e, or 8c).

An age model for the paleostrandlines, presented on Figure 7-44, is based on the preferred ages for stratigraphic reflections mapped as horizons H30 and H40 (PG&E, 2013) and the observed stratigraphic relationships between these horizons and the depths of the mapped paleostrandlines (Figures 7-27 and 7-28). Reflected in the age model is an assumption that little tectonic uplift has occurred in central San Luis Obispo Bay since the paleostrandlines formed during the late Quaternary. The best evidence for estimating the age of the shorelines is exhibited on Figure 7-27, where unconformity H40 (~250–

240 ka) appears to be stratigraphically lower than the paleostrandlines. The H40 horizon laps onto the bedrock surface southwest of the paleostrandlines, at a depth of approximately 120 m, whereas unconformity H30 (~135–125 ka) lies stratigraphically higher than the paleostrandlines and is thus considered younger than the strandlines. Therefore, the paleostrandlines are interpreted to have incised into Upper Pleistocene deposits (Figure 7-1) sometime between 185 ka and 155 ka (MIS 6c through 6e), when sea levels stabilized for several tens of thousands of years at depths between 75 m and 92 m below modern sea level (Figures 7-28 and 7-44). Given this age model, a preferred slip rate of 0.06 mm/yr is estimated using a preferred offset of 10 m (see Table 7-12 for a full analysis). In consideration of the other potential ages for the formation of the paleoshorelines, a minimum preferred slip rate would be 0.01 mm/yr for MIS 14 (~550 ka with a minimum offset of 3.4 m) and a maximum preferred slip rate of 0.51 mm/yr for MIS 2 (~70–28 ka, with a maximum offset of 15.2 m).Estimating the age of initial channel incision is based on a subjective examination of the sea-level curves and selecting the points on the curves when sea level was low enough to allow fluvial erosion of the bedrock (Figure 1-8). It is commonly assumed that most shallow pre-Holocene channels preserved on continental shelves worldwide, when buried by only Holocene-age marine deposits, were incised during the LGM (MIS 2). However, this assumption may not be applicable to the study area, as some of the channels in the San Luis Obispo Bay data set crosscut other channels and are often incised into bedrock well below the depth of the older channel thalwegs at the same location (Plate 5).

Age models for the paleochannels identified in the San Luis Obispo Bay 3D survey area are presented on Figure 7-45. The channels are bracketed stratigraphically by two key unconformities that extend across most of the survey area. The lower unconformity is the bedrock surface (Figures 7-7; Plate 5), and the upper unconformity is H10. The H10 horizon is located at the base of the Holocene, which is interpreted to represent the pre-Holocene transgressive surface (PG&E, 2013) formed during the sea-level rise from MIS 2 to MIS 1 (~19–7 ka, respectively; Figures 1-8 and 7-46). The age of the bedrock surface is poorly constrained, as it has been subject to erosion during repeated sea-level transgressions and regressions throughout the late Quaternary.

Using the crosscutting relationships and bifurcation of the paleochannels, varying ages of initial channel incision and reoccupation of the channels are estimated, although channel crossovers and avulsion can occur within a single sea-level lowstand. Therefore, the relative ages of initial channel incision (Figure 7-23; Plates 5 and 6) are inferred based on channel depths, incisions as shown in the bedrock surface contour map, and geomorphic relationships at channel crossings. Crosscutting relationships of the upper (youngest) channel fill deposits in each channel and their stratigraphic position and relationship to inferred Holocene marine and upper Quaternary non-marine shelf deposits were also evaluated and used in developing paleochannel age models (see Section 7.2.1.5).

Channels A, G, and H are considered the oldest preserved bedrock channels mapped in the San Luis Obispo Bay 3D survey area (see Section 7.1.1.3 and Plate 5). Channel A is incised and cut by Channels B and C, and Channels G and H are incised by Channels F and I. Channels G and H do not cross the Shoreline or Oceano faults, however, so they do not provide piercing points and are not included in the age model.

The age of initial incision of Channel A is poorly constrained. However, given the observed bedrock channel morphology, piercing point offsets, incised channel fill deposits, and nested younger channel west of Souza Rock (Figures 7-33 and 7-35), Channel A is likely significantly older than MIS 2, and likely older than MIS 6. Sea-level curve metrics and stratigraphic control provided by the observed relationship between the Channel A fill and Upper Pleistocene deposits provide additional constraints on the channel's age.

Channels A, F, and I extend south of the onlap edge of the Upper Pleistocene deposits, and thus appear to have been initially incised prior to deposition of these sediments in the late Pleistocene, when the southernmost, deeper parts of these channels were buried (Plate 5). There is clear evidence that some channels have been repeatedly reoccupied (see Section 7.1.1.3). Channel I is incised into the Upper Pleistocene deposits at the Shoreline fault piercing point, and the channel fill deposits are overlain by Holocene sediments, demonstrating that the channel was reoccupied during MIS 2 (Figure 7-38d, e, and f). The timing of initial incision of Channel F into the bedrock surface is unclear based on the 3D data set, but given the depth of this channel and its inferred stratigraphic position where unconformity H40 laps onto the bedrock surface to the southwest of the study area at approximately 120 m (Figure 7-46), it may be coeval with the formation of horizon H40 (MIS 8b).

A shallow channel incised into bedrock approximately 35 m below horizon H40 (~155 m) on USGS Line PBS-319 to the southwest of the 3D survey area (Figure 7-46) may represent Channel I. This location is 5 km south of the 3D survey area, and the uncertainty in this age is large. The preferred age model for Channel I is that it was initially incised during MIS 10 (~345 ka), when sea level was at approximately 125 m (Figures 1-8 and 7-45). Given the elevation of inferred Channels F and I on USGS Line PBS-319, this would imply that this part of San Luis Obispo Bay has undergone net subsidence in the last several hundred thousand years.

Initial incision of Channels C, D, E, and J is interpreted to have occurred more recently than Channels A, B, F, and I. Channels K and L appear to be locally sourced (no known river or creek input) and are interpreted to have been initially incised into the exposed shelf during MIS 3 or 4, prior to deposition of the uppermost Pleistocene sediments (Plate 5). During this period (MIS 3 and 4), sea levels varied between –50 m and –80 m, and the shoreline was near or adjacent to the Oceano fault zone scarp at the location of Channels K and L. Differential uplift across the Oceano fault led to greater channel incision into the hanging wall (eastern structural block) relative to the footwall (Central block), creating a fault-line scarp that may have coincided with the shoreline during MIS 3 (Figures 7-41 and 7-45). This explains why Channels K and L, as fluvial channels, are only incised into the eastern structural block bedrock to the north of the Oceano fault zone, and why they are not present on the bedrock of the central structural block.

To summarize, the ages of the paleochannels in San Luis Obispo Bay (Figures 7-7 and 7-45; Plate 5) are estimated as follows:

- Channels C, D, and E were incised during MIS 2 (~20–10 ka).
- Channels K and L were incised during MIS 3 and 4 (~70–40 ka).

- Channels B and J originated during stage 6b and 6c (~160–140 ka).
- Channel F originally formed during MIS 8b and 8c (~275–245 ka).
- Channel A may have originated during sea-level lowstands recorded during MIS 8b/8c, 10, or 12.
- Channel I may have been incised during MIS 10 (~350–340 ka).

As previously noted, Channels A, B, F, and I appear to have been reoccupied during subsequent sea-level lowstands. While it is considered unlikely that any of the channels are older than MIS 16, the upper-bound maximum age of the initial incision of all the channels is conservatively placed at approximately 1.4 Ma, at the beginning of the MPT transition (Figure 6-2).

The highest preferred age model for Channel A, based on the eustatic sea-level curve metrics, is MIS 12, the sea-level lowstand that stabilized approximately 450–430 ka. During this lowstand, sea level fell below −80 m elevation for approximately 45,000 years (470–425 ka, as shown on Figure 1-6), which is the longest duration of any lowstand since the end of the MPT (Figure 6-2). Sea levels only below the −80 m elevation for approximately 20 kyr during MIS 10, and for 30 kyr during MIS 8. The elevation of sea level during MIS 12 was also lower than during MIS 10 and 8b (Figures 6-2 and 7-45).

The lowest preferred age model for Channel A (Figure 7-45), based on the eustatic sea-level curves and on the estimated age of unconformities outside the 3D survey area, such as horizons H30 and H40 (PG&E, 2013), is MIS 8b and 8c, the sea-level lowstand that stabilized between approximately 275 and 245 ka. The alternate age model is weakly supported from interpretations of USGS seismic-reflection profiles PBS-09 and PBS-319 (Figure 7-46), which show a possible channel incised into bedrock to a depth of approximately 110–120 m, where it lies below the H30 horizon and at about the same depth as the H40 horizon. On PBS-319, the channel is shallow (~3 m) and is approximately 100–150 m wide, likely due to being close to base level on a relatively flat coastal floodplain. Based the location of this channel in relation to the 3D survey area, however, it is more likely to be the seaward extension of Channel F. Channel A appears not to be imaged on USGS seismic-reflection Profile PBS-319 (Figure 7-46), and may have been destroyed by erosive coastal processes during MIS 10, 8b/c, and/or 6b/c. Thus, within the extents of 3D survey area (Figure 7-7), the highest preferred age model is for Channel A to have initially incised into the bedrock surface during the extended MIS 12 sea-level lowstand, during an extended period of time when sea levels were within a depth range between approximately 80 and 130 m below modern sea level (Figure 7-46).

Using the highest preferred age of approximately 430 ka (MIS 12) and the preferred Channel A thalweg piercing point offset of approximately 30 m, an estimated slip rate of approximately 0.07 mm/yr (within range of 0.02–0.12 mm/yr) is calculated for the Shoreline fault zone using Channel A. Using the lower preferred age of approximately 250 ka (MIS 8b/8c) and the preferred Channel A thalweg piercing point offset of approximately 30 m, the estimated slip rate is approximately 0.12 mm/yr (within range of 0.04–0.20 mm/yr). Considering the other potential ages (135 ka of MIS 6b, and 1.4 Ma of MIS 45) for Channel A incision, a minimum estimated slip rate of 0.01 mm/yr (using 1.4

Ma at 10 m minimum offset) and a maximum estimated slip rate of 0.37 mm/yr (using 135 ka at 50 m maximum offset) is calculated for the fault zone.

With the exception of Channel A, no other channel is distinctly offset by the Shoreline fault. Channels F and I were considered for slip-rate analysis of the Shoreline fault, as the thalweg width for both channels is estimated to be approximately 6 m; thus, while a maximum offset of 6 m could have occurred, it is not clearly detected in the 3D imagery (Figures 7-37 and 7-38) because of geological uncertainty and instrument resolution. The preferred offset is 1 m, which would indicate a slip rate of 0.05 mm/yr along the Shoreline fault zone at the locations of the Channel F and I piercing points. Using a maximum offset of 6 m and the preferred age of 20 ka for reoccupation of Channels F and I results in a maximum slip rate of 0.30 mm/yr. The minimum slip rate on the Shoreline fault for Channels F and I is 0 mm/yr over the past 20,000 years (see Table 7-20).

The overall slip rate on the Shoreline fault zone as calculated using both the paleoshorelines and paleochannels is estimated to range from approximately 0.06 mm/yr (with an uncertainty of 0.01–0.51 mm/yr) based on offset of the paleoshorelines to approximately 0.07 to 0.12 mm/yr (with an uncertainty of 0.01–0.37 mm/yr) based on offset of paleochannel Ae/Ac and 0.0.5 mm/yr (with an uncertainty of 0.0–0.30 mm/yr) for Channels F and I. The most reasonable analysis and highest confidence level comes from the paleostrandline piercing points.

8.3   Comparison with Published Slip Rates

The results of this 3D LESS investigation have yielded estimated slip rates of the HFZ and the Shoreline and Oceano fault zones, which have been compared to previously estimated slip rates. Figures 8-1, 8-2, and 8-3 summarize the horizontal slip rates determined for these fault zones in the San Luis Obispo Bay study area and described in this report. Cumulative offsets are plotted with respect to the age of the offset. For each piercing point, the range of offset and age is shown as rectangles, with the preferred value shown as a filled circle. Reference rates of 1 cm/yr and 1 mm/yr, 0.1 mm/yr, and 0.01 mm/yr are shown as diagonal lines.

8.3.1   The Hosgri Fault Zone

The preferred slip rates estimated for each of the two HFZ study sites are nearly equivalent (1.6 mm/yr in the Estero Bay study area and 1.8 mm/yr in the Point Sal study area), suggesting relatively uniform slip rates along this portion of the HFZ in the late Quaternary. This is not consistent with recent models that suggest a northward increase in slip along the HFZ (Johnson and Watt; 2012; Langenheim et al., 2013).

As seen on Figure 8-1, the offset ages used for HFZ slip-rate estimates cluster in three distinct age ranges: 10 ka, 0.2–4 Ma, and 11–18 Ma. In the first age cluster, recent offsets (~10 ka), measured onshore at San Simeon (Hall et al., 1994; Hanson et al., 2004) and offshore north of Estero Bay along an eastern splay of the HFZ (Johnson et al., 2013), yield slip rates of 2.6 ± 0.9 mm/yr.

Older offset deposits used in the second age cluster (4–0.2 Ma) indicate similar slip rates. Sediments sampled at San Simeon date between 500 ka and 200 ka and yield rates of 0.7–2.6 mm/yr (Hanson and Lettis, 1994). To the south, near Point Sal, Sorlien et al. (1999) estimated an average post-Miocene slip rate of approximately 2 mm/yr, based on a total displacement of 10.5 km, including 7 km of dextral shear from the clockwise rotation of tectonic blocks east of the HFZ and 3.5 km of fault slip measured from restored structural contour maps of deformed Pliocene (mid–Sisquoc Formation) horizons south of Point Sal. Within the limits of resolution, the data on Figure 8-1 indicate that the slip rate on the HFZ during the last 4 Myr has been relatively constant (2 ± 1 mm/y).

The third cluster of ages (~18–11 Ma) on Figure 8-1 represents cumulative slip rates associated with older piercing points as defined by estimated offsets of the Point Sal/San Simeon and Point Buchon/Point Sur ophiolite pairs (Hall, 1975; Dickinson et al., 2005; Langenheim et al., 2013), as well as offsets correlative with the early Miocene Lospe Formation conglomerates exposed at Point Sal and San Simeon (Hall, 1975; Graham and Dickinson, 1978a; Johnson and Stanley, 1994). These older offsets indicate substantially faster average slip rates (8–11 mm/yr) along the HFZ for the past 11–12 Myr (Clark, 1998; Dickinson et al., 2005; Langenheim et al., 2013).

When compared with the younger (<4 Ma) offsets on Figure 8-1, these data indicate a decrease in overall HFZ slip rate during the last 12 Myr. The period between approximately 12 Ma and 4 Ma was coincident with most of the more than 90-degree clockwise rotation of the Transverse Ranges (beginning in early Miocene, ~20 Ma; Hornafius et al., 1986; Nicholson et al., 1994), regional transpression (beginning ~5 Ma; Atwater and Stock, 1988; Clark et al., 1991), and the eastward jump of the East Pacific spreading center into the Gulf of California.

A second phase of northeast-southwest crustal shortening related to an abrupt 11-degree clockwise rotation of the direction of Pacific Plate motion occurred in Central California between approximately 3.9 Ma and 3.4 Ma (Cox and Engebretson, 1985; Harbert and Cox, 1989). Strong transpression and associated uplift of the Santa Maria Basin, possibly as a consequence of this tectonic event, resulted in erosion and development of the basin-wide ELP unconformity, as well as northwest-southeast-trending folds and faults (Hanson et al., 2004; Willingham et al., 2013). Large-scale structural inversion of Miocene normal faults as transpressional oblique reverse faults may have also occurred during this period. Block rotation rates and slip rates on the HFZ (and likely other faults in the Los Osos domain and western Transverse Ranges) appear to have decreased considerably over the past several million years (Langenheim et al., 2013), although the predominant tectonic regime continues to be transpressional in nature.

8.3.2　The Shoreline and Oceano Fault Zones

The estimated range of slip rates for the combined Shoreline and Oceano fault zones northwest of Souza Rock from the Channel A piercing point in this study is 0.01–0.37 mm/yr, with a preferred slip rate of 0.7 to 0.12 mm/yr (Figure 8-2). This compares with an estimated range of slip rates of 0.05 to 1.0 mm/yr in the Shoreline Fault Zone Report

(PG&E, 2011b). The estimated slip rate for the Shoreline fault zone south of Souza Rock, exclusive of any slip that may be transferred onto the Oceano fault, is lower. Based on offset paleostrandlines located in the southern part of the 3D survey area, the preferred dextral slip rate for the Shoreline fault zone is 0.06 mm/yr, with a range of 0.01–0.51 mm/yr.

The estimated preferred vertical slip rate on the Shoreline fault zone based on observed 0.8–1.6 m vertical separation of the paleoshoreline is 0.01 mm/yr (see Section 8.2.4; Figure 6-28b). This vertical slip rate is significantly less than a published vertical slip rate of up to 0.33 mm/yr for the South Pecho fault near the Shoreline fault zone paleostrandline piercing point (Figures 7-15 and 7-29), which was based on up to 6 m vertical separation of a the MIS 2 (late Wisconsinan) unconformity with an estimated age of 18 ka (Lettis et al., 1994). The estimated preferred vertical slip rate on the Oceano fault zone based on estimated 1 to 3 m vertical separation of paleochannels that cross the Oceano fault line scarp is 0.01 to 0.1 mm/yr (see Section 7.1.2.6; Figure 8-3).

Onshore, the apparent vertical separation of the Franciscan Complex by the Oceano fault is 122–183 m (PG&E, 1988). Oil well data near the coast show vertical separation by the Oceano fault of the Top Foxen Formation at between 77 m and 126 m (PG&E, 1988). Lettis et al. (1994) state that the Oceano fault clearly displaces Tertiary strata and estimate vertical slip rates of 0.04 to 0.20 mm/yr for the Oceano fault beneath Nipomo Mesa, and 0.01 to 0.04 mm/yr at the coast.

The results of this study indicate that the Oceano fault zone has a preferred reverse slip rate of approximately 0.1 mm/yr, within a range of estimated slip rates of 0.0–0.25 mm/yr. Consequently, the estimated slip rate for the Oceano fault determined by this study (0–0.1 mm/yr) falls within the published slip-rate estimates of 0.01–0.20 mm/yr for the Oceano fault (Lettis et al., 1994), and is comparable to the estimated slip rate of the Shoreline fault southeast of Souza Rock.

9.0   CONCLUSIONS

The two main objectives of the 3D LESS were to (1) identify the southern extension, geometry, and connectivity of the Shoreline fault zone, and (2) determine slip rates for the Shoreline fault zone and the HFZ, both of which were successfully achieved. In addition, buried paleochannels, newly discovered faults, and other structures were well imaged, providing insight into the tectonic complexity, kinematics, and rheology of the region. This investigation, while limited to three small distinct, disparate study areas, represents the most detailed and focused geophysical surveys undertaken in the region to date and provides data that can be used to focus on the connectivity of structures both offshore and onshore.

Excellent-quality 2D and 3D marine geophysical data were collected using a state-of-the-art high-resolution 3D LESS system that included a P-Cable with 14 hydrophone streamers and a triple-plate boomer acoustic source. The data were collected by Fugro Consultants, Inc., of Ventura, California, and processed by Fugro Seismic Imaging, Inc., and CGG Veritas of Houston, Texas. A popular, sophisticated 3D processing software system, IHS Kingdom, produced detailed 3D volumes that were used to interpret the data and construct selected cross sections, time slices, and attributes. The Kingdom RSA software module was used to calculate geometric (multi-trace) seismic attributes (i.e., similarity and smoothed dip of maximum similarity), which were invaluable in detecting and enhancing fault splays and paleochannel margins. Interpretation and mapping were also aided by the use of seismic-reflection profiles from previous 2D seismic-reflection surveys and potential field (i.e., magnetic anomaly) data to identify deeper structures in the survey areas (Figure 2-1).

The high-resolution 3D data acquired in this study significantly improved the ability to recognize and map geologic structures (e.g., faults and folds) and geomorphology (e.g., channels and shorelines) within the uppermost approximately 40–240 m (~50–300 ms) stratigraphic section of the study areas. Lower-resolution, deeper-penetration PG&E legacy archive data were also used in this study, along with the recently collected (2009–2010) USGS low-energy single-channel seismic-reflection profile data. Several additional faults, and new details of fault geometry, relationships to folding, and interconnectivity of faults are now recognized relative to previous mapping in these areas. The improved data density and resolution reveal details of the bedrock surface that improve the understanding of style and location of fault deformation, as well as details of the locations and geometry of channels incised into the continental shelf and slope.

Piercing points identified for constraining offsets along the Shoreline, Oceano, and Hosgri faulft zones were identified with the high-resolution 3D seismic images; buried paleochannels and paleoshorelines (paleostrandlines) were the best geomorphic features to use in evaluating offsets. The accuracy of offset and age estimates needed to determine slip rates was found to be dependent on the quality of the spatial and temporal (stratigraphic age) data, as well as dependent on the level of confidence in the interpretations (geologic confidence). Generally, the quality of the spatial data is good and the range of confidence levels of interpretation is from high to low, with those piercing points used for offset estimates having a medium to high confidence level. Ages

used in estimating temporal aspects of piercing point offsets are based on the evaluation of current global paleo–sea-level curves, offshore well data, and sequence stratigraphy.

The following sections discuss the study's conclusions resulting from the interpretation of the LESS data of each survey area for determining slip rates on the HFZ and the Shoreline fault zone and for delineating the southern extension of the Shoreline fault zone. Also, the slip rates estimated for the HFZ and the Shoreline, Pecho, and Oceano fault zones are compared with previously reported and published slip rates.

9.1   The Hosgri Fault Zone

The 3D LESS that focused on the HFZ was undertaken along selected parts of the fault zone in areas offshore of Estero Bay and Point Sal. These studies reveal a more complex fault zone than had previously been mapped, including providing evidence of offset piercing points.

9.1.1   The Estero Bay Study Area

In the Estero Bay study area (Survey Area 1), located just south of the intersection of the Los Osos fault zone with the HFZ (Figure 1-1; Plate 2), the 3D LESS imagery exhibits details and complexities of the fault zone's geometry (Figure 6-3) not seen before. The interpretation of the bedrock surface (Figure 6-5) resulted in the mapping of previously unknown patterns of uplift and subsidence at the top of bedrock.

The HFZ in the Estero Bay study area consists of two primary subparallel fault strands, faults labeled 10001 and 10006 on Figure 6-8b, with minor secondary strands to the northeast and southwest within the survey area. Where well imaged, the strands of the HFZ are generally steeply dipping to vertical, consistent with previous characterizations of the HFZ as a dominantly right-lateral strike-slip fault zone (e.g., Hanson et al., 2004; Johnson and Watt, 2012; Willingham et al., 2013). The sense of vertical separation across the HFZ in the study area is dominantly down to the west, as indicated by the presence of the broad, beveled bedrock surface to the east and a relatively thick sedimentary section to the west (Figure 6-4). Faults within the HFZ have produced slivers of structural blocks that are are called here the Eastern, Central, and Western blocks.

9.1.1.1   Channel Correlations

Paleochannels are imaged on both sides of the HFZ within the Estero Bay study area. Alternative channel correlations were tested by restoring offset on the HFZ to match potential offset equivalent channels across the zone. A preferred correlation (Alternative A) is selected because it matches each of the three well-imaged channels west of the HFZ with candidate equivalent channels east of the HFZ (Figure 7-3). Other alternatives are rejected because either they provide poor matches for other potential offset channels or they require left-lateral slip on the fault, which contradicts existing well-documented research on the fault (e.g., Hall et al., 1994; Lettis and Hanson, 1994; Hanson et al., 2004; Johnson and Watt, 2012), or both. An alternative working hypothesis is that there is no channel correlation across the HFZ; this cannot be ruled out because the image quality of the 2D seismic-reflection profiles is variable west of the western

primary strand of the HFZ, to the west of the 3D survey area, and because these profiles are the only image data available of the channels west of the HFZ.

The preferred channel correlation matches offset channels across the two primary strands of the HFZ, faults 10001 and 11006. This correlation matches Channel De (east of the HFZ) with Channel Ee (between strands of the HFZ) with Channel DBw (west of the HFZ). Fault offset is measured by projecting channel thalwegs to strands of the HFZ from each side. Uncertainties in offset measurements are estimated based on the range of reasonable thalweg projections. The fault offset measurements and uncertainties are as follows:

- A right-lateral offset of 260 ± 60 m and a vertical separation of 40 ± 8 m, down to the west, across fault 11006, the eastern primary strand of the HFZ.
- A best estimate of right-lateral offset between approximately 700 and 1,000 m, with uncertainty ranging from 450 m to 1,650 m and a vertical separation of 100 ± 25 m, down to the west, across fault 10001, the western primary strand of the HFZ.

The total dextral offset across both strands of the fault is 1,230 +450/–390 (within a high [90%] confidence level). Total vertical separation is estimated as 140 ± 30 m, down to the west.

9.1.1.2 Slip Rates

Channel offsets and their interpreted ages yield a preferred lateral slip rate for the HFZ in Estero Bay of approximately 1.6 ± 0.8 mm/yr within a high (90%) confidence interval. Accounting for uncertainties in ages and offset estimates, the range in lateral slip rate is between approximately 0.2 mm/yr and 3.6 mm/yr.

9.1.2 The Point Sal Study Area

The Point Sal study area (Survey Area 3) is located approximately 45 km south of the Estero Bay study area (Figure 1-1) and here, like to the north in Estero Bay, the HFZ is found to be more complex than previously mapped. Three major strands of the fault zone and many secondary fault strands are identified within a 7 km long, approximately 1 km wide paired bend in the HFZ. The eastern and western primary fault strands bound a central structural block, which is cut by a primary central fault strand and numerous other faults (Figure 6-28). The major central and eastern strands are curved, forming a restraining bend (a change in fault trend of ~10°) and a releasing bend (a change in fault trend of ~20°), with the western strand forming a paired-bend bypass fault (Figure 6-27).

The new mapping resulting from this study shows that from south to north, the HFZ splits from a single strand with little or no vertical separation to multiple splays with substantial vertical and dextral shear, which converge to form a single strand once more. The three primary strands are located in the central part of the 3D survey area, with transtension displayed in the south and transpression displayed in the north. There is an approximate 6-degree change in the strike of the HFZ from approximately 336 degrees in the south to approximately 330 degrees in the north (Figure 6-27). To the north of the 3D survey area,

the HFZ extends north-northwest across San Luis Obispo Bay with an average trend of 340 degrees (Johnson and Watt, 2012), approximately 10 degrees more northerly than the strike of the fault in the northern part of the 3D study area (Plate 1B). Other faults interpreted from the 3D data set indicate that the northwest-trending Lions Head fault and other faults converge with the HFZ in the north of the 3D study area. North/northeast–south/southwest shortening appears to be exhibited with an inferred buried fault, the "Blind Thrust fault NE" (Figure 6-29), within the Casmalia/Point Sal block and southwest of the location of the 29 May 1980 Point Sal 5.1 M_w earthquake (Figure 9-1). The 1980 Point Sal event and a 1984 M_w 3.8 aftershock are located near the surface trace of the Casmalia fault, southeast of the intersection of the Casmalia fault and the HFZ. Focal mechanisms for both events show a nearly pure reverse fault, northwest-striking planes on a steeply (55°–80°) southwest-dipping fault (Eaton, 1984; McLaren and Savage, 1987; Hanson et al., 2004). Active northeast-southwest-directed shortening within the Los Osos domain east of the HFZ as shown here (Figures 6-29, 6-34, and 7-20; Plate 1B) has been documented by other studies (Sorlien et al., 1999; Lettis et al., 2004; Willingham et al., 2013).

9.1.2.1　Channel Correlations

Seven buried paleochannels (Channels A through G) were identified in the 3D volume and 2D seismic-reflection profiles in the Point Sal study area. The channels occur above the ELP/NTN unconformity, which was mapped across the entire survey area using 3D LESS data and deep-penetration, high-energy 2D PG&E legacy archive data correlated with key Neogene stratigraphic horizons in nearby offshore oil wells (Figure 6-18). The paleochannels are located on the middle and outer continental shelf and consist of single channels, as well as channel complexes of multiple nested channels incised into lower (older) channel fill. Many of the channels exhibit a stratigraphy characteristic of a submarine origin (see Figure 1-9).

Channels B and F exhibit significant separation across one or more of the primary strands of the HFZ (Figures 6-36 and 6-51a and b). However, Channel Complex F exhibits relatively linear thalweg geometry in the 3D survey area; it is the only channel or channel complex that crosses all the primary faults and structural blocks of the HFZ, and thus it is used in the HFZ slip-rate estimates. The preferred Channel F correlation is selected because the buried channel geometry and relationship with the ELP/NTN unconformity and bedrock structure matches the well-imaged channels east and west of the HFZ (Figure 6-51a and b).

9.1.2.2　Slip Rates

Channel Complex F (Channels Fe3, Fc1, and Fw3) provides the preferred piercing points for estimating slip rates on the HFZ in the Point Sal area. Using the preferred age of approximately 342 ka (MIS 10) and the preferred Channel F thalweg piercing point offset of approximately 600–650 m, an estimated slip rate of approximately 1.75–1.90 mm/yr is calculated for the HFZ. The preferred rate based on Channel F piercing points, as well as the combined rates for the western and eastern strands of the fault from Channel A and B piercing points, is 1.8 mm/yr. Considering the two other potential ages (138 ka of MIS 6b

and 1.4 Ma) for Channel F incision, a minimum estimated slip rate of 0.39 mm/yr (1.4 Ma at 550 m minimum offset) and a maximum estimated slip rate of 5.07 mm/yr (138 ka at 700 m maximum offset) is calculated for the HFZ at Point Sal.

9.2   The Shoreline Fault Zone

The southern extension of the Shoreline fault zone was investigated thoroughly, with 3D attributes and other images clearly defining this fault zone and other faults. Many buried paleochannels and a set of paleoshorelines (paleostrandlines) cross the Shoreline fault zone, and all were considered potential piercing points to constrain offsets along the fault zone. The potential ages of the piercing points were estimated based on sea-level curves, and their relationships to sequence-stratigraphic horizons.

9.2.1   The San Luis Obispo Bay Study Area

In the San Luis Obispo Bay study area (Survey Area 2) the 3D LESS imagery reveals new details and complexities of fault geometry and convergences (Figure 7-3). Here, because faults of the Shoreline fault zone are strike slip in motion, cleanly cut strata with little or no deformation, and are fairly linear, identification in the seismic-reflection profiles is difficult to impossible. However, time slices constructed from the 3D volume imaged these faults in great detail and provided the ability to confidently map the faults.

In the northwestern and central area of the 3D study area, several faults converge near the location of Souza Rock (Figure 7-7). The Shoreline fault zone is mapped as a straight, throughgoing structure, extending southeastward through the survey area. The fault zone bifurcates at Souza Rock, where a northern strand, the Oceano fault trends toward the east, while the Shoreline fault continues in a more southerly direction with a southeasterly strike. The Los Berros fault intersects the Shoreline fault zone near the northern boundary of the 3D survey area (Plate 4). The 10 August 2000 M_L 3.5 earthquake epicenter is shown to be located immediately north of these converging faults' intersection (Hardebeck, 2010). A dextral strike-slip focal mechanism with a nodal plane parallel to the Shoreline fault zone (see Figure 7-43), in combination with offset paleostrandlines revealed by this study, shows it to be an active right-lateral fault zone.

In the southeastern part of the 3D survey area, the Oceano fault zone is expressed on the bedrock surface as a fault-line scarp (Figures 7-3, 7-6, 7-7, and 7-41b; Plate 7). Just north of Souza Rock, the western terminus of the Los Berros fault appears to be truncated by or bifurcates from the Shoreline fault zone. A general east-west-trending inferred fault, here called the North Pecho fault, intersects the Shoreline fault zone in the central part of the survey area, and a more westerly inferred strand, called the Pecho fault, appears to bifurcate from the North Pecho fault strand near the northwest corner of the survey area, extending a short distance to the southeast (Figure 7-15b). A well-defined east-west-trending unnamed fault intersects the Shoreline fault zone in the central part of the survey area, just south of where the North Pecho fault terminates at the Shoreline fault zone (Plate 4).

Outside the 3D San Luis Obispo Bay survey area, interpretations of 2D seismic-reflection profiles suggest that the offshore Oceano fault zone aligns with the Santa Maria River

and Oceano fault zones onshore (Plate 1B; Figures 7-15 and 9-1). The total length of the Oceano fault from Souza Rock to the shoreline is 10.7 km.

The Shoreline fault zone is extended 13.7 km from the southeast edge of the 3D survey area southeast to near the mouth of the Santa Maria River (Figure 7-21a), where it connects with a 3 km long fault mapped in the Guadalupe Oil Field onshore (CDOGGR, 1992). This distance added to the 5.3 km length of the fault zone imaged in the 3D volume extends the newly mapped part of the Shoreline fault zone by 22 km. Assuming that the Point Buchon fault zone is part of the Shoreline fault zone (PG&E, 2012), then the fault zone length north of the San Luis Obispo Bay 3D survey area is approximately 23 km, making the entire Shoreline fault zone approximately 45 km long.

9.2.1.1   Strandlines and Channel Piercing Points

A significant conclusion from the evaluation of the standlines and channel piercing points within San Luis Obispo Bay is that no evidence of recent fault ruptures within the last 10 to 15 ka was identified. Fault rupture along the Shoreline, Oceano and other fault zones mapped appear to have occurred before MIS 2.

Two paleoshorelines (paleostrandlines), the 84 and 92 m deep strandlines, exhibit equal lateral and vertical separation across the Shoreline fault zone. Vertical separation is estimated to be approximately 0.8 to 1.6 m, and dextral offset is 9.4 ± 6 m, with a preferred value of 10 m (Figure 7-29). The ratio of vertical to horizonal slip is approximately 10 to 1, and the preferred vertical slip-rate value is 0.006 mm/yr. Given the clear geomorphologic expression of the paleostrandlines that erode reflections of Upper Pleistocene age and the unambiguous, distinct measurable dextral and vertical separations across the fault zone, offset estimates of the mapped paleostrandline piercing points are considered of the highest confidence level (see Section 3.6; Figures 7-22 to 7-29).

Of the 12 buried paleochannels (Channels A through L on Figures 7-2, 7-7, 7-22, 7-31, and 7-32) incised into the bedrock within the San Luis Obispo Bay study area (Figure 7-22; Plates 5 and 6), the thalwegs and margins of three (Channel Complex A and Channels Fw and Iw) are considered the most promising for piercing points to use in determining fault offsets and slip rates. All channels imaged lie on the inner shelf area of San Luis Obispo Bay (Plate 4) and range in geomorphology from fairly narrow, straight, and V-shaped (primarily, thread channels) to broad, meandering, and U-shaped (braided channels); all appear to be of fluvial origin. The channels are interpreted to have formed at glacially induced sea-level lowstands during the late Quaternary, and were likely sourced from ancestral San Luis Obispo Creek and Pismo Creek, and locally, from drainages on the then exposed continental shelf in San Luis Obispo Bay (Figure 7-30). Thread channels are primarily restricted to the eastern structural block of the study area, east of the Shoreline and Oceano fault zones (Plate 4). Braided channels are primarily concentrated on the eastern and central structural blocks, with their proximal parts related to knickpoints associated with vertical offsets and uplift in the hanging walls of the Oceano and Los Berros fault zones (Figures 7-10, 7-17, 7-18, and 7-20; Plate 5). This change in channel geomorphology occurs at the basement traces of the Oceano and Los

Berros fault zones, suggesting fault control of the fluvial styles and channel formation. These channels are interpreted to be of different ages, with some channels cutting across and eroded into other channels (Figures 6-32 and 6-35b).

Most of these channels cross the mapped faults in the area but have little or no observed lateral separation (see Section 7.1.1.3). Channel A piercing points and channel fill, however, exhibit distinct evidence of fault offset. The Shoreline fault is interpreted to dextrally offset the shallow (~50 m below sea level) Channel Complex A's margins by 20 to 40 ± 10 m (Figure 7-35). The channel margin on the southeast side is disrupted, and apparent dextral offset on the Shoreline fault zone is greater than that observed on the northwest channel margin (Figures 7-33 and 7-35). The east channel margin also appears to be vertically offset by the Oceano fault zone (Figure 7-33b and c; Figures 7-34 and 7-35); vertical separation at this location is estimated as 3 ± 2 m. The Oceano fault zone style is reverse, north side up. Souza Rock is uplifted in the hanging wall of the Oceano fault zone at this location, which is near the point of bifurcation from the Shoreline fault zone.

Two other well-defined channels, Channels Fw and Iw, cross the Shoreline fault zone in the southern part of the 3D survey area (Figure 7-2; Plate 5). Channel Fw is very straight and its thalweg and margin piercing points appear not to be significantly offset by the fault zone. Channel Iw is more sinuous than Channel Fw but appears not to be offset significantly by the Shoreline fault zone. Although no offsets of either channel's piercing points are clearly observed in the 3D data, given the approximately 6 m horizontal and 2 m vertical resolution and the geological constraints of the canyon morphology, it is possible that approximately 6 m of offset has occurred since channel abandonment.

9.2.1.2   Slip Rates

The paleostrandlines located in the southern part of the 3D survey area have a preferred offset of 10 m since 160 ka, which yields a slip rate of 0.06 mm/yr (with a range of 0.01–0.51 mm/yr) for the Shoreline fault zone.

With the exception of Channel A, no other channel exhibits distinct lateral offsets of its piercing points. While a maximum offset of 6 m could have occurred, it is not detected in the 3D data because of geological uncertainty and instrument resolution. Channel F may have been initially incised during MIS 8b and 8c, or possibly as recently as MIS 6b. Initial incision of Channel I appear older, possibly forming as early as MIS 10. Parts of Channels F and I have been reoccupied since initial incision, during subsequent lowstands at MIS 8b, 6b, and/or 2. The preferred lateral offset for both channels is 1 m, which would indicate a slip rate of 0.05 mm/yr along the Shoreline fault zone at the location of the Channel F and I piercing points since channel abandonment. However, using a maximum offset of 6 m and the preferred age of 20 ka for Channel F and I reoccupation results in a maximum slip rate of 0.30 mm/yr (Tables 7-20 and 7-21).

The overall slip rate on the Shoreline fault zone is calculated using the piercing points of both the paleoshorelines and paleochannels. The slip rate estimates for the Shoreline fault range from approximately 0.06 mm/yr (preferred with a range of 0.01–0.51 mm/yr) on the paleoshorelines to 0.07 to 0.12 mm/yr (preferred with a range of 0.01–0.37 mm/yr)

for paleochannel Ae/Ac and 0.5 mm/yr (with an uncertainty of 0.0–0.30 mm/yr) for Channels F and I.. The most compelling analysis is based on those paleostrandline piercing points that cross the Shoreline fault.

The results of this study indicate that the Oceano fault zone has a preferred reverse slip rate of approximately 0.1 mm/yr, within a range of estimated slip rates of 0.0–0.25 mm/yr. Consequently, the estimated reverse slip rate for the Oceano fault determined by this study appears to be comparable to the estimated slip rate of the Shoreline fault to the southeast of where these two faults bifurcate near Souza Rock.

10.0 LIMITATIONS

Attachment 7.3 of the PG&E Geosciences' Department Procedure CF3.GE2, Quality Related Technical Reports, states that any technical report produced by, or for the Geosciences Department "Address any limitations on the use of results and conclusions" of such report. Therefore, in this section we address limitations of the results and conclusions made herein that may be used within other Geosciences reports.

Because the intent of, and the data used for this report is restricted to the shallow subsurface, the use of the results and conclusions presented in this report to characterize structure at depth, especially within the seismogenic zone is limited. Faults mapped in this study were not correlated with faults and microseismicity at depth, as the 3D seismic-reflection acoustics did not penetrate to depths that would have allowed for such a correlation.

Age estimates are based on the most recent global sea-level curves because biostratigraphic, radiometric, or radiocarbon ages were not available, and age uncertainties of applicable sea-level curves were considered in the development of the slip rate ranges.

11.0 IMPACT EVALUATION

Attachment 7.3 of the PG&E Geosciences' Department Procedure CF3.GE2 Quality Related Technical Reports, CF3.GE2 R1 ATTACHEMNT 7.3, states: "Provide an evaluation of the impact that the results/conclusions have on other Geosciences documents." For this report the impact to other Geosciences documents is unknown at this time.

12.0 REFERENCES

Adeogba, A.A., McHargue, T.R., and Graham, S.A., 2005. Transient fan architecture and depositional controls from near-surface 3-D seismic data, Niger Delta continental slope, *American Association of Petroleum Geologists Bulletin* **89**: 627–643.

Atwater, T., and Stock, J., 1988. Pacific–North American plate tectonics of the Neogene southwestern United States: An update: in Ernst, W.G., and Nelson, C.A. (editors), *Integrated Earth and Environmental Evolution of the Southwestern United States*, Bellwether Publishing, Columbia, Md., pp. 393-420.

Atwater, T.M., 1970. Implications of plate tectonics for the Cenozoic tectonic evolution of western North America, *Geological Society of America Bulletin* **81**: 3513–3536.

Ben-Avraham, Z., and Zoback, M.D., 1992. Transform-normal extension and asymmetric basins: An alternative to pull-apart models, *Geology* **20**: 423–426.

Berger, A., Li, X.S., and Loutre, M.F., 1999. Modelling northern hemisphere ice volume over the last 3 Ma, *Quaternary Science Reviews* **18**: 1–11.

Bintanja, R., and van de Wal, R.S.W., 2008. North American ice-sheet dynamics and the onset of 100,000-year glacial cycles, *Nature* **454**: 869–872.

Boggs, S., Jr., 2005. *Principles of Sedimentology and Stratigraphy*, Fourth Edition, Prentice Hall.

Brown, A.R., 2004. Interpretation of three-dimensional seismic data, *American Association of Petroleum Geologists*, Memoir 42, 6th Edition, Tulsa, Okla., 541 pp.

California Department of Conservation, Division of Oil, Gas, and Geothermal Resources (CDOGGR), 1992. California Oil & Gas Fields, Volume II—Southern, Central Coastal, Offshore California Oil and Gas Fields, 645 pp.

(California) Department of Water Resources (DWR), 2002. Water Resources of the Arroyo Grande—Nipomo Mesa Area, Southern District Report, 157 pp. and 6 appendices; available at www.dpla.water.ca.gov/sd/water_quality/arroyo_grande/arroyo_grande-nipomo_mesa.html.

California Energy Commission, 2008. *An Assessment of California's Nuclear Power Plants: AB 1632 Report*, Commission Report CEC-100-2008-009-CMF, 42 pp.

Carlson, A.E., 2008. Why there was not a Younger Dryas-like event during the Penultimate Deglaciation, *Quaternary Science Reviews* **27**: 882–887.

Chiocci, F.L., and Normark, W.R., 1992. Effect of sea-level variation on upper-slope depositional processes offshore of Tiber delta, Tyrrhenian Sea, Italy, *Marine Geology* **104**: 109–122.

Clark, D.G., 1990. Late Quaternary tectonic deformation in the Casmalia Range, coastal south-central California: in Lettis, W.R., Hanson, K.L., Kelson, K.I., and Wesling, J.R. (editors), *Neotectonics of South-Central Coastal California*, Friends of the Pleistocene Pacific Cell, 1990 Fall Field Trip Guidebook, pp. 349–383.

Clark, D.H., Hall, N.T., Hamilton, D.H., and Heck, R.G., 1991. Structural analysis of late Neogene deformation in the central offshore Santa Maria Basin, California, *Journal of Geophysical Research* **96** (B4), 6435–6457.

Clark, J.C., 1998. Neotectonics of the San Gregorio fault zone: Age dating controls on offset history and slip rates, *American Association of Petroleum Geologists Bulletin* **82** (5A): 844–845.

Clark, J.C., Brabb, E.E., Greene, H.G., and Ross, D.C., 1984. Geology of the Point Reyes Peninsula and implications for San Gregorio fault history: in Crouch, J.K., and Bachman, S.B. (editors), *Tectonics and Sedimentation Along the California Margin*, Pacific Sections, Society of Economic Paleontologists and Mineralogists, Vol. 38, pp. 67–85.

Clark, P.U., and Pollard, D., 1998. Origin of the middle Pleistocene transition by ice sheet erosion of regolith, *Paleoceanography* **13** (1): 1–9.

Compton, J.S., 1991. Porosity reduction and burial history of siliceous rocks from the Monterey and Sisquoc Formations, Point Pedernales area, California, *Geological Society of America Bulletin* **103** (5): 625–636.

Cox, A., and Engebretson, D., 1985. Change in motion of Pacific plate at 5 Myr BP, *Nature* **313**: 472–474.

Crowell, J.C., 1974. Origin of late Cenozoic basins in southern California: in Dickinson, W.R. (editor), *Tectonics and Sedimentation*, Society of Economic Paleontologists and Mineralogists Special Publication 22, pp. 190–204.

Dartnell, P., and Gardner, J.V., 2009. Seafloor terrain analysis and geomorphology of the greater Los Angeles margin and San Pedro Basin, Southern California: in Lee, H.J., and Normark, W.R. (editors), *Earth Science in the Urban Ocean*, Geological Society of America Special Paper 454, pp. 9–28.

Dickinson, W.R., 2004a. Evolution of the North American Cordillera, *Annual Reviews of Earth and Planetary Sciences* **32**: 13–45.

Dickinson, W.R., 2004b. Kinematics of transrotational tectonism in the California Transverse Ranges and its contribution to cumulative slip along the San Andreas Transform Fault System; http://seismo.berkeley.edu/~rallen/teaching/S04_SanAndreas/Resources/BlockRotationTransrotationalTectonism.pdf.

Dickinson, W.R., Ducea, M., Rosenberg, L.I., Greene, H.G., Graham S.A., Clark, J.C., Weber, G.E., Kidder, S., Ernst, W.G., and Brabb, E.E., 2005. *Net Dextral Slip, Neogene*

San Gregorio-Hosgri Fault Zone, Coastal California: Geologic Evidence and Tectonic Implications, Geological Society of America Special Paper 391, 43 pp.

Eaton, J.P., 1984. *Focal Mechanisms of Near-Shore Earthquakes Between Santa Barbara and Monterey, California*, U.S. Geological Survey Open-File Report 84-477, 9 pp.

Field, M.E., Gardner, J.V., and Prior, D.B., 1999. Geometry and significance of stacked gullies on the northern California slope, *Marine Geology* **154**: 271–286.

Fugro Consultants, Inc., 2012a. *Field Operations Report 2010-2011, High-Resolution Marine Survey Offshore Diablo Canyon Power Plant, Central California*, Fugro Project No. 04.B0992017, prepared for PG&E, May, 875 pp.

Fugro Consultants, Inc., 2012b. *Software Validation of Uniseis and 3D Data Qualification of 2010-2011 High-Resolution Marine Survey Data, Offshore Diablo Canyon Power Plant, Central Coastal California Seismic Imaging Project*, Report No. PGEQ-PR-03 (Rev0), FSI Project No. 2011-4493, June, 67 pp.

Fugro Consultants, Inc., 2012c. *Software Validation for Seismic Processing Workshop and Qualification of 2010-2011, High-Resolution 2D Marine Seismic Reflection Data, Rev. 1, Offshore Diablo Canyon Power Plant, Central California*, Report No. PGEQ-PR-06 (Rev1), Fugro Project No. 04.B0992017, prepared for PG&E, November, 43 pp.

Fugro Consultants, Inc., 2012d. *2012 PG&E P-Cable 3D Low-Energy Seismic Survey Field Operations Report, Diablo Canyon Power Plant, Central Coastal California Seismic Imaging Project*, Report No. PGEQ-PR-11, Rev0, prepared for PG&E, December, 319 pp.

Fugro Consultants, Inc., 2012e. *2011 PG&E P-Cable Seismic Survey, 3D Data Processing Report, San Luis Bay, Central Coastal California Seismic Imaging Project*, Report No. PGEQ-PR-05, Rev0, FSI Project No. 2012-4509, prepared for PG&E, December, 92 pp.

Fugro Consultants, Inc., 2012f. *Validation of the Commercial Software IHS Kingdom Version 8.6 Hotfix 4 2d/3dPAK, VuPAK, and Rock Solid Attributes, Diablo Canyon Power Plant, Central Coastal California Seismic Imaging Project*, Report No. PGEQ-PR-07, Rev0, prepared for PG&E, December, 216 pp.

Fugro Consultants, Inc., 2013a. *2D Data Processing Report for the 2012 Offshore High-Resolution P-Cable Seismic Reflection Data, Diablo Canyon Power Plant, Central Coastal California Seismic Imaging Project*, Report No. PGEQ-PR-13, Rev0, prepared for PG&E, February, 23 pp.

Fugro Consultants, Inc., 2013b. *2012 PG&E P-Cable Low-Energy Seismic Survey 3D Data Processing Report, San Luis Obispo Bay, Diablo Canyon Power Plant, Central Coastal California Seismic Imaging Project*, FSI Project Number 2012-4574, Report No. PGEQ-PR-17, Rev0, prepared for PG&E, August, 65 pp.

Fugro Consultants, Inc., 2013c. *2012 PG&E P-Cable Low-Energy Seismic Survey 3D Data Processing Report, Point Sal, Diablo Canyon Power Plant, Central Coastal California Seismic Imaging Project*, FSI Project Number 2012-4574, Report No. PGEQ-PR-18, Rev0, prepared for PG&E, August, 59 pp.

Fugro Consultants, Inc., 2013d. *2012 PG&E P-Cable Low-Energy Seismic Survey 3D Data Processing Report, Estero Bay, Diablo Canyon Power Plant, Central Coastal California Seismic Imaging Project*, FSI Project Number 2012-4574, Report No. PGEQ-PR-19, Rev0, prepared for PG&E, August, 53 pp.

Fugro Consultants, Inc., 2013e. *PG&E 3D P-Cable Survey- Field Operations Report, 2011 Low-Energy Seismic Survey, Diablo Canyon Power Plant, Central Coastal California Seismic Imaging Project*, Report No. PGEQ-PR-1, Rev0, prepared for PG&E, November, 160 pp.

Galloway, W.E., 1975. Process framework for describing the morphologic and stratigraphic evolution of deltaic depositional systems: in Broussard, M.L. (editor), *Deltas: Models for Exploration*, Houston Geological Society, Houston, Tex., pp. 87–98.

Gardner, M.H., Borer, J.M., Melick, J.J., Mavilla, N., Dechesne, M., and Wagerle, R.N., 2003. Stratigraphic process-response model for submarine channels and related features from studies of Permian Brushy Canyon outcrops, West Texas, in Mutti, E., Steffens, G.S., Pirmez, C., Orlando, M., Roberts, D. (editors), special issue on Turbidites: Models and Problems, *Marine and Petroleum Geology* **20**: 757–787.

Graham, S.A., and Dickinson, W.R., 1978. Apparent offsets of on-land geologic features across the San Gregorio-Hosgri fault zone: in Silver, E.A., and Normark, W.R. (editors), San Gregorio-Hosgri fault zone, California: California Division of Mines and Geology Special Report 137, pp. 13–23

Greene, H.G., Maher, N.M., and Paull, C.K., 2002. Physiography of the Monterey Bay National Marine Sanctuary and implications about continental margin development, *Marine Geology* **181**: 55–82.

Grossman, E.E., Eittreim, S.L., Field, M.E., and Wong, F.L., 2006. Shallow stratigraphy and sedimentation history during high-frequency sea-level changes on the central California shelf, *Continental Shelf Research* **26**: 1217–1239.

Hall, C.A., Jr., 1973. Geologic map of the Morro Bay South and Port San Luis quadrangles, San Luis Obispo County, California, *U.S. Geological Survey Miscellaneous Field Studies Map MF-511*, scale 1:24,000.

Hall, C.A., Jr., 1975. San Simeon–Hosgri fault system, coastal California; Economic and environmental implications, *Science* **190**: 1291–1293.

Hall, T., Hunt, T.D., and Vaughan, P.R., 1994. Holocene behavior of the San Simeon fault zone, south-central coastal California: in Alterman, I.B., McMullen, R.B., Cluff,

L.S., and Slemmons, D.B. (editors), *Seismotectonics of the Central California Coast Range*, Geological Society of America Special Paper 292, pp. 167–189.

Hanson, K.L., and Lettis, W.R., 1994. Estimated Pleistocene slip rate for the San Simeon fault zone, south-central coastal California: in Alterman, I.B., McMullen, R.B., Cluff, L.S., and Slemmons, D.B. (editors), *Seismotectonics of the Central California Coast Range*, Geological Society of America Special Paper 292, pp. 133–150.

Hanson, K.L., Lettis, W.R., McLaren, M.K., Savage, W.U., and Hall, N.T., 2004. Style and rate of Quaternary deformation of the Hosgri fault zone, offshore south-central California: in Keller, M.A. (editor), *Evolution of Sedimentary Basins/Onshore Oil and Gas Investigations—Santa Maria Province*, U.S. Geological Survey Bulletin 1995-BB, 33 pp.

Hanson, K.L., Wesling, J.R., Lettis, W.R., Kelson, K.I., and Mezger, L., 1994. Correlation, ages, and uplift rates of Quaternary marine terraces, south-central California: in Alterman, I.B., McMullen, R.B., Cluff, L.S., and Slemmons, D.B. (editors), *Seismotectonics of the Central California Coast Range*, Geological Society of America Special Paper 292, pp. 45–72.

Harbert, W., and Cox, A., 1989. Late Neogene motion of the Pacific Plate, *Journal of Geophysical Research: Solid Earth* **94** (B3): 3052–3064.

Hardebeck, J.L., 2010. Seismotectonics and fault structure of the California central coast, *Seismological Society of America Bulletin* **100**: 1031–1050, doi: 10.1785/0120090307.

Hardebeck, J.L., 2013. Geometry and earthquake potential of the Shoreline Fault, Central California, *Bulletin of the Seismological Society of America* **103** (1): 447–462.

Hays, J.D., Imbrie, J., and Shackleton, N.J., 1976. Variations in the earth's orbit: Pacemaker of the ice ages, *Science* **194**: 1121–1132.

Hill, M.L., and Dibblee, T.W., Jr., 1953. San Andreas, Garlock, Big Pine faults: A study of the character, history, and tectonic significance of their displacements, *Geological Society of America Bulletin* **64** (4): 443–458.

Hornafius, J.S., Luyendyk, B.P., Terres, R.R., and Kamerling, M.J., 1986. Timing and extent of Neogene rotation of western Transverse Ranges, California, *Geological Society of America Bulletin* **97**: 1476–1487.

Howell, D.G., Crouch, J.K., Greene, H.G., McCulloch, D.S., and Vedder, J.G., 1980. Basin development along the late Mesozoic and Cainozoic California margin: A plate tectonic margin of subduction, oblique subduction and transform tectonics: in Ballance, P.F., and Reading, H.G. (editors), *Sedimentation in Oblique-Slip Mobile Zones*, International Association of Sedimentologists Special Publication, chap. 4, pp. 43–62.

Jennings, C.W., and Bryant, W.A., 2010. 2010 Fault Activity Map of California, California Geological Survey, Geologic Data Map No. 6, California Geological Survey.

Johnson, S.Y., Dartnell, P., Cochrane, G.R., Golden, N.E., Phillips, E.L., Ritchie, A.C., Kvitek, R.G., and 11 others, 2013. California State Waters Map Series—Offshore of Ventura, California: in Johnson, S.Y., and Cochran, S.A. (editors), U.S. Geological Survey Scientific Investigations Map 3254, pamphlet 42 pp., 11 sheets; http://pubs.usgs.gov/sim/3254/.

Johnson, S.Y., Hartwell, S.R., and Dartnell, P., 2014. Offset of Latest Pleistocene shoreface reveal slip rate on the hosgri strik-slip fault, offshore central California, *Bulletin of the Seismological Society of America* **104** (4), doi:10.1785/012013057.

Johnson, S.Y., and Stanley, R.G., 1994. Sedimentology of the Conglomeratic Lower Member of the Lospe Formation (Lower Miocene), Santa Maria Basin, California: in Keller, M.A. (editor), *Evolution of Sedimentary Basins/Onshore Oil and Gas Investigations—Santa Maria Province*, U.S. Geological Survey Bulletin 1995-D; http://pubs.usgs.gov/bul/1995de/report.pdf.

Johnson, S.Y., and Watt, J.T., 2012. Influence of fault trend, bends, and convergence on shallow structure and geomorphology of the Hosgri strike-slip fault, offshore central California, *Geosphere* **8** (6): 1632–1656.

Keller, E., and Pinter, N., 2002. *Active Tectonics: Earthquakes, Uplift, and Landscape*, 2nd Edition, Prentice Hall, Upper Saddle River, NJ, 355 pp.

Kingma, J.T., 1958. Possible origin of piercement structures, local unconformities, and secondary basins in the Eastern Geosyncline, New Zealand, *New Zealand Journal of Geology and Geophysics* **1**: 269–274.

Knox, J.C., 1995. Fluvial systems since 20,000 years BP: in Gregory, K.J., Starkel, L., and Baker, V.R. (editors), *Global Continental Paleohydrology*, John Wiley & Sons, Chichester, pp. 87–108.

Langenheim, V.E., Jachens, R.C., Graymer, R.W., Colgan, J.P., Wentworth, C.M., and Stanley, R.G., 2013. Fault geometry and cumulative offsets in the central Coast Ranges, California: Evidence for northward increasing slip along the San Gregorio–San Simeon–Hosgri fault, *Lithosphere* **5** (1): 29–48.

Lease, R.O., McQuarrie, O.M., and Leier, A., 2009. Quantifying destral shear on the Bristol-Granite Mountain Fault Zone: successful geologic prediction from kinematic compatibility of the Eastern California Shear Zone, *Journal of Geology* **117**: 37–53.

Lee, S.E., Talling, P.J., Ernst, G.G.J., and Hogg, A.J., 2002. Occurrence and origin of submarine plunge pools at the base of the U.S. continental slope, *Marine Geology* **185**: 363–377.

Lettis, W.R., Hanson, K.L., Unruh, J.R., McLaren, M., and Savage, W.U., 2004. Quaternary tectonic setting of south-central coastal California: in Keller, M.A. (editor), *Evolution of Sedimentary Basins/Offshore Oil and Gas Investigations—Santa Maria Province*, U.S. Geological Survey Bulletin 1995-AA, 24 pp.

Lettis, W.R., Kelson, K.I., Wesling, J.R., Angell, M., Hanson, K.L., and Hall, N.T., 1994. Quaternary deformation of the San Luis Range, San Luis Obispo County, California: in Alterman, I.B., McMullen, R.B., Cluff, L.S., and Slemmons, D.B. (editors), *Seismotectonics of the Central California Coast Ranges*, Geological Society of America Special Paper 292, pp. 111–132.

Lisiecki, L.E., and Raymo, M.E., 2005. A Pliocene-Pleistocene stack of 57 globally distributed benthic δ^{18}O records, *Paleoceanography* **20** (1), doi:10.1029/2004PA001071, 17 pp.

Luyendyk, B.P., 1991. A model for Neogene crustal rotations, transtension, and transpression in Southern California, *Geological Society of America Bulletin* **103**: 1528–1536.

Maier, K.L., Fildani, A., McHargue, T.R., Paull, C.K., Graham, S.A., and Caress, D.W. 2012. Punctuated deep-water channel migration: High-resolution subsurface data from the Lucia Chica channel system, offshore California, *Journal of Sedimentary Research* **82**: 1–8, doi:10.2110/jsr.2012.10.

Maier, K.L., Fildani, A., Paull, C.K., McHargue, T.R., Graham, S.A., and Caress, D.W., 2013. Deep-sea channel evolution and stratigraphic architecture from inception to abandonment from high-resolution Autonomous Underwater Vehicle surveys offshore central California, *Sedimentology* **60** (4): 935–960.

Mann, P., 2007. Global catalogue, classification and tectonic origins of restraining- and releasing-bends on active strike-slip fault systems: in Cunningham, W.D., and Mann, P. (editors), *Tectonics of Strike-Slip Restraining and Releasing Bends*: Geological Society, London, Special Publications, Vol. 290, pp. 13–142.

McClay, K., and Bonora, M., 2001. Analog models of restraining stepovers in strike-slip fault systems, *American Association of Petroleum Geologists Bulletin* **85** (2): 233–260.

McCulloch, D.S., 1987. Regional geology and hydrocarbon potential of offshore central California continental margin: in Scholl, D.W., Grantz, A., and Vedder, J.G. (editors), *North America and Adjacent Ocean Basins—Beaufort Sea to Baja California*, Circum-Pacific Council for Energy and Mineral Resources, Earth Science Series Volume 6, Houston, pp. 353–401.

McFarland, F.S., Lienkaemper, J.J., and Caskey, S.J., 2009. *Data from Theodolite Measurements of Creep Rates on San Francisco Bay Region Faults, California: 1979-2013*, USGS Open-File Report 2009-1119, Report, 18 pp. and data files.

McLaren, M.K., and Savage, W.U., 1987. Relocation of earthquakes offshore from Point Sal, California (abs.): *EOS Transactions, American Geophysical Union* **68** (44): 1366.

McLaren, M.K., and Savage, W.U., 2001. Seismicity of south-central coastal California: October 1987 through January 1997, *Bulletin of the Seismological Society of America* **91** (6): 1629–1658.

Mitchell, N., and Huthnance, J., 2007. Comparing the smooth, parabolic shapes of interfluves in continental slopes to predictions of diffusion transport models, *Marine Geology* **236** (3-4): 189–208.

Muller, R.A., and MacDonald, G.J., 1995. Glacial cycles and orbital inclination, *Nature* **377**: 107–108.

Naish, T.R., and Wilson, G.S., 2009. Constraints on the amplitude of Mid-Pliocene (3.6–2.4 Ma) eustatic sea-level fluctuations from the New Zealand shallow-marine sediment record, *Philosophical Transactions of the Royal Society* **367**: 169–187.

Nicholson, C., Sorlien, C.C., Atwater, T., Crowell, J.C., and Luyendyk, B.P., 1994. Microplate capture, rotation of the western Transverse Ranges, and initiation of the San Andreas transform as a low-angle fault system, *Geology* **22**: 491–495.

Nishenko, S., Hogan, P., and Kvitek, R., 2012. Seafloor mapping for earthquake, tsunami hazard assessments, *Sea Technology* **53** (6): 15–20.

Normark, W.R., Piper, D.J.W., Romans, B.W., Covault, J.A., Dartnell, P., and Sliter, R.W., 2009. Submarine canyon and fans systems of the California Continental Borderland: in Lee, H., and Normark, W.R. (editors), *Earth Science in the Urban Ocean; The Southern California Continental Borderland*, GSA Special Paper 454, pp. 141–168.

O'Connell, D.R.H., Unruh, J.R., and Block, L.V., 2001. Source characterization and ground-motion modeling of the 1892 Vacaville-Winters earthquake sequence, California, *Bulletin of the Seismological Society of America* **91** (6): 1471–1497.

Onderdonk, N.W., 2005. Structures that accommodated differential vertical axis rotation of the western Transverse Ranges, California, *Tectonics* **24** (4), 15 pp., doi:10.1029/2004TC001769.

Orange, D.L., 1999. Tectonics, sedimentation and erosion in northern California; Submarine geomorphology and sediment preservation potential as a result of three competing processes, *Marine Geology* **154**: 369–382.

Pacific Gas and Electric Company (PG&E), 1988. *Final Report of the Diablo Canyon Long Term Seismic Program*, U.S. Nuclear Regulatory Commission Enclosure 1, PG&E letter DCL-05-002, Docket No. 50-275 and No. 50-323.

Pacific Gas and Electric Company (PG&E), 1990. Long Term Seismic Program: Response to Question GSG 16. U.S. Nuclear Regulatory Commission Docket No. 50-275 and No. 50-323, March.

Pacific Gas and Electric Company (PG&E), 2011a. *Progress Report on the Analysis of the Shoreline Fault Zone, Central Coastal California*, report to the U.S. Nuclear Regulatory Commission, PG&E Letter DCL-10-003, 36 pp.

Pacific Gas and Electric Company (PG&E), 2011b. *Shoreline Fault Zone Report: Report on the Analysis of the Shoreline Fault Zone, Central Coastal California*, report to the

U.S. Nuclear Regulatory Commission, January; www.pge.com/myhome/
edusafety/systemworks/dcpp/shorelinereport/.

Pacific Gas and Electric Company (PG&E), 2012. *DCPP 3D/2D Seismic-Reflection
Investigation of Structures Associated with the Northern Shoreline Seismicity
Sublineament of the Point Buchon Region*: PG&E Technical Report
GEO.DCPP.TR.12.01.

Pacific Gas and Electric Company (PG&E), 2013. *Stratigraphic Framework for
Assessment of Fault Activity Offshore of the Central California Coast Between Point San
Simeon and Point Sal*: PG&E Technical Report GEO.DCPP.TR.13.01.

Peltier, W.R., 2004. Global glacial isostasy and the surface of the ice-age earth: The ICE-
5G (VM2) Model and GRACE, *Annual Review of Earth and Planetary Sciences* **32**: 111–
149.

Posamentier, H.W., and Allen, G.P., 1999. Siliciclastic Sequence Stratigraphy: Concepts
and Applications: SEPM Concepts in Sedimentology and Paleontology No. 7, *Society for
Sedimentary Geology*, 210 pp.

Pratson, L.F., Nittrouer, C.A., Wiberg, P.L., Steckler, M.S., Swenson, J.B., Cacchione,
D.A., Karson, J. A., and 15 others, 2007. Seascape evolution on clastic continental
shelves and slopes: in Nittrouer, C.A., Austin, J.A., Jr., Field, M.E., Kravitz, J.H.,
Syvitski, J.P.M., and Wiberg, P.L. (editors), *Continental Margin Sedimentation, From
Sediment Transport to Sequence Stratigraphy* Special Publication No. 37 of the
International Association of Sedimentologists, Blackwell Publishing, Ltd., pp. 339–373.

Pratson, L.F., Ryan, W.B.F., Mountain, G.S., and Twichell, D.C., 1994. Submarine
canyon initiation by downslope-eroding sediment flows; evidence in late Cenozoic strata
on the New Jersey continental slope, *Geological Society of America Bulletin* **106** (3):
395–412.

Quennell, A.M., 1958. The structural and geomorphic evolution of the Dead Sea Rift,
Quarterly Journal of the Geological Society of London **114**: 1–14.

Raymo, M.E., Lisiecki, L.E., and Nisancioglu, K.H., 2006. Plio-Pleistocene ice volume,
Antarctic climate, and the global δ^{18}O record, *Science* **313**: 492–495.

Raymo, M.E., and Mitrovica, J.X., 2012. Collapse of polar ice sheets during the stage 11
interglacial, *Nature* **483**: 453–456.

Reading, H.G., 1980. Characteristics and recognition of strike-slip fault systems: in
Ballance, P.F., and Reading, H.G. (editors), *Sediment in Oblique-Slip Mobile Zones*,
International Association of Sedimentologists Special Publication 4, pp. 7–26.

Reneau, S.L., Dietrich, W.E., Donahue, D.J., Jull, A.J.T., and Rubin, M., 1990. Late
Quaternary history of colluvial deposition an erosion in hollows, central California Coast
Ranges, *Geological Society of America Bulletin* **102**: 969-982.

Rivero, C., and Shaw, J.H., 2011. Active folding and blind thrust faulting induced by basin inversion processes, inner California borderlands: in McClay, K., Shaw, J., and Suppe, J. (editors), *Thrust Fault-Related Folding*, American Association of Petroleum Geologists Memoir 94, Ch. 9, pp. 187–214.

Romans, B.W., Normark, W.R., McGann, M.M., Covault, J.A., and Graham, S.A., 2009. Coarse-grained sediment delivery and distribution in the Holocene Santa Monica Basin, California: Implications for evaluating source-to-sink flux at millennial time scales, *Geological Society of America Bulletin* **121** (9-10):1394–1408.

Ross, D.C., and Brabb, E.E., 1972. Petrography and structural relations of granite basement rocks in the Monterey Bay area, California, *Journal of Research of the U.S. Geological Survey* **1** (3): 273–282.

Shepard, F.P., 1965. Types of submarine valleys, *American Association of Petroleum Geologists Bulletin* **49** (3): 304–310.

Sheriff, R.E., 1982. *Structural Interpretation of Seismic Data*, American Association of Petroleum Geologists, 73 pp.

Sheriff, R.E., and Geldart, L.P., 1995. *Exploration Seismology*, Cambridge University Press, Second Edition.

Siddall, M., Rohling, E.J., Almogi-Labin, A., Hemleben, C., Meischner, D., Schmelzer, I., and Smeed, D.A., 2003. Sea-level fluctuations during the last glacial cycle, *Nature* **423**: 853–857, doi:10.1038/nature01690.

Sims, J.D., 1993. Chronology of displacement on the San Andreas Fault in central California: Evidence from reversed positions of exotic rock bodies near Parkfield, California: in Powell, R.E., Weldon, R.J., III, and Matti, J.C. (editors), *The San Andreas Fault System: Displacement, Palinspastic Reconstruction, and Geologic Evolution*, Geologic Society of America Memoir 178, Ch. 6, pp. 231–256.

Sliter, R.W., Triezenberg, P.J., Hart, P.E., Watt, J.T., Johnson, S.Y., and Scheirer, D.S., 2009 (revised 2010). *High-Resolution Seismic Reflection and Marine Magnetic Data Along the Hosgri Fault Zone, Central California*, U.S. Geological Survey Open-File Report 2009-1100, version 1.1.

Sommerfield, C.K., Ogston, A.S., Mullenbach, B.L., Drake, D.E., Alexander, C.R., Nittrouer, C.A., Borgeld, J.C., Wheatcroft, R.A., and Liethold, E.L., 2007. Oceanic dispersal and accumulation of river sediment: in Nittrouer, C.A., Austin, J.A., Field, M.E., Kravitz, J.H., Syvitski, J.P.M., and P.L. Wiberg (editors), *Continental Margin Sedimentation, From Sediment Transport to Sequence Stratigraphy* (Special Publication No. 37 of the International Association of Sedimentologists, Blackwell Publishing, Ltd., pp. 157–205.

Sorlien, C.C., Kamerling, M.J., and Mayerson, D., 1999. Block rotation and termination of the Hosgri strike-slip fault, California, from three-dimensional map restoration, *Geology* **27** (11), 1039–1042.

Sorlien, C.C., Nicholson, C., Luyendyk, B.P., Miller, K.C., and Meltzer, A.S., 1999. Miocene extension and post-Miocene transpression offshore of south-central California. Structure and tectonics of the central offshore Santa Maria and Santa Lucia basins, California: Results from the PG&E/EDGE seismic reflection survey: in Keller, M.A. (editor), *Evolution of Sedimentary Basins/Onshore Oil and Gas Investigations—Santa Maria Province*, U.S. Geological Survey Bulletin 1995-Y, 38 pp.

Spinelli, G.A., and Field, M.E., 2001. Evolution of continental slope gullies on the Northern California margin, *Journal of Sedimentary Research* **71**: 237–245.

Surpless, K.D., Ward, R.B., and Graham, S.A., 2009. Evolution and stratigraphic architecture of marine slope gully complexes: Monterey Formation (Miocene), Gaviota Beach, California, *Marine and Petroleum Geology* **26**: 269–288.

Swanson, M.T., 2005. Geometry and kinematics of adhesive wear in brittle strike-slip zones, *Journal of Structural Geology* **27** (5): 871–887, doi:10.1016/j.jsg.2004.11.009.

Tamisiea, M.E., and Mitrovica, J.X., 2011. The moving boundaries of sea level change: understanding the origins of geographic variability, *Oceanography* **24** (2): 24–39.

Townend, J., and Zoback, M.D., 2001. Implications of earthquake focal mechanisms for the frictional strength of the San Andreas fault system, in Holdsworth, R.E., Strachan, R.A., Magloughlin, J.F., and Knipe, R.J. (editors), *The Nature and Tectonics Significance of Fault Zone Weakening*, Geological Society, London Special Publication 186, pp. 13–21.

Tziperman, E., and Gildor, H., 2003. On the mid-Pleistocee transition to 100-kyr glacial cycles and the asymmetry between glaciation and deglaciation times, *Paleoceanography* **18** (1): 1001–1008.

Waelbroeck, C., Labeyrie, L., Michel, E., Duplessy, J.C., McManus, J.F., Lambeck, K., Balbon, E., and Labracherie, M., 2002. Sea-level and deep water temperature changes derived from benthic foraminifera isotopic records, *Quaternary Science Reviews* **21**: 295–305.

Watt, J.T., Johnson, S.Y., Hartwell, S.R., and Roberts, M., [in preparation]. Offshore geology and geomorphology maps from Piedras Blancas to Pismo Beach, San Luis Obispo and Santa Barbara counties, California: *U.S. Geological Survey Scientific Investigations Map XXXX*, pamphlet XX pp., 6 sheets, 1:35,000 scale, and database. Draft dated February 15, 2012.

Wentworth, C.M., and Zoback, M.D., 1989. The style of late Cenozoic deformation at the eastern front of the California Coast Ranges, *Tectonics* **8** (2): 237–246.

Willingham, C.R., Rietman, J.D., Heck, R.G., and Lettis, W.R., 2013. Characterization of the Hosgri Fault Zone and adjacent structures in the offshore Santa Maria Basin, south-central California: in Keller, M.A. (editor), *Evolution of Sedimentary Basins/Onshore Oil and Gas Investigations—Santa Maria Province*, U.S. Geological Survey Bulletin 1995-CC, 105 pp. (revised version of 1995 report).

Yilmaz, O., 2001. *Seismic Data Analysis: Processing, Inversion, and Interpretation of Seismic Data*, Volume II, 2nd Ed., Investigations in Geophysics No. 10, Society of Exploration Geophysicists, Tulsa, OK, 2,027 pp.

Zoback, M.D., Zoback, M.L., Mount, V.S., Suppe, J., Eaton, J.P., Healy, J.H., Oppenheimer, D., Reasenberg, P., Jones, L., Raleigh, C.B., Wong, I.G., Scotti, O., and Wentworth, C., 1987. New evidence on the state of stress of the San Andreas Fault system, *Science* **238**: 1105–1111.

ATTACHMENT 1

REPORT VERIFICATION SUMMARY

An Independent Technical Reviewer (ITR) provided reviews of the Technical Report and supporting documents. Professor Stephan Graham of Stanford University reviewed the report for technical accuracy, including use of proper interpretation methods. He also reviewed the Fugro Field and Data Processing reports for completeness and accuracy as QA acceptance of the data collection and processing.
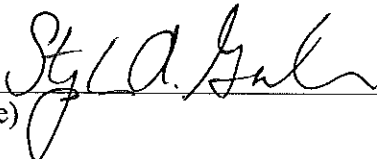
Item	Parameter	Yes	No*	N/A*
1	Purpose is clearly stated, and the report satisfies the Purpose.	XXX		
2	Data to be interpreted and/or analyzed are included or referenced.	XXX		
3	Methodology is appropriate and properly applied.	XXX		
4	Assumptions are reasonable, adequately described, and based on sound geotechnical principles and practices.	XXX		
5	Software is identified and properly applied. Validation is referenced or included and is acceptable. Input files are correct and accurate.	XXX		
6	Interpretation and/or Analysis is complete and accurate and leads logically to Results and Conclusions.	XXX		
7	Results and Conclusions are accurate, acceptable, and reasonable compared to the Data, Interpretation and/or Analysis, and Assumptions.	XXX		
8	The Limitation on the use of the Results has been addressed and is accurate and complete.	XXX		
9	The Impact Evaluation has been included and is accurate and complete.	XXX		
10	References are valid for intended use.	XXX		
11	Appendices are complete and accurate and support the text.		XXX	

Report Verification Summary by Independent Technical Reviewer

Comments:
From mid-2013 through July, 2014, I attended three meetings with the author of this report and his associated investigators to observe the evolution of the study. In my role as ITR for GEO.DCPP.TR.14.02 R0, I reviewed an October, 2013, draft version of the report. Recommendations from my review included numerous slight clarifications of language, grammatical errors, correction of certain geologic terms. The most significant technical recommendation concerned estimates of timing of channel incision. Report author Greene subsequently made the requested changes in response to these recommendations. I reviewed a later version of the report in mid-June, 2014, and made a limited number of additional recommendations of a minor nature; report author Greene accepted these recommendations, as verified by me in reviewing the July 23, 2014, version of the report.
Item 11 of the Verification Summary Report: 'No'—Review of appendices was not in the scope of this review.

Verifier (ITR): ___Dr. Stephan A. Graham___ _(signature)_ ~ 27 July 2014
                        (name/signature)   (date)